



UNIVERSITAT DE
BARCELONA

Identification of PfAP2-HS as the master regulator of the heat shock response in the human malaria parasites *Plasmodium falciparum*

Elisabet Tintó Font

ADVERTIMENT. La consulta d'aquesta tesi queda condicionada a l'acceptació de les següents condicions d'ús: La difusió d'aquesta tesi per mitjà del servei TDX (www.tdx.cat) i a través del Dipòsit Digital de la UB (diposit.ub.edu) ha estat autoritzada pels titulars dels drets de propietat intel·lectual únicament per a usos privats emmarcats en activitats d'investigació i docència. No s'autoritza la seva reproducció amb finalitats de lucre ni la seva difusió i posada a disposició des d'un lloc aliè al servei TDX ni al Dipòsit Digital de la UB. No s'autoritza la presentació del seu contingut en una finestra o marc aliè a TDX o al Dipòsit Digital de la UB (framing). Aquesta reserva de drets afecta tant al resum de presentació de la tesi com als seus continguts. En la utilització o cita de parts de la tesi és obligat indicar el nom de la persona autora.

ADVERTENCIA. La consulta de esta tesis queda condicionada a la aceptación de las siguientes condiciones de uso: La difusión de esta tesis por medio del servicio TDR (www.tdx.cat) y a través del Repositorio Digital de la UB (diposit.ub.edu) ha sido autorizada por los titulares de los derechos de propiedad intelectual únicamente para usos privados enmarcados en actividades de investigación y docencia. No se autoriza su reproducción con finalidades de lucro ni su difusión y puesta a disposición desde un sitio ajeno al servicio TDR o al Repositorio Digital de la UB. No se autoriza la presentación de su contenido en una ventana o marco ajeno a TDR o al Repositorio Digital de la UB (framing). Esta reserva de derechos afecta tanto al resumen de presentación de la tesis como a sus contenidos. En la utilización o cita de partes de la tesis es obligado indicar el nombre de la persona autora.

WARNING. On having consulted this thesis you're accepting the following use conditions: Spreading this thesis by the TDX (www.tdx.cat) service and by the UB Digital Repository (diposit.ub.edu) has been authorized by the titular of the intellectual property rights only for private uses placed in investigation and teaching activities. Reproduction with lucrative aims is not authorized nor its spreading and availability from a site foreign to the TDX service or to the UB Digital Repository. Introducing its content in a window or frame foreign to the TDX service or to the UB Digital Repository is not authorized (framing). Those rights affect to the presentation summary of the thesis as well as to its contents. In the using or citation of parts of the thesis it's obliged to indicate the name of the author.

Identification of PfAP2-HS as the master regulator of the heat shock response in the human malaria parasite *Plasmodium falciparum*

Elisabet Tintó Font

La present tesi s'ha dut a terme a l'Institut de Salut Global de
Barcelona (ISGlobal), sota la direcció del Dr. Alfred Cortés Closas i
la tutela del Dr. Antonio Zorzano Olarte.

Programa de Doctorat en Biomedicina
Universitat de Barcelona

Setembre de 2019



UNIVERSITAT DE
BARCELONA

ISGlobal **Barcelona**
Institute for
Global Health

Seguirem somniant
ensorrarem els murs
anirem sempre més lluny.

Sopa de Cabra

INDEX

INTRODUCTION	13
1 MALARIA	15
1.1 Malaria context and epidemiology	15
1.2 Life cycle	16
1.3 Clinical manifestations	18
1.4 Malaria control	20
2 TRANSCRIPTIONAL REGULATION IN <i>P. FALCIPARUM</i>	24
2.1 Genome characteristics	24
2.2 General aspects of transcription	24
2.3 Transcription factor regulation	26
2.4 Epigenetic regulation	34
2.5 Post-transcriptional regulation	37
3 FEVER	39
3.1 General mechanisms of fever	39
3.2 Biological basis of malarial fever	43
4 HEAT SHOCK RESPONSE REGULATION	49
4.1 Types of stress response	49
4.2 Heat shock response in eukaryotes	50
4.3 Heat shock response in <i>P. falciparum</i>	58
HYPOTHESIS AND OBJECTIVES	65
MATERIALS AND METHODS	69
1 PARASITE LINES	71
2 <i>P. FALCIPARUM</i> CULTURE	72
2.1 Basic maintenance	72
2.2 Cryopreservation of parasite stocks	73
2.3 Parasite synchronization	73
3 <i>P. BERGHEI</i> CULTURE	75
3.1 Basic mice maintenance	75
3.2 <i>In vitro</i> culture	75
3.3 Parasite stocks	76
3.4 Schizonts purification	76

4	DETERMINATION OF PARASITEMIA	76
4.1	Giemsa-staining and light microscopy	76
4.2	Flow cytometry	77
5	NUCLEIC ACIDS EXTRACTION	77
5.1	gDNA extraction	77
5.2	RNA extraction	78
6	GENERATION OF TRANSGENIC LINES	79
6.1	Protocols used for cloning	79
6.2	Constructs generated for parasite transfection	82
6.3	<i>P. falciparum</i> transfection	85
6.4	<i>P. berghei</i> transfection	87
7	MEASUREMENT OF THE GROWTH RATE	88
8	DETERMINATION OF THE NUMBER OF MEROZOITES PER SCHIZONT	89
9	MEASUREMENT OF THE INTRAERYTHROCYTIC CYCLE LENGTH	89
10	HEAT SHOCK ASSAY	90
10.1	<i>P. falciparum</i> heat shock assay	90
10.2	<i>P. berghei</i> heat shock assay	92
11	DETERMINATION OF SENSITIVITY TO OTHER STRESS CONDITIONS	93
11.1	DHA sensitivity assay	93
11.2	DTT and H ₂ O ₂ sensitivity assays	94
12	PROTEIN DETECTION ANALYSIS	94
12.1	Western blot	94
12.2	Immunofluorescence assay	98
13	WHOLE-GENOME SEQUENCING	99
14	TRANSCRIPTIONAL ANALYSIS	100
14.1	Reverse transcription quantitative PCR	100
14.2	Microarrays analysis	102
15	ATAC-seq	105
16	PRIMERS	108
17	GENERAL RECIPES	111
RESULTS		113
1	PREVIOUS RELEVANT RESULTS	115

1.1	Adaptation of the 3D7-A line to periodic HS _____	115
1.2	Optimization of the heat shock assay _____	116
1.3	Transcriptional analysis of 3D7-A-HS and unselected 3D7-A populations _____	117
1.4	Assessment of the association between <i>clag2</i> and the heat shock-resistant phenotype _____	119
2	IDENTIFICATION OF THE DETERMINANT OF HEAT SHOCK	
	SUSCEPTIBILITY _____	120
2.1	Whole genome sequencing of 3D7-A and 3D7-A-HS lines _____	120
2.2	Association of the premature Q3417X mutation in PF3D7_1342900 with the heat shock-sensitive phenotype _____	123
2.3	Description of the PF13_42900 gene that carries the Q3417X mutation _____	123
2.4	Effect of the Q3417X mutation in the the regulation of <i>hsp70-1</i> and <i>hsp90</i> _____	124
3	NEW TOOLS TO STUDY PfAP2-HS _____	127
3.1	Generation of Δ PfAP2-HS transgenic lines _____	127
3.2	Generation of transgenic lines with inducible AP2-HS degradation and mislocalization _____	128
3.3	Generation of transgenic lines expressing tagged PfAP2-HS and PbAP2-HS _____	129
4	CHARACTERIZATION OF THE INVOLVEMENT OF PfAP2-HS IN PARASITE DEVELOPMENT _____	130
4.1	Functional characterization of PfAP2-HS under basal conditions _____	130
4.2	PfAP2-HS-dependent transcriptional regulation under basal conditions _____	132
5	CHARACTERIZATION OF THE ROLE OF PfAP2-HS IN THE HEAT SHOCK RESPONSE _____	135
5.1	Essentiality of PfAP2-HS under heat shock _____	135
5.2	Transcriptomic analysis of the heat shock response _____	135
5.3	PfAP2HS DNA-binding motifs involved in the heat shock response _____	146
5.4	Analysis of the role of PfAP2-HS in other types of stress _____	156
6	PRELIMINARY CHARACTERIZATION OF THE <i>P. BERGHEI</i> ORTHOLOG OF PfAP2-HS _____	160
	DISCUSSION _____	163
1	<i>P. FALCIPARUM</i> PARASITES CAN RESPOND TO HEAT STRESS _____	165
1.1	<i>P. falciparum</i> can activate directed transcriptional responses _____	165
1.2	Heat shock induces global transcriptional alterations _____	166

1.3	Different mechanisms are involved in the heat shock response _____	167
2	PfAP2-HS IS ANALOGOUS TO THE EUKARYOTIC HSF1 _____	171
2.1	PfAP2-HS is structurally different from HSF1 _____	171
2.2	Genetic variations in <i>pfap2-hs</i> _____	174
2.3	PfAP2-HS and HSF1 play a similar role under basal and stress conditions _ _____	176
2.4	Possible mechanisms of PfAP2-HS regulation analogous to HSF1 _____	179
2.5	DNA-binding motifs that recruit PfAP2-HS under basal and heat shock conditions _____	182
2.6	Conservation of the role of PfAP2-HS in other <i>Plasmodium</i> species _____	184
3	UNANSWERED QUESTIONS AND FUTURE PERSPECTIVES _____	186
	CONCLUSIONS _____	189
	ACKNOWLEDGEMENTS _____	193
	BIBLIOGRAPHY _____	197
	ANNEX _____	227
	ANNEX – I: Product references _____	229
	ANNEX – II: Generation and characterization of <i>P. falciparum</i> and <i>P. berghei</i> transgenic lines _____	233
	ANNEX – III: RT-qPCR validation of microarray analysis _____	242
	ANNEX – IV: Published and unpublished work _____	244

ABBREVIATIONS

3xHA	Triple human influenza hemagglutinin	CNTF	Ciliary neurotropic factor
aa	Amino acid	CSA	Chondroitin sulfate A
ACDC	AP2-coincident domain mostly at the C-terminus	CTM	C-terminal modulator domain
ACT	Artemisinin-based combination therapies	DBD	DNA-binding domain
AFC	Average fold-change	DD	Destabilization domain
aMAFC	Adjusted maximum average fold-change	DDT	Dichlorodiphenyltrichloroethane
AP2	Apetala2	DHA	Dihydroartemisinin
AP2/ERF	Apetala2/ethylene response factor	DSIF	DRB sensitivity-inducing factor
ApiAP2	Apicomplexan AP2 family	DTT	Dithiothreitol
APS	Ammonium persulfate	EDTA	Ethylenediaminetetraacetic acid
AR1/2	Transcriptional activation regions 1 and 2	eEF1A	Elongation factor 1-alpha 1
ATAC-seq	Assay for transposase accessible chromatin with high-throughput sequencing	EhHSF	<i>Entamoeba histolytica</i> HSF1
ATF6	Activating transcription factor 6	EMSA	Electrophoretic mobility shift assays
ATSB	Attractive toxic sugar bait	EP3	Prostaglandin receptor E 3
BBB	Blood brain barrier	ER	Endoplasmic reticulum
bp	Base pair	eYFP	Enhanced yellow fluorescent protein
BRG1	Brahma-related gene-1	FACT	Facilitates chromatin transcription
BSA	Bovine serum albumin	FBS	Fetal bovine serum
CDS	Coding sequence	FC	Fold change
CE2	Conserved element 2	FKBP	FK506 binding protein
ChIP-seq	Chromatin immunoprecipitation sequencing	FRB	FKBP rapamycin binding
clag	Cytoadherence-linked asexual gene family	GAF	GAGA factor
CNP	Copy number polymorphism	GCN5	General control nonderepressible 5
		CSP	<i>P. falciparum</i> circumsporozoite protein
		DMA	N,N-dimethylacetamide

gDNA	Genomic DNA	HSP	Heat shock protein
GDV1	<i>P. falciparum</i> gametocyte development 1	HSR	Heat shock response
gexp02	Gametocyte exported protein 2	HSR-1	Heat shock RNA-1
GFP	Green fluorescent protein	IC₅₀	Half maximal inhibitory concentration
GO	Gene ontology	Indels	Insertions and deletions
GPA	Glycophorin A	i.p.	Intraperitoneally
GPI	Glycophosphatidylinositol	i.v.	Intravenous
GSEA	Gene set enrichment analysis	IDC	Intraerythrocytic developmental cycle
GSR	General stress response	IFA	Immunofluorescence assay
GTF	General transcription factor	IFN-γ	Interferon-γ
H₂O₂	Hydrogen peroxide	IL	Interleukin
H3K4me3	Trimethylation of histone H3 lysine 4	indels	Insertions and deletions
H3K9ac	Acetylation of histone H3 lysine 9	Inr	Initiator element
H3K9me3	Trimethylation of histone H3 lysine 9	IPTi	Intermittent preventive treatment in infancy
HAT	Histone acetyltransferase	IPTp	Intermittent preventive treatment in pregnant women
HDAC	Histone deacetylase	IRS	Indoor residual spraying
hdhfr	Human dihydrofolate reductase	ITN	Insecticide-treated mosquito net
HDM	Histone demethylase	kb	Kilo base pairs
HMGB	High mobility group box	kDa	Kilo Daltons
HMT	Histone methyltransferase	KS	Knocksideways
hpi	Hours post-invasion	LAMP	Loop-mediated isothermal amplification
HR	Homology regions	LB	Luria-Bertani medium
HR-A/B/C	Heptad repeats A/B/C	lisp1	Liver specific protein 1
HRP	Horseradish peroxidase	LPS	Lipopolysaccharide
HS	Heat shock	LysoPC	Lysophosphatidylcholine
HSBP1	Heat shock binding protein 1	MPMP	Malaria parasite metabolic pathways
HSE	Heat shock element	mqH₂O	Ultrapure milli-Q H ₂ O
HSF1	Heat shock factor 1		

mRNA	Messenger RNA	PfLDH	<i>P. falciparum</i> lactate dehydrogenase
Msn2/4	Multicopy suppressor of <i>SNF1</i> mutation proteins 2 & 4	pfmc-2tm	<i>P. falciparum</i> two transmembrane Maurer's cleft protein family
MSP	Merozoite surface protein	pfmdr1	<i>P. falciparum</i> multidrug resistance transporter 1 gene
ncRNA	Non-coding RNA	PfSir2A	NAD-dependent deacetylase sirtuin-2A
NEF	Nucleotide-exchange factor	PfSR1	<i>P. falciparum</i> Ser/Arg-rich protein 1
NELF	Negative elongation factor	PGE₂	Prostaglandin E ₂
NFE2L2	Nuclear factor erythroid 2 like 2	PI	Phosphatidylinositol
ORF	Open reading frame	PIC	Preinitiation complex
OSR	Oxidative stress response	POA	Preoptic area of the hypothalamus
OVLT	Organum vasculosum of the laminae terminalis	Pol II	Polymerase II
PAMP	Pathogen associated molecular pattern	PR	Pentapeptide-repeat-like
PARP1	Poly(ADP)-ribose polymerase 1	PREBP	<i>Prx</i> regulatory element binding protein
PBM	Protein binding microarrays	PSAC	Plasmodial surface anion channel
PBS	Phosphate buffered saline	P-TEFb	Positive transcription elongation factor
PCR	Polymerase chain reaction	PTM	Post-translational modification
PFA	Paraformaldehyde	Rapa	Rapamycin
pfcr1	<i>P. falciparum</i> cloroquine resistance transporter gene	RBC	Red blood cell
pfdhfr	<i>P. falciparum</i> dihydrofolate reductase gene	RD	Central regulatory domain
pfdhps	Hydroxymethyldihydropterin pyrophosphokinase-dihydropteroate synthase gene	RDT	Rapid diagnostic test
PfDZ50	<i>P. falciparum</i> DOZI homologue	rif	Repetitive interspersed family
PfEMP1	<i>P. falciparum</i> erythrocyte membrane protein-1	ROS	Reactive oxygen species
PfHP1	<i>P. falciparum</i> heterochromatin protein 1	RPA	Replication protein A
PfHRP2	<i>P. falciparum</i> histidine-rich protein 2	rpm	Revolutions per minute
pfk13	<i>P. falciparum</i> Kelch13 gene	rRNA	Ribosomal RNA

RT-qPCR	Reverse transcription quantitative PCR	UPR	Unfolded protein response
s.e.m	Standard error of the mean	uRBC	Uninfected red blood cell
S2P	Site 2 protease	UTR	Untranslated region
ScHSF1	<i>Saccaromices cerevisiae</i> HSF1	WB	Western blot
SDS	Sodium dodecyl sulfate	WT	Wild type
sgRNA	Single guide RNA	yfcu	Yeast bifunctional enzyme gene
Shld	Shield 1		
sHSP	Small heat shock protein		
SMC	Seasonal malaria chemoprevention		
SNP	Single nucleotide polymorphism		
SRF	Serum response factor		
stevor	Subtelomeric variable open reading frame gene family		
STF	Specific transcription factor		
SWI/SNF	SWItch/sucrose non fermentable		
TAD	Transcriptional activation domain		
TBE	Tris/Borate/EDTA buffer		
TBP	TATA-box binding protein		
Td-Gbox	Tandem G-box		
Td-Tomato	Tandem Tomato		
TE	Tris-EDTA buffer		
TEMED	Tetrametiletildiamina		
TFII	Transcription factor II		
TLR	Toll-like receptor		
TM	Transmembrane		
TNF-α	Tumour necrosis factor- α		
TRiC	TCP1 ring complex		
TSS	Transcription start site		
uce	Ubiquitin-conjugating enzyme gene		

The background of the entire page is a repeating pattern of light teal circles, each containing a different microscopic cell structure. Some circles show a nucleus with a nucleolus, others show multiple nuclei, and some show a granular cytoplasm. A solid teal horizontal band is positioned across the middle of the page, containing the title text.

INTRODUCTION

1 MALARIA

1.1 Malaria context and epidemiology

Malaria has been a **global disease** since ancient times and remains as a major problem worldwide, especially for people from resource-limited areas. Nearly half of the world's population is at risk of malaria, being children under 5 years of age and pregnant women particularly vulnerable to this disease. An estimated 435,000 deaths and 219 million cases occurred in 2017, most of them in the African region (92%), followed by the Southeast Asia (5%) and the Eastern Mediterranean regions (2%) (**Fig. 1**). Although more than half of the countries that had endemic malaria twenty years ago have reduced or eliminated malaria, today up to 90 countries still remain endemic for malaria^{1,2}. Within this context, the new goal for 2030 is to reach malaria elimination in at least 35 more countries, with the ultimate vision of achieving a malaria-free world².

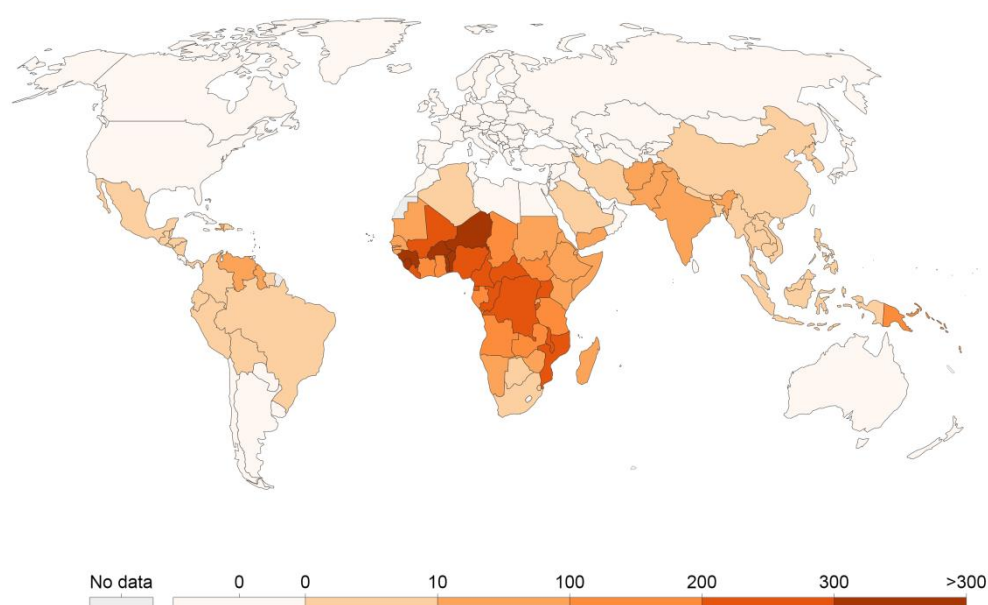


Figure 1. Malaria incidence in 2017. Number of new malaria infections per 1,000 people in each country in 2017. Reproduced from *Our World in Data*³.

Malaria disease is caused by protozoan ***Plasmodium sp. parasites***, eukaryotic organisms that belong to the phylum Apicomplexa. More than 100 species of *Plasmodium* have been identified, infecting many animal species such as reptiles, birds and mammals. However, only four of them (*P. falciparum*, *P. vivax*, *P. ovale* and *P. malariae*) produce infection exclusively in humans. Of those, *P. falciparum* and *P. vivax* are the most common species and responsible for the majority of cases worldwide. *P. falciparum* is found in tropical areas, mainly in Africa, and is responsible for most malaria-related deaths, killing around 1,200 African children each day⁴. In contrast, *P.*

vivax is the most widespread species, found in both tropical and temperate areas mainly from Southeast Asia, Central and South America. Both *P. ovale* and *P. malariae* cause mildest infections and are especially present in West Africa. Other species infecting non-human primates, such as *P. knowlesi* that naturally infects macaques, can also cause zoonotic malaria in humans.

The main mode of transmission in humans is through the bite of an infected female **Anopheles mosquito**, although other sources of transmission are known (i.e. transfusion of infected blood or transplacental infection). There are about 40 malaria-competent *Anopheles* species, which are broadly distributed worldwide and show differences in the efficacy of transmission based on their location, feeding habitats and behaviour. *A. gambiae*, for instance, is a major and highly efficient vector in tropical Africa⁵. Climate, economic and social conditions also indirectly affect the ability of the mosquito to sustain malaria transmission.

1.2 Life cycle

The *Plasmodium* life cycle is divided between two different hosts: a vertebrate host (humans and other animals) and an invertebrate host (mosquitoes) (**Fig. 2**). Female *Anopheles* mosquitoes transmit malaria during a blood feed by inoculating ~20 **sporozoites**, the infective form of the parasite. In less than 45 minutes, sporozoites reach hepatocytes, where they multiply by several rounds of asexual fissions producing from 10,000 to more than 30,000 daughter merozoites per sporozoite (pre-erythrocytic phase). During this period, which can last about 6-7 days for *P. falciparum* infections in naïve individuals, the peripheral blood is still not infected and the patient remains asymptomatic⁶. Some species (e.g. *P. vivax* and *P. ovale*) can persist in the liver as dormant stages (hypnozoites) and cause relapses weeks or years later.

After exponential multiplication, infected hepatocytes burst, releasing all the merozoites into the blood stream. They invade red blood cells (RBCs) to start the intraerythrocytic developmental cycle (IDC), which takes 48 h for *P. falciparum*, *P. vivax* and *P. ovale*, 72 h for *P. malariae* and 24 h for *P. knowlesi*, a period during which parasites develop into different asexual stages⁷. Merozoites of some species can infect both reticulocytes and mature erythrocytes (i.e. *P. falciparum*), whereas other species have marked preference to invade only reticulocytes (i.e. *P. vivax*). Upon invasion, merozoite is surrounded by a parasitophorous vacuolar membrane originated from the erythrocyte plasma membrane and altered by parasite-derived proteins. Merozoites first progress to the **ring stage** (~0-24 h post-invasion, hpi), in which the thin cytoplasm and the

small chromatin dots give them the characteristic “ring” appearance. Early after invasion, ring-stage parasites start endocytosing the host cytoplasm, creating small food vacuoles within the parasite cytoplasm that become a single large vacuole at later stages. Afterwards, the parasite enters a maturation phase of high metabolic activity known as **trophozoite stage** (~24-38 hpi), characterized by the accumulation of hemozoin as a product of hemoglobin degradation and major changes in the host RBC. Such modifications are mainly driven by the export of hundreds of parasite-encoded proteins into the RBC cytoplasm and surface, affecting RBC deformability, adhesion and permeability. Lastly, during the **schizont stage** (~38-48 hpi) parasites undergo repetitive nuclear division forming ~30 daughter **merozoites**. The cycle culminates with RBC rupture, releasing new merozoites into the bloodstream to reinvade new RBCs. This IDC, continuously repeated in the human blood stream, is responsible for the clinical manifestations of the disease.

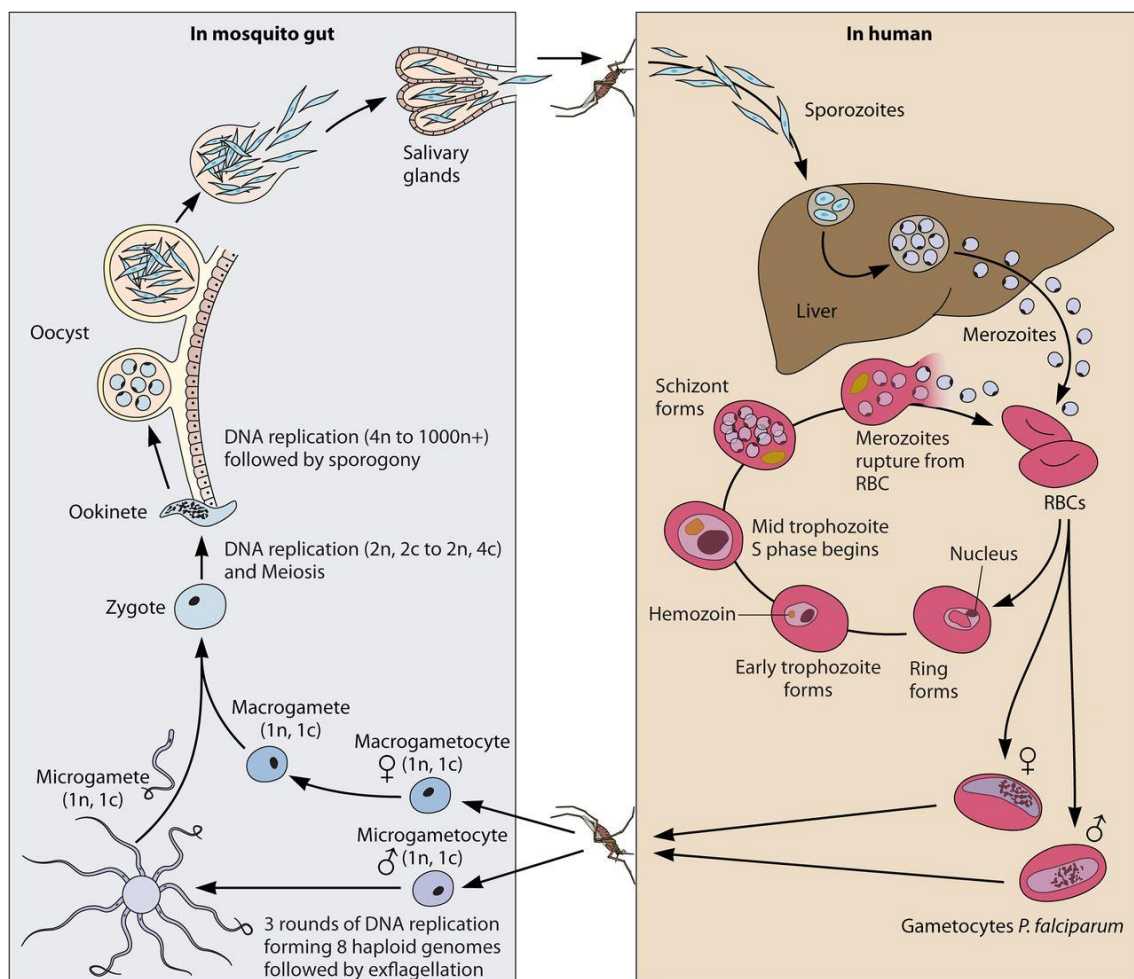


Figure 2. *Plasmodium falciparum* life cycle. Malaria parasites' complete life cycle, which includes the mosquito (left) and human (right) hosts. Reproduced from Andrew H. Lee et al.⁸

During each cycle, a small fraction of the parasites abandons the cyclical growth and develops into non-replicating female and male sexual stages called **gametocytes**, which are sequestered in the bone marrow and other tissues until they complete their maturation process⁹. Once mature, gametocytes can access again the peripheral bloodstream and remain in circulation until they are ingested by a new mosquito during a blood meal¹⁰.

The uptake of gametocytes by a mosquito induces their activation to gametes in the mosquito midgut and triggers the typical male gamete exflagellation. Afterwards, flagellated male gametes fertilize the female counterpart, allowing sexual recombination that generates genetic diversity among malaria parasite populations. The resultant **zygote** develops into a motile and elongated **ookinete** that invades the mosquito midgut wall and transforms into an **oocyst**, which generates thousands of sporozoites. After oocyst rupture, sporozoites are released into the mosquito body cavity and invade the salivary glands (~10-18 days after gametocyte ingestion), where they stay until inoculation into a new host during the next mosquito blood meal¹¹.

1.3 Clinical manifestations

The onset of malaria symptoms is related with the intraerythrocytic stages and occurs about 9-30 days after *P. falciparum* infection. The clinical manifestations of malaria are dependent on the previous immune status of the host and vary according to the level of acquired immunity developed after repetitive exposure¹². Apart from malaria specific host immunity, factors such as *Plasmodium* species, host ethnicity, parasite load or previous exposure to anti-malarial drugs have key relevance in determining the severity of the disease. Thus, completely different symptomatology is described in different malaria-infected patients, which can be categorized as asymptomatic, uncomplicated, severe and placental malaria¹³.

Asymptomatic malaria is characterized by the absence of symptoms even though there are circulating parasites in the blood stream. It is common in >5-year-old children and adults from regions with high malaria transmission. In consequence of the frequent exposure to *Plasmodium* parasites, these individuals have developed tolerance to the infection and do not experience malaria symptomatology. Thus, they constitute an important reservoir for *Plasmodium* parasites, leading to continued transmission of the disease^{14,15}.

In **uncomplicated malaria**, the onset of the disease is mostly accompanied by early nonspecific symptoms shared with other diseases, including headache, arthralgia,

nausea, diarrhoea, anorexia, dyspepsia, epigastric discomfort and muscle pain^{13,16}. The hallmark of symptomatic malaria is periodic fever, which typically occurs every 48 h (but it can also occur daily or every 36 h). Symptoms are mainly due to the direct effects of RBC infection and destruction by parasites, and the host's reaction to this process. Even though the infected individual may not appear very ill, serious complications may develop at any stage if the appropriate treatment is not started.

In some cases, uncomplicated malaria may progress to **severe malaria**, characterized by general and organic complications involving the central nervous, pulmonary, renal or hematopoietic systems, which are the principal cause of malaria-related deaths^{13,17}. It is defined by at least one of the following clinical manifestations: impaired consciousness or coma (cerebral malaria), prostration and generalized weakness, convulsions, pulmonary oedema, respiratory failure causing acidosis, abnormal spontaneous bleeding, jaundice, hepatic dysfunction, circulatory collapse, severe anemia, hypoglycemia, hemoglobinuria and acute kidney failure, as well as opportunistic bacterial infections^{13,17}. These complications are related with increased binding of infected RBCs to endothelial cells, as well as to either other infected (agglutination) or non-infected (rosetting) RBCs, altogether causing microvascular obstruction and local inflammation in vital organs^{18–20}. It commonly occurs in naïve individuals that have no or low previous malaria immunity and therefore are more susceptible to develop symptomatology, such as children below 5 years of age, travellers or immunocompromised patients, as well as individuals from low transmission areas. While uncomplicated malaria can be caused by all *Plasmodium* species, severe malaria is usually caused by infection with *P. falciparum*, although less frequently it can also be caused by *P. vivax* or *P. knowlesi*.

Placental malaria is one type of severe malaria, characterized by sequestration of *P. falciparum*-infected erythrocytes within the intervillous spaces of the placenta, which leads to poor outcomes for both the fetus and the mother^{21,22}. In such situation, high parasitemia in the placenta results in alteration of the exchange system between mother and fetus, causing abortions, neonatal death, still births, preterm births, intrauterine growth retardation and low birth weight. Congenital malaria can also occur, transmitting the infection from the mother to her fetus prenatally or perinatally. At the same time, pregnant women can suffer the typical severe malaria complications, such as severe anemia, generalized edema, pulmonary edema, hypoglycemia and cerebral malaria. Many women presenting these symptoms die during or shortly after labour, highlighting the risk of fatality in placental malaria. In high transmission areas, although women may already have acquired immunity against malaria disease, once they are

pregnant, they are exposed to different antigenic forms of the parasite and thus they have again high risk of severe malaria, like non-immune individuals²³. Women who are pregnant for the first time (primigravidae) are especially susceptible to adverse effects, a risk that diminishes over successive pregnancies due to the development of specific immunity against pregnancy-associated malaria.

1.4 Malaria control

The control of malaria disease, with the ultimate goal of eradication, represents one of the major global public health challenges of the 21st century. Although the global strategies for fighting malaria have changed during the last years, they are based on three main lines of work: diagnosis, treatment and prevention.

1.4.1 Diagnosis

Early and accurate diagnosis of malaria is essential for both effective disease management and malaria surveillance. However, malaria disease shares many common symptoms with other diseases, such as influenza or dengue, leading to frequent wrong diagnoses. Thus, although one of the main criteria for malaria diagnosis is the presence of periodic fever, other microscopic and molecular techniques based on detection of parasites in the blood need to be used to discriminate malaria from other infections.

Light **microscopy examination** of thick or thin blood smears stained with Giemsa is the main method used for malaria diagnosis, due to its low cost and availability in poor countries. However, the quality of microscopy-based diagnosis is frequently inadequate and has many limitations, such as the need of highly trained staff and the low sensitivity²⁴. Another widely used diagnostic technique are malaria rapid diagnostic tests (**RDTs**), which can be used in remote areas with limited access to microscopy services^{24,25}. They are based on the immunological detection of parasite antigens that are present in the blood of infected individuals (e.g. PfHRP2 and PfLDH), being able to detect single or multiple *Plasmodium* species and even distinguish between them. They are simple to use, require little training and allow rapid and easy diagnosis. However, they also have disadvantages, such as the limited sensitivity or the obtenance of either false-negative or false-positive results due to PfHRP2 deficiency or interaction with other infections, respectively.

While microscopy and RDTs are the primary choices for diagnosing malaria in the field, neither of them is able to detect low parasitemia infections or dormant liver stages,

leading to false-negative results that compromise malaria surveillance. Thus, other highly sensitive molecular techniques may be used. The most sensitive tests are based on the detection of parasite genetic material by nucleic acid amplification, such as polymerase chain reaction (**PCR**) or loop-mediated isothermal amplification (**LAMP**)^{24,26}. These techniques detect low-density parasitemia, multiple pathogens simultaneously and different strains, enabling an accurate diagnosis of the infectious agents. Nevertheless, they have limitations in low-resource settings, including the need for equipment and supplies, experienced personnel, high cost or long processing time.

1.4.2 Treatment

Malaria treatment can achieve a rapid and full elimination of parasites from the patient's blood, preventing progression to severe disease or chronic infections and at the same time reducing transmission to other individuals. It currently relies on the use of antifolates, quinolines and artemisinins, the two latter derived from plants whose medicinal values had been noted for centuries. They all differ in the mechanism of action and act at different stages of the parasite life cycle, most of them being effective against the asexual intraerythrocytic stages^{27,28}. The **antifolate** drugs include sulfadoxine, pyrimethamine, atovaquone, proguanil and dapson, all of which interfere with the synthesis of precursors needed for DNA replication^{29,30}. **Quinolines** (e.g. chloroquine, amodiaquine, quinidine, mefloquine, piperazine, lumefantrine, primaquine and halofantrine, among others) are derived from quinine, the first antimalarial drug used in Europe in the early 17th century. Their mechanism of action relies on the interference with the process of hemozoin formation, resulting in the accumulation of toxic free heme in the intraerythrocytic stages, except for primaquine, which also kills hepatic and gametocyte stages³¹. **Artemisinin** is derived from the plant *Artemisa annua*, which was used as an antimalarial medicine in China for more than 2,000 years. Its derivatives include dihydroartemisinin (DHA), artesunate, arthemeter, artemisone or artemiside. These drugs appear to act by alkylation of biomolecules such as heme, proteins and lipids, leading to the generation of free reactive oxidative radicals that are toxic for the parasite³². They rapidly induce killing of blood stages of all *Plasmodium* species and are also partially active against gametocytes. The use of artemisinins has been key in the fight against malaria, being present in the majority of current treatments. However, given the short half-life of artemisinins, they are mainly used in combination therapy with other long-acting antimalarials.

As resistance to many individual antimalarial drugs has been reported in the last decades, the use of combinations of drugs with different mechanisms of action is often

preferred to reduce the risk of resistance development and treatment failure^{28,33}. **Artemisinin-based combination therapies** (ACTs), which combine the highly effective short-lived artemisinins with a longer-acting partner, are the most effective antimalarial medicines available today and the recommended treatment for both uncomplicated and severe *P. falciparum* malaria.

Distinct treatments are used depending on the severity of the disease, the parasite species and the region³⁴. In *P. falciparum* infections, the treatment of choice for uncomplicated malaria is a three-day ACTs oral dose, which has high efficacy and few adverse effects. A single dose of primaquine can also be administered as antigametocyte drug. Instead, severe malaria requires hospitalization and long periods (>24 h) of parenteral administration of artemisinin derivatives (e.g. artesunate or artemether) or quinine, that rapidly clear the parasites from blood. Pregnant women must be treated with antimalarials that are known to be safe for the fetal development, such as quinine, chloroquine, clindamycin or proguanil in the first trimester, or ACTs in the second and third trimesters of pregnancy.

1.4.3 Prevention

Prevention of *Plasmodium spp.* infection can be accomplished by different strategies. On the one hand, **prophylaxis** is used in chemoprevention campaigns of specific vulnerable groups^{35,36}. This is the case of the intermittent preventive treatment of pregnant women (IPTp) and infants (IPTi), in which doses of sulphadoxine-pyrimethamine are administered in the antenatal and childhood programmed visits. Also, seasonal malaria chemoprevention (SMC) campaigns are performed during acute seasonal transmission periods, where sulphadoxine-pyrimethamine plus amodiaquine is monthly given to children. Prophylactic treatments may also be provided to individuals entering an area of high endemicity, such as tourists and non-immune migrants. This protection is achieved by daily atovaquone-proguanil or weekly mefloquine treatments administered prior, during and upon return from their travel to the endemic region.

On the other hand, many efforts have been put in the development and clinical trials of a malaria **vaccine**, which would have a great impact on malaria elimination efforts. The most advanced candidate vaccine to date is RTS,S/AS01, which contains a recombinant protein with parts of the *P. falciparum* circumsporozoite protein (CSP) combined with the hepatitis B virus surface antigen^{37,38}. The phase III trial of RTS,S/AS01 showed that a 3-dose vaccination reduced clinical malaria cases by 18% and 28% in young infants and children, respectively, and by 26% and 36% after the

addition of a booster dose³⁹. However, this efficacy waned over time, meaning that this vaccine is not ideal for long-term protection.

Vector control is another key aspect of malaria prevention. Several vector characteristics (e.g. population size, longevity or human biting habits) are strongly influenced by climate, local ecology or human behaviour, and consequently can be altered by distinct strategies with the aim of reducing mosquito availability and malaria transmission^{35,40}. The main strategies of malaria elimination campaigns include insecticide-treated mosquito nets (ITNs) and indoor residual spraying (IRS), both of which reduce vector-human contact⁴¹. Use of insecticides such as dichlorodiphenyltrichloroethane (DDT) at large-scale has helped to reduce malaria transmission by controlling its vector, but mosquitoes have started to develop resistance to them. Moreover, some specific insecticides, such as DDT, have also been restricted due to the risk they involve for the health and environment⁴². Management of mosquito breeding sites with activities such as drainage of stagnant water, introduction of larvae predators or application of larvicides can also reduce the number of mosquito populations³⁵. A new method of vector control is the attractive toxic sugar bait (ATSB), which kills mosquitoes by attracting them to a solution that contains both a feeding stimulant and an oral toxin⁴³.

2 TRANSCRIPTIONAL REGULATION IN *P. FALCIPARUM*

2.1 Genome characteristics

P. falciparum contains a 23 Mb nuclear genome organized in 14 chromosomes that encodes ~5,500 genes⁴⁴. In addition to the nuclear genome, mitochondrion and apicoplast organelles also have their own extrachromosomal genomes, which are much smaller (6 kb and 35 kb, respectively) and maternally inherited⁴⁵.

The highly compacted and AT rich (~80% overall and greater than 90% in noncoding regions) genome of *P. falciparum* has abundant repetitive regions, especially rich in short tandem repeats and other low complexity sequences^{44,46}. These characteristics increase the chances of strand mispairing during DNA replication, consequently causing spontaneous genetic diversity. Insertions and deletions (indels) of short tandem repeats (e.g. microsatellites) are the most common polymorphism in *P. falciparum* parasites, especially abundant in noncoding regions⁴⁷. Similarly, major genomic changes, such as gene copy number polymorphisms (CNPs) and translocations, are common sources of variation that affect larger genomic DNA segments, mainly in subtelomeric regions^{48,49}. Single nucleotide polymorphisms (SNPs) are also abundant in the *P. falciparum* genome, with a non-homogeneous distribution among chromosomal regions and genes^{50,51}.

Genetic variants may confer a functional advantage that can be selected and transmitted to the next generations. Thus, this heritable, non-reversible and slow adaptive mechanism is one of the fundamental ways of adaptation to the environment found in malaria parasites⁵². One of the most studied examples is the development of drug resistance, which has been associated with specific SNPs in genes encoding transporters and enzymes such as *pfcr*, *pfmdr1*, *pfdhfr*, *pf dhps* and *pfk13*. For instance, point mutations in *pfcr* and *pfmdr1* permit the efflux of cloroquine and quinine from the site of drug action^{53–55}, whereas mutations in *pf dhfr* and *pf dhps* are associated with decreased affinity of antifolate drugs^{56,57}.

2.2 General aspects of transcription

During the 48 h IDC, *P. falciparum* expresses over 80% of its genes in a coordinated and time-specific manner, showing a transcriptional cascade that progress throughout the lifecycle. Most genes involved in specific processes are expressed just once per

cycle when their products are needed, fitting with the so-called “**just-in-time**” **transcriptional profile**^{58–60}. Several mechanisms take part simultaneously in this process to tightly control gene expression throughout the whole development.

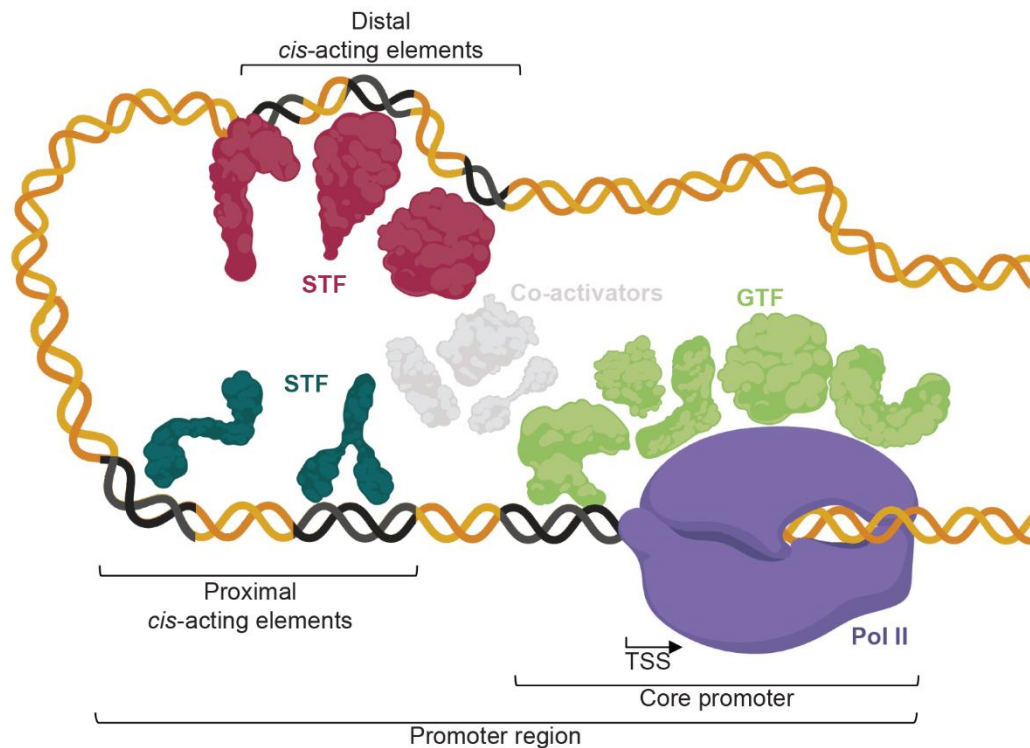


Figure 3. Promoter organization. Transcription initiates at gene core promoters, where general transcription factors (GTFs) recruit the RNA polymerase II (Pol II) to the transcription start site (TSS) to form the pre-initiation complex and lead transcription initiation. The pre-initiation complex activity can be regulated by specific transcription factors (STFs), which bind to specific distal and proximal DNA sequences (*cis*-acting elements). Other co-activator factors may take part in the pre-initiation complex regulation. Distal *cis*-acting elements are known as enhancers or silencers, depending on their activator or repressor function, respectively. Adapted from Levine & Tjian⁶¹ and Tuteja et al.⁶². Created with BioRender.com.

In model eukaryotes, genes have an upstream proximal promoter region called **core promoter**, essential for the assembly of the transcriptional pre-initiation complex (PIC) and for the regulation of transcriptional activity⁶³ (Fig. 3). It includes the **RNA polymerase II** (Pol II), constituted by twelve subunits, and **general transcription factors** (GTFs). As Pol II is unable to locate and bind to promoters by itself, GTFs can recognize DNA sequences located next to the PIC (***cis*-acting elements**), such as the TATA box or the initiator (Inr) element, and attract Pol II to the transcription start site (TSS) to establish the transcription direction and starting point. *P. falciparum* gene promoters have a similar structure to eukaryotes⁶⁴. The twelve Pol II subunits and many eukaryotic GTFs are conserved in malaria parasites, including the TATA-binding protein (TBP) and other TFIIIs^{65–67}. Some *cis*-acting elements, such as the TATA box-like and the Inr-like sequences, have also been functionally characterized in *P. falciparum*^{68,69}, although their relevance remains unclear.

2.3 Transcription factor regulation

While the core promoter is responsible for the basal level of transcriptional activity, **specific transcription factors** (STFs) can either activate or repress the transcriptional activity in that locus by regulating the PIC assembly and function⁷⁰. STFs recognize proximal and distal *cis*-acting elements that confer specificity and also bind to co-activator factors to regulate PIC activity (**Fig. 3**). Distal *cis-acting* elements are known as enhancers or silencers, depending on their activator or repressor function, respectively. It has been shown that *P. falciparum* has a relative paucity of STFs and their specific *cis*-regulatory elements, which have low similarity to known regulatory elements or factors in other eukaryotes.

2.3.1 Specific transcription factors

To date, only a few STFs have been identified in *P. falciparum* (ApiAP2, zinc finger proteins and helix-turn-helix families), whereas many of the STF families found in other eukaryotes are absent^{66,67,71,72}. Different hypothesis may explain this paucity of STFs in *Plasmodium* species. On the one hand, due to their distant evolutionary relationship with other eukaryotes, it is possible that malaria parasites contain a completely different set of STFs, which are difficult to identify using the currently available homology-based tools^{66,73}. Moreover, the extremely AT-rich genome and the abundance of repeats insertions may also pose a challenge for the bioinformatics prediction of transcription factors. The identification of the *P. falciparum* apicomplexan AP2 (ApiAP2) family of transcription factors (typically found in plants, but not in mammals or yeast) was crucial to understand the transcriptional regulation mechanism in malaria parasites, highlighting the differences with other model eukaryotes^{71,72}.

Also, several potential *cis*-acting sequences are clustered together in the promoter regions of *P. falciparum* genes, suggesting a combinatorial mode of gene regulation in which multiple factors contribute to the overall promoter activity of a specific gene⁷⁴. The ability of some STFs to form dimers also supports a multifactorial regulation mechanism in *Plasmodium* species. This would provide the diversity required to specifically control a large number of genes using a small set of factors, explaining the apparent lack of transcription factors in *P. falciparum*.

ApiAP2 proteins

ApiAP2 is the largest and most studied transcription factors family in *P. falciparum*. This family includes apetala2 (AP2) domain-containing proteins, homologous to the apetala2/ethylene response factor (AP2/ERF) family of DNA-binding proteins from plants⁷⁵. AP2/ERF proteins are characterized by the presence of AP2 DNA-binding domains, a 60-amino acids (aa) sequence that binds to DNA by a triple stranded β -sheet stabilized by a C-terminal α -helix structure⁷⁶. They can either activate or repress gene expression and are involved in different functions depending on the number of AP2 domains present in the protein. While AP2/ERF proteins with only one AP2 domain generally regulate genes involved in pathogenesis and environmental stress responses, AP2/ERF transcription factors with two AP2 domains are generally related with development⁷⁶.

Several AP2-domain containing proteins are conserved among apicomplexan parasites such as *Theileria*, *Cryptosporidium*, *Plasmodium* or *Toxoplasma* species^{67,72}. Similar to plants, ApiAP2 proteins contain up to four AP2 domains, which are also ~60 aa in length and conserve the triple β -sheet structure that directly makes contact with DNA⁷⁷. In *P. falciparum*, 27 putative ApiAP2 members and their cognate DNA-binding motifs (discussed below) have been identified and most of them appear to be conserved in other *Plasmodium* species⁷⁸ (**Fig. 4**). ApiAP2s greatly vary in size, ranging from 200 to more than 4,000 aa, and may also contain additional domains such as the AT-hook, the zinc finger, the Acyl-CoA-N-acetyltransferase, the pentapeptide-repeat-like (PR) or the AP2-coincident domain mostly at the C-terminus (ACDC) domains⁷⁹ (**Fig. 4**). The presence of an AT-hook close to the AP2 domain has been proposed to increase affinity through nonspecific interactions with DNA⁸⁰, whereas the function of the rest of domains is still unclear.

Apart from binding DNA, ApiAP2s can also interact with other transcription-related proteins, such as chromatin remodelling factors (e.g. GCN5, HMGB-type and bromodomain proteins)^{79,81,82}. Binding to both DNA and proteins may serve to recruit the chromatin-related factors to specific locations and facilitate interactions with the transcription machinery. However, it is still unclear whether these protein interactions are driven by AP2 domains as in plants⁸³ or by other regions within the protein. It has also been suggested that ApiAP2s can undergo dimerization, forming either homo or heterodimers, as shown in the crystal structure of PfAP2-SP/Exp⁷⁷.

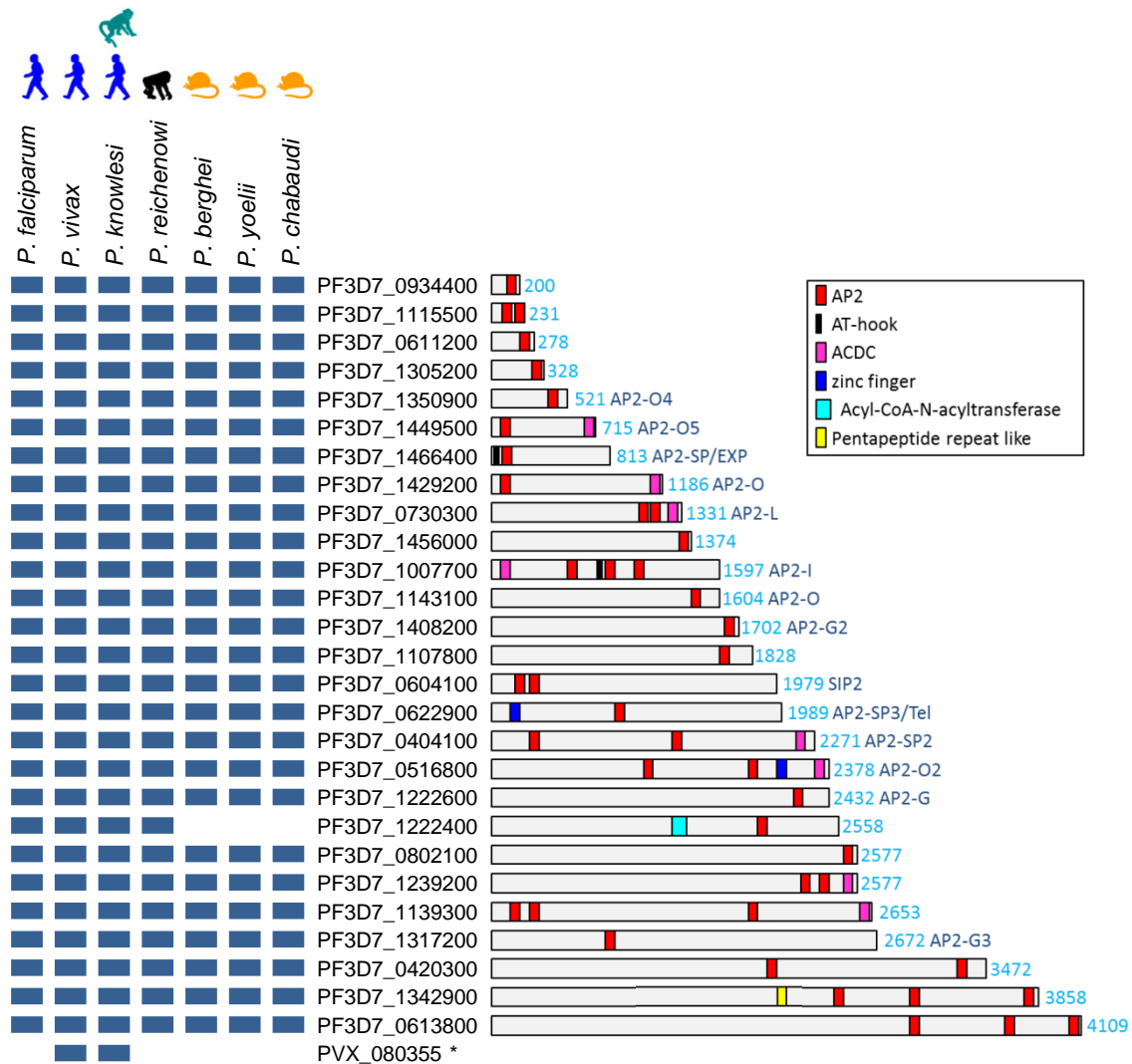


Figure 4. Apicomplexan AP2 family. Conservation of ApiAP2 members in some *Plasmodium* species infecting humans (blue icon), monkeys (green icon), chimpanzees (black icon) or rodents (yellow icon). Gene ID refers to *P. falciparum* ID, except for the member marked with a star (*) that refers to *P. vivax* gene ID. On the right, schematic of the proteins and their domains. The total length and the common protein name are provided at the end in light or dark blue, respectively. ACDC, AP2-coincident domain mainly at the C-terminus. Adapted from Jeninga et al.⁷⁹ and Painter et al.⁷⁸.

Similar to the IDC transcriptional cascade, ApiAP2 expression also occurs in a sequential manner. In *P. falciparum*, a cascade of ApiAP2s expression and co-expression of 4-6 ApiAP2 are observed in specific stages, which indicate that they likely play a coordinated role in regulating life cycle progression^{72,84}. Furthermore, it has been suggested that this ApiAP2 expression is self-regulated, as binding motifs for many ApiAP2 factors are present upstream of other ApiAP2 genes. Recent systematic knockout screens targeting the ApiAP2 family in rodent malaria parasites has led to the identification of new roles for many of the ApiAP2 members^{85,86}. From the total 27 ApiAP2 members, more than half were refractory to knockout, suggesting that they are essential for asexual blood stage development *in vivo*⁸⁵ (Fig. 5). Among them, AP2-I is one of the most characterized, described to drive the expression of genes necessary

for merozoite invasion⁸⁷. The remaining ApiAP2s have putative roles in gametocyte, ookinete, sporozoite and liver stages, as well as driving heterochromatin formation and telomere maintenance across the life cycle. One of the most studied members is AP2-G, which is key for sexual conversion and drives gametocyte development together with AP2-G2 and AP2-G3^{88–90}. Ookinete formation and development in the mosquito midgut is probably mediated by four transcription factors: AP2-O, AP2-O2, AP2-O3, AP2-O4 and AP2-O5^{85,86,90–92}. Three ApiAP2 members are related with sporozoite development: AP2-SP/Exp, AP2-SP2 and AP2-SP3/Tel^{85,86,93}. Finally, one ApiAP2 plays an essential role in liver stages, AP2-L^{85,86,94}.

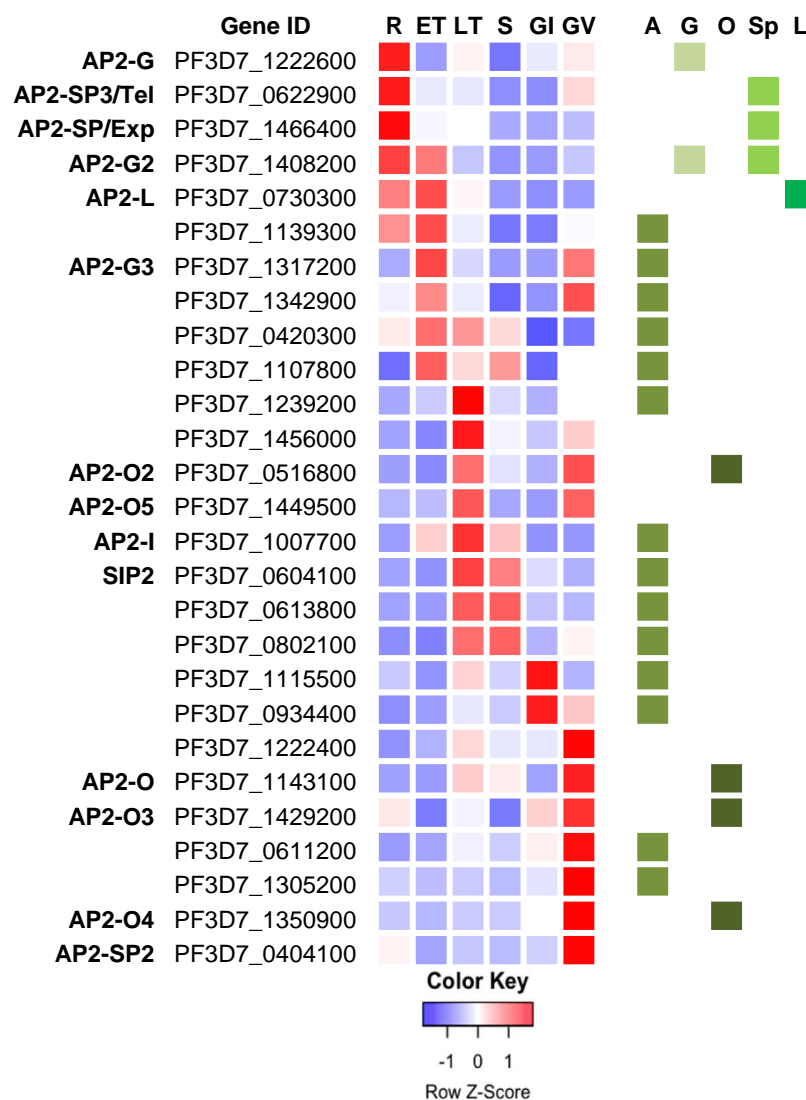


Figure 5. ApiAP2 expression and role in the parasite life cycle. *P. falciparum* ApiAP2 transcript levels throughout the intraerythrocytic cycle at the ring (R), early trophozoite (ET), late trophozoite (LT) and schizont (S) asexual stages, as well as gametocyte stage II (GII) and V (GV). The right green columns indicate an essential role in the asexual cycle (A), gametocyte (G), ookinete (O), sporozoite (Sp) or liver (L) stages. Adapted from Modrzynska et al.⁸⁵.

While most ApiAP2 members play important roles during development, other members have shown different functions beyond life cycle progression. This is the case of SIP2, which plays a role in heterochromatin formation and genome integrity⁹⁵. Also, in addition to sporozoite formation, AP2-SP/Exp is involved in the regulation of clonally variant genes⁹⁶ and AP2-SP3/Tel may also be related with chromatin maintenance and telomere biology⁹⁷. However, new studies using conditional approaches are needed to elucidate the specific role of the remaining ApiAP2 members in parasite progression through the life cycle, specially those that are essential for IDC progression and hence cannot be knocked out.

[Zinc finger proteins](#)

The **zinc finger proteins** group includes a diverse set of proteins, such as C2H2, C3H4 and CCCH types, all of them presenting zinc finger domains that coordinate DNA-binding. Particularly, the CCCH-type is highly over-represented in *Plasmodium falciparum*, but their role in transcriptional regulation is still unclear⁶⁷.

[Helix turn helix proteins](#)

The helix-turn helix group comprises **Myb** domain-containing proteins. One of the main studied members is PfMyb, which is expressed throughout the erythrocytic developmental stages and its inhibition causes reduced growth, suggesting that PfMyb1 is essential for normal parasite growth^{98,99}.

[Other STFs](#)

Apart from the families mentioned above, other individual transcription factors and their associated DNA motifs have been described, such as the cold-shock protein⁶⁶, the *Pfx* regulatory element binding protein (PREBP)¹⁰⁰ or the PfNF-YB¹⁰¹, but their functional relevance remains to be determined.

2.3.2 Specific *cis*-acting elements

As other eukaryotes, the malaria parasite genome contains specific *cis*-regulatory sequences located between 100 to >1000 base pairs (bp) upstream of the TSS, which are needed to recruit STFs to the promoter and regulate the level and time of expression of a specific gene⁶⁴. However, due to the high AT content in intergenic regions, only a few specific *cis*-acting elements have been identified in *Plasmodium* species.

		D1	D2	D3
	PF3D7_0934400			
	PF3D7_1115500			
	PF3D7_0611200			
	PF3D7_1305200	T C A C A C A C		
AP2-O4	PF3D7_1350900	A T C T A G A A		
AP2-O5	PF3D7_1449500			
AP2-SP/Exp	PF3D7_1466400	T G C A T G C A		
AP2-O	PF3D7_1429200			
AP2-L	PF3D7_0730300	A A T T T C C	A A T T T C C	
	PF3D7_1456000	C A C A C A C A C		
AP2-I	PF3D7_1007700	G G T C G A C C C	T T T T G C C	G T G C A C T A
AP2-O	PF3D7_1143100	A G C T A G C T		
AP2-G2	PF3D7_1408200	T C C A C C A		
	PF3D7_1107800	A G C A T A C		
SIP2	PF3D7_0604100	G G T G C A C C	G G T G C A C C	
AP2-SP3/Tel	PF3D7_0622900			
AP2-SP2	PF3D7_0404100			
AP2-O2	PF3D7_0516800		T G A C A T C A	
AP2-G	PF3D7_1222600	G G T A C C		
	PF3D7_1222400	T A T A T A T A		
	PF3D7_0802100	C A C A C A C A		
	PF3D7_1239200	T C T A C A A A	T C T A C A A A	
	PF3D7_1139300	T A G A A C A A		
AP2-G3	PF3D7_1317200	T A G C T C A A		
	PF3D7_0420300	C A C A C A C	G T G T T A C A C	
	PF3D7_1342900	C C G G G G C		
	PF3D7_0613800	T A A G C C C A	C T C T A G A G	

Figure 6. ApiAP2 cis-acting elements. Diagram showing the number of AP2 domains (D1, D2, D3; blue boxes) found in the *P. falciparum* ApiAP2 members and the predicted DNA motif recognized by each one⁸⁴. Empty boxes stand for AP2 domains without predicted cis-acting motif. Genes are ordered by size, as in fig. 4.

Most of them were predicted bioinformatically by searching over-represented regulatory elements upstream genes of the same family¹⁰² or sharing similar expression profiles^{74,103–107}, as well as using comparative genomics^{108,109}. Although these approaches led to the discovery of many putative motifs, they poorly overlap. Other approaches aimed to identify regulatory elements by exploring the accessible chromatin environment during the IDC, such as using the transposase accessible

chromatin sequencing (ATAC-seq) technique^{110–113}. Recent ATAC-seq studies, for instance, have identified similar motifs to the previously predicted and in some cases they showed nearly complete overlap with chromatin immunoprecipitation sequencing (ChIP-seq) data, highlighting the accuracy of the approach¹¹¹. Nevertheless, the cognate STF of many of these identified motifs and their function remain unknown.

Protein binding microarrays (PBM), which defines the *in vitro* sequence preference of recombinant domains, also revealed several potential *cis*-acting elements associated with different members of the apicomplexan AP2 family (A_{pi}AP2) of STFs^{80,84,102} (**Fig. 6**). A relevant example for the thesis is the PF3D7_1342900 A_{pi}AP2, which was shown to recognize the (A/G)NGGGG(C/A) sequence, known as **G-box**. These studies also showed that different AP2 domains within the same protein have distinct DNA binding specificity and that an individual domains can bind to multiple motifs, which significantly increases the number of potential target genes that can be regulated by one factor⁸⁴. Although the identification of these *cis*-regulatory elements was highly powerful to predict potential A_{pi}AP2 target genes and function, the direct binding to the STFs has only been corroborated by ChIP-seq experiments for a few *P. falciparum* A_{pi}AP2s, including PfAP2-I, PfAP2-G, PfAP2-O and PfAP2-TeI^{82,87,92,97}

2.3.3 Transcription factor regulation in the context of adaptation

In addition to controlling development, eukaryotic STFs have also been related with directed transcriptional responses to changes in the environment. This strategy involves a sensing mechanism that enables the detection of external changes and induces a signal transduction cascade that leads to a transient and non-heritable transcriptional change driven by one or more STFs, with the final aim of ensuring survival to the new condition. During the whole life cycle, *P. falciparum* parasites are exposed to several fluctuations in the environment. In blood stages, for instance, parasites must face variable conditions, including host metabolic state, immunity, drugs and fever fluctuations. However, the capacity of *P. falciparum* to drive directed responses to external cues similar to other eukaryotes is questioned and has been a controversial issue for many years¹¹⁴.

Some studies proposed that malaria parasites possess a **hard-wired transcriptional program**, unable to mount a protective response to external perturbations. For instance, no specific effect on the parasite transcriptome was observed after exposure to several drugs. Although in some cases a transcriptional change was reported upon treatment, it generally was of low magnitude, non-reproducible and mainly a consequence of the cell damage induced by the compound rather than a directed

protective response^{115–119}. In other cases, the reported transcriptional alterations were directly linked with the impairment of the functions targeted and thus did not reflect a protective response^{120–122}.

In contrast, other studies suggested that malaria parasites can **sense and induce specific transcriptional responses** to physiological external cues, such as changes in oxygen pressure, nutrient availability, presence of drugs or temperature. Regarding the nutrient availability, many studies have tested the effect of deprivation of amino acid, lipids, glucose and other micronutrients (e.g. iron, zinc or vitamins)¹²³. A transcriptional response has been reported under these conditions, such as the developmental stop and induction of a “hibernatory” state during amino acid starvation¹²⁴ or the up-regulation of *var* and sexual-specific genes upon glucose deprivation¹²⁵. Also, lethal doses of artesunate and DTT induced deregulation of several pathways that may be reflecting particular mechanisms of gene regulation, although it remains unclear which alterations are part of a specific protective response and which are only a direct consequence of the lethal injury^{126,127}. Exposure of blood stage parasites to hyperoxic conditions, such as those found in mosquito stages, alters the transcriptome affecting protein folding, translation, antioxidant metabolism and glycolysis¹²⁸. High parasitemia has also been related with global transcriptional changes involving cell remodelling, clonal antigenic variation, metabolism and apoptosis-like death¹²⁹. Another source of stress for malaria parasites is the high temperature reached during malarial fever episodes. It has been shown that parasites can activate a temperature-dependent response, involving expression of chaperones and many other stress response genes, as well as death-related mechanisms¹³⁰. Although all these examples suggest that malaria parasites may have the capacity to respond transcriptionally to diverse stimuli, the protective response is not well understood. Moreover, the observed responses involve only modest transcriptional changes, of much lower amplitude than in other eukaryotes such as yeast^{131,132}.

Interestingly, two recent findings clearly confirmed the capacity of *Plasmodium sp.* parasites to sense fluctuating conditions in their environment and respond at the transcriptional level. First, it was shown that asexual blood-stage *P. berghei* parasites have an intrinsic capacity to respond to a nutrient-poor environment by reducing their replicative capacity. The mediator of this response is a serine/threonine kinase termed KIN (PBANKA_131800), which drives a nutrient-sensing mechanism that is activated upon caloric restriction of the host. Thus, in a less-favourable metabolic landscape, KIN induces a signalling cascade that leads to transcriptional regulation of genes related with proliferation rate and virulence¹³³. Secondly, it was found that intraerythrocytic *P.*

falciparum parasites can sense the levels of the host lipid lysophosphatidylcholine (LysoPC) and activate a transcriptional response when there is limited availability of this lipid. Apart from affecting the phosphatidylcholine synthesis pathway and other metabolism-related genes, low amount of LysoPC also acts as an environmental sensor to induce expression of *pfap2-g* (possibly through GDV1 activation), which drives differentiation of asexual parasites towards the transmissible gametocyte stage^{134,135}. Altogether, both studies support the idea that malaria parasites can sense fluctuations in their environment and drive an adaptive transcriptional response. However, the complete mechanism involved in sensing, signal transduction and transcriptional regulation upon nutrient or LysoPC depletion is still poorly understood. Altogether, these examples show that malaria parasites can respond to several external cues, opposing the idea of a hard-wired transcriptome. Although it seems as the capacity to sense changes in the environment and induce a directed transcriptional response is conserved in *Plasmodium*, the STF's associated with these adaptive responses are not identified.

2.4 Epigenetic regulation

Epigenetic regulation of gene expression in malaria parasites mainly occurs at the chromatin level. The relevance of DNA methylation, which plays key roles in many eukaryotes as an epigenetic mechanism, remains unknown in malaria parasites¹³⁶.

As in other eukaryotes, *Plasmodium* species organize the genetic material in nucleosomes, in which 146 bp of DNA sequence are wrapped around a histone octamer. Malaria parasites contain four canonical core histones (H2A, H2B, H3 and H4) and four alternative histones (H2A.Z, H2Bv, H3.3 and CenH3) needed for core nucleosome assembly^{137,138}. Nucleosomes are regularly spaced along the genome forming the chromatin fibre. Chromatin not only efficiently packs DNA, but also plays an important role in the regulation of gene expression. Depending on the degree of nucleosome compaction, eukaryotic chromatin can be found in two main dynamic conformations: euchromatin or heterochromatin. **Euchromatin** refers to the relaxed, accessible and transcriptionally competent chromatin, whereas a highly compacted, inaccessible and transcriptionally silent chromatin is termed **heterochromatin**. Facultative heterochromatin refers to the heterochromatin regions that are able to convert between euchromatin and heterochromatin states¹³⁹. This chromatin landscape determines RNA polymerases and transcription factors accessibility to the promoter region. In *P. falciparum*, heterochromatin is highly enriched in low expression areas, such as telomeric and sub-telomeric regions, whereas lower levels are found in the

main body of the chromosomes¹⁴⁰. In contrast to other eukaryotes, heterochromatin is not present in *P. falciparum* centrosome regions^{141,142}.

2.4.1 Histone modification and other epigenetic mechanisms

Chromatin architecture and compaction is mainly determined by **post-translational modifications** (PTMs) occurring in some residues of the histone N-terminal tails^{137,140,143}. These modifications include mainly acetylation and methylation of lysine residues, but also other less common modifications such as sumoylation, phosphorylation and ubiquitination (**Fig. 7**).

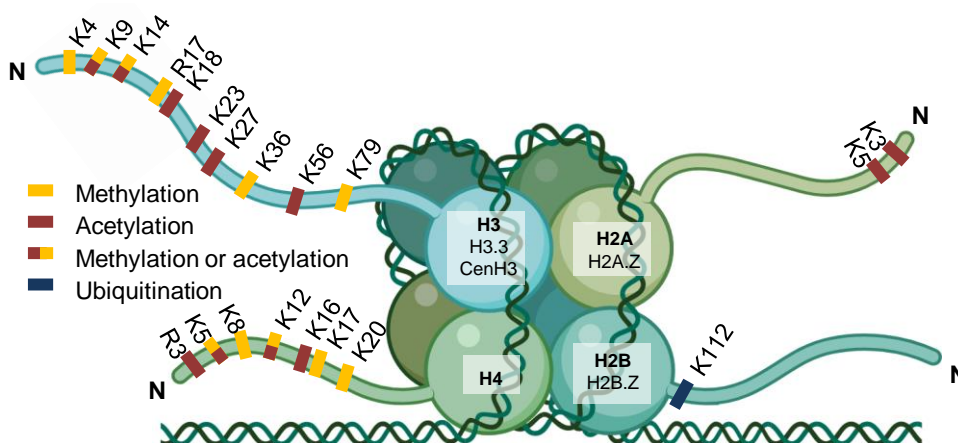


Figure 7. Histone PTMs described in *P. falciparum*. Specific histone PTMs (methylation, acetylation and ubiquitination) described in the main *P. falciparum* histones (H3, H2A, H4 and H2B). K, lysine; R, arginine. Adapted from Bechtsi & Waters¹⁴⁴. Created with BioRender.com.

Histone **acetylation** is generally associated with gene activation (e.g. H3K9ac), and it affects the histone interaction with DNA by neutralizing the charge on the histone tail, making the DNA more accessible for transcription¹³⁸ (**Fig. 8**). It also facilitates the binding of many chromatin remodelers and transcription factors, such as bromodomain proteins. Histone acetylation is mediated by histone acetyltransferases (HATs), whereas histone deacetylases (HDACs) remove the acetylation marks^{145,146}. Histone **methylation** can be associated with both gene activation (e.g. H3K4me3) and silencing (e.g. H3K9me3)^{138,143} (**Fig. 8**). The addition of methylation marks is controlled by histone methyltransferases (HMTs), whereas histone demethylases (HDMs) remove methyl groups on particular residues¹⁴⁷. Methylation recruits other chromatin-remodeler proteins (e.g. chromodomain-containing factors), which form large multiprotein complexes that alter chromatin structure¹⁴⁸. A well-known example is the heterochromatin protein 1 (PfHP1), a chromatin effector that binds specifically to H3K9me3^{141,149}.

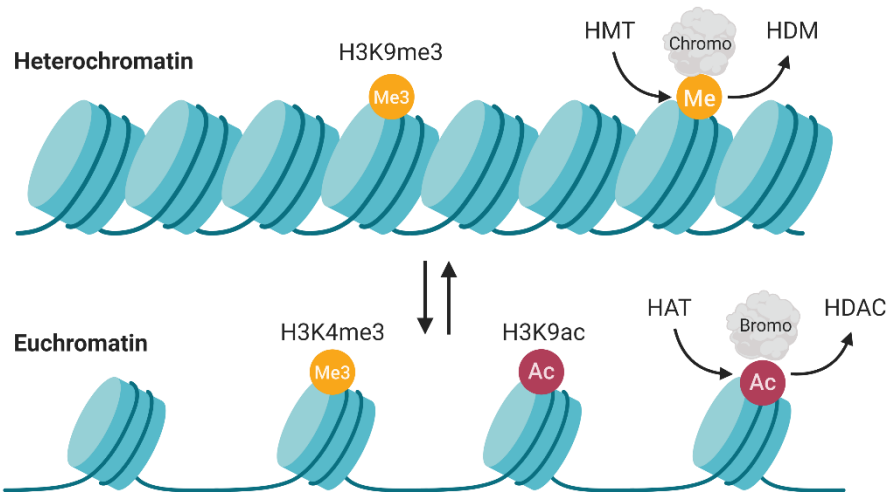


Figure 8. Main histone PTMs associated with euchromatin and heterochromatin states in *P. falciparum*. Schematic of the methylation (Me) and acetylation (Ac) marks typically found in the euchromatin (transcriptionally permissive) and heterochromatin (transcriptionally silent) states. Enzymes that add or remove the methylation and acetylation marks, as well as the factors that can bind to these post-translational modifications, are also indicated. H3K9me3, trimethylation of histone H3 lysine 9; H3K4me3, trimethylation of histone H3 lysine 4; H3K9ac, acetylation of histone H3 lysine 9; HMT, histone methyltransferase; HDM, histone demethylase; HAT, histone acetyltransferase; HDAC, histone deacetylase; Chromo, chromodomain-containing factor; Bromo, bromodomain protein. Adapted from Bechtis & Waters¹⁴⁴. Created with BioRender.com.

Other epigenetic mechanisms also play a role in transcriptional regulation. Canonical histones, for instance, can be exchanged with alternative histones, which have different PTMs and confer different properties to nucleosomes. Also, some factors (e.g. high mobility group box, HMGB) induce the physical movement of nucleosomes along the DNA strand¹⁵⁰. Non-coding RNAs (ncRNAs) can also exert positive and negative regulation of gene expression (e.g. *var* genes)¹⁵¹. Moreover, chromatin distribution within the nucleus, which fluctuates during the IDC, is also implicated in transcriptional activation or silencing of a locus^{152–155}.

2.4.2 Epigenetic variation in the context of adaptation

P. falciparum has multiple families of clonally variant genes, characterized by their intrinsic property of being in different transcriptional states among genetically identical parasites at the same stage of the life cycle¹⁵⁶. Differences in the transcriptional state of these genes can result in different antigenic properties and phenotypes. This transcriptional state is maintained by epigenetic mechanisms and stably transmitted from one generation to the next (epigenetic memory). However, infrequent stochastic switches between active and silent states occur during normal growth, increasing the phenotypic heterogeneity between individual parasites. This pre-existing diversity permits the selection of parasites with the most advantageous combination of active and repressed genes under different conditions of the environment, an adaptive strategy known as **bet-hedging**^{52,157}. Although this strategy does not ensure survival of

individual cells, it enables population survival upon changes in the environment by selection of cells that have a higher fitness under the new condition. It is a fast and heritable mechanism that has been linked to some adaptation processes in malaria parasites, such as immune evasion or drug resistance. The most studied example involves the **var family**, composed by 60 genes that encode different forms of *P. falciparum* erythrocyte membrane protein-1 (PfEMP1), a protein located on the membrane of infected erythrocytes. The ability of parasites to express only a single *var* gene at a time (mutually exclusive expression) and periodically switch expression to alternative *var* gene variants allows the evasion of the host's immune system and the change of binding specificity of the infected cell^{158,159}. The best example of such association is the expression of *var2csa*, linked to chondroitin sulfate A (CSA) binding and placental malaria¹⁶⁰. Clonally variant expression of *rif*, *stevor* and *Pfmc-2tm* families is also likely linked to antigenic variation and immune evasion^{161,162}. Another well-known clonally variant gene family are **clag genes**, involved in solute transport (i.e. nutrients and toxic compounds) across the RBC membrane. This family includes five members, among which *clag2*, *clag3.1* and *clag3.2* are clonally variant¹⁶³. Moreover, *clag3.1* and *clag3.2* also present mutually exclusive expression, and parasites expressing different combinations of *clag3* genes associated with different solute permeability phenotypes can be selected under different conditions such as presence of toxic compounds^{164–166}.

2.5 Post-transcriptional regulation

It has been shown that malaria parasite's transcriptional profile fit with a “just-in-time” model, such that life cycle progression is mainly controlled at the transcriptional level. However, a consistent delay is observed between transcript peak and accumulation of the resultant protein, differently affecting distinct transcripts^{167,168}. Indeed, in some cases no correlation is observed between transcript and protein levels. For instance, low abundant transcripts can be efficiently translated leading to high protein amount, whereas others are poorly translated even though the high presence of transcript. This observation suggests an important contribution of post-transcriptional mechanisms to **regulate protein levels**.

Regulation at this level involves mechanisms to control different post-transcriptional steps, such as mRNA maturation and stability, transfer into the cytoplasm, translation efficiency, PTMs and protein half-life¹⁶⁹. Translation efficiency is a key post-transcriptional regulation mechanism. Some *cis*-acting elements in specific *var* and sexual-stage genes have been shown to inhibit translation^{170,171}. Similarly, *trans*-acting

factors can control translation by regulating binding of specific mRNAs to the ribosome (e.g. PfAlba1) or repressing the translation machinery (e.g. PfDZ50)^{172,173}. Also, structurally different types of ribosomal RNAs (rRNAs) have been described in *P. falciparum*, each of them expressed in specific stages, suggesting a putative additional level of regulation by the ribosome complex¹⁷⁴. Apart from translation initiation, processes such as mRNA splicing, decay and stabilization are other levels of regulation, in which exonucleases (e.g. PfRNaseII) and other *trans*-acting factors (e.g. PfSR1) may exert a regulatory role^{175,176}. Moreover, the mRNA stability pattern changes in a time-dependent and gene-specific manner throughout the IDC and has been related with developmental transitions^{107,177,178}.

3 FEVER

3.1 General mechanisms of fever

Fever is a type of innate immune response characterized by a resetting of the body's thermostatic setpoint, which leads to a temporary 1.5-5°C increase of core temperature¹⁷⁹. It involves not only a rise in core temperature but also the generation of acute-phase reactants and the activation of several physiologic, endocrinologic and immunologic pathways¹⁸⁰.

Although a strong association between fever and infection has been recognized for a long time, this response is not restricted to infectious diseases. Fever is also observed in response to injury, such as surgery, trauma, chemicals or thermal insults, and in some cases can accompany internal stimuli, including tumours or autoimmune diseases^{180,181}. In fact, fever is considered a non-specific host defence, part of the innate immune system, that acts in parallel with other mechanisms (e.g. inflammation) with the final aim to inactivate the pathogenic agents or heal the damaged areas¹⁸². Fever induced by these situations must be distinguished from hyperthermia, such as the hyperthermia induced by a heat stroke or ambient exposure, characterized by a dysregulation of the mechanisms of body temperature control leading to a sustained elevation in core temperature¹⁸⁰.

3.1.1 Pyrogens and cryogens

Substances that can raise core temperature (pyrogens) are divided into two general categories depending on their source^{183,184}. **Exogenous pyrogens** are microorganism products and foreign antigens, such as cell wall components (e.g. lipopolysaccharide, LPS) or toxins (e.g. enterotoxins). They can either directly induce fever by themselves or induce the release of cytokines that elicit a febrile response by different mechanisms. In contrast, **endogenous pyrogens** are derived from host cells and include a special class of cytokines that are intrinsically pyrogenic. Some of the known pyrogenic cytokines are interleukin-1 (IL-1 α and IL-1 β), IL-6, tumour necrosis factor- α (TNF- α), ciliary neurotropic factor (CNTF) and interferon- γ (IFN- γ), among others^{180,185}. They are produced by immune cells such as neutrophils, macrophages and lymphocytes, as well as other cell types such as endothelial cells, astrocytes and glial cells, in response to exposure to exogenous pyrogens or other stimuli. Most of them are undetectable under basal conditions in healthy subjects and their synthesis is highly induced in response to specific stimuli, being essential for the immune system. Once released, each pyrogenic cytokine is recognized by a highly specific surface

receptor present in many different host cell types, inducing local and systemic effects within only a few minutes. Other substances are known to play an antipyretic role (**cryogens**) by inhibiting the synthesis of pyrogenic cytokines, blocking the cytokine receptors or increasing heat loss. This group of cryogens includes some cytokines (e.g. IL-10 and TNF- α , the latter with both pyrogenic and antipyretic properties), hormones, neuroendocrine products and cytochrome P-450, among others^{186,187}. The interaction between pyrogens and cryogens determines the height and duration of the febrile response.

3.1.2 Generation of fever

Both exogenous pyrogens and pyrogenic cytokines drive a fever cascade that is sensed by a hypothalamic region called *organum vasculosum of the laminae terminalis* (OVLT). It ultimately stimulates the POA, one of the anterior-preoptic hypothalamic structures that contains thermal neurons (warm and cold sensitive neurons), and considered the main thermoregulatory region of the brain¹⁸⁸. All signalling pathways leading to a reset of the thermoregulatory circuit culminate in the POA via two distinct pathways: humoral and neural^{189–191}. The choice of pathway appears to depend on the specific pyrogen and its route of delivery, and often more than one signalling pathway is used to regulate the different phases of fever initiation and maintenance¹⁸⁵.

The **humoral pathway** is characterized by the signalling of the pyrogenic cytokines or components of microbial products (**Fig. 9**). Each exogenous microorganism shows differential signature molecules, known as pathogen associated molecular pattern (PAMP), which are specifically recognized by Toll-like receptor (TLR) family members. Humans have at least ten different TLRs that are able to recognize a broad spectrum of pathogens. One group of the TLR family is located on the cell surface (TLRs 1, 2, 4, 5, 6 and 10) and is specialized in recognizing cell wall components of microorganisms, whereas another group of TLRs is intracellular (TLRs 3, 7, 8 and 9) and recognizes microbial nucleic acids (double- and single-stranded RNA and DNA)^{192,193}. Each TLR subtype recognize specific microbe-associated PAMPs. It is known, for instance, that LPS recognition is driven by TLR 4^{192,194}. Binding of PAMPs to specific TLRs on peripheral macrophages or cerebral endothelial cells leads to release of pyrogenic cytokines, as well as prostaglandin E₂ (PGE₂).

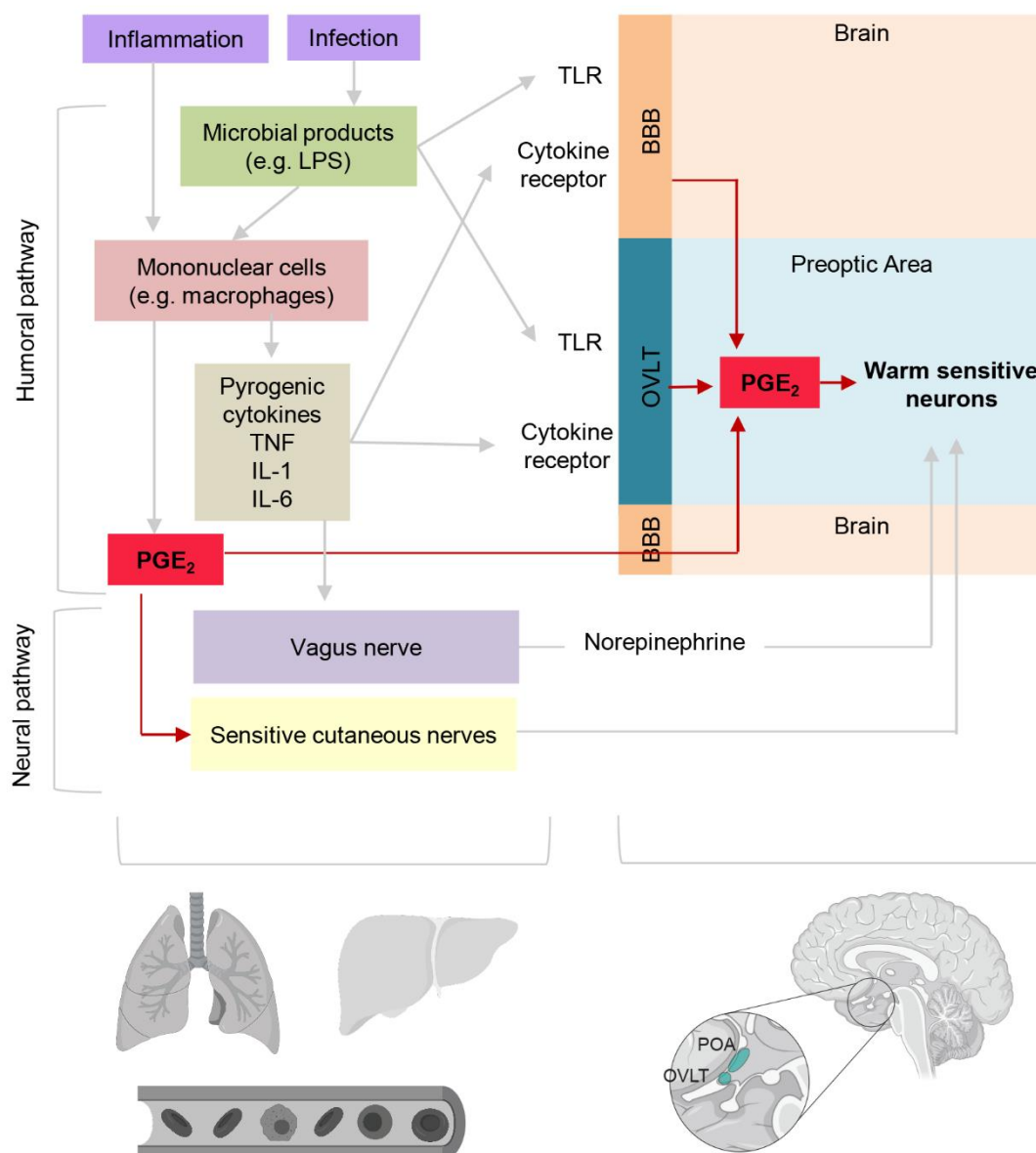


Figure 9. Pathways leading to fever. Microbial products can lead to fever by inducing the production of PGE₂ in the periphery and the brain, either directly (stimulation of endothelial cells in the brain) or indirectly (through macrophages activation, which releases PGE₂ and pyrogenic cytokines that can stimulate endothelial cells in the brain). PGE₂ acts in the preoptic area (POA) of the hypothalamus, activating warm sensitive neurons by binding to the EP3 receptor (humoral pathway). Localized PGE₂ and pyrogenic cytokines may also activate cutaneous nerves and the vagus nerve, able to transmit fever signals directly to the POA (neural pathway). PGE₂, prostaglandin E₂; TNF, tumor necrosis factor; TLR, Toll-like receptor; IL, interleukin; BBB, blood brain barrier; OVL, organ of the laminae terminalis. Adapted from Sajadi & Mackowiak¹⁸⁰. Created with BioRender.com.

Pyrogenic cytokines transmit fever signals by activating specific cytokine receptors in the endothelial cells of the OVL, leading to release of PGE₂ directly in the POA^{180,195}. In this case, OVL acts as a sensor for circulating cytokines and transfers febrile signals to the POA situated nearby. Moreover, cytokines can cross the blood brain barrier (BBB) and access cytokine receptors of the vascular, glial and neuronal structures of the brain, which also stimulate PGE₂ synthesis and promote increased cytokine production by the brain¹⁹⁵. PGE₂ can also be synthesized on the periphery

(e.g. lung and liver macrophages) and cross the BBB. This peripheral PGE₂ is more related with the initiation of the febrile response, whereas the one synthesized in the brain (i.e. OVLT) is involved in its maintenance. Once in the POA, PGE₂ binds to specific receptors (EP3 receptors) and activates thermal neurons^{180,196–198}. The final result is a slowdown of the firing rate of the warm sensitive neurons, which results in an increase in body temperature. In addition to these pathways, cytokines and other inflammatory mediators can also directly activate the thermal neurons in a PGE₂-independent pathway¹⁸⁹.

In contrast, the **neural pathway** is characterized by a febrile signal communication through peripheral nerves, either involving transmission through cold-sensitive cutaneous nerves or the vagus nerve (**Fig. 9**). In the first case, localized synthesis of PGE₂ at sites of inflammation may activate cold-sensitive cutaneous nerves, which transmit fever signals to the POA of the hypothalamus¹⁹⁹. In contrast, the vagus nerve is stimulated by pyrogenic cytokines synthesized by the Kupffer cells in the liver, and it may convey these signals to the hypothalamus through a noradrenergic pathway^{189,191}. Neural pathways have the potential to respond more rapidly than humoral pathways, which rely on the sequential synthesis and transport of pyrogenic mediators²⁰⁰.

Hypothalamic thermal neurons integrate core and peripheral thermal information, both obtained from the humoral and neural pathways, which allows the identification of the nature of the inflammatory challenge. Immediately after, they begin an efferent signalling that will be transmitted through the dorsomedial hypothalamus and the *rostral raphe pallidus nucleus* to finally raise body temperature.

3.1.3 Symptomatology of fever

Several **local and systemic changes** are induced during fever generation in order to increase core temperature. In most cases, shivering is the primary symptom that reflects that heat production is enhanced. The circulatory system determines the temperature of various body parts and the rate at which heat is lost from body surfaces to the environment¹⁸⁰. Thus, this system is critical to induce the increased temperature needed during fever. At a vascular level, changes occur rapidly and involve vasodilatation, vascular stasis and increased capillary permeability. Also, vasoconstriction in the skin capillaries is induced to decrease cutaneous blood flow and avoid heat dissipation at the skin surface, producing the chills typical of fever. Other heat gain mechanisms are also activated, including increased muscle contraction that leads to rigors. Specific behavioural mechanisms are also used to avoid heat loss, such as adopting fetal position to reduce the body surface area or wearing thick clothes

and seeking warmer environments¹⁸⁰. Once the fever signal is no longer present in the central nervous system, the thermal point drops to normal, activating heat loss mechanisms such as sweating to re-establish the normal core temperature.

The increased core temperature is only one of many features of the febrile response. Thus, it may be accompanied by other symptoms such as headache, malaise, anorexia and other sickness behaviours, all of which are mediated by members of the same group of pyrogenic cytokines that activate the thermal response of fever¹⁸⁰.

3.1.4 Risk-benefit considerations

Fever would have first appeared over 600 million years ago and it is nowadays widespread within the animal kingdom, being present in several mammals, reptiles, amphibians, fish and invertebrate species¹⁷⁹. The evolutionary persistence of fever is even more remarkable considering its substantial **metabolic cost**, requiring an over 10% increase in metabolic rate per °C increase in core temperature in humans²⁰¹. Moreover, it has been reported that the same febrile response used for pathogen elimination could increase the risk of collateral injuries due to either induction of ischemia in essential tissues or excessive enhancement of cytotoxic activities.

Thus, from the evolutionary point of view, fever may have offered a clear benefit for many organisms to be maintained along evolution despite its harmful consequences. Many studies demonstrate that increased body temperature is directly related with **enhanced resistance** of animals to viral and bacterial infections, whereas fever suppression is associated with increased mortality during infection^{202,203}. Moreover, it seems that other immunologic processes that are usually active in the presence of fever have evolved to function optimally at febrile rather than basal temperatures¹⁷⁹. Altogether, fever offers a **defence** to exogenous microorganisms, which would explain its maintenance as an adaptive host defence response.

3.2 Biological basis of malarial fever

Fever is one of the most common symptoms of malarial infections, characterized by **periodic febrile paroxysms** during which body temperature can rise to >40°C for a few hours (**Fig. 10**). As described by Karunaweera et al., *P. falciparum*-induced fever follows a regular sequence of events that typically last 5-7 h: it begins with chills, followed by the rise in temperature and rigor; afterwards the temperature falls slowly, finishing with a severe sweating²⁰⁴.

3.2.1 Fever as a malaria symptom

Classical malaria paroxysms are cyclical (intermittent pattern) (Fig. 10), triggered by schizonts burst at the end of each asexual blood cycle. As *Plasmodium* species differ in their IDC length, the frequency of the febrile episode induced by each infection is also variable. In primary infections malaria fever occurs with a periodicity of 48 h (**tertian fever**) in species such as *P. falciparum*, *P. vivax* and *P. ovale*, or 72 h (**quartan fever**) in *P. malariae*, according to their respectively asexual blood cycle length. In contrast to other species, sometimes the pattern observed in *P. falciparum* infections is not regular and fever can occur daily (**quotidian fever**) or every 36 h (**subtertian fever**) in early infections, when parasite synchronicity is not yet established (Fig. 10). Non-classical patterns are also common, and can be attributed to the simultaneous presence of multiple parasite populations operating at different synchronicities and to the host immune status, among other factors²⁰⁰.

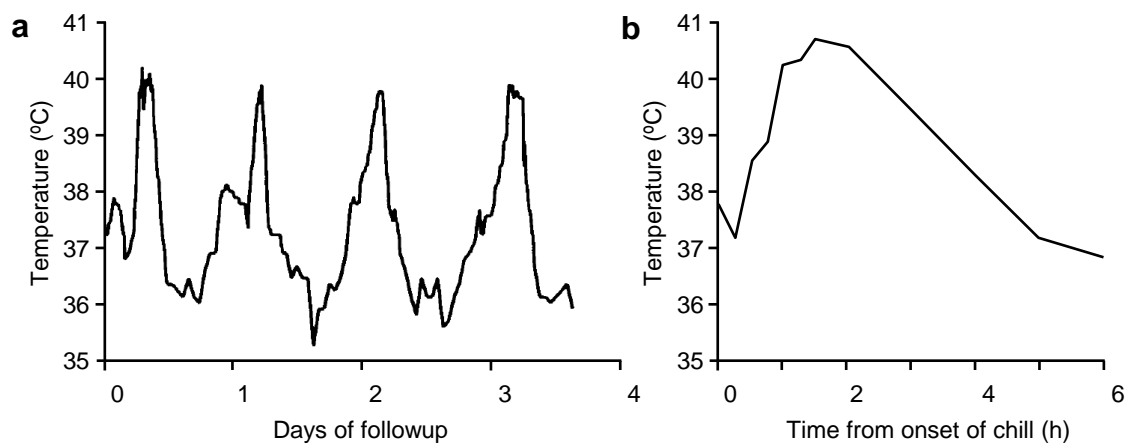


Figure 10. Pattern of *P. falciparum*-induced fever. **a**, Fever pattern from a symptomatic *P. falciparum*-infected patient, followed during some days before starting the antimalarial treatment. Adapted from Gravenor & Kwiatowsky²⁰⁵. **b**, Single fever paroxysm experienced by a *P. vivax*-infected patient. Body temperature was measured during all the episode, starting at the time when chills were first observed. Adapted from Karunaweera et al.²⁰⁴.

During the first days of infection, parasitemia increases exponentially, but fever only occurs when a certain parasitemia is reached (**pyrogenic threshold**) and thus a high proportion of schizonts are bursting at the same time²⁰⁵. Although many studies tried to estimate this pyrogenic threshold, it has been shown that it varies depending on many factors, such as transmission levels, season, *Plasmodium* species and host immunity^{206–211}. For instance, in areas with intense *P. falciparum* transmission, young children have a higher pyrogenic threshold than adults, meaning that they can tolerate much higher levels of parasitemia in the absence of fever^{208,209}.

3.2.2 Mechanism of fever induction in malaria disease

At the end of each intraerythrocytic cycle, schizont rupture releases both invasive merozoites and many other parasite-derived toxins into the bloodstream, which trigger the febrile response^{200,212,213} (**Fig. 11**). **Glycophosphatidylinositol** (GPI) has been suggested as the main toxin involved in fever induction, being recognized at the cell surface by receptor TLR2 heterodimers (TLR2-TLR6 and TLR2-TLR1) and TLR4 homodimers^{214–217}. This glycolipid structure comprises a glycan backbone linked at one end to the C-terminus of a protein and at the other end to the phosphatidylinositol (PI), which permits to anchor proteins to the surface membrane lipid bilayer^{218,219}. Although GPIs are expressed ubiquitously by eukaryotes, they are particularly common among protozoa, differing in structure, size and heterogeneity from the human GPIs. In *Plasmodium*, GPI is mainly found anchoring parasite surface proteins, such as merozoite surface proteins (MSP1, MSP2 and MSP4), although it can also be found free or bound to other cellular elements. Other studies propose **hemozoin** (“malaria pigment”) as another toxin triggering malaria fever^{220,221}. Hemozoin is formed during intraerythrocytic stages due to the crystallization of toxic free heme residues derived from the digestion of hemoglobin by the parasite²²². Detoxification of heme by formation of this pigment is essential for the survival of malaria and some other apicomplexan parasites. Despite the intracellular TLR9 is the receptor involved in the hemozoin-induced response, it is still unclear whether hemozoin is directly recognized by TLR9 or it only acts as a carrier to present other attached molecules, such as plasmodial DNA^{223,224}.

Although hemozoin and GPI are the main studied toxins, other parasite-derived molecules may also induce a proinflammatory response^{212,213}. This is the case of plasmodial **DNA** and **RNA**, recognized by TLR9 and TLR7, respectively^{223,225}. Moreover, plasmodial nucleic acids may also activate TLR-independent cytosolic sensors²²⁶. RBC lysis also releases **heme**, which activates TLR4 and also leads to inflammation by inducing tissue injury²²⁷. Another example is the strong inflammatory response observed to **uric acid**, accumulated in the infected RBC as a degradation product of purine metabolism²²⁸.

Interaction of both GPI and hemozoin/DNA with TLRs induces the fever signalling cascade, consequently increasing secretion of PGE₂ and several pyrogenic cytokines, such as TNF- α , IL-6 and IL-1. The **TNF** response is the most studied in malaria infections^{204,229}. While these pyrogenic cytokines cause fever, they are also responsible for the most severe malaria symptoms such as cerebral malaria, anemia or multi-organ

dysfunction²¹⁶. However, the knowledge of all these toxins and how they induce malaria fever is still scant. Indeed, there are still some doubts about whether GPI and hemozoin can really induce TNF production, as many studies on the role of these toxins in fever induction are hampered by contamination of the *P. falciparum* cultures with *Mycoplasma*, which is a potent macrophage-stimulator²³⁰. Thus, although both GPI and hemozoin may play a role in fever induction, further analysis must be performed to determine the true role of these and other putative malaria toxins, as well as the role of TNF in malaria fever.

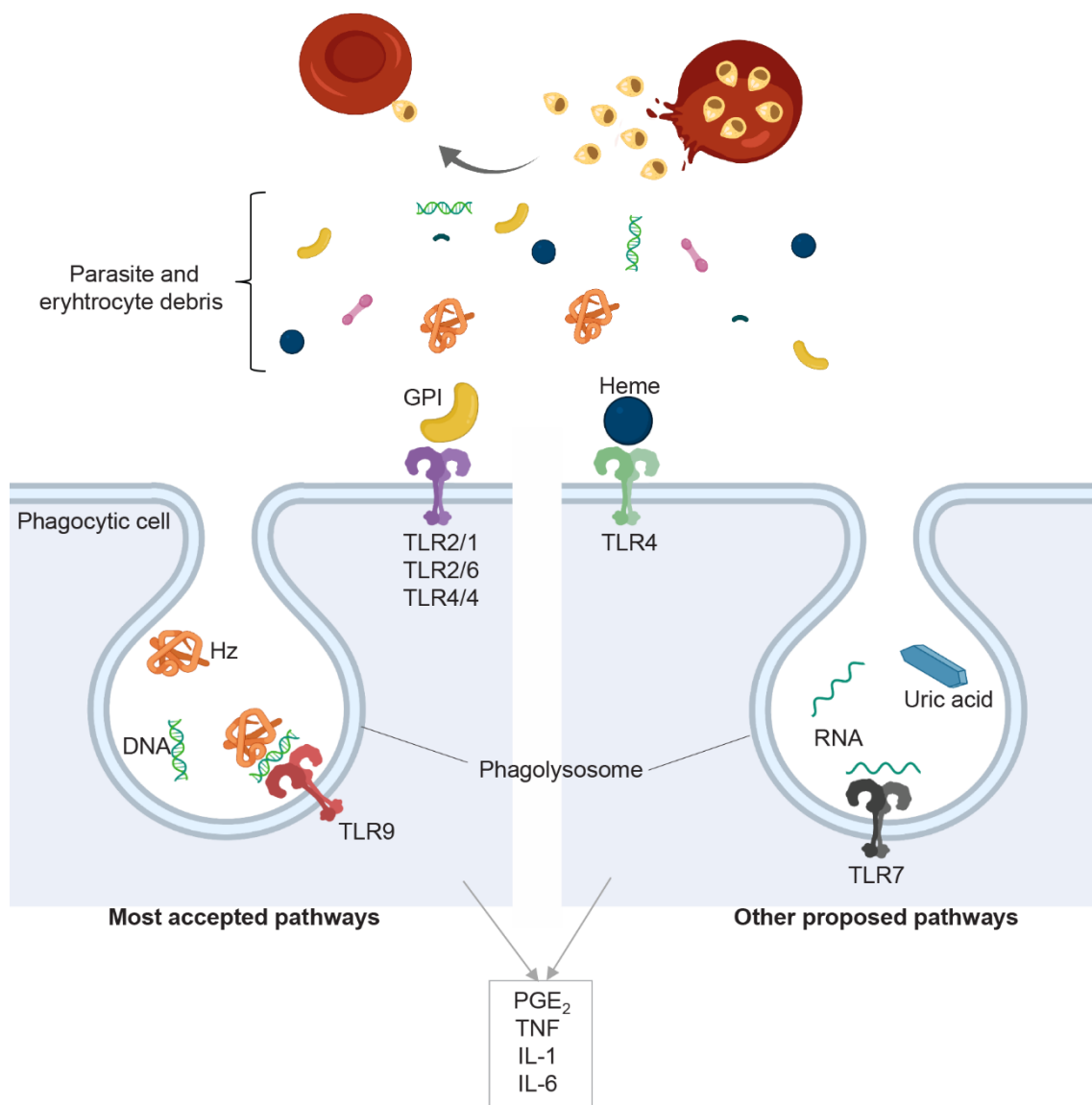


Figure 11. Proposed mechanisms of malaria fever induction. Malaria fever is linked to schizonts burst at the end of each intraerythrocytic cycle, which releases the new formed merozoites, together with all the parasite-derived and erythrocyte-derived compounds, into the bloodstream. Phagocytes and other immune cells can recognize some of these toxins by specific Toll-like receptors (TLRs) or other receptors and induce the production of pyrogenic cytokines and prostaglandin E₂ (PGE₂), which transduce signals to the brain and finally induce the febrile response. GPI, glycosphosphatidylinositol; Hz, hemozoin; TNF, tumor necrosis factor; IL, interleukin. Adapted from Gazzinelli et al.²¹². Created with BioRender.com.

3.2.3 Effect of fever on parasite survival and growth

Heat shock (HS) assays have been used to mimic physiological fever episodes *in vitro* and to determine the effect of this heat stress on parasites. Several HS exposure times and temperatures have been tested in the last decades, and conclusions from independent studies are the same: increased temperature of just a few degrees during a short period of time **inhibits growth and development** of *P. falciparum* parasites. Exposure of synchronous parasite cultures to 40°C for 24 h either during the first or the latter half of the intraerythrocytic cycle showed that only late-stage parasites were affected by the high temperature, whereas HS-exposed rings could develop normally²³¹. Similarly, ~80% of ring-stage parasites could survive a 12 h HS at 40°C whereas only ~20% of trophozoites were able to progress correctly²³². Shorter time of exposure (41°C for 2 h) had a similar impact on parasite development, also showing ~80-40% survival of ring-stage parasites and <20% in trophozoites¹³⁰. Altogether, these studies show that ring-stage parasites are less affected by HS, whereas **late-stages are especially vulnerable** to high temperature exposure, a variability that has been explored as a method of synchronization of mixed-stage parasite cultures²³¹.

In all cases, decreased survival was linked to an increased number of “**crisis forms**”, corresponding to dead parasites, which are characterized by **pyknotic** nucleus, hyposegmented schizonts, swelling and vacuolated cytoplasm^{130,231–234}. Some data suggests that heat stress may induce programmed cell death, although the pathway is still unclear, as it shows some markers similar to eukaryotic apoptosis, autophagy and necrosis^{233,234}. Paradoxically, while a single HS exposure inhibits intraerythrocytic parasite development, recurrent fever may actually promote it^{235,236}. It was observed that a short HS at the ring stage confers several advantages to further HS exposures, such as cytoprotection, developmental stimulation and increased invasion rate²³⁵. These results suggest that parasites may have developed mechanisms to respond to continued temperature peaks seen in malaria fever, although more evidence from independent studies is needed to test this hypothesis.

Although other types of stress, such as endoplasmic reticulum (ER) stress, can induce gametocyte commitment¹²⁶, a similar situation has not been reported for heat stress conditions. It is possible that high temperatures alter parasite or host metabolism in some way that affects gametocytemia, but there is no clear evidence to support or refute such speculation²³⁷.

3.2.4 Benefits of fever for host and parasite

Fever is usually seen as beneficial for the host due to its damaging effect on mature intraerythrocytic malaria parasites. However, HS-induced growth inhibition is not 100% effective, as after each fever episode a proportion of the parasites can still survive.

Some studies conceive it as a mechanism of population density regulation that benefits both the parasite and the host, allowing host survival during acute infection by reducing the parasite burden and at the same time providing the parasite enough time to ensure transmission of the infection^{231,238,239}. Other studies show that fever promotes parasite synchronization, which in turn reinforces fever induction²³⁸. It has also been suggested that recurrent fever paroxysms enhance cell stiffening and cytoadherence^{240–242}, which entangles parasite clearance. Moreover, other studies propose that fever may promote intraerythrocytic parasite development^{235,236}. Altogether, these results suggest that fever could be seen both as a protective innate immune response and fever induction as an adaptive strategy of the parasite to ensure maintenance of the infection.

4 HEAT SHOCK RESPONSE REGULATION

4.1 Types of stress response

In eukaryotic cells, there are sophisticated mechanisms of protein quality control, which help polypeptides folding, distinguish misfolded proteins from those with native forms, and clear away conformationally aberrant and toxic proteins²⁴³. Altogether, these mechanisms maintain protein homeostasis (proteostasis) to ensure cell survival. However, many stress conditions can deregulate proteostasis and lead to a proteotoxic situation, which many organisms overcome by activating a protective stress-response machinery that detects and neutralizes protein damage. Different pathways may be activated depending on the type of stress, although they are interconnected and may share some elements^{244–246} (**Fig. 12**). The **heat shock response** (HSR) is induced by a variety of stress conditions leading to misfolded or aggregated proteins in the cytosol, such as elevation in temperature or heavy metal exposure. In contrast, conditions such as nutrient deficiency, hypoxia, oxidative stress or shifts in pH mainly induce the accumulation of unfolded proteins in the ER and mitochondria organelles, activating the **unfolded protein response** (UPR). Many other stress responses have been identified in eukaryotic cells, such as the **oxidative stress response** (OSR), triggered by the toxic effect of reactive oxygen species (ROS), the **DNA damage response**, caused by exposure to genotoxic agents or endogenous damaging events, or the **osmotic stress response**, induced by a change in solute concentration.

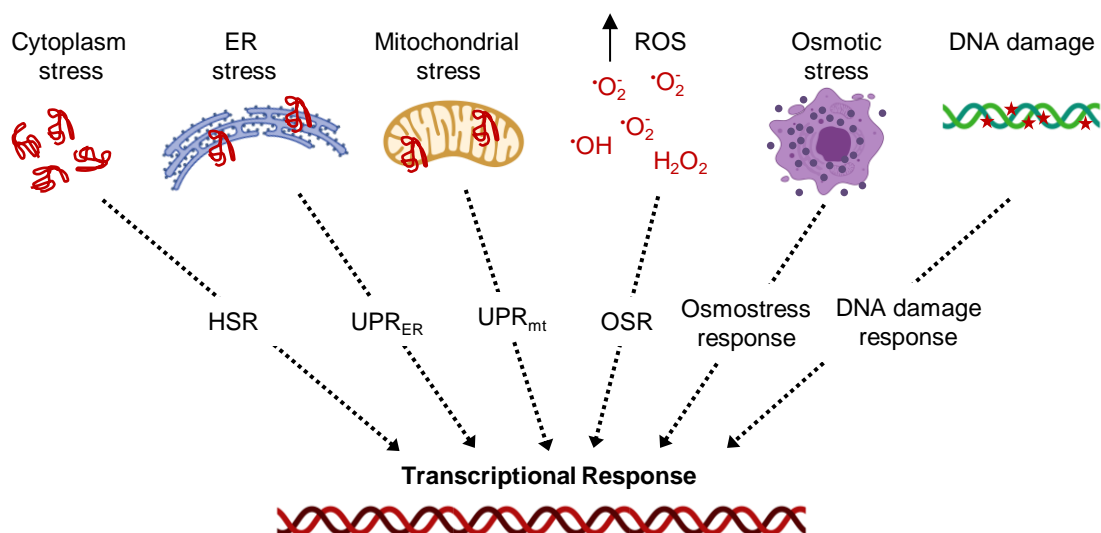


Figure 12. Types of stress and cellular responses commonly found in eukaryotic cells. Unfolded proteins trigger the heat shock response (HSR) in the cytoplasm and the unfolded protein response in the endoplasmic reticulum (UPR_{ER}) and mitochondrion (UPR_{mt}). The oxidative stress response (OSR), the osmotic stress response and the DNA damage response, among other types of stress responses, are also commonly found in eukaryotes. ER, endoplasmic reticulum; ROS, reactive oxygen species. Created with BioRender.com.

4.2 Heat shock response in eukaryotes

Most prokaryotes and eukaryotes are able to produce a protective response following heat stress with a relatively conserved mechanism that mediates survival in front of HS damage. Many thermosensory structures are affected by thermal stress (e.g. proteins, DNA, RNA or lipids) and can have a direct effect or lead to the activation of a signal transduction pathway²⁴⁶. For instance, the accumulation of denatured proteins is the main trigger of the HSR. This directed transcriptional response is mediated by a transcription factor that induces increased synthesis of chaperones and other stress-response genes that help to maintain proteostasis²⁴⁷.

4.2.1 Chaperones

Several different classes of molecular chaperones exist in cells, most of which belong to the **heat shock proteins** (HSPs) group. It includes more than 300 members in higher eukaryotes, involved in a diverse proteome-maintenance functions under stress and nonstress conditions, including assistance of *de novo* folding and refolding, protein trafficking, signal transduction, aggregate prevention and proteolytic degradation²⁴⁸. HSPs can be divided in nine families according to their molecular weight and properties, among which HSP100, HSP90, HSP70, HSP60, HSP40 and small HSPs are the main known families^{248,249}.

HSP100 chaperones, members of the AAA+ protein family (Adenosine triphosphatases with diverse activities), are heat inducible proteins that help organisms to survive under extreme stress conditions. The yeast HSP104 is the best characterized member, involved in modulation of protein aggregation and thermotolerance²⁵⁰.

HSP90s are the most abundant chaperones in the cell, localized in the cytosol and ER. Members of this family mainly play a role downstream of HSP70 in the regulation of numerous pathways in eukaryotic cells (e.g. regulating the activity of signalling proteins), as well as stabilizing misfolded proteins during basal and stress conditions²⁵¹. They also cooperate with co-chaperones and other co-factors (e.g. Hop), which in some cases provide a direct link between HSP70 and HSP90 that allows substrate transfer²⁵².

The **HSP70 family** is the biggest family of chaperones, each member showing a different pattern of expression and subcellular location. In humans, 11 members have been identified, including HSP70 (heat-induced), HSC70 (cytosol), GRP78 (ER) and GRP75 (mitochondrion). They are central players in proteostasis maintenance both

under basal and stress conditions, some of them being constitutively expressed (e.g. HSC70) and others induced upon stress (e.g. HSP70)²⁵³. Their affinity to proteins is assisted by **HSP40 co-chaperones** and nucleotide-exchange factors (NEFs), which regulate the cycle between ADP- and ATP-bound forms^{254–256}.

HSP60s (Type I chaperonins) are present in the mitochondria and chloroplasts where they assist folding of proteins transported to these organelles, although under certain cellular stress they can also migrate to the cytosol²⁵⁷. As other chaperones, HSP60s have co-chaperones (HSP10s) and also work together with HSP70s²⁵⁸. A second class of chaperonins (Type II chaperonins) include the eukaryotic cytoplasmic chaperonin TCP1 ring complex (**TRiC**), independent of HSP10 cooperation and involved in folding of cytoskeletal proteins, although its role is still poorly understood²⁵⁷.

HSP40 co-chaperones accelerate the ATP hydrolysis in HSP70 chaperones that aids proper folding. HSP40s also bind to protein substrates and target them to HSP70, regulating substrate specificity of HSP70s²⁵⁶.

Finally, **small heat shock proteins** (sHSPs) are a diverse family of chaperones with a molecular mass <40 kilodaltons (kDa). They oligomerize and mainly play a role during oxidative and heat stress by binding to non-native proteins to prevent their aggregation. Similar to HSP60s, sHSPs can work together with the HSP70/HSP40 complex^{259,260}.

4.2.2 Transcriptional regulation of the heat shock response

The overall HSR includes both repression and activation of gene expression, although there are many more genes that are transcriptionally repressed than induced. In prokaryotes, the σ^{32} subunit of the bacterial RNA polymerase is responsible for driving this HSR. In eukaryotes, the HSR is much more complex and different regulatory mechanisms may co-exist, each of them regulating a specific subset of genes at specific times²⁶¹. The main regulators of this response are specific transcription factors, named **heat shock factors** (HSF), among which HSF1 is the best characterized and largely conserved from yeast to humans^{247,262}. Although HSF1 is considered as the main regulator of the HSR, only a 10 and 13% of the transcriptional alteration induced by HS is dependent on this transcription factor in yeast and mammals, respectively^{131,261}. This HSF1-dependent response is mainly restricted to chaperone gene expression²⁶³. Thus, other transcription factors also contribute to the regulation of heat-induced transcriptional changes, such as Msn2 and Msn4 from yeast, which drive a general stress response (GSR) to respond to a variety of stress types^{264,265}. However, Msn2/4 factors appear to play different roles from HSF1: while HSF1 is essential for

recovery from a brief exposure to an extreme temperature, Msn2/4 is required for long-term survival at high temperature²⁶⁶. In mammals, the HSF1-independent HSR includes induction of cytoskeletal genes and apoptotic pathways, and down-regulation of genes related with metabolism, cell cycle, protein synthesis, mRNA processing and transport²⁶¹. Other factors, such as SRF, have been predicted *in silico* to regulate this mammalian HSF1-independent response, although there is no experimental evidence²⁶¹.

In this thesis, we have focused on the HSFs since they are the key specific factors of the HSR. While plants and vertebrates have at least four HSF members (HSF1-4), other organisms such as yeast or invertebrates only have **HSF1**. Although HSF1 may not be responsible for the whole HS transcriptional response, this transcription factor plays a key role inducing the main chaperones and other stress response genes essential to rescue the protein aggregation and damage found during stress^{261,267}. Moreover, its conserved and widespread presence in eukaryotes reflects its biological importance.

4.2.3 HSF1 structure

HSF family members share a highly conserved helix-turn-helix domain in the N-terminal region, named DNA-binding domain (DBD) (**Fig. 13**). Through this domain, HSF1 can recognize a conserved motif called **heat shock element** (HSE), formed by three contiguous inverted nGAAn DNA sequence repeats^{268–270}. Although the HSE architecture is highly conserved among organisms including mammals or yeast, HSF1 can also bind to variations of HSE. For instance, in *S. cerevisiae*, three different HSE have been described to be recognized by HSF1 upon HS: the *perfect* HSE (also called *typical*), which contains at least three contiguous nGAAn motifs, the *gap*-type HSE, composed by two consecutive nGAAn followed by a another nGAAn unit after a gap of 5 bp, and the *step*-type HSE that have 5 bp spacers between each nGAAn repeat^{271,272}. HSF1 from *C. elegans* shows affinity for the *consensus* HSE during HS, but under basal conditions it binds to a *degenerate* HSE that contain mismatches in the nGAAn motif²⁷³. Also, HSF1 may regulate transcription by binding to non-HSE sequences, perhaps in association with other transcriptional regulators²⁷⁴.

Mammalian HSF1 contains a C-terminal transcriptional activation domain (TAD), involved in the transcriptional activation of target genes and regulation of the magnitude of HSF1 activation. In the absence of stress, TAD is restrained by a central regulatory domain (RD), which exerts a negative control and prevents HSF1

activation²⁴⁷. Three oligomerization domains (heptad repeats HR-A, HR-B and HR-C) also control HSF1 activation by mediating triplet formation, needed to bind to the HSE. HR-A and HR-B permit HSF1 trimerization, a process that is inhibited by HR-C under nonstress conditions to maintain HSF1 in a monomeric form²⁴⁷. Contrarily, yeast HSF1 contains two activation domains, AR1 and AR2, located at the N-terminal and C-terminal ends, respectively. These domains are not essential under basal conditions, but instead are needed for transient (AR1) or sustained (AR2) HSF1 activation during HS^{275,276}. Interestingly, while both AR1 and AR2 can activate HSF1 bound to *perfect* HSEs, only AR2 activates HSF1 when it is bound to *gap*-type HSEs²⁷⁷. Yeast HSF1 also contains a negative regulatory domain termed conserved element 2 (CE2) that represses HSF1 activity, regulated by a C-terminal modulator domain (CTM). This CTM is also needed for HSF1 binding to *gap*-type HSEs during the HSR²⁷⁵.

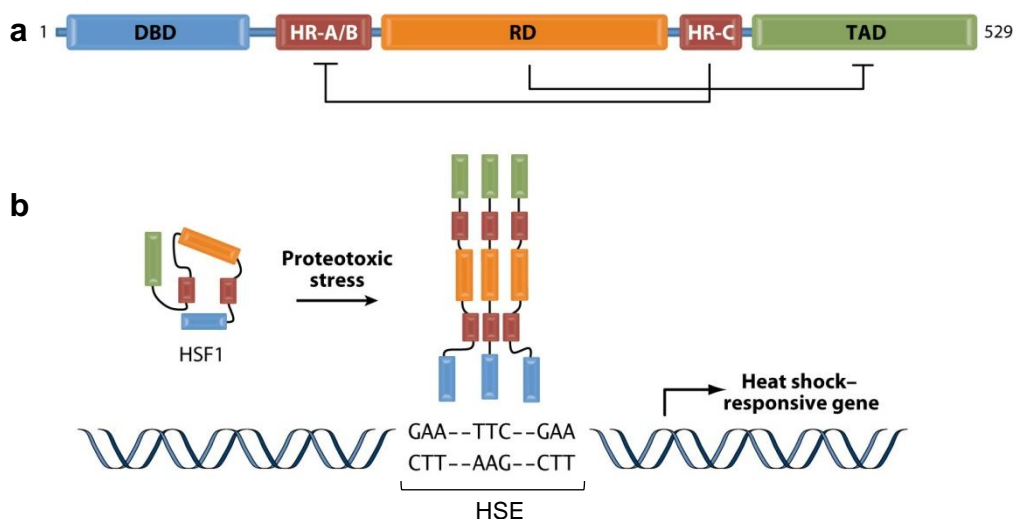


Figure 13. Mammalian HSF1 structure and DNA-binding. **a**, Schematic of the structure of mammalian heat shock factor 1 (HSF1). Black lines indicate negative regulation. **b**, Different stress conditions induce HSF1 trimerization and activation needed for DNA-binding to the heat shock element (HSE) present in the promoter of genes that are transcriptionally regulated by HSF1. Adapted from Anckar & Sistonen²⁴⁷.

4.2.4 Stress sensing and HSF1 regulation

The proteotoxic signals that initiate HSF1 activation can be of various origins, such as HS, heavy metals, osmotic deregulation, oxidants, proteotoxic agents, starvation and bacterial and viral infections^{247,275}. However, it is likely that different types of stress result in HSF1 activation by different mechanisms, with HS inducing a rapid response and other stress types inducing a slower response²⁷⁸.

In the absence of stress, HSF1 is mostly kept inactive as a monomer in the nucleus and cytoplasm. However, in yeast, an inactive trimeric form of HSF1 may also be already bound to DNA in the promoter region of a small subset of genes^{279–281}. What

maintains HSF1 in the inactive state and how it senses stress is not completely understood, although in both mammal and yeast organisms the most accepted mechanism relies on chaperone and PTM regulation.

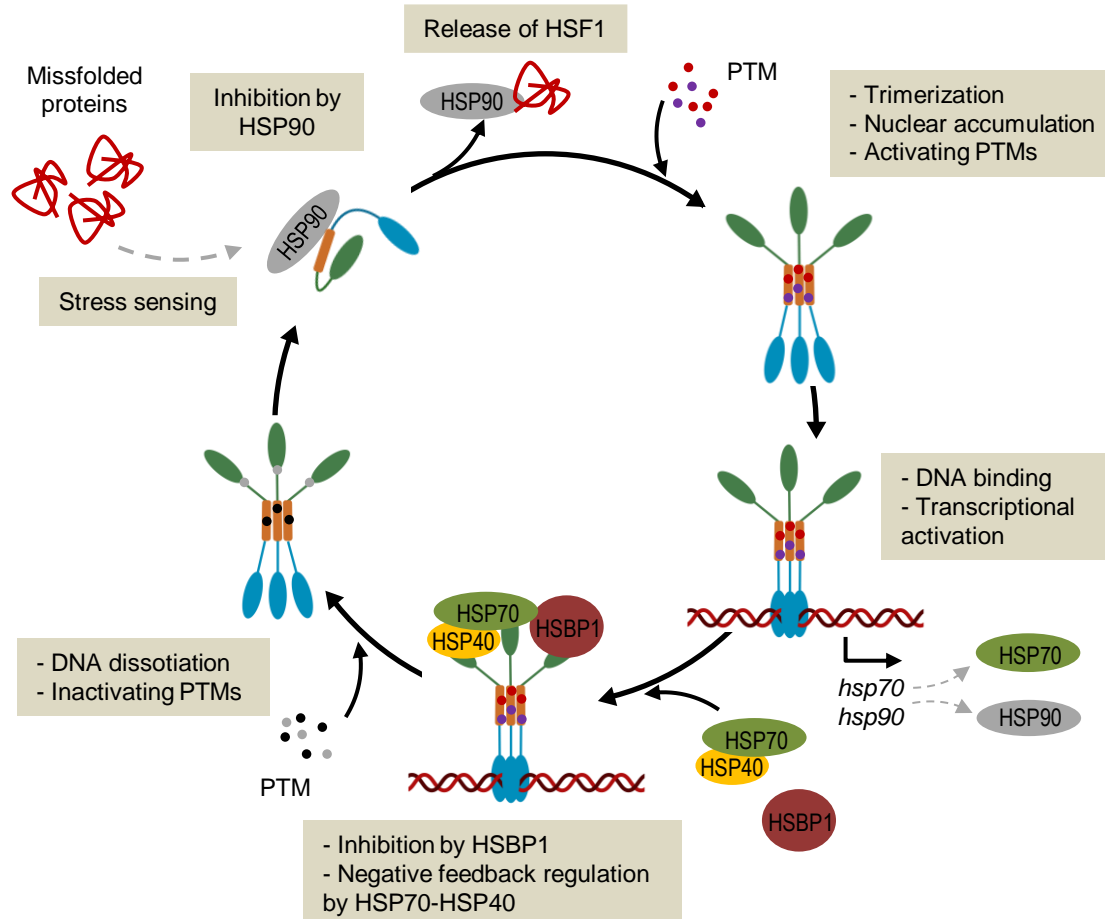


Figure 14. Mammalian HSF1 activation and attenuation cycle. In the absence of stress, heat shock factor 1 (HSF1) is bound to HSP90, which maintains it cytoplasmic in a monomeric inactive form. Proteotoxic stress conditions (e.g. HS) induce HSP90 binding to the accumulated misfolded proteins, releasing and activating HSF1. HSF1 translocated to the nucleus, undergoes trimerization and is modified by several activating post-translational modifications (PTMs), such as acetylation, phosphorylation and sumoylation. Altogether, these changes promote binding to the heat shock elements (HSE) and transcriptional activation of target genes, including *hsp70* and *hsp90*, which codify for heat shock proteins (HSPs). During recovery, the accumulation of HSP70 chaperone, together with its co-chaperone HSP40, inhibits HSF1 transcriptional activity. Heat shock binding protein 1 (HSBP1) also interacts and negatively regulates HSF1 trimers, and also plays a role in recruiting HSP70-HSP40 complexes. HSF1 attenuation also involves modification with inactivating PTMs, which induce DNA dissociation and trimer disgregation.

In nonstressed cells, **HSP90** chaperones maintain the HSF1 transcription factor in an inactive state by inhibiting HSF1 oligomerization and DNA binding^{247,275} (Fig. 14). Negative regulation is also driven by **HSP70**, when accumulation of this chaperone occurs during recovery from stress. In this case, chaperone HSP70 together with its co-chaperone HSP40 also bind to active HSF1, inhibiting the HSF1 capacity to activate transcription (*trans-acting capacity*)^{282,283}. Increasing numbers of misfolded proteins

upon HS compete with HSF1 for chaperone binding, which allows HSF1 liberation and activation²⁸⁴. This activation involves HSF1 trimerization, nuclear accumulation, DNA binding and several PTMs^{284,285}. Both HSP90 and HSP70 are target genes of HSF1 and consequently highly expressed during HS. The accumulation of such chaperones during continuous HS or upon recovery drives a negative regulatory feedback that induces decreased HSF1 activity, conversion to the inactive state and loss of DNA binding (attenuation phase)^{284,286}. This negative regulatory feedback has also been reported for other HSF1 target genes, such as the cytosolic chaperonin TRiC²⁸⁷.

The **heat shock binding protein 1** (HSBP1) is also considered a negative regulator of HSR, as it has been described to interact with HSF1 trimers and recruit HSP70/HSP40 to negatively regulate HSF1 activity during the attenuation phase²⁸⁸. The hexameric form of HSBP1 is highly unstable, which may serve as a sensor for the environmental changes and led to regulation of HSF1-interaction in response to stress²⁸⁹.

PTMs (i.e. phosphorylation, acetylation and sumoylation) are key in the HSF1 activation cycle, having both activation and inhibition effects. They are involved in regulation of HSF1 oligomerization, conformational changes, DNA binding, protein-protein interactions and *trans*-activating capacity^{247,282}. Phosphorylation and sumoylation processes occur rapidly upon HS and modulate the transcriptional activation of HSF1, whereas acetylation events are delayed and inhibit the HSF1 activity during the attenuation phase^{247,282}.

Although the model described above is the most widely accepted, the rapidity of HSF1 activation is difficult to explain only through the release of the repression exerted by accumulated HSPs. Thus, a complementary mechanism was proposed, relying on a constitutively expressed noncoding RNA named **heat shock RNA-1** (HSR-1). Heat may induce a conformational change of HSR-1 that, together with the translation elongation factor eEF1A, may contribute to HSF1 activation²⁹⁰. Another proposed sensing mechanism relies on the intrinsic ability of HSF1 itself to undergo stress-induced conformational changes^{291,292}.

4.2.5 HSF1 target genes under basal and heat shock conditions

HSF1 controls several physiological processes both under stress and nonstress conditions. HSF1^{-/-} mice and cell models have revealed that *hsf1* is needed to activate expression of *hsp* genes, maintain protein homeostasis and ensure cell integrity and survival during stress conditions²⁶². In mammals, a total of nine genes were identified as the HSF1-dependent targets activated upon HS, including four members of the

HSP70 family, an HSP90, three co-chaperones (HSP40 and others) and a non-chaperone gene²⁶³. In *S. cerevisiae*, many of the ScHSF1 target genes induced upon HS are also stress response genes, including the orthologs of HSP70, HSP90 and small HSPs^{264,285}.

Under basal conditions, HSF1 has a different subset of target genes. In *S. cerevisiae*, in addition to regulating protein folding, protein degradation and detoxification, ScHSF1 has been shown to activate transcription of genes involved in cell wall and cytoskeleton, transport, energy generation, carbohydrate metabolism and signal transduction^{285,293}. Although ScHSF1 is involved in all these pathways, its essential role in yeast relies in maintaining high *hsp70* and *hsp90* expression levels under basal conditions²⁶³. In contrast, mammalian HSF1 is not essential, but its deletion has severe consequences, impairing brain development, placenta formation and immunity, as well as producing growth retardation and female infertility^{262,294}. Similar to yeast, mammalian HSF1 has many other roles beyond proteostasis maintenance, such as the regulation of cell cycle progression, lipid metabolism and transport^{263,273,295} (Fig. 15). The role of HSF1 has also been related with ageing diseases that involve protein misfolding, such as Parkinson's or Huntington's diseases, as well as with some types of human cancer, in which proteotoxic and oxidative stress is usually found²⁸².

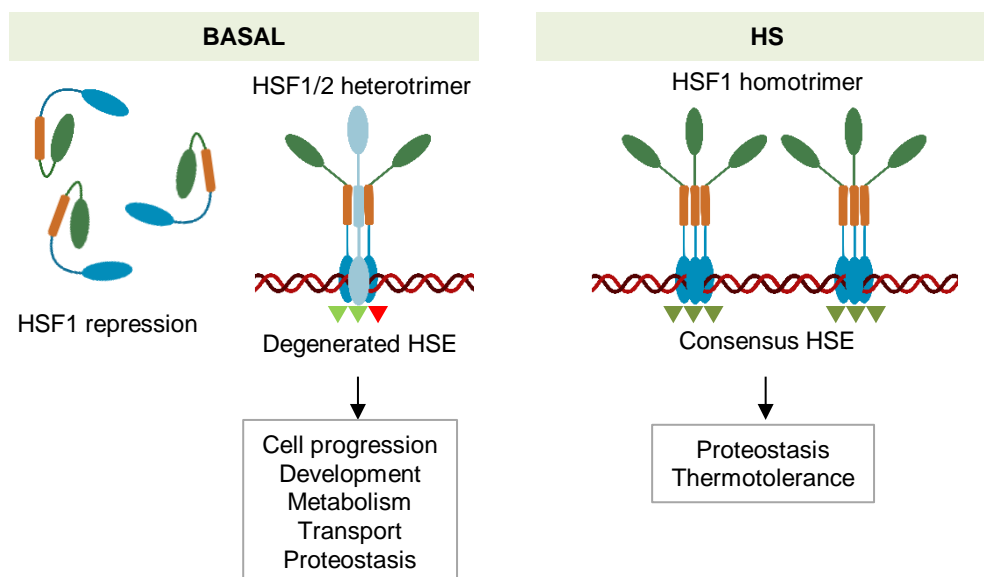


Figure 15. Proposed mechanisms that may explain HSF1 differential target gene specificity under basal and HS conditions. HSF1-HSF2 heterotrimer formation and binding to a *degenerated* HSE have been proposed as the mechanisms that allow HSF1-target gene activation under basal conditions in mammals and *C. elegans* (left). In contrast, HSF1 homotrimer formation and recognition of multiple copies of *consensus* HSE are involved in the HS-induced response (right).

In mammals, this variation in transcriptional regulation between stress and nonstress conditions may rely on the differential HSF1 activation and cooperativity with other HSFs, such as HSF2, providing the differential target gene specificity²⁹⁶ (**Fig. 15**). Another layer of regulation was proposed to be driven by the architecture of the HSE, which in *C. elegans* appears to be different between genes regulated under stress or nonstress conditions (**Fig. 15**). For instance, while high number of *consensus* HSE are found in the HS-induced promoters, only a single copy of a *degenerate* HSE is typically found in genes induced under basal conditions²⁷³.

While *hsp70* regulation is associated with binding of HSF1 to its promoter, it has been shown that many other HSF1-dependent genes do not have HSF1 bound in their promoter region, and vice versa, some genes that do have HSF1 bound in their upstream region are not regulated by HSF1²⁶¹. This observation suggests that HSF1 may exert its activating or repressive role from a distant enhancer region²⁶¹. Also, HSF1 activity is known to be strongly influenced by chromatin structure and the presence of coactivators, which restrict HSF1 activity to only a small subset of HSEs^{270,275}. For instance, the presence of a GC-rich motif (recognized by the E2F/DP cofactor) adjacent to the HSE is required for HSF1-dependent expression during *C. elegans* development, but dispensable for the HSR²⁷³.

4.2.6 HSF1-induced promoter organization in target genes

Induction of *hsp70* expression upon HS has been extensively studied in *Drosophila*, serving as a model for other HSF1 target genes. It has been shown that chromatin status plays a key role in the HSR²⁹⁷. In the absence of stress, the *hsp70* promoter is maintained in a nucleosome-free state by the GAGA factor (GAF), whereas in mammals this state is maintained by the action of chromatin remodelers such as the replication protein A (RPA), the facilitates chromatin transcription (FACT) factor or the chromatin-remodeling complex containing BRG1^{298,299}. Under nonstress conditions, the *hsp70* open promoter is occupied by a transcriptionally paused elongation complex, formed by Pol II and a DRB sensitivity-inducing factor (DSIF) (**Fig. 16**). This complex is maintained in a paused state by the negative elongation factor (NELF), recruited by GAF approximately 20-40 bp downstream the TSS^{300,301}.

Upon HS, the promoter landscape of *hsp70* undergoes a dramatic reorganization within only minutes after the onset of the stress (**Fig. 16**). As pausing maintains an open chromatin environment, the promoter is accessible to transcriptional activators such as HSF1 or SRF. Binding of HSF1 to the promoter is critical for the release of paused Pol

II²⁶⁷. However, HSF1-binding by itself does not activate a gene, but instead it requires the assembly of many different factors at the promoter³⁰². HSF1 is needed to recruit the positive transcription elongation factor (P-TEFb) kinase to the promoter, although no direct interaction between the two proteins has been reported²⁷⁰. HSF1 directly recruits the Mediator complex, which allows a functional interaction between HSF1 and the core promoter by collaborating with factors such as P-TEFb³⁰³. P-TEFb kinase activity is needed to phosphorylate both the Pol II and the DSIF–NELF complex, dissociating NELF from the complex and enabling Pol II to start a productive elongation³⁰⁴. At the same time other Pol II continuously enter into the paused site and are released to maintain high gene transcription. It was proposed that HSF1 itself could maintain the *hsp70* promoter open by recruiting specific chromatin remodelling machinery that displace nucleosomes, such as SWI/SNF or the poly(ADP)-ribose polymerase 1 (PARP1)^{305,306}. The final result is a rapid transcriptional response, involving the expression of several genes to overcome the thermal stress.

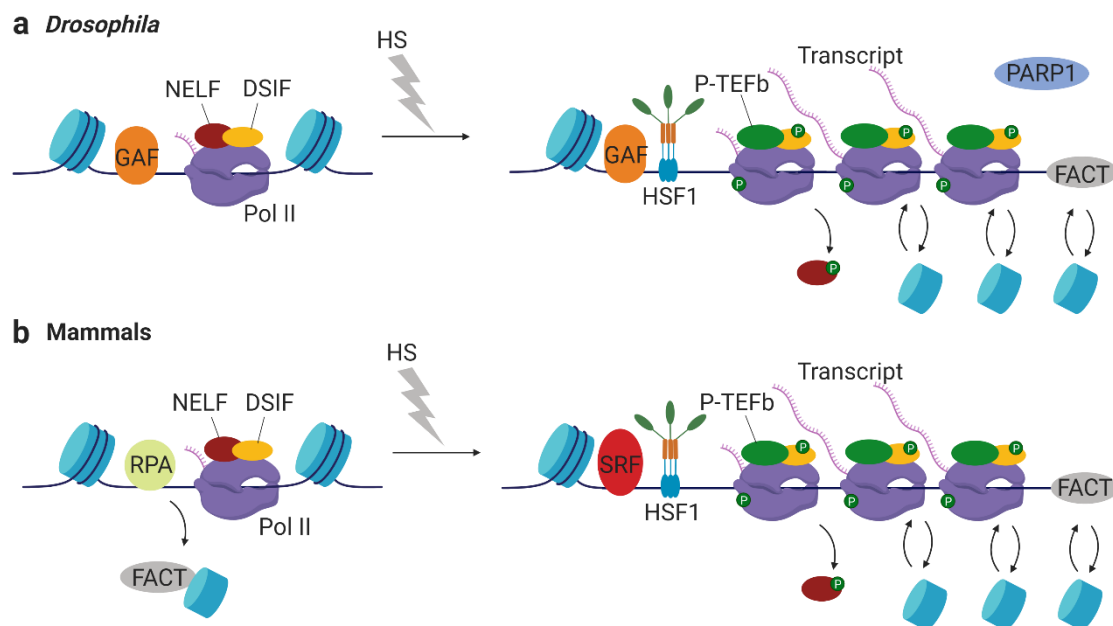


Figure 16. Promoter reorganization upon HS. Diagram of the *hsp70* promoter organization under basal conditions (left) and upon HS (right), comparing *Drosophila* (a) and mammalian (b) mechanisms of gene activation. GAF: GAGA-factor; PIC: pre-initiation complex; NELF: negative elongation factor; DSIF: DRB sensitivity-inducing factor; Pol II: RNA polymerase II; HSF1: heat shock factor 1; P-TEFb: positive transcription elongation factor b; FACT: facilitates chromatin transcription; RPA: replication protein A; SRF: serum response factor. Adapter from Vihervaara et al.²⁹⁸. Created with BioRender.com.

4.3 Heat shock response in *P. falciparum*

HS has been found to be an external signal that controls certain life cycle transitions of several apicomplexa parasites, such as *Entamoeba histolytica*, *Giardia lamblia* and

Toxoplasma gondii, in which the HSR drives some development and differentiation steps³⁰⁷. Moreover, the various temperatures that protozoan parasites experience during their life cycle in multiple hosts suggest that the HSR is essential for their survival. Malaria parasites, for instance, experience an abrupt temperature change during transmission from the mosquito (~25°C) to the human hosts (37°C), in addition to the periodic HS of up to 41°C to which they are exposed during the cyclical febrile episodes of the patient. Parasites thus need a robust HSR to adapt to such regular temperature changes.

4.3.1 Chaperones

As much as 2% of the *P. falciparum* genome encodes for chaperones and chaperonins that are expressed at various stages of the life cycle and are involved in parasite development and survival^{308–311}. They play a role in folding, refolding, aggregation suppression, translocation and degradation of proteins, as well as driving a housekeeping role during the parasite life cycle³⁰⁹. Thus, these proteins are critical to maintain cellular proteostasis, not only upon thermal stress but also during normal parasite growth. More than 90 chaperones and chaperonins have been identified in the parasite, as well as several co-chaperone factors. The best characterized chaperones are members of the HSP90, HSP70, HSP60 and HSP40 families, and many of them use ATP binding or hydrolysis as the energy source for their folding-unfolding activities³¹⁰ (**Table 1**). Also, *P. falciparum* encodes more than 90 proteases, such as the proteasome components or the Clp family, that complement chaperone tasks by clearing the cells from misfolded or short-lived proteins in a selective manner³⁰⁹.

The *P. falciparum* genome encodes four ***hsp90*** genes, of which the best characterized is HSP90, also known as HSP86, located in the cytosol and expressed throughout the life cycle, showing high levels in the schizont stage³⁰⁹. It is essential for the parasite, being involved in signal transduction of pathways related with cell growth and differentiation (e.g. transition from ring to trophozoite stage), intracellular communication and the stress response³¹². Similar to mammals, it has been shown that *P. falciparum* HSP90 can bind to other co-chaperones and functionally interact with HSP70-1^{309,313}. However, it is still not known if HSP90 plays a role as a negative regulator of HSF1 under nonstress conditions. The other three genes encode putative organellar HSP90s: GRP94, HSP90-A and TRAP1, predicted to be localized in the ER, apicoplast and mitochondria, respectively³⁰⁹.

	Gene ID	Name	Cellular localization	Expression stage	Other information
HSP70	PF3D7_0818900	HSP70-1	N, C	T, S	
	PF3D7_0917900	HSP70-2	ER	S	
	PF3D7_1134000	HSP70-3	M	S	
	PF3D7_0831700	HSP70-X	C, ER, Exp	S	
	PF3D7_1344200	HSP70-Y (HSP110)	ER	S	
	PF3D7_0708800	HSP70-Z (HSP110c)	C	S	
HSP90	PF3D7_0708400	HSP90	C	S	
	PF3D7_1222300	GRP94	ER	T, S	
	PF3D7_1118200	TRAP1	A	GV	
	PF3D7_1443900	HSP90-A	A	S, O	
HSP60	PF3D7_1015600	HSP60	M	R, S	
	PF3D7_1232100	CPN60	A	R, T, S	
	PF3D7_1215300	CPN10	M	R, S	Interaction with HSP60
	PF3D7_1333000	CPN20	A	R, S	Interaction with HSP60
HSP40	PF3D7_1437900	HSP40	C	T, Me.	Interaction with HSP70-1
	PF3D7_0201800	KAHsp40	Exp	R	
	PF3D7_1253000	GECO	Exp	GI-GIV	
	PF3D7_0409400	Pfj1 (DnaJ)	A	Const.	Interaction with HSP70-1; DNA replication
	PF3D7_1108700	Pfj2	ER	Const.	Interaction with HSP70-2
	PF3D7_1211400	Pfj4	C	T, S	Interaction with HSP70-1
	PF3D7_0501100	HSP40	J-dots	T, S	Interaction with HSP70-x
	PF3D7_0113700	HSP40	J-dots	Const.	Interaction with HSP70-x

Table 1. Main *P. falciparum* chaperones. Summary of the members of HSP70, HSP90, HSP60 and HSP40 (only best characterized HSP40 proteins) families identified in *P. falciparum*³⁰⁹. Gene ID and protein name are shown, together with additional information about cellular localization and expression stage. Information about their role or interactions with other HSPs is also included. N, nucleus; C, cytoplasm; ER, endoplasmic reticulum; M, mitochondrion; A, apicoplast; Exp, exported protein; R, ring; T, trophozoite; S, schizont; Me, merozoite; O, ookinete; GI, gametocyte stage-I; GIV, gametocyte stage-IV; Const, constitutively expressed.

Six *hsp70* genes have been described in *P. falciparum*: HSP70-1, HSP70-2, HSP70-3, HSP70-X, HSP70-Y/HSP110 and HSP70-Z/HSP110c^{308,309}. Among these, HSP70-1 is the major cytosolic HSP70 chaperone in erythrocytic stages, driving proteostasis maintenance activities that include folding of nascent polypeptides, refolding of misfolded and aggregated proteins and protein translocation into organelles such as the apicoplast, although it is translocated into the nucleus upon HS^{309,314}. It has been shown that HSP70-1 interacts with HSP90, as well as with methyltransferases and the translation elongation factor eF1A²³⁶. HSP70-2 is the homolog of the mammalian Glucose-regulated Protein 78 kDa (GRP78, also known as BiP), largely localized in the ER³⁰⁹. This protein has a major role regulating the UPR in higher eukaryotes, a role that is conserved in *P. falciparum*³¹⁵. HSP70-3 is exported to Maurer's clefts, which are involved in protein sorting and export to the RBC plasma membrane³¹⁶. HSP70-X is found in the cytoplasm, parasitophorous vacuole and partially in Maurer's clefts, and it can be exported to the host erythrocyte and interact with HSP40 proteins³¹⁷. HSP70-Y/HSP110 and HSP70-Z/HSP110c possess nucleotide exchange factor activity, suggesting that they may drive the hydrolysis of the ATP from other HSP70s in the ER

or cytoplasm, respectively³⁰⁹. HSP70-Z/HSP110c has shown to be essential for HS survival, and also to play a central role in preventing aggregation of the asparagine repeats-rich *P. falciparum* proteins³¹⁸.

P. falciparum has two members of the **HSP60** family, also known as chaperonins. HSP60 is localized in the mitochondria, whereas CPN60 is found in the apicoplast³⁰⁹. Other smaller chaperonins are also described in malaria parasites: CPN10 and CPN20, localized in the mitochondria and apicoplast, respectively. This localization pattern seems to suggest the existence of the HSP60-CPN10 complex in the mitochondria and the HSP60-CPN20 complex in the apicoplast, although their biological function is still undetermined.

HSP40 class are HSP70 co-chaperones that recruit and modulate interaction of HSP70 molecules with other proteins and enhance their ATPase activity³⁰⁹. This gene family is largely expanded in malaria parasites compared to other organisms, encoding for up to 44 HSP40 proteins in *P. falciparum*³¹⁹. Many of them are exported to the erythrocyte cytosol, erythrocyte plasma membrane or other structures like Maurer's clefts or J-dots, and could be involved in chaperoning membrane-associated proteins, as well as remodelling red blood cells by interacting with host cell HSP70 and HSP90³⁰⁹. Some examples of secreted HSP40s are KAHSP40 or GECO. In contrast, other HSP40s are located within the parasite, either in the cytoplasm, nucleus or parasite organelles, and are thought to assist protein export and prevent aggregation. Cytosolic HSP40 (Pf3D7_1437900) and Pfj4 were shown to directly interact with HSP70-1. Pfj2 is predicted to reside in the ER, where it could serve as a HSP70-2 co-chaperone. In contrast, Pfj1 is located in the apicoplast and it was proposed to aid in apicoplast DNA replication³¹⁹.

4.3.2 Transcriptional regulation of the heat shock response

Although many HSPs have been identified in apicomplexa, the regulation of the HSR is relatively poorly understood in these organisms. If the mechanism is conserved among eukaryotes, we would expect to find a transcriptional regulator ortholog to HSF1 able to activate the expression of stress response genes. Apicomplexan orthologs of HSF1 have been identified so far only in *Entamoeba histolytica* (EhHSF1, EhHSF2 and EhHSF3), sharing ~50-70% sequence homology with other HSF1 and a conserved (but much shorter) DNA-binding domain³²⁰. However, a transcription factor regulating the HSR similarly to the classical **HSF1 has not been found** so far in any *Plasmodium* species, nor in other apicomplexan organisms.

Despite the absence of a classical HSF, an ortholog of human HSBP1, a negative regulator of HSF1, has been identified in *P. falciparum* (**PfHSBP**, Pf3D7_1120900)³²¹. Although HSBP homologues within the animal and plant kingdoms are very similar, PfHSBP is very distant (only shares 28% of similarity with human HSBP1). However, the structure of the core domain is highly conserved, suggesting that its function may also be conserved across species. PfHSBP is present as a trimer or hexamer and predominantly localized in the cytoplasm under normal conditions, but translocates to the nucleus upon HS. Moreover, it is able to interact with HSP70-1, similar to human HSBP1, which suggests a potential role in the regulation of the HSR³²¹. The identification of a functional PfHSBP in *P. falciparum* suggests that an HSF ortholog may also be present in this species. However, it may be a distant ortholog of the classical eukaryotic HSF1, sharing low sequence and structure similarity, which would explain why its identification has not been possible so far.

4.3.3 Transcriptional changes upon heat shock

Transcriptional alterations upon HS have been described in *P. falciparum* parasites. Oakley et al. identified several pathways that may be part of a HSR in *P. falciparum*¹³⁰. Pathways related with protein stability and folding were specially up-regulated, involving HSPs and other proteins acting as chaperones or chaperonins. HSP70-1 is the main studied chaperone related to HS, as a moderate increase of mRNA and protein has been detected in several studies upon heat stress^{314,322–325}. Other studies also reported induction of HSP90, HSP40, Pfj1 or Pfj4, and decreased transcription of chaperones like Pfj2^{324–327}.

Also, some families of protein kinases involved in phosphorylation-dependent signalling cascades were up-regulated upon HS¹³⁰. Altered expression was also described for genes participating in processes as diverse as protein secretion, DNA repair and replication, signal transduction pathways, mRNA metabolism, splicing or the ubiquitin proteasome pathways¹³⁰. Some specific pathways were down-regulated, including the GPI anchor biosynthesis or the ubiquitin metabolism pathways¹³⁰. In this same study, a high proportion of genes with altered transcription upon HS were found to be either transmembrane or secreted proteins, which might contribute to increased parasite-host interactions and parasite sequestration¹³⁰. Indeed, higher parasite cytoadherence to vascular endothelium was reported upon HS, especially in the brain, highlighting the potential pathological consequences of fever *in vivo*^{240,328}. Although Oakley et al. provided initial insight on the general transcriptional changes and biochemical pathways affected during HS¹³⁰, new approaches are needed to distinguish actual

protective HSRs from transcriptional alterations related with delayed cell cycle progression during HS or with parasite death.

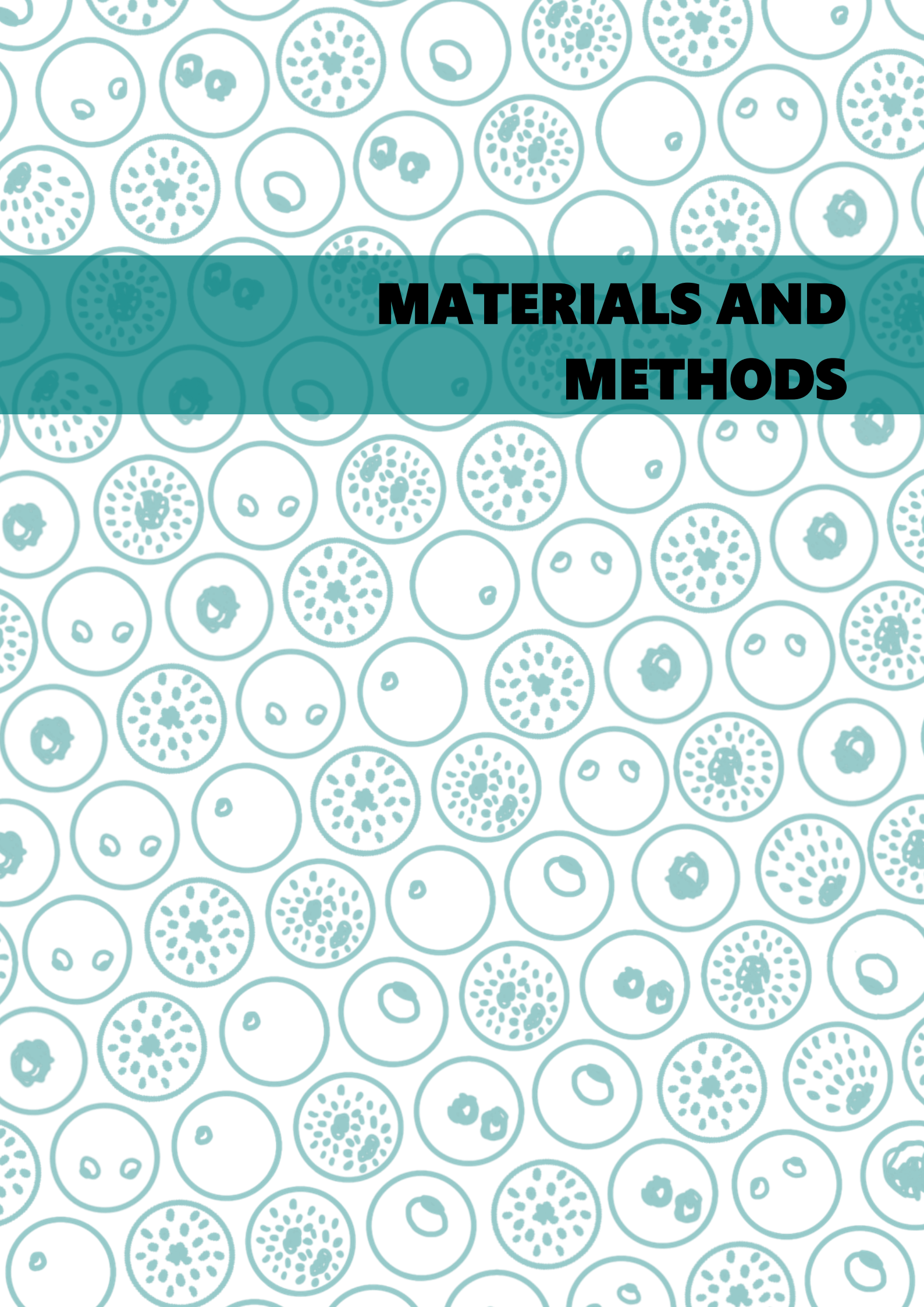
The background of the slide is a repeating pattern of various microscopic cells, likely yeast or bacteria, shown in different stages of division or morphology. The cells are rendered in a light teal color against a white background. A solid teal horizontal band is positioned across the middle of the slide, containing the title text.

HYPOTHESIS AND OBJECTIVES

We hypothesize that, similar to model eukaryotes, *P. falciparum* can sense heat stress and activate a transcription factor analogous to the conserved eukaryotic HSF1, which drives a protective transcriptional HSR. HSF1 is also involved in the response to other types of stress and mediates housekeeping functions under basal conditions, reason which led us to hypothesize that the analogous transcription factor in *P. falciparum* may also perform these roles. The identification of such a transcription factor may provide the first identification of the transcription factor driving a protective response to a fluctuating environmental condition in malarial blood stages, helping to settle the current controversy about the capacity of malaria parasites to mount rapid protective transcriptional responses.

The aim of this PhD Thesis is to characterize the transcriptional regulation of the protective HSR in malaria parasites. The specific objectives are as follows:

- To identify the gene(s) that determine susceptibility of *P. falciparum* to HS *in vitro*, using HS-adapted lines.
- To characterize the PfAP2-HS transcription factor and assess its role under basal and stress conditions, including HS and other types of stress.
- To define the transcriptional alteration induced by HS exposure and distinguish the directed PfAP2-HS-dependent protective response from other PfAP2-HS-independent alterations.
- To gain initial insight on the conservation of the HSR in other *Plasmodium* species.



MATERIALS AND METHODS

1 PARASITE LINES

The 3D7-A stock of the clonal *P. falciparum* line 3D7, the 3D7-A subclones 10G, 1.2B, 10E, 4D, 6D, 1.2F, W4-1, W4-2, W4-4, W4-5, and the HS-adapted line 3D7-A-HS have been previously described^{156,329–331} (Table 2). The *P. berghei* ANKA cl15cy1 clone and the FRB::mCherry::TM transgenic line were previously described^{332,333} (Table 3). The generation of the new transgenic lines is described below.

Parasite line	Description
3D7-A	Stock of the 3D7 clonal line ³³⁰ .
3D7-A-HS	HS-adapted line, obtained after periodic exposure of 3D7-A to HS ¹⁵⁶ .
10G	Subclone of 3D7-A obtained by limiting dilution ³²⁹ .
1.2B	Subclone of 3D7-A obtained by limiting dilution ³²⁹ .
10E	Subclone of 3D7-A obtained by limiting dilution ³²⁹ .
4D	Subclone of 3D7-A obtained by limiting dilution ³²⁹ .
6D	Subclone of 3D7-A obtained by limiting dilution ³²⁹ .
W4-1	Subclone of 3D7-A obtained by limiting dilution after transfection with the plasmid E140-0 ³³¹ .
W4-2	Subclone of 3D7-A obtained by limiting dilution after transfection with the plasmid E140-0 ³³¹ .
W4-4	Subclone of 3D7-A obtained by limiting dilution after transfection with the plasmid E140-0 ³³¹ .
W4-5	Subclone of 3D7-A obtained by limiting dilution after transfection with the plasmid E140-0 ³³¹ .
8A_PfAP2-HS::DD	Subclone transgenic line generated from 1.2B that expresses endogenous PfAP2-HS tagged with a destabilization domain (DD) and 3xHA.
12E_PfAP2-HS::DD	Subclone transgenic line generated from 1.2B that expresses endogenous PfAP2-HS tagged with a destabilization domain (DD) and 3xHA.
10E_PfAP2-HS::eYFP	Transgenic line generated from 10E that expresses endogenous PfAP2-HS tagged with an eYFP in the C-terminal end.
10E_PfAP2-HS::3xHA	Transgenic line generated from 10E that expresses endogenous PfAP2-HS tagged with an 3xHA in the C-terminal end.
10E_eYFP::PfAP2-HS	Transgenic line generated from 10E that expresses endogenous PfAP2-HS tagged with an eYFP in the N-terminal end.
10E_Δpfap2-hs	Transgenic line generated from 10E in which the endogenous <i>pfap2-hs</i> gene was deleted.
10G_Δpfap2-hs	Transgenic line generated from 10G in which the endogenous <i>pfap2-hs</i> gene was deleted.

Table 2. List of the *P. falciparum* lines used.

Parasite line	Description
PbANKA cl15cy1	Clone 15cy1 obtained from 8417 HP clone, which was derived from the original ANKA strain ³³³ .
FRB::mCherry::TM	Transgenic line derived from PbANKA cl15cy1 that expresses FRB fused to a transmembrane protein anchored into the cell plasma membrane. This line is needed as a background to generate the knocksideways (KS) transgenics ³³² .
C2m2_PbAP2-HS::KS	Subclone transgenic line generated using the background FRB::mCherry::TM that expresses PbAP2-HS tagged with FKBP and GFP (knocksideways, KS) in the C-terminal end, which induces PbAP2-HS mislocalization when Rapamycin is added.
C1m3_PbAP2-HS::KS	Subclone transgenic line generated from PbANKA cl15cy1 that expresses PbAP2-HS tagged with FKBP (knocksideways) in the C-terminal end, which induces PbAP2-HS mislocalization when Rapamycin is added.
PbAP2-HS::3xHA	Subclone transgenic line generated from PbANKA cl15cy1 that expresses PbAP2-HS tagged with 3xHA in the C-terminal end.

Table 3. List of the *P. berghei* lines used.

2 *P. FALCIPARUM* CULTURE

2.1 Basic maintenance

P. falciparum parasites were cultured in B+ erythrocytes at a 3% hematocrit, maintained in sterile conditions. Total blood was purchased every four weeks and weekly washed to obtain the RBCs. For this, the total blood was centrifuged for 5 min at 1,360 x *g* at room temperature and the supernatant (containing the plasma and the buffy coat) was removed by aspiration. Two rounds of washes of the resultant erythrocyte pellet were performed by adding incomplete medium, centrifuging for 10 min at 1,360 x *g* and discarding the supernatant. All spins were performed with low deceleration. The washed RBC pellet was resuspended in one pellet volume of complete media and stored for up to one week at 4°C.

Cultures were grown in petri dishes under low oxygen atmosphere (5% CO₂, 3% O₂, balance N₂) in air-tight modular hypoxia incubator chambers. Hypoxic incubators with the same atmosphere mixture were only used when specifically stated. All cultures were maintained at 37°C, except for the experiments including 10E_Δ*pfap2-hs* and 10G_Δ*pfap2-hs* lines, which were maintained at 35°C.

An RPMI-based complete medium (containing Albumax II and without human serum) from Invitrogen was used for routinely culture maintenance, supplemented monthly with glutamine to a final concentration of 2 mM (1:100 dilution of a 200 mM stock) (Table 4). Prewarmed media was routinely changed every second day, except for specific experiments in which high parasitemia was needed. Incomplete medium was custom made (Table 4) and used for the washing steps of several procedures.

Complete medium (1 l)	Incomplete medium (1 l)
Custom RPMI-Albumax medium (041-91762A): 10.4 g RPMI-1640 medium 2.3 g NaHCO ₃ 5.957 g HEPES 0.025 g Gentamycin 0.05 g Hypoxanthine 2 g Glucose 5 g Albumax II mqH ₂ O pH 7.2 Add 10 ml/l of 200 mM sterile glutamine monthly [store at 4°C]	10.43 g RPMI (with L-glutamine, without NaHCO ₃) 5.95 g HEPES mqH ₂ O pH 7.4 (adjusted using 10 M NaOH) [filter-sterilize and store at 4°C]

Table 4. Complete and incomplete medium recipes used for *P. falciparum* culture.

2.2 Cryopreservation of parasite stocks

2.2.1 Freezing stocks

Only ring-stage parasites survive to freezing and thawing. Ideally, cultures must have 5% rings or higher. Cultures were centrifuged 5 min at 453 x *g*, supernatant were removed by aspiration and two pellet volumes of freezing solution (**Table 5**) were slowly added (drop by drop) to the RBC pellets, mixing constantly, and transferred to cryotubes. Cells were incubated at room temperature for 5 min and then frozen directly to liquid N₂.

2.2.2 Thawing stocks

Parasite stocks were removed from liquid N₂, warmed in the hand until thawing and transferred to a tube. Prewarmed thawing solutions (**Table 5**) were added drop-wise very slowly and constantly swirling. First, 0.2 ml volumes of thawing solution-1 were added to the cryopreserved samples, followed by 10 volumes of thawing solution-2 and finally 10 volumes of thawing solution-3. Samples were then centrifuged for 5 min at 290 x *g* and pellets were washed by slow addition of 10 ml of incomplete medium. After another 5 min centrifugation at 290 x *g*, supernatants were removed and pellets were used to establish new cultures, adding the appropriate amount of complete medium and washed RBCs.

Freezing solution (50 ml) 0.324g NaCl 1.512 g D-sorbitol 14 ml Glycerol 36 ml mqH ₂ O [filter-sterilize and store at -20°C]	Thawing solution-1 (100 ml) 12 g NaCl [12% (w/v)] PBS [filter-sterilize and store at 4°C]
Thawing solution-2 (100 ml) 1.6 g NaCl [1.6% (w/v)] PBS [filter-sterilize and store at 4°C]	Thawing solution-3 (100 ml) 0.9 g NaCl [0.9% (w/v)] 0.2 g Glucose [0.2% (w/v)] PBS [filter-sterilize and store at 4°C]

Table 5. Freezing and thawing solutions recipes used for *P. falciparum* culture.

2.3 Parasite synchronization

2.3.1 Sorbitol: ring-stage synchronization

Standard ring-stage synchronization was performed using sorbitol, which only enters and kills late-stage parasites (>20-25 hpi). Cultures were first transferred to tubes and centrifuged for 5 min at 453 x *g*. After removing supernatants, pellets were resuspended in 7 pellet volumes of 5% sorbitol (**Table 6**) and incubated for 7 min at 37°C. Samples were centrifuged again for 5 min at 453 x *g* and remaining pellets were

washed with 10 ml of incomplete medium. After another centrifugation for 5 min at 453 x *g*, supernatants were removed, and pellets were finally resuspended in complete medium to establish the synchronized culture.

2.3.2 Percoll: late-stage synchronization

Late-stage infected RBCs have a different density than ring-stage parasites and uninfected RBCs, and consequently can be purified using a density gradient such as a Percoll gradient. For this, cultures were transferred to tubes and centrifuged for 5 min at 453 x *g*. For each sample, most of the supernatant was removed, leaving ~3 ml to resuspend the pellet, which was slowly applied on top of a tube containing 10 ml of 70% Percoll (**Table 6**). A maximum of 1.8 ml of erythrocyte pellet (corresponds to 30 ml of culture at 3% hematocrit) can be applied to a single tube of Percoll. Samples were then centrifuged for 11 min at 1,065 x *g*, using a low deacceleration. The upper dark layers, which contained the schizonts, were transferred to new tubes containing 40 ml of incomplete medium and centrifuged for 6 min at 652 x *g*. Supernatants were discarded, and schizont-infected erythrocyte pellets were used to establish new cultures, adding the corresponding amount of complete medium and RBCs.

Sorbitol 5% (500 ml)

25 g D-sorbitol
500 ml m_qH₂O
[filter-sterilize and store at 4°C]

Percoll 70% (142.86 ml) *

10 ml PBS 10x
90 ml Percoll
42.86 ml incomplete media
[filter-sterilize and store at 4°C]

* This Percoll preparation in reality contains 63% Percoll.

Table 6. Sorbitol 5% and Percoll 70% recipes.

2.3.3 Tight synchronization

In some specific assays, tight synchronization (1, 2 or 5 h age window) was needed to ensure that all the transcriptional and phenotypical differences observed between strains were not due to differences in parasite age. This synchronization was performed by first purifying schizont-stage parasites with Percoll, usually when >2 rings were counted per each schizont, which indicated that many schizonts were already bursting. Once purified, these schizonts were used to establish a culture and left undisturbed at 37°C (or 35°C for the *Δpfap2-hs* lines) for 1, 2 or 5 h. After this time, sorbitol lysis was used to purify the new ring-stage parasites that had appeared during this period. Consequently, the resultant parasites were all 0-1 hpi, 0-2 hpi or 0-5 hpi after the tight synchronization. In the synchronization to a 1 h age window, to ensure complete removal of late stage parasites, the volume of sorbitol used for the lysis was increased to 30 pellet volumes, the time of incubation increased to 10 minutes and two washes were performed instead of one.

Given the slower IDC progression of 10E_Δ*pfap2-hs*, cultures of this parasite line were synchronized to 0-5 hpi 3 h earlier than 10E and 10G cultures, such that at the time of starting HS or DHA exposure (in parallel for all lines) all cultures were approximately at the same stage of IDC progression.

3 *P. BERGHEI* CULTURE

3.1 Basic mice maintenance

Parasites were routinely propagated in Theiler's original outbred mice of 6-8 weeks of age, whereas BALB/c mice of 6-8 weeks of age were used as the recipients of the experiments (all weighting ~25 g). All animal research was conducted in accordance with the UK Home Office licencing, using protocols reviewed by the ethics committee of the Wellcome Trust Sanger Institute.

For new infections, ~200 µl of cryopreserved stocks were injected intraperitoneally (i.p.). For passage, blood was collected by a terminal cardiac puncture using syringes pre-loaded with 100 µL of heparin (30 U/mL) and injected i.p. to uninfected mice. Parasite harvesting for genomic DNA (gDNA) or protein extraction was also done with a terminal cardiac puncture. Intravenous (i.v.) injection in the tail vein was only used for the HS assays and transfections. Rodents were anesthetized by i.p. injection of 10 ml/kg of a solution containing 12% ketamine and 0.16% xylazine in PBS.

In specific experiments, 1 mg/kg of Rapamycin (Rapa) was daily injected i.p. into mice. For this, Rapamycin was dissolved in N,N-dimethylacetamide (DMA) to a final concentration of 4 mg/ml and then the appropriate amount for injection was diluted in 200 µl of vehicle solution containing 4% DMA, 10% polyethylene glycol (molecular weight 400) and 17% Tween 20. The same proportions of DMA (instead of Rapa) and the vehicle solution were injected i.p. to control mice.

3.2 *In vitro* culture

P. berghei cultures were established in freshly prepared schizont culture medium (Table 7), gassed with the hypoxic gas mixture (1% O₂, 3% CO₂, 96% N₂) and incubated at 36.5°C with gentle shaking using sterile Erlenmeyer flasks.

Schizont culture medium (50 ml)
36 ml RPMI-1640 (25 mM HEPES)
12.5 ml FBS [25% (v/v)]
0.5 ml Penicillin/Streptomycin 10,000 U/ml
1 ml NaHCO ₃ 1.2 M pH 7.2 [24 mM]

Table 7. Schizont culture medium recipe used for *P. berghei* culture.

3.3 Parasite stocks

Parasite stocks were prepared with a 1:2 ratio of infected blood and freezing solution (Table 8) and maintained frozen at -80°C . Upon thawing, stocks were immediately injected i.p. into mice.

Freezing solution
90% v/v Alsever's solution
10% v/v Glycerol

Table 8. Freezing solution recipe used for *P. berghei* culture.

3.4 Schizonts purification

Nycodenz gradient was used to purify schizonts. Cultures were transferred to tubes and centrifuged for 14 min at $300 \times g$ (low acceleration and deceleration). Supernatants were discarded, leaving ~ 3 ml to resuspend the pellet, which was gently added on top of 5 ml of 55% Nycodenz (Table 9). After 20 min centrifugation at $300 \times g$, top dark layers were collected and washed in 30-50 ml of freshly prepared complete medium (Table 9). Samples were centrifuged for 3 min at $450 \times g$ and supernatants were discarded to obtain schizont pellets.

Nycodenz 55% (10 ml)	Complete medium
5.5 ml Nycodenz	10 ml FBS
4.5 ml PBS	40 ml RPMI-1640 (25 mM Hepes)

Table 9. Reagents needed for schizonts *P. berghei* schizonts purifications using Nycodenz gradient.

4 DETERMINATION OF PARASITEMIA

4.1 Giemsa-staining and light microscopy

Giemsa-stained thin smears were routinely made for basic culture maintenance and parasitemia determination. For *P. falciparum* cultures, smears were made using 3-4 μl of erythrocyte pellet, whereas for *P. berghei* infections, smears were made from one drop ($\sim 3 \mu\text{l}$) of tail blood. Smears were air dried and fixed with methanol for ~ 10 s. The excess of methanol was decanted, and slides were stained with Giemsa diluted 1:10 in Sorenson's buffer (Table 10) or H_2O . After 10 min staining, slides were rinsed with abundant distilled water and tissue-dried.

Light microscopy examination of Giemsa-stained smears was used to determine culture parasitemia and parasite growth. An Eclipse E200 (Nikon) optical microscope was used for routine observation, whereas an Eclipse 50i (Nikon) microscope was used to obtain high magnification ($\times 1000$) pictures. For routine parasitemia

determination, the proportion of infected versus non-infected RBCs was calculated from ~1,500 RBCs (~5 different fields). For accurate parasitemia determination (e.g. DHA sensitivity assay), the total RBCs counted was different in each condition depending on the parasitemia: 1,000 RBCs if parasitemia was >5%, 2,000 RBCs if parasitemia was 2-5% or 3,000 RBCs if parasitemia was <2%).

Sorenson's buffer (1 l)

3 g Na ₂ HPO ₄ 0.6 g KH ₂ PO ₄ mqH ₂ O to 1 l pH 7.2 (adjusted using 1 M KH ₂ PO ₄) [sterilize and store at room temperature]

Table 10. Sorenson's buffer recipe.

4.2 Flow cytometry

In many assays, parasitemia was accurately measured by flow cytometry (FACScalibur flow cytometer, Becton Dickinson) using the green-fluorescent Syto11 to stain nucleic acids and the fluorescence channel 488-530/30 as previously described^{334,335}.

For parasitemia quantification, 5 µl of homogenized culture were resuspended in 800 µl of room temperature PBS and incubated with 1 µl Syto11 0.5 mM for 1 min before analysing. Uninfected RBCs maintained in the same conditions that the *Plasmodium*-infected RBCs were always used to determine the autofluorescence background signal (typically ~0.03%) in each experiment and subtracted from the rest of parasitemia measurements.

In some assays, Td-Tomato and Syto11 signal were simultaneously detected in a LSRFortessa™ flow cytometer (Becton Dickinson) using the fluorescence channels 561-582/15-A and 488-525/50-505LP-A, respectively. Autofluorescence was established using infected RBCs that did not express Td-Tomato. Data analysis was performed using Summit™ (v.4.3)³³⁶ and Flowing (v.2.5.1)³³⁷ softwares.

5 NUCLEIC ACIDS EXTRACTION

5.1 gDNA extraction

To extract *P. falciparum* gDNA, cultures were transferred to tubes and centrifuged for 5 min at 453 x *g*. Pellets were resuspended in 4 pellet volumes of buffer A (Table 11) and 1 pellet volume of 18% SDS, mixed by inversion and incubated for 2 min at room temperature. Afterwards, 6 pellet volumes of phenol:chloroform at room temperature were added and mixed well by inverting several times before centrifuging for 10 min at

805 x *g*. DNA was precipitated from the recovered upper-phase using an overnight incubation at -20°C in 1/10 volume of 3 M NaAc pH 5.2 and 2.5 volumes of ethanol. After a centrifugation at 10,600 x *g* for 15 min at 4°C, pellets were resuspended with 500 µl of Tris-EDTA buffer (TE). An equal volume of room temperature phenol:chloroform was added, mixed and centrifuged at full speed for 5 min at room temperature. DNA was again ethanol-precipitated from the upper phase as explained above. Samples were then spun for 30 min at full speed at 4°C, washed with 600 µl of 80% ethanol and centrifuged again for 10 min at full speed at 4°C. Resultant pellets were air dried for 5-10 min and resuspended in 50 µl of mqH₂O.

For *P. berghei* gDNA extraction, blood samples were collected by cardiac puncture, transferred to a 1.5 ml tube and centrifuged for 1 min at 1,000 x *g*. Supernatants were removed and cell pellets were lysed using 1 ml of cold lysis buffer (Table 11). After 15 min of incubation on ice, samples were centrifuged for 1 min at 1,000 x *g*. Pellets were resuspended with 1 ml PBS and spun for 1 min at 1,000 x *g*. Total DNA from remaining pellets was resuspended in 200 µl PBS and purified using DNeasy Blood & Tissue Kit, following manufacturer instructions, and eluted with 100 µl AE buffer.

Buffer A (50 ml)	Lysis buffer (1 l)
0.833 ml NaAc 3 M pH 5.2 [50 mM] 2.5 ml NaCl 2 M [100 mM] 0.1 ml EDTA 0.5 M pH 8 [1 mM] 46.567 ml mqH ₂ O	8.02 g NH ₄ Cl [150 mM] 1 g KHCO ₃ [10 mM] 0.372 g Na ₂ EDTA [1 mM] mqH ₂ O to 1 l pH 7.4

Table 11. Buffer A and lysis buffer recipe.

5.2 RNA extraction

The TRIzol method was used to collect RNA from *P. falciparum* and *P. berghei* cultures, as previously described³³⁸. Cultures were transferred to tubes, spun for 6 min at 515 x *g* and supernatants were removed. Erythrocyte pellets were resuspended in 12 (ring-stage parasites) or 20 (trophozoite and schizont-stage parasites) volumes of prewarmed TRIzol reagent, well homogenized and incubated for 5 min at 37°C to ensure complete dissolution. Samples were frozen at -80°C until RNA extraction.

For total RNA purification, TRIzol samples were thawed and centrifuged for 2 min at 805 x *g*. Supernatants were transferred to new tubes and 0.2 volumes of chloroform were added and mixed well by inversion. After centrifugation at 8,000 x *g* for 40 min at 4°C, RNA was precipitated from the recovered upper phase using isopropanol (5/6 of the recovered volume) overnight incubation at 4°C. Samples were centrifuged for 50 min at 8,000 x *g* at 4°C, resultant pellets were washed with 6-8 ml of cold 70% ethanol

(diluted using RNase-free H₂O) and spun again at 8,000 x *g* for 20 min at 4°C. Remaining pellets were air-dried for 5 min at room temperature and resuspended for 5 min at 55°C in 30-45 µl of RNase-free H₂O. Samples were transferred to 1.5 ml tubes and frozen at -80°C until use.

6 GENERATION OF TRANSGENIC LINES

6.1 Protocols used for cloning

6.1.1 PCR amplification

Standard PCR amplification were performed using *Taq* DNA polymerase or GoTaq® (e.g. confirmation of genomic edition or fragment integration in a cloning step). *LA Taq*® DNA polymerase was used for high fidelity and difficult PCR amplifications (e.g. amplification of fragments for cloning or sequencing, long fragments and promoter regions) (**Table 12**). Primers used for PCR amplification are listed in **Table 35**.

Taq DNA Polymerase reaction (25 µl) 5 µl Taq PCR Buffer 5x (with MgCl ₂ 7.5 mM) 0.25 µl Taq DNA Polymerase 2.5 µl dNTP mix 2 mM each 0.25 µl Primer forward 50 µM 0.25 µl Primer reverse 50 µM X µl DNA template mqH ₂ O to 25 µl	Taq Polymerase thermal cycle DENATURALIZATION 95°C, 2 min CYCLING (x25-30) 95°C, 20 s * °C, 1 min 68°C, ** min FINAL ELONGATION 68°C, 3 min
LA Taq Polymerase reaction (25 µl) 2.5 µl LA PCR Buffer II (Mg ²⁺ free) 10x 2 µl MgCl ₂ 25 mM 0.25 µl LA Taq polymerase 4 µl dNTP mix 2.5 mM each 0.25 µl Primer forward 50 µM 0.25 µl Primer reverse 50 µM X µl DNA template mqH ₂ O to 25 µl	LA Taq Polymerase thermal cycle DENATURALIZATION 92°C, 1 min CYCLING (x25-30) 92°C, 20 s * °C, 1 min 60°C, ** min FINAL ELONGATION 68°C, 5 min
GoTaq® Polymerase reaction (25 µl) 12.5 µl GoTaq Green Master Mix 2x 1 µl Primer forward 10 µM 1 µl Primer reverse 10 µM X µl DNA template mqH ₂ O to 25 µl	GoTaq Polymerase thermal cycle DENATURALIZATION 95°C, 5 min CYCLING (x25-30) 95°C, 30 s * °C, 1 min 62°C, ** min FINAL ELONGATION 62°C, 10 min

* Annealing temperature was ~4°C lower than the estimated primer melting temperature.

** Elongation time was calculated depending on the amplification length (1 min/Kb).

Table 12. PCR reaction and thermal cycle using *Taq*, GoTaq® Green Premix or *LA Taq*® polymerases.

6.1.2 Restriction enzyme digestion

DNA digestion was routinely performed by incubation of the DNA with the selected restriction enzymes and buffer for more than 1 h to overnight at 37°C, following manufacturer (Takara or New England Biolabs) instructions. If the digested DNA was

needed for cloning, purification was performed using the GFX PCR DNA & gel band purification kit.

6.1.3 Oligonucleotide annealing for sgRNA cloning

Annealing of the oligonucleotide sequences for the single guide RNA (sgRNA) was performed by mixing 10 μl of each oligonucleotide (resuspended in mqH_2O to a final concentration of 50 μM) with 2.2 μl of NEB2 buffer, and allowing slow cooling from 95°C to room temperature ($\sim 25^\circ\text{C}$) in a thermometer-controlled water bath. The annealed oligonucleotides were diluted in Tris 5 mM pH 8 to a final concentration of 25 μM (dilution 1:50). Oligonucleotides used for annealing are listed in [Table 35](#).

6.1.4 T4 DNA Ligation

To ligate two digested fragments with sticky or blunt ends we used the T4 ligase enzyme in a 10 μl reaction, following manufacturer instructions. For this, 100 ng of the vector and the appropriate amount of insert, calculated using a molar ratio of 1:3 vector to insert, were typically used. The reaction was incubated for 1 h at 16°C, followed by an incubation of 1 h at room temperature.

6.1.5 In-Fusion cloning

The In-Fusion® HD cloning kit was used to clone sgRNA and PCR-amplified fragments in a digested vector, in a final 5 μl reaction volume. For sgRNA cloning, 100 ng of vector (digested with *BtgZI*) and 1.5 μl of annealed oligos at 25 μM were used. For cloning of single or multiple PCR-amplified fragments, we used ~ 50 ng of vector and the appropriate amount of each fragment, calculated using a molar ratio of 1:10 or 1:10:10 vector to fragments ([Table 13](#)).

sgRNA In-Fusion (5 μl)

X μl Linearized vector *
1.5 μl annealed oligos 25 μM
1 μl In-Fusion HD Enzyme Premix 5x
 mqH_2O to 5 μl

PCR In-Fusion (5 μl)

X μl Linearized vector *
X μl PCR-purified fragments **
1 μl In-Fusion HD Enzyme Premix 5x
 mqH_2O to 5 μl

* <10 kb: 50-100 ng; >10 kb: 50–200 ng

** <0.5 kb: 10-50 ng; 0.5 to 10 kb: 50–100 ng; 10 kb: 50–200 ng

Table 13. In-Fusion® reactions used for cloning of sgRNA or PCR-amplified fragments.

6.1.6 Bacterial transformation and growth

For bacterial transformation, 4 μl of T4-ligated plasmid or 2.5 μl In-Fusion-generated plasmid were used to transform 50 μl of DH5 α or Stellar competent cells. Mixtures were incubated on ice for 30 min, heat-shocked for 45 s at 42°C and kept on ice for 2 min. After the addition of 450 μl of room temperature S.O.C medium, samples were

incubated for 1 h at 37°C in shaking. Transformed cells were then spread on prewarmed 0.02% ampicillin-LB agar plates and incubated overnight at 37°C.

For minipreps, single colonies or glycerol stocks were picked from the agar plates using sterile plastic tips and inoculated in individual tubes containing 5 ml LB broth with 100 µg/ml ampicillin (1:1,000 dilution from a 100 mg/ml stock). Bacterial cultures were incubated overnight at 37°C under shaking (180-200 rpm). Glycerol 15% stocks were also routinely made by mixing 750 µl of LB-culture with 250 µl of glycerol 60%.

For maxipreps, single colonies or glycerol stocks were picked and incubated for ~7 h shaking (180-200 rpm) in 5 ml LB medium with 100 µg/ml ampicillin. Afterwards, part or the whole bacterial culture was transferred to a sterile Erlenmeyer flask containing 150-200 ml LB broth and the selection antibiotic: 100 µg/ml ampicillin for high-copy plasmids or 50 µg/ml carbenicillin (1:1,000 dilution from a 50 mg/ml stock) for low-copy plasmids. Bacterial cultures were incubated overnight at 37°C in shaking.

6.1.7 Plasmid purification from bacteria

After an overnight incubation at 37°C, cultures were harvested and plasmid extraction was performed using either the QIAprep Spin Miniprep Kit or the EndoFree Plasmid Maxi Kit, following manufacturer instructions.

6.1.8 Agarose electrophoresis

Agarose electrophoresis were routinely used to detect PCR amplification, DNA digestion and tagmentation products. A HORIZON 58 Gel electrophoresis system (GibcoBRL) was mainly used to prepare the SYBR-stained gel in TBE 0.5x (diluted from TBE 5x in m_qH₂O) (Table 14) and electrophoresis was run in TBE 0.5x buffer at 80 V for 1-2 h. Samples were diluted 1:6 in Orange-G 6x loading buffer before loading. Images were taken using a G:Box system (Syngene).

TBE 5x (1 l)
54 g Tris
27.5 g Boric acid
20 ml EDTA 0.5 M pH 8
m _q H ₂ O to 1 l
pH 8.3 (adjusted with HCl)
[sterilize and store at room temperature]

Table 14. TBE 5x recipe.

6.1.9 Sanger sequencing

Sanger sequencing was routinely used after each cloning step to confirm the correct plasmid or gDNA edition. PCR-amplified DNA or plasmids were sent to Genewiz together with the sequencing primers used.

6.1.10 PlasmogEM protocols

Plasmids for *P. berghei* transfection were obtained in collaboration with the PlasmogEM team, following their specific cloning protocols^{339,340}.

6.2 Constructs generated for parasite transfection

6.2.1 Δ pfap2-hs

Given the large size of *pfap2-hs* (11,577 bp), to knock this gene out with the CRISPR/Cas9 system we used two sgRNAs (also referred as guides) (see Results, section 3.1). One guide targets a sequence near the 5' end of the gene (position 866-885 from the start codon, primers C1/2) whereas the other recognizes a sequence near the 3' end (positions 11,486-11,505, primers C3/4). The 5' guide was cloned into a modified pL6-*egfp* donor plasmid³⁴¹ in which the *yfcu* cassette had been removed by digestion with *NotI* and *SacII*, end blunting and religation. Homology regions (HR1: positions -2 to 808 bp relative to the *pfap2-hs* start codon; HR2: positions 11,520 bp of the gene to 490 bp after the stop codon) were PCR-amplified using primers C5/6 and C7/8 respectively. HR1 and HR2 were also cloned in this plasmid, flanking the *hdhfr* expression cassette, to generate plasmid pL7-pfap2hs_KO_sgRNA5'. The 3' guide was cloned into a modified version of the pDC2-Cas9-U6-hdhfr³⁴² plasmid, in which we previously removed the *hdhfr* expression cassette by digesting with *NcoI* and *SacII*, end blunting and religation, and replaced the *BbsI* guide cloning site by a *BtgZI* site. The resulting plasmid was termed pDC2_wo/hdhfr_pfap2hs_sgRNA3'. All guides were cloned using the In-Fusion system, whereas homology regions were PCR-amplified from gDNA and cloned by ligation using restriction sites *SpeI* and *AflII* (HR1), and *EcoRI* and *NcoI* (HR2) (**Annex II – Fig. 1**).

6.2.2 PfAP2-HS tagged with a destabilization domain

To tag PfAP2-HS with a 3xHA-ddFKBP tag we used a single homologous recombination approach (**Annex II – Fig. 2**). To generate the pfap2hs_HA-ddFKBP plasmid, we replaced the *pfap2-g* homology region in plasmid PfAP2-G-ddFKBP⁸⁹ by a PCR-amplified fragment (primers C9/10) including positions 9,551 to 11,574 bp of *pfap2-hs* in frame with the tag. The fragment was cloned using restriction sites *EagI* and *XhoI*.

6.2.3 PfAP2-HS C-terminal taggings

For constructs aimed at C-terminal tagging of *pfap2-hs* using CRISPR/Cas9 (10E_*pfap2-hs*_eYFP-Cterm and 10E_*pfap2-hs*_3xHA-Cterm lines) we used a guide corresponding to positions 11,508 to 11,527 bp of the gene. The guide (primers C11/12) was cloned in the pDC2-Cas9-U6-hdhfr³⁴² plasmid to obtain pDC2_*pfap2hs*_sgRNA-C. The donor plasmid for tagging with eYFP (pHR-C_*pfap2hs*_eYFP) was based on plasmid pHRap2g-eYFP³⁴³, with the *pfap2-g* homology regions and *hsp90* 3' sequence replaced by *pfap2-hs* homology regions (**Annex II – Fig. 3**). The 5' HR1 was generated with a PCR-amplified fragment spanning from nucleotide 10,964 to the sequence of the guide (recodoned, primers C13/14), and a 47 bp fragment (generated by annealing two complementary oligonucleotides, primers C15/16) consisting of a recodoned version of the remaining nucleotides to the end of the gene. The two fragments were cloned simultaneously, using the In-Fusion system, into *SpeI*-*BglII* sites. The 3' HR2 was a PCR fragment spanning positions 1 to 590 bp after the *pfap2-hs* stop codon (primers C17/18), and was cloned into *XhoI*-*AatII* restriction sites. The donor plasmid for 3xHA C-terminal tagging (pHR-C_*pfap2hs*_3xHA_*hsp90*-3') was also based on plasmid pHRap2g-eYFP³⁴³, with the eYFP coding sequence replaced by the 3xHA sequence (amplified from plasmid pHH1inv-*pfap2-g*-HAX3⁸⁹ using primers C19/20 and cloned into *XhoI*-*BglII* sites) and the same homology regions as in plasmid pHR-C_*pfap2hs*_eYFP (but HR2 was amplified using primers C21/22 and cloned using the In-Fusion system into *EcoRI*-*AatII* sites, because in this construct the *hsp90* 3' region in pHRap2g-eYFP was maintained) (**Annex II – Fig. 4**).

6.2.4 PfAP2-HS N-terminal tagging

For N-terminal tagging (10E_*pfap2-hs*_eYFP-Nterm line), we cloned a guide targeting *pfap2-hs* positions 73 to 92 bp (primers 23/24) in the pDC2-Cas9-U6-hDHFRyFCU plasmid³⁴⁴ to obtain plasmid pDC2_*pfap2hs*_sgRNA-N (**Annex II – Fig. 5**). The donor plasmid (*pfap2hs*_HR-N_eYFP) consisted of a 5' HR1 including positions -366 to -1 relative to the *pfap2-hs* start codon, the eYFP gene and an in frame 3' HR2 spanning positions 4 to 756 bp of the gene (excluding the ATG) in which the nucleotides up to the position of the guide were recodoned. HR1 was PCR-amplified using primers C25/26, whereas HR2 was amplified in two steps using a nested PCR approach to add the recodoned sequences (primers C27-30). HR1 and HR2 were cloned in the *SacII*-*NcoI* and *SpeI*-*EcoRI* restriction sites, respectively, of the pL1144400-F1.1-yFCU vector (a variation of the previously described pL1144400-F1.1³⁴⁵ that contains the *yfcu*

selection marker in the *NotI*/*SacII* sites). The eYFP fragment (PCR-amplified from plasmid pHR-C_pfpap2hs_eYFP using primers C31/32) was finally cloned using the In-Fusion system into *SpeI*/*NcoI*, eliminating both restriction sites in the final construct.

6.2.5 Modified *hsp70-1* promoter driving *Td-Tomato* expression

To assess the role of the tandem G-box (Td-Gbox) in regulating *hsp70-1* expression, we generated plasmids to integrate different modified version (containing 0, 1 or 2 G-boxes) of the *hsp70-1* promoter controlling the expression of the fluorescent reporter *tandem Tomato* (*Td-Tomato*) in the *lisp1* locus using CRISPR-Cas9 technology. We used the previously generated *gexp02-tdTomato-lisp1* vector, which included the *lisp1* HR1 and HR2, and the *Td-Tomato* reporter gene under the control of the *gexp02* promoter³⁴⁶ (**Annex II – Fig. 6**). For the wild type Td-Gbox *hsp70-1* promoter, the first 2,000 bp of the *hsp70-1* upstream region were PCR-amplified from *P. falciparum* gDNA using primers C33/34 and cloned by In-Fusion in the *gexp02-tdTomato-lisp1* plasmid digested with *SalI*/*NotI* (replacing the *gexp02* promoter and eliminating both restriction sites in the final construct), generating the 2Gbox_ *hsp70-1*_TdT_ *lisp1* vector. For the *hsp70-1* promoter versions containing either 1 or 0 G-boxes, two fragments with overlapping modified sequences in the G-box region were PCR-amplified: one of them spanning from the Td-Gbox to the -2,111 bp position, and the other from the Td-Gbox to the ATG. For the 1 G-box approach, the first fragment spanned from -2,111 to -1,109 bp (primers C33/35) and the second from -1,117 to 3 bp (primers C36/34); whereas for the 0 G-box approach, fragments spanned from -2,111 to -1,121 (primers C33/37) and from -1,117 to 3 bp (primers C38/34) relative to the *hsp70-1* start codon. We cloned these fragments in a single In-Fusion step to obtain 1Gbox_ *hsp70-1*_TdT_ *lisp1* and 0Gbox_ *hsp70-1*_TdT_ *lisp1* vectors, which have one or both G-boxes disrupted, respectively.

6.2.6 PbAP2-HS knocksideways

For the PbAP2-HS knocksideways (KS) construct, we used a double homology recombination approach. The PbGEM-646603 vector was previously generated by the PlasmogEM team³³⁹ from a pJAZZ-OK vector using the Red/ET recombineering and Gateway technology. The RecUp consisted in the last 50 bp of *pbap2-hs* (excluding the stop codon) and the RecDown included the 50 bp following the stop codon. This vector contained the FKBP, a 3xHA, *hdhfr* and *yfcu* in frame with the PBANKA_1356000 sequence (**Annex II – Fig. 7**).

6.2.7 PbAP2-HS 3xHA C-terminal tagging

For the 3xHA C-terminal tagging of *pbap2-hs*, we used a double homology recombination approach. The PbGEM-060890 vector was previously generated by the PlasmogEM team³³⁹ from a pJAZZ-OK vector using the Red/ET recombineering and Gateway technology. The RecUp consisted in the last 50 bp of *pbap2-hs* (excluding the stop codon) and the RecDown included the 50 bp following the stop codon. This vector contained a 3xHA, *hdhfr* and *yfcu* in frame with the PBANKA_1356000 sequence (**Annex II – Fig. 8**).

6.2.8 Premature stop codon in PbAP2-HS

To reproduce the *pfap2-hs* non-sense mutation in *P. berghei*, we used a double homology recombination approach. By alignment of the protein sequence of PfAP2-HS and PbAP2-HS (PBANKA_1356000), the equivalent location of the Q3714X mutation in *P. berghei* was determined to be at position 3,239 aa (positions 9,715-9,717 bp). The Rec166 vector was generated from the genomic library PbG01-2388b11 (based on a pJAZZ-OK vector) using a combination of Red/ET recombineering and Gateway technology, in collaboration with the PlasmogEM team³³⁹. The specific primers used for this cloning were Rec166-RecUp, corresponding to positions 9,665 to 9,714 bp, and Rec166-RecDown, including positions -52 to 0 bp relative to the *pbap2-hs* start codon (**Annex II – Fig. 9a**). The final vector contained an in frame 3xHA tag, *hdhfr* and *yfcu* selection markers, following the truncation at position 9,714 bp (**Annex II – Fig. 9b**). Using this construct, we engineered parasites to express a truncated PbAP2-HS and additionally added a 3xHA tag to the truncated protein.

6.3 *P. falciparum* transfection

6.3.1 Plasmid linearization and DNA preparation

For *P. falciparum* CRISPR-Cas9-based edition strategies, 15 µg of the donor vector were linearized with the *PvuI* restriction enzyme in a 50 µl digestion volume (cleaving the ampicillin resistance gene of the donor plasmid). After confirming the correct digestions by agarose electrophoresis, a phenol:chloroform extraction was performed to purify the DNA. For this, DNA was resuspended with mqH₂O to a final volume of 200 µl, and 200 µl phenol:chloroform were added. After centrifugation at full speed (20,800 x g) for 5 min at room temperature, the upper aqueous layer was recovered adjusted to a final volume of 270 µl with mqH₂O. DNA was precipitated with 30 µl of 3 M NaAc pH 5.2 and 750 µl of cold ethanol and incubated at -20°C overnight or until the day of transfection.

For circular vectors, the plasmid was diluted to a final volume of 270 μ l in mqH₂O and ethanol-precipitated as described above. For CRISPR-Cas9-based editions, 60 μ g of the Cas9-containing circular plasmid were precipitated, whereas 100 μ g of the circular vector were used for the single homologous recombination strategy.

Before transfecting, precipitated DNAs were centrifuged at full speed for 30 min at 4°C and maintained under sterile conditions. The supernatant was removed, and the pellet was washed with 1 ml of cold 70% ethanol. After centrifuging at full speed for 10 min at 4°C, the supernatant was removed and the pellet air dried in sterile conditions for 5 min and resuspended in 30 μ l of sterile TE buffer. In CRISPR-Cas9 strategies, where double transfection was needed, both donor and Cas9 plasmids were resuspended in the same 30 μ l volume.

6.3.2 Rings electroporation

Transgenic *P. falciparum* lines were generated using 1.2B, 10G or 10E subclones. Transfections were performed by electroporation of ring stage cultures with 100 μ g of plasmid (HA-ddFKBP tagging) or with a mixture of 12 μ g linearized donor plasmid and 60 μ g of circular Cas9-containing plasmid (CRISPR-Cas9 system).

Cytomix (250 ml)
15 ml 2 M KCl
18.75 ml 2 M CaCl ₂
2.5 ml 1 M K ₂ HPO ₄ /KH ₂ PO ₄ pH 7.6
25 ml 250 mM Hepes / 20 mM EGTA pH 7.6
1.25 ml 1 M MgCl ₂
mqH ₂ O to 250 ml
pH 7.6 (adjusted with ~500-650 μ L 10 M KOH)
[filter-sterilise and store at 4°C]

Table 15. Cytomix recipe.

A total of 200 μ l of erythrocyte pellet was used for each transfection. Before electroporating, a culture with 5-8% ring-stage parasites was sorbitol-synchronized and incubated under standard culture conditions for ~1 h. For the electroporation, the 30 μ l of DNA (containing either one or two vectors needed for the transfection) were mixed with 370 μ l of cold cytomix (**Table 15**). The synchronized culture was centrifuged for 5 min at 453 x g, the supernatant was removed, and 200 μ l of erythrocyte pellet was mixed with the DNA and cytomix dilution and transferred to an electroporation cuvette (2 mm electrode gap). Electroporation was performed using Bio-Rad Gene Pulser Xcell™ system, at a 310 V of voltage, 950 μ F of capacitance and without resistance. The electroporated cells were recovered with a fine plastic Pasteur pipette and the cuvette was washed twice with complete medium, all used to establish a new 10 ml culture, adding 150 μ l of RBCs and the appropriate volume of complete. The RBCs

used in the initial culture and in the culture establishment after electroporation were washed from fresh blood extractions (<1-week-old), to avoid high hemolysis upon electroporation.

6.3.3 Maintenance and selective pressure

For parasite selection, WR99210 was added to cultures to a final concentration of 10 nM. For this, an WR99210 20 μ M dilution was prepared in incomplete media (1:1,000 dilution from a WR99210 20 mM stock) and maintained at 4°C for up to one month. It was added 12-24 h after transfection and media was changed daily for the first 3-4 days. In transfections using the CRISPR-Cas9 system, this selective pressure was maintained for four days as previously described³⁴⁴. In contrast, cultures transfected with the pfap2hs_HA-ddFKBP plasmid were maintained under continuous selective pressure until parasites were observed, followed by 3 off/on drug cycles and subcloning by limiting dilution. Transfected cultures were weekly diluted 1:2 with fresh uninfected RBCs until parasitemia was observed in Giemsa-stained thin smears, usually 2-3 weeks post-transfection. In all cases, to assess correct integration we used analytical PCR of gDNA with specific primers.

6.3.4 Subcloning by limiting dilution

Prior to *P. falciparum* subcloning, late-stage cultures were incubated for 24 h in shaking conditions (40 rpm) to reduce the double-infections. Rings-stage parasites were sorbitol-synchronized, parasitemia was determined flow cytometry and cultures were sequentially diluted to a final concentration of 0.3 parasites/100 μ l. The diluted culture was split into 40 wells (each containing 100 μ l) in a 96-well plate. Controls containing 1,000 and 100 parasites/100 μ l were also included. Media was changed every 48 h and parasitemia was checked by Giemsa-stained thin smears from day 10 onwards, expecting growth in <50% of the wells.

6.4 *P. berghei* transfection

6.4.1 Plasmid linearization and DNA preparation

For *P. berghei*, 10 μ l of vector were linearized by an overnight *NotI* digestion (100 μ l digest volume), releasing the targeting vectors from the bacterial vector arms. DNAs were precipitated by adding 250 μ l of cold ethanol and 11 μ l of 3 M NaAc pH 5.2 and incubating at -20°C for 1 h. After centrifugation at full speed for 30 min at 4°C, pellets were washed with 500 μ l of 70% ethanol and centrifuged again for 5 min at 4°C at full

speed. After, supernatant was completely removed and pellet was dried at 65°C for 10 min, resuspended for 5 min at 65°C in 10 µl mqH₂O.

6.4.2 Schizonts electroporation

Transgenic *P. berghei* lines were generated using the PbANKA cl15cy1 (wild type)³³³ and the FRB::mCherry::TM (only used for the KS strategy)³³² lines. Blood was harvested from an infected mouse when parasitemia reached 1-5% and used for up to 2-3 transfections. This infected blood was used to set up a culture using schizont culture medium (50 ml for one mouse or 100 ml for 2-3 mice) and gassed for 5 min. It was cultured 20-22 h at 36.5°C in shaking (50-100 rpm) before schizonts were isolated using a 55% Nycodenz gradient and electroporated using the 4D Nucleofector System (Lonza). For this, 18 µl/transfection of P3 Primary Cell 4D-Nucleofector solution were added to the schizonts pellet. Finally, 20 µl of this mixture were added to 10 µl of each digested plasmid, transferred to an individual well of a 16-well Nucleocuvette™ Strip and pulsed using the Amaxa™ 4D-Nucleofector electroporator, programme FI-115.

6.4.3 Mice injection and selective pressure

Transfected parasites were injected i.v. into BALB/c mice and drug selection was initiated 24 h post-inoculation using pyrimethamine (70 mg/l in drinking tap water). Infections were monitored daily until parasitemia arose, usually on day 4-8 post-transfection. To assess correct integration we performed analytical PCR of gDNA using specific primers, following PlasmoGEM guidelines³³⁹.

6.4.4 Subcloning by limiting dilution

For *P. berghei* subcloning, a Theiler's original mouse was infected with the mutant line and blood was harvested when parasitemia reached ~1%. This infected blood was diluted in PBS by successive dilutions to a final concentration of 2 parasites/100 µL and 100 µL of this dilution were injected i.p. into 10 mice. Parasitemia was checked at day 9 post-infection, expecting 3-4 positive infections.

7 MEASUREMENT OF THE GROWTH RATE

To determine growth rates at different temperatures, cultures were sorbitol-synchronized and parasitemia was determined by flow cytometry and adjusted to 1%. The same uninfected RBCs diluent was used to adjust parasitemia for all cultures, previously ensuring that the hematocrit was the same between the cultures and the diluent by comparing pellet volumes after centrifugation. The resultant parasitemia after

dilution was confirmed by flow cytometry. Cultures were then split in three dishes, each of them placed in a different air-tight chamber and maintained in parallel in incubators at different temperatures (35, 37 and 37.5°C). Temperature in each condition was confirmed and adjusted by a mercury-based thermometer (temperature range: -10 to +50°C) in water. After ~60 h post-synchronization (when all schizonts had already burst), parasitemia at the next cycle was again determined by flow cytometry. Growth rate was calculated as the final parasitemia divided by the initial parasitemia.

8 DETERMINATION OF THE NUMBER OF MEROZOITES PER SCHIZONT

Mature schizonts were Percoll-purified and used to prepare Giemsa-stained smears. We obtained pictures from multiple, high magnification fields (1000x) of each slide by light microscopy (Nikon Eclipse 50i) and manually counted the number of merozoites per schizont on a computer screen. For each condition, a total of 100 fully mature schizonts were used, identified as schizonts with defined and clearly independent merozoites. We excluded schizonts with non-defined or overlapping merozoites, as well as those with multiple hemozoin pigment that likely identify multiple-infected erythrocytes.

9 MEASUREMENT OF THE INTRAERYTHROCYTIC CYCLE LENGTH

To measure the duration of the IDC (at 35°C) in the different parasite lines we used a recently described method based on synchronization to a 1 h age window¹⁵⁶. Cultures containing abundant schizonts (~2-4% parasitemia) were tightly synchronized to 0-1 hpi. Parasitemia was determined by flow cytometry and adjusted to 1.5% by dilution with uninfected erythrocytes maintained at 37°C for the previous 48 h. The same uninfected RBCs diluent was used for all cultures, previously ensuring that the hematocrit was the same between the cultures and the diluent by comparing pellet volumes after centrifugation. Cultures were split in 12 different 100 µl volume cultures in a 96-wells plate and left undisturbed in a hypoxia incubator until they were harvested for flow cytometry analysis. To ensure minimal disturbance of the culture, each 96-wells plate was used only for two time points.

Flow cytometry was used to determine ring (1-4 nuclei) and schizont (>4 nuclei) parasitemias during the whole assay. Initial ring parasitemia was determined at ~20 hpi, and the value of schizont parasitemia at this time point was subtracted from the

subsequent measurements as it corresponded to dead schizonts that were not removed by sorbitol treatment. Ring and schizont parasitemias were determined at 2 h intervals during the period in which most schizont bursting and reinvasion events occurred, from 44-45 hpi to 62-53 hpi. The final time point was at 75-76 hpi, when all viable schizonts had burst.

At each time point, the cumulative number of new rings was calculated as the proportion of rings relative to the total number of rings at the end of the assay. Data was fitted to a sigmoidal dose-response curve with variable slope using GraphPad Prism and used to interpolate the time to generate 50% of new rings in each population.

10 HEAT SHOCK ASSAY

10.1 *P. falciparum* heat shock assay

Two different types of HS assays were performed in this thesis. While one aimed only at determining the HS survival of specific populations, the other aimed to collect samples at different time points.

10.1.1 Synchronization and culture establishment

To only measure HS survival, cultures were first synchronized in parallel using sorbitol lysis. Parasitemia was determined by flow cytometry and adjusted to 1% using the same uninfected RBCs diluent for all the samples. Diluted cultures were then split into two identical petri dishes (~1.6 ml culture in a 10 cm² petri dish), corresponding to HS and control conditions (**Table 16**).

When sample collection was needed during the HS assay, cultures were tightly synchronized to a 0-2 h (reverse transcription quantitative PCR, RT-qPCR) or a 0-5 h (microarray and ATAC-seq) age window. For these experiments, the 10E_Δ*pfap2-hs* line was tightly synchronized 3 h earlier than the other lines but exposed to HS in parallel, to account for its slower IDC progression. For Western blot (WB) analysis, parasites were only sorbitol-synchronized. After sorbitol treatment, parasitemia was determined by flow cytometry and adjusted to either 1% (RT-qPCR and WB) or 2-2.5% (microarray and ATAC-seq). For the dilution, the same uninfected erythrocyte diluent for all the samples, ensuring that the hematocrit was the same between the samples and the diluent. Diluted cultures were then split into several identical petri dishes (~10 ml culture in a 78 cm² petri dish), each of them corresponding to a different time point

and condition. Another culture diluted to 1% was also prepared, from which two identical cultures were established (~1.6 ml culture in a 10 cm² petri dish) to determine HS survival at the end of the assay to confirm that the HS worked well (**Table 16**).

Control and HS-exposed cultures were disposed in independent air-tight incubation chambers and maintained undisturbed at 37°C until HS exposure (or 35 °C in experiments including the *Δpfap2-hs* line). Also, cultures used for sample collection after only 1.5 h of HS were placed in an independent chamber.

		HS sensitivity		WB		RT-qPCR		Microarrays		ATAC-seq	
		37°C	HS	37°C	HS	37°C	HS	37°C	HS	37°C	HS
Synchronization		Sorbitol		Sorbitol		Percoll-Sorbitol (0-2 h)		Percoll-Sorbitol (0-5 h)		Percoll-Sorbitol (0-5 h)	
HS exposure		20-25 h post-Sorb.		20-25 h post-Sorb.		33-35 hpi		30-35 hpi		30-35 hpi	
Established cultures	0 h	-	-	-	-	5-10 *	-	13 #	-	8 #	-
	1.5 h	-	-	-	-	5-10 *	5-10 *	13 #	13 #	-	-
	3 h	-	-	8 *	8 *	5-10 *	5-10 *	13 #	13 #	8 #	8 #
	2 h post	-	-	-	-	5-10 *	5-10 *	13 #	13 #	-	-
	4 h post	-	-	-	-	5-10 *	5-10 *	-	-	-	-
	6.5 h post	-	-	8 *	8 *	-	-	-	-	-	-
	Flow Cytometry	1.6 *	1.6 *	1.6 *	1.6 *	1.6 *	1.6 *	1.6 *	1.6 *	1.6 *	1.6 *

Table 16. Summary of the preparation and sample collection of diverse HS assay. For each assay, the type of synchronization, the specific time point of HS exposure and the culture volume (ml) prepared for collection are specified. Colours stand for different air-tight chambers, such that cultures for control (green), 1.5 h HS exposure (yellow) and 3 h HS exposure (red) conditions were placed in separated chambers. Cultures were either established at 1% (*) or 2-2.5% (#) initial parasitemia. WB, Western blot; RT-qPCR, reverse transcription quantitative PCR.

10.1.2 Heat shock exposure and samples collection

Cultures were exposed to HS when the majority of parasites were at the trophozoite stage. In sorbitol-synchronized cultures, the HS exposure was typically performed 20-25 h after sorbitol lysis, whereas in cultures tightly synchronized to a 0-5 h or 0-2 h age window HS was performed at 30-35 or 33-35 hpi, respectively. As the 10E_Δ*pfap2-hs* line was tightly synchronized 3 h earlier than the other lines, at the time of HS exposure this line was 33-38 hpi. Parasite stage before HS was always checked by a Giemsa-stained smear.

For HS, the full incubation chamber was transferred to an incubator at 41.5 °C for 3 h, and then placed back to 37 or 35 °C. The chamber with the control cultures was always maintained at 37 or 35 °C. The temperature of the incubators was confirmed and

adjusted using a mercury-based thermometer (temperature range: -10 to +50°C) in water.

In some experiments (e.g. WB, RT-qPCR, microarrays and ATAC-seq analysis), samples were collected before (0 h), during (1.5 h) and after (3 h, 2 h post, 4 h post or 6.5 h post) the HS exposure, trying to ensure minimal disturbance of the rest of cultures contained within the air-tight chamber. Giemsa-stained smears were taken for each culture and condition at the time of sample collection.

10.1.3 Heat shock survival

HS survival was calculated for each population by dividing the parasitemia at the next generation of control and HS-exposed cultures, measured by flow cytometry. It was typically measured 60-65 h after sorbitol treatment, a time point that ensures that all parasites had completed the cycle, including parasites subjected to HS that showed delayed progression through the IDC. Giemsa-stained smears were taken for each culture and condition at the time of sample collection for flow cytometry.

10.2 *P. berghei* heat shock assay

10.2.1 Mice bleeding and setting up the culture

Blood was collected from mice by cardiac puncture (~1 ml of blood per mouse) when parasitemia reached ~10%. For each parasite line, 2 ml of collected blood were used to set up a 50 ml culture in schizont culture medium. After homogenization, this culture which was split into two equal 25 ml volumes, in which we added either 25 µl DMSO or Rapamycin to a final concentration of 100 nM (dilution 1:1,000 of the 100 µM stock). For the wild type lines, we set-up a single 25 ml culture, in which we added 25 µl DMSO. Each culture was used to establish identical 12 ml cultures in flasks, corresponding to control and HS conditions, which were gassed and left for ~1 h at 37°C with gentle shaking.

10.2.2 Heat shock exposure, samples collection and mice re-injection

When parasites were mainly at the trophozoite stage, cultures were moved to an incubator set at 40°C for 3 h, while their controls were maintained at 37°C. After HS, 6 ml of each culture (~120 µl of pellet) were used to collect RNA samples, using the TRIzol method. The remaining 5 ml (~100 µl of pellet) were centrifuged for 5 min at 500 x g, and the pellet was resuspended in 120 µl of PBS and split into two 110 µl aliquots. Two mice were injected i.v. with 100 µl of infected blood for each condition.

10.2.3 Heat shock survival

Parasitemia was determined 2 days after re-injection by microscopic analysis of Giemsa-stained smears. HS survival was determined as the parasitemia in mice infected with HS-exposed versus mice infected with control parasites.

11 DETERMINATION OF SENSITIVITY TO OTHER STRESS CONDITIONS

11.1 DHA sensitivity assay

P. falciparum cultures were tightly synchronized (0-5 h of age window) in parallel, except for the 10E_Δ*pfap2-hs* line, which was synchronized 3 h earlier to account for its slower IDC progression. Parasitemia was determined by flow cytometry and adjusted to 1% using the same uninfected erythrocyte diluent for all the samples. Diluted cultures were then split into 6 identical wells (~500 µl culture in a 1.8 cm² 24-well plate), each corresponding to a different DHA concentration. Complete medium with 200 nM DHA was added in one of the cultures and left throughout the assay, corresponding to a control condition where all parasites are killed. Cultures were maintained undisturbed at 35 °C.

These tightly synchronized cultures were exposed to different concentrations of DHA (2.5 nM, 5 nM, 10 nM, 20 nM and 200 nM) either at ring (10-15 hpi) or trophozoite (30-35 hpi) stages. For this, different volumes of an intermediate 2 µM DHA solution (diluted in sterile mqH₂O from a 20 mM DHA stock) were added to the cultures, which were well homogenized with the drug and maintained at 35°C for 3 h. After this period, cultures were transferred to a 1.5 ml tube, centrifuged for 30 s at 1,568 x *g* and supernatants were discarded. To completely remove the drug, pellets were washed using 500 µl of incomplete media centrifuging for 30 s at 1,568 x *g*, and finally resuspended in 500 µl of complete media and placed back in culture. Cultures were then maintained undisturbed at 35°C.

Parasitemia was measured by light microscopy analysis of Giemsa-stained smears at the next cycle (typically ~70-75 h after Percoll-sorbitol synchronization). DHA sensitivity was calculated for each population by dividing the parasitemia at the next generation of each DHA-exposed culture relative to its control.

11.2 DTT and H₂O₂ sensitivity assays

Parasitemia from sorbitol-synchronized cultures was determined by flow cytometry or microscopy and adjusted to 1% using the same uninfected erythrocyte diluent for all the samples. Diluted cultures were then split into several identical petri dishes (~1.6 ml culture in a 10 cm² petri dish), each corresponding to a different dithiothreitol (DTT) or hydrogen peroxide (H₂O₂) condition, and incubated under standard conditions for ~20-25 h until the vast majority of the parasites had reached the trophozoite stage. After this period, several dilutions of both compounds were freshly prepared using complete medium and filter-sterilized. DTT solutions (0.2 mM, 0.5 mM, 1 mM, 2 mM and 4 mM) were prepared from a 1 M DTT stock, whereas H₂O₂ solutions (0.1 mM, 0.5 mM, 1 mM, 5 mM, 10 mM, 50 mM and 10 mM) were prepared by sequential dilution from a 1 M H₂O₂ stock.

For drug exposure (~20-25 h post-sorbitol), media was directly aspirated from cultures, and 1.6 ml of the diluted compounds were added to each culture plate. Cultures were placed again into the air-tight chamber, gassed and incubated in the air-tight chamber at 37°C for either 30 min or 3 h (H₂O₂), or 30 min or 1 h (DTT). After this exposure, medium from the cultures was removed by direct aspiration and replaced by complete medium. Cultures were then maintained undisturbed at 37°C in air-tight chambers.

Stress-survival was calculated for each population dividing by the parasitemia at the next generation of the DTT- or H₂O₂-exposed cultures by the parasitemia of their controls, measured by flow cytometry. It was typically measured 60-65 h after sorbitol treatment, a time point that ensured that all parasites had completed the first cycle. Giemsa-stained smears were taken for each culture and condition at the time of sample collection for flow cytometry.

12 PROTEIN DETECTION ANALYSIS

12.1 Western blot

12.1.1 Total protein extraction

For *P. falciparum* protein extraction, we first purified parasites by saponin lysis, which lyses the RBC membrane but not the parasite plasma membrane. For this, cultures were first transferred to tubes, centrifuged for 5 min at 515 x *g* and the supernatant removed. Pellets were resuspended with 2.2 pellet volumes of cold 0.15% saponin (**Table 17**), mixed and incubated for 5 min on ice. After the incubation, samples were

centrifuged at 1,578 x *g* for 5 min at 4°C, dark supernatants were carefully removed, and remaining pellets were washed twice with 5-10 pellet volumes of cold 1x PBS, centrifuging at 1,578 x *g* for 5 min at 4°C. For the second wash with PBS, samples were transferred to a 1.5 ml tube and centrifuged at 6,800 x *g* for 5 min at 4°C. For total protein extraction, remaining pellets were resuspended with 2x Laemmli sample buffer (Table 17) and PBS to a final volume of 20 pellet volumes, boiled at 95°C for 5 min and frozen at -80°C.

Saponin 0.15% (100 ml)	Laemmli sample buffer 2x (20 ml)
0.15 g Saponin 100 ml PBS [filter-sterilize and store at 4°C]	151.4 mg Tris-HCl [62.5 mM TrisHCl, pH 6.8]* 5 ml Glycerol [25% glycerol] 2 ml 20% SDS [2% SDS] 200 µl 1% bromophenol blue [0.01% bromo. blue] mqH ₂ O to 20 ml [stable for one year at room temperature] * Adjust pH in the Tris-HCl + H ₂ O solution.
Saponin 0.02% (100 ml)	
20 mg Saponin 100 ml PBS [filter-sterilize and store at 4°C]	

Table 17. Saponin and Laemmli sample buffer recipes.

For *P. berghei* protein extraction, blood collected from one mouse was diluted 1:5 in PBS and passed through a Plasmodipur filter (previously activated with PBS) to remove leucocytes. More PBS was added to assist the blood moving through the filter. The flow-through was collected and centrifuged for 5 min at 500 x *g*, the supernatant was discarded, and the pellet was resuspended in 5 pellet volumes of saponin 0.02% (Table 17). After incubation for 20 min on ice, samples were centrifuged at full speed for 5 min at 4°C and the pellet was washed with cold PBS twice (centrifugations at full speed for 5 min at 4°C). Pellets were resuspended in 200 µl RIPA buffer (Table 18) and protease inhibitor cocktail (dilution 1:7) and incubated for 30 min at 4°C in rotation. Afterwards, samples were centrifuged at 4°C for 15 min at full speed, supernatants containing the total protein extract were transferred to a new 1.5 ml tube and pellets were resuspended in 50-100 µl PBS.

RIPA buffer (10 ml)	Lysing buffer (10 ml)	Extracting buffer (10 ml)
0.5 ml Tris HCl pH 8 1 M [50 mM] 0.9 ml NaCl 5 M [450 mM] 1 ml NP-40 10% [1%] 0.5 ml sodium deoxycholate 10% [0.5%] 50 µl SDS 20% [0.1%]	1 ml HEPES pH 7.9 100 mM [10 mM] 1 ml KCl 100 mM [10 mM] 10 µl EDTA 0.1 M [0.1 mM] 10 µl DTT 1 M [1 mM] 1.428 ml Protease inhibitor cocktail 7x * 6.552 ml H ₂ O	2.5 ml HEPES pH 7.9 100 mM [25 mM] 800 µl NaCl 5 M [0.4 M] 20 µl EDTA 0.1 M [0.2 mM] 8 µl EGTA 250 mM [0.2 mM] 10 µl DTT 1 M [1 mM] 2 ml Glycerol 50% [10%] 1.428 ml PIC 7x * 6.552 ml H ₂ O

* Protease inhibitor cocktail was added to the buffer just before use.

Table 18. RIPA buffer recipe for total protein extraction and lysing and extracting buffers for nuclear protein extraction used in *P. berghei* samples.

To specifically isolate nuclear proteins from the saponin pellet, another extraction protocol was followed as previously described³⁴⁷. Briefly, saponin-lysed blood was resuspended in 500 μ l of lysing buffer (**Table 18**), incubated for 15 min on ice, and NP-40 was added to a final concentration of 0.65% and homogenized by vortexing. Samples were centrifuged for 20 s at 14,000 \times g at 4°C, supernatants were recovered, and nuclear pellets were resuspended in 100 μ l of extraction buffer (**Table 18**). After incubation under shaking for 15 min at 4°C, samples were centrifuged for 5 min at 14,000 \times g at 4°C, supernatants were recovered (nuclear protein extract) and pellets were resuspended in 100 μ l PBS. All samples were stored at -80°C.

12.1.2 Polyacrylamide gel preparation

Polyacrylamide gels were prepared in gel cassettes (Mini-PROTEAN® Tetra cell), following manufacturer instructions. The separating gel solution containing 15% polyacrylamide was first prepared (5 ml/gel) (**Table 19**) and transferred to the glass, adding a small layer of isopropanol on the top prior to polymerization. For large molecular weight proteins, 5% polyacrylamide separating gels were prepared. Once the gel had polymerized, isopropanol was removed and the 4% stacking gel solution (~2 ml/gel) was prepared (**Table 19**) and transferred to the glass on top of the separating gel. A 10-well comb was inserted until full polymerization was achieved.

Resolving gel solution (15%, 10 ml) *	Stacking gel solution (4%, 3.75 ml)
2.6 ml Resolving gel buffer 4x 3.750 ml Acrylamide 40%/Bis solution 3.7 ml mqH ₂ O 50 μ l APS 10% 5 μ l TEMED	937.5 μ l Stacking gel buffer 4x 375 μ l Acrylamide 40%/Bis solution 2.394 ml mqH ₂ O 40 μ l APS 10% 4 μ l TEMED
Resolving gel buffer 4x Tris-HCl 1.5 M pH 8.8 (100 ml)	Stacking gel buffer 4x Tris-HCl 1.5 M pH 6.8 (100 ml)
18.16 g Tris [1.5 M Tris] 50 ml 20% SDS [10% SDS] mqH ₂ O to 100 ml pH 8.8 (adjusted with 1 M HCl) [stable at 4°C for one year]	18.16 g Tris [1.5 M Tris] 50 ml 20% SDS [10% SDS] mqH ₂ O to 100 ml pH 6.8 (adjusted with 1 M HCl) [stable for one year at 4°C]
Ammonium persulfate (APS) 10%	
10 mg APS 100 μ l mqH ₂ O	

* For large molecular weight proteins, 5% polyacrylamide gels were prepared.

Table 19. Reagents and recipe to prepare 15% polyacrylamide gels.

12.1.3 SDS-PAGE Electrophoresis

The electrophoresis module (Mini-PROTEAN® Tetra cell), containing the polymerized gels, was assembled and filled with freshly prepared running buffer (**Table 20**). Before loading the gel, samples were diluted using Laemmli sample buffer (**Table 17**) and PBS. β -mercaptoethanol was added to a final concentration of 4% and samples were

boiled at 95°C for 5 min. Samples and the PageRuler™ Plus Prestained Protein Ladder were loaded and the electrophoresis run at 30 V for 30 min, followed by 100 V for 2-3 h for complete resolution.

NuPAGE™ 3-8% Tris-acetate precast gels were also used for large molecular weight proteins. In this case, samples were diluted with NuPAGE™ LDS sample buffer and reducing agent, boiled at 70°C for 10 min or 95°C for 5 min before loading into gel and run for ~4 h at 200 V in a XCell SureLock™ Mini-Cell electrophoresis system with NuPAGE™ Tris-acetate SDS buffer.

Tris-Glycine 5x

15.14 g Tris [125 mM]
71.3 g Glycine [950 mM]
mqH₂O to 1 l
pH 8.3-8.6 (do not adjust)

Running buffer (750 ml)

150 ml Tris-Glycine 5x [25 mM]
596 ml mqH₂O [190 mM]
3.75 ml 20% SDS [0.1%]
pH 8.3-8.6 (do not adjust)

Table 20. Tris-Glycine and running buffer recipes.

12.1.4 Protein transfer

Transfer sandwiches (from the negative to the positive pole: foam pad, filter paper, resolving gel, nitrocellulose membrane, filter paper, foam pad) were assembled using gel holder cassettes (Mini Trans-Blot® module or XCell II™ Blot Module) in a tray with cold transfer buffer (custom-made or NuPAGE®) (**Table 21**). For large molecular weight proteins, different percentage of methanol and SDS were added to the transfer buffer. The assembled transfer cassettes were inserted in the appropriate transfer module filled with cold 1x transfer buffer and run at 100 V for 1-4 h at 4°C or overnight at 30 V at 4°C.

Transfer buffer (1 l)

160 ml Tris-Glycine 5x [80%]
200 ml Methanol [20%] *
640 ml mqH₂O

Transfer buffer (1 l) – Large protein

160 ml Tris-Glycine 5x [80%]
100 ml Methanol [10%] *
5 ml SDS 20% [0.1%]
735 ml mqH₂O
[Transfer buffer adapted for large proteins]

* Methanol was added just before use.

Table 21. Custom-made transfer buffer recipe.

12.1.5 Membrane blocking and blotting

Membranes were blocked for 30 min rolling at room temperature with blocking solution (**Table 22**). Incubations with the primary and secondary antibodies, listed in **Table 23**, were performed either for ≥1 h at room temperature or overnight at 4°C. After each antibody incubation, membranes were washed three times for 5 min rolling at room temperature with Tween-TBS washing solution (**Table 22**).

Blocking solution (10 ml) 0.5 g Milk powder [5%] 10 ml PBS	Antibody solution (10 ml) 2 ml blocking solution [1% milk] 8 ml PBS Diluted antibody
TBS 10x (200 ml) 4.85 g Tris-HCl 1.12 g Tris 16 g NaCl mqH ₂ O to 200 ml pH 7.6	Tween-TBS 1x (250 ml) 25 mL TBS 10x 225 ml mqH ₂ O 250 µl Tween-20

Table 22. Recipe of the solutions used for membrane blocking, antibody incubation and washing.

	Antibody	Animal	WB Dilution	IFA Dilution	Vendor	Ref.
Primary	Anti-HSP70-1	Rabbit	1:10,000-20,000	-	StressMarq Biosciences	SPC-186C
	Anti-HSP70-1, monoclonal	Mouse	1:1,000	-	Kindly provided by J. Przyborsky	
	Anti-HSP70-1, polyclonal	Rabbit	1:2,000	-	Kindly provided by J. Przyborsky	
	Anti-GPA	Mouse	1:400	-	Sigma	G7650
	Anti-3xHA	Rat	1:100	1:1,000	Roche	11867423001
	Anti-H3	Rabbit	1:1,000	-	Cell Sign	9715
Secondary	Anti-GFP	Rabbit	-	1:1,000	Invitrogen	A11122
	Anti-mouse HRP	Goat	1:1,000	-	Sigma	A4416
	Anti-rabbit HRP	Goat	1:5,000	-	Millipore	AP307P
	Anti-rat HRP	Goat	1:500	-	Invitrogen	A10549
	Anti-rabbit Alexa 488	Goat	-	1:1,000	Invitrogen	A11034
Anti-rat Alexa 488	Goat	-	1:2,000	Invitrogen	A11006	

Table 23. Antibodies used for protein detection in western blot (WB) and immunofluorescence assays (IFA).

12.1.6 Signal detection

Pierce™ ECL Western blotting substrate was used for protein detection, incubating membranes for 1 min with the substrate (ratio 1:1 of reagents 1 and 2). Signal detection was carried out on ImageQuant LAS4000 (GE Healthcare) or on x-ray film.

12.1.7 Stripping

Stripping was performed by incubating membranes for 5 min rocking at 37°C with 10 ml of Pierce™ stripping buffer, followed by incubation for 3 min at room temperature and two washes with Tween-TBS for 5 min. Afterwards, membranes were blocked again with the blocking solution, as explained above.

12.2 Immunofluorescence assay

12.2.1 Cell fixation, permeabilization and blocking

Smears were prepared and the regions of interest were delimited with a hydrophobic pen. All steps were performed by directly adding the solution on top of the slide, except for the PBS washes, in which a glass staining jar was used. After fixation with 1% paraformaldehyde (PFA) (Table 24) for 10 min, smears were washed twice in PBS for 10 min shaking (120 rpm) at room temperature. The excess of PBS was decanted and

permeabilization of the cells was performed by adding 0.1% Triton X-100 on the slide and incubating it for 5 min shaking (60 rpm). After two 5 min washes in PBS, slides were blocked shaking (60 rpm) with PBS-3% BSA (**Table 24**) for 30 min at room temperature or overnight at 4°C.

Paraformaldehyde 1% (1.2 ml)	PBS-3% BSA (10 ml)
75 µl PFA 16%	0.45 g BSA
1125 µl PBS	10 ml PBS

Table 24. Recipe of the solutions used for cell fixation and blocking.

12.2.2 Antibody incubation

The primary and secondary antibodies (**Table 23**) were diluted in PBS-3% BSA and centrifuged for 2 min at full speed before using the supernatant. DAPI staining was added in the secondary antibody solution to a final concentration of 5 µg/ml. Incubations with the primary and secondary antibodies were performed under shaking (60 rpm) either for ≥1 h at room temperature or overnight at 4°C. After each antibody incubation, slides were washed five times with PBS for 5 min shaking (120 rpm) at room temperature. Slides were maintained in dark conditions from the addition of the secondary antibody onwards.

12.2.3 Signal detection

The excess of PBS was decanted and a drop of Vectashield solution was added on the slide to mount the cover slip, avoiding the appearance of bubbles. The slide and cover slip were sealed with nail polish and kept at 4°C in dark conditions overnight before observation. The Olympus IX51 microscope was used to detect signal and take high magnification (x1,000) pictures. Images were analysed using Image J software (v.50i)³⁴⁸.

13 WHOLE-GENOME SEQUENCING

13.1 Library preparation and sequencing

To sequence the full genome of control and HS-adapted 3D7-A lines, we used PCR-free whole-genome Illumina sequencing. In brief, RNase-treated gDNA was sheared to ~150-400 bp fragments using a Covaris S220 ultrasonicator, purified using 2.3x AmpurBeadsXP and analysed using an Agilent 2100 Bioanalyzer. For library preparation we used the NEBNext DNA Library Prep Master Mix Set for Illumina in a final reaction volume of 50 µl, using 1.25 µl of indexed TruSeq Illumina adaptors specific for each sample (**Table 25**). Two purification steps were performed with 1.25x AmpurBeadsXP, following manufacturer instructions, and quality was checked by

qPCR. A total of >6 million 150 bp paired reads were obtained for each sample using an Illumina MiSeq sequencing system at the Functional Genomics Service of IDIBAPS.

Name	TruSeq Illumina index sequence	Sample
Index-2	CGATGT	3D7-A rep.1
Index-4	TGACCA	3D7-A rep.2
Index-6	GCCAAT	3D7-A-HS rep.1
Index-12	CTTGTA	3D7-A-HS rep.2

Table 25. TruSeq Illumina index sequences used for whole-genome sequencing.

13.2 Data analysis

Read quality was confirmed using FastQC (v.0.11.2)³⁴⁹ and adaptors were trimmed using Cutadapt (v.1.8)³⁵⁰. Sequence reads were mapped to the *P. falciparum* 3D7 reference genome version 24 (obtained from PlasmoDB³⁵¹) using Bowtie2 (v.2.1.0)³⁵². For the alignment, default values were used except for using the local alignment (--local) algorithm and limiting the maximum fragment length for valid paired-end alignment to 1,000 (-X 1000). Alignment quality was assessed by Qualimap (v.2.1.1)³⁵³. Reads from two sequencing rounds were merged using Picard-tools (v.1.138)³⁵⁴. Variant calling was performed using GATK-UnifiedGenotyper (Genome Analysis Toolkit v.3.4-46³⁵⁵) and following a pipeline based on GATK best practices to identify SNPs and small indels. Multiple mapping reads were not excluded of the analysis (-T PrintReads --read_filter MappingQualityZero). Variants with low calling quality (Phred QUAL<20) and low read depth (DP<10) were filtered out using GATK-VariantFiltration (Genome Analysis Toolkit v.3.4-46), and only variants present in both biological replicates were considered. Differences in SNP/indel frequency between control and HS-adapted lines were calculated for each SNP/indel, and those showing <25% difference in any of the two replicates were filtered out. Integrative Genomics Viewer (v.2.3.66)³⁵⁶ was used to visualize alignments and variants.

14 TRANSCRIPTIONAL ANALYSIS

14.1 Reverse transcription quantitative PCR

14.1.1 DNase treatment

RNA from cultures was obtained using the TRIzol method described above. For each *P. falciparum* sample, 5-20 µg of the purified RNA were treated with DNase in a 100 µl reaction for 10 min at room temperature using the RNase-free DNase I kit instructions. Afterwards, treated RNAs were purified using the RNeasy MinElute cleanup kit, eluted in 16 µl of RNase-free H₂O and stored at -80°C. *P. berghei* samples were treated using

DNA-free™ DNase treatment & Removal reagents following manufacturer instructions, and finally stored at -80°C (**Table 26**).

<i>P. falciparum</i> DNase treatment (100 µl)	<i>P. berghei</i> DNase treatment (33.4 µl)
X µl RNA sample	30 µl RNA sample
10 µl RDD buffer	3.4 µl Buffer 10x
2.5 µl DNase I	1 µl DNase
X µl RNase-free H ₂ O to 100 µl	+ 3 µl DNase inactivation reagent

Table 26. DNase treatment reactions used for *P. falciparum* and *P. berghei* RNA samples.

14.1.2 cDNA synthesis

For *P. falciparum* samples, reverse transcription of 500 ng of DNase-treated RNA was performed using the AMV reverse transcription kit, in a final reaction volume of 10 µl (**Table 27**). Prior to reverse transcription, RNAs were incubated for 10 min at 70°C and 2 min on ice. Reverse transcription reactions were incubated for 10 min at room temperature, 60 min at 42°C, 5 min at 95°C and 5 min on ice. A negative control reaction without the reverse transcriptase enzyme was included in parallel for each sample. Afterwards, samples were diluted in RNase-free H₂O and stored at -20°C.

<i>P. falciparum</i> Reverse transcription (10 µl)	<i>P. berghei</i> Reverse transcription (20 µl)
2 µl MgCl ₂ 25 mM	2 µl RT buffer 10x
1 µl Reverse transcriptase buffer 10x	2 µl RT random primers 10x
1 µl dNTP mixture 10 mM	0.8 µl dNTP mixture 100 mM 25x
0.25 µl Recombinant RNasin ribonuclease inhibitor	1 µl Multiscribe™ Reverse transcriptase
0.3 µl AMV reverse transcriptase (or 0 µl in the negative control)	1 µl RNase inhibitor
0.5 µl Mix oligo(dT)15 and random primers	3.2 µl RNase-free H ₂ O
X µl DNase-treated RNA sample (500 ng)	10 µl DNase-treated RNA sample
X µl RNase-free H ₂ O to 10 µl	

Table 27. Reverse transcription reactions used for *P. falciparum* and *P. berghei* samples.

For *P. berghei* samples, the High capacity cDNA Reverse transcription kit was used to retrotranscribe DNase-treated RNAs. In this case, 10 µl of DNase-treated RNA was mixed with the reverse transcription reaction in a final volume of 20 µl (**Table 27**) and incubated for 10 min at room temperature, 1 h at 37°C and 5 min at 95°C. After this, samples were diluted in RNase-free H₂O and stored at -20°C.

14.1.3 RT-qPCR reaction and thermal cycler conditions

For qPCR analysis we used the Power SYBR Green master mix (**Table 28**) or the Light Cycler® 480 SYBR Green I master (**Table 28**) in a final reaction volume of 10 µl or 20 µl, respectively. The standard curve method was used, using several dilutions (10-0.001 ng/µl) of 3D7-A gDNA for each primer pair. Primers used for RT-qPCR analysis, listed in **Table 36**, were used at a final concentration of 200 or 400 nM. Reactions were placed in 96-well or 384-well reaction plates, sealed with optical adhesive film, vortexed

and spun for 1 min at 2,500 x *g*. The 7900HT fast real-time PCR (Applied Biosystems) or the LightCycler® 480 II (Roche) instruments were used for the amplification. Fluorescence measurements were taken during the extension phase and melt curves were analysed for the presence of multiple amplification peaks or primer dimers.

Unless otherwise indicated, transcript levels were normalized against *serine--tRNA ligase* (PF3D7_0717700), which shows relatively stable expression throughout the IDC. In the case of DTT and H₂O₂ treatment, *actin1* (PF3D7_1246200) was used for normalization, similar to previous studies¹²⁶.

Power SYBR Green master mix	
qPCR reaction (10 µl)	Thermal cycler conditions
5 µl Power SYBR Green PCR master mix 2x 0.04 µl Primer forward 50 µM [200 nM] 0.04 µl Primer reverse 50 µM [200 nM] 2.92 µl mqH ₂ O 2 µl cDNA	<p>HOLDING 95°C, 10 min</p> <p>CYCLING (x40) 95°C, 15 s 57°C, 30 s 60°C, 30 s (measure)</p> <p>MELT CURVE 95°C, 15 s 60°C, 1 min 0.3°C/min increment (measure) 95°C, 15 s (measure)</p>
Light Cycler® 480 SYBR Green I master mix	
qPCR reaction (20 µl)	Thermal cycler conditions
10 µl Light Cycler® 480 SYBR Green I master 2x 0.08 µl Primer forward 100 µM [400 nM] 0.08 µl Primer reverse 100 µM [400 nM] 8.84 µl mqH ₂ O 1 µl cDNA	<p>HOLDING 95°C, 5 min</p> <p>CYCLING (x40) 95°C, 10 s 57°C, 30 s 72°C, 30 s (measure)</p> <p>MELT CURVE 95°C, 5 s 65°C, 1 min 5°C increment (measure) 97°C (measure)</p>

Table 28. Power SYBR green master mix and Light Cycler® 480 SYBR green I master amplification reaction and thermal cycler.

14.2 Microarrays analysis

14.2.1 Microarray design

We used two-colour long oligonucleotide-based custom Agilent microarrays. The microarray design was based on Agilent design AMADID n° 037237^{357,358}, but we modified it by adding new probes for some genes that didn't have any unique probe, and also included probes for some reporter genes (new design AMADID n° 084561). The array was also reannotated to exclude probes that, according to blast analysis, may not recognize any target or recognized multiple transcripts.

14.2.2 cDNA synthesis

RNA from cultures was obtained using the TRIzol method described above, and sample preparation and microarray hybridization were performed essentially as described³⁵⁸. In addition to samples, a common reference pool (used to normalize the microarray data) was also prepared using equal starting amounts of RNA from rings, trophozoites and schizonts obtained from a 3D7-A culture. For reverse transcription, 10 µg of the purified RNA were mixed with 2 µl of oligo-dT/random primer mix to a final volume of 33 µl, incubated at 70°C for 10 min and kept on ice for 10 min. Afterwards, 1.5 µl of aa-dUTP/dNTPs 30x custom-made stock, and 9 µl of 5x RT buffer and 1.5 µl of RT enzyme from the RevertAid H Minus M-MuLV reverse transcriptase kit were added individually to each reaction and incubated for 2 h at 42°C. To each reaction, 10 µl of 0.5 M EDTA pH 8 and 10 µl of 1 M NaOH were added and incubated at 65°C for 15 min (**Table 29**). Afterwards, cDNAs were purified using the MinElute PCR purification kit, eluted in 10 µl of EB buffer (Tris-HCl 10 M pH 8.5) and stored at -80°C.

Reverse transcription	aa-dUTP/dNTPs 30x (113.33 µl)
2 µl oligo-dT/random primer mix	dNTP Set 100 mM:
X µl RNA (10 µg)	34 µl dATP
RNase-free H ₂ O to 33 µl	17 µl dTTP
9 µl 5x RT buffer	17 µl dCTP
1.5 µl aa-dUTP 30x	17 µl dGTP
1.5 µl RT enzyme	17 µl aa-dUTP
10 µl of EDTA 0.5 M pH 8	11.33 µl RNase-free H ₂ O
10 µl of NaOH 1 M	[store at -20°C]

Oligo-dT/random primer mix (100 µl)
26.5 µl oligo-dT 25-mer primer 1 M (200 µg)
73.5 µl random 9-mer primer 1 M (200 µg)
[store at -20°C]

Table 29. Reagents needed for RNA reverse transcription for microarrays analysis.

14.2.3 cDNA labelling

For labelling, 1 µg of cDNA/aa-dUTP was used, in which 2 µl of 0.5 M sodium bicarbonate pH 9 and RNase-free H₂O were added to a final volume of 10 µl. To this reaction, 1 µl of either cyanine dye Cy5 (samples) or Cy3 (reference pool) was added and incubated in the dark for 1-4 h at room temperature (**Table 30**). The labelled cDNA/aa-dUTP was purified using MinElute PCR purification kit, eluting in 12 µl RNase-free H₂O.

Labelling reaction (11 µl)	Cyanine dyes (Cy3 or Cy5)
X µl cDNA/aa-dUTP (1 µg)	40 nmol Cy3 or Cy5 (one dye pellet)
2 µl 0.5 M NaHCO ₃ pH 9	12 µl DMSO
RNase-free H ₂ O to 10 µl	
1 µl Cy3 or Cy5	

Table 30. Cy3/Cy5 cDNA labelling reaction.

14.2.4 Hybridization and washing

The cDNA/aa-dUTP quantity and Cy3/Cy5 labelling was quantified using Nanodrop. Equal amounts of Cy5-labelled (sample) and Cy3-labelled (reference pool) cDNA/aa-dUTP were combined in a 1.5 ml microcentrifuge tube, such that each channel contained 250-1,000 ng of cDNA and 2.5-5 pmol of dye. The total volume was adjusted to 22 μ l, and 5.5 μ l of Agilent 10x GE blocking agent and 27.5 μ l of 2x Hi-RPM hybridization buffer were added for the hybridization reaction (**Table 31**). The solution was hybridized with an Agilent microarray slide using a silicone Agilent gasket in rotation at 12 rpm for ~17 h at 65°C.

After this period, microarray slides were separated from the gasket and washed with freshly prepared washing buffer A for 1 min, washing buffer B for 1 min and acetonitrile for 20 s (**Table 31**).

Hybridization reaction (55 μl) X μ l Cy5-cDNA/aa-dUTP (sample) X μ l Cy3-cDNA/aa-dUTP (reference pool) mqH ₂ O to 22 μ l 5.5 μ l GE blocking agent 10x 27.5 μ l Hi-RPM hybridization buffer 2x	SSPE 20x (1 l) 175.3 g NaCl 27.6 g NaH ₂ PO ₄ 7.4 g EDTA mqH ₂ O to 1 l pH 7.4 (adjusted with ~24 ml of 10 M NaOH) [sterilize and store at room temperature]
Washing buffer A (1 l) 300 ml SSPE 20x 700 ml mqH ₂ O 0.25 ml 20% N-laurylsarcosine [store for two days at room temperature]	Washing buffer B (1 l) 3 ml SSPE 20x 997 ml mqH ₂ O 0.25 ml 20% N-laurylsarcosine [store for two days at room temperature]

Table 31. Hybridization reaction and washing buffers.

14.2.5 Scanning

Microarray images were obtained using a DNA Microarray Scanner (n° G2505C, Agilent Technologies) located in a low ozone area, and initial data processing was performed using the GE2 _1105_Oct12 extraction protocol in Agilent Feature Extraction 11.5.1.1 software.

14.2.6 Data analysis

Agilent microarray data was analysed using Bioconductor in an R environment (R version 3.5.3). For each individual microarray, we calculated Cy3 and Cy5 background signal as the median of the 100 lowest signal probes for each channel, and probes with both Cy3 and Cy5 signals below three times the array background were excluded. Gene level $\log_2(\text{Cy5/Cy3})$ values, statistical estimation of parasite age³⁵⁹ and estimation of average fold-change (AFC) expression differences across a time interval (for the comparison between parasite lines in the absence of HS) were performed as

described¹⁵⁶. Expression fold-change (FC) upon HS was calculated by dividing, for each gene and time point, the $\log_2(\text{Cy5/Cy3})$ in the HS-exposed sample by the $\log_2(\text{Cy5/Cy3})$ in the control sample at the same parasite age, calculated using linear interpolation in the $\log_2(\text{Cy5/Cy3})$ vs estimated age plot. Visual inspection was used to exclude from further analysis genes with apparent artefacts. Genes missing data for ≥ 2 time points (or ≥ 1 for the comparison across a time interval), or with values within the lowest 15th percentile of expression intensity (Cy5 sample channel) in all samples, were also excluded from further analysis.

To assess the level of similarity to a reference nonstressed transcriptome (HB3 line) with high temporal resolution⁵⁸ we calculated the Pearson correlation between each sample and the time point with which it has higher similarity. Heatmaps and hierarchical clustering based on Spearman or Pearson correlation were generated using Multiple Experiment Viewer (MeV) 4.9³⁶⁰. Expression trend plots for each cluster were generated using ggplot2, with LOESS smoothing, and Venn diagrams using the eulerr package (both in an R environment). Motif analysis (5 to 8 bp) was performed using MEME 5.0.3³⁶¹ software. Functional enrichment analysis using gene ontology (GO) terms annotated in PlasmoDB³⁵¹ version 43 was performed using Ontologizer 2.1 software³⁶² with the topology-elim method³⁶³. Gene set enrichment analysis (GSEA) was performed using GSEA v3.0 Preranked³⁶⁴, using the following gene sets: GO terms, MetaCyc and KEGG functional groups as in PlasmoDB³⁵¹ version 43, Malaria Parasite Metabolic Pathways (MPMP)³⁶⁵, gene families¹⁵⁶, and other gene lists corresponding to the functional groups chaperones³¹¹, transcription factors⁶⁶ and ABC transporters³⁶⁶.

15 ATAC-seq

15.1 Nuclei preparation

Tightly synchronized 10E, 10G and 10E_Δ*pfap2-hs* cultures were used to collect ring parasites (10-15 hpi) maintained under control conditions, and trophozoites after HS exposure (33-38 hpi) or maintained under control conditions. Parallel to ATAC-seq sample collection, RNA samples were harvested using TRIzol method. At these specific timepoints, parasitemia was determined from Giemsa-stained smears and the volume of culture containing 10^7 (rings) or 5×10^6 (trophozoites) parasites was harvested in a 1.5 ml tube and kept on ice during the whole processing. ATAC-seq samples were prepared in collaboration with Dr. Gómez-Díaz's group, approximately as described^{112,367}. Samples were first centrifuged at $564 \times g$ for 3 min in a

microcentrifuge, the supernatant was discarded and 10 volumes of saponin 0.15% (**Table 17**) were added to the pellet. After 5 min incubation on ice, it was centrifuged at 1,700 x *g* for 3 min at 4°C, the supernatant was discarded and the remaining pellet was washed twice with 1 ml of cold PBS, centrifuging for 5 min at 1,700 x *g* at 4°C and discarding the supernatant.

The parasites pellet was resuspended with 50 µl of freshly prepared lysis buffer (**Table 32**) and well homogenized to permeabilize membranes. Immediately after lysis, nuclei were spun for 10 min at 660 x *g* at 4°C and the supernatant was removed.

ATAC-seq lysis buffer (1 ml)
5 µl Tris-HCl 2 M pH 7.4 [10 mM]
2.5 µl NaCl 4 M [10 mM]
3 µl MgCl ₂ 1 M [3 mM]
10 µl Igepal CA-630 10% [0.1%]
979.5 µl mqH ₂ O

Table 32. ATAC-seq lysis buffer recipe.

15.2 Transposition

Immediately following the nuclei preparation, the pellet was resuspended in 50 µl of transposition reaction mix (**Table 33**), gently pipetted up and down to resuspend well and incubated for 30 min at 37°C. Directly following transposition, transposed DNA was purified using the Qiagen MiniElute kit following manufacturer instructions, eluted in 10 µl elution buffer and stored at -20°C. As a control, 50 ng of gDNA were resuspended in 50 µl of transposition reaction and incubated for 5 min at 55°C for transposition.

Transposition reaction (50 µl)	TD buffer 2x (10 ml)
25 µl TD buffer 2x	0.2 µl Tris 1 M [20 mM]
1.25 µl Tn5 transposase	0.1 ml MgCl ₂ 1 M [10 mM]
23.75 µl mqH ₂ O	1 ml Dymethylformamide [20 %]
	mqH ₂ O to 10 ml
	pH 7.6 (adjust with acetic acid)
	[sterilize and store at -20°C for 6 months]

Table 33. Tn5 transposition reaction.

15.3 Library preparation

Libraries of transposed DNA fragments were prepared by PCR amplification (PCR-2) using KAPA HiFi polymerase and Nextera-indexed primers (**Table 37**) in a 50 µl reaction, approximately as previously described^{112,367}. To reduce GC and size bias in PCR, the optimal number of PCR cycles was determined using quantitative PCR (qPCR-1). To do this, we amplified the full libraries for 25 cycles in a final volume reaction of 10 µl and determined the number of cycles that allowed amplification before saturation, equal in all samples. In this experiment, samples and gDNA control libraries were amplified for 9 or 6 cycles, respectively.

Libraries were then purified using the Qiagen PCR cleanup kit, eluted in 20 µl elution buffer (10 mM Tris pH 8) and stored at -20°C. A small aliquot was run on a 1% agarose gel electrophoresis and analysed in a 4200 TapeStation System (Agilent Technologies) to confirm the correct concentration and library size, expecting a distribution between 40 bp to 1 kb with a predominant size of ~120 bp (mononucleosomes), ~260 bp (dinucleosomes) and ~390 bp (trinucleosomes).

qPCR-1 KAPA HiFi hot-start reaction (10 µl)	PCR-2 KAPA HiFi hot-start reaction (50 µl)
5 µl KAPA HiFi mix hot-start 2x	25 µl KAPA HiFi mix hot-start 2x
1 µl SYBR Green 10x	1.25 µl Primer forward (Ad_F1) 25 µM
0.6 µl Primer forward (Ad_F1) 2.5 µM	1.25 µl Primer reverse (Ad_R) 25 µM
0.6 µl Primer reverse (Ad_R) 2.5 µM	9.5 µl Transposed DNA
0.5 µl Transposed DNA	13 µl mqH ₂ O
2.3 µl mqH ₂ O	

KAPA HiFi thermal cycle	
DENATURALIZATION	72°C, 5 min
HOT START	98°C, 45 s
CYCLING	98 °C, 10 s
(x25 or x6-9*)	63°C, 30 s
	72°C, 30 s
FINAL ELONGATION**	72°C, 1 min

* In PCR-1, 25 cycles were used; in PCR-2, 6 or 9 cycles were used.

** Final elongation step was not added in PCR-1.

Table 34. ATAC-seq library preparation reaction.

15.4 Sequencing and data analysis

ATAC-seq libraries were sequenced using Illumina HiSeq2000 sequencer at the Genomics Unit of CRG and ~30 M of 2 x 50 bp paired-end sequencing reads were obtained per sample.

Data analysis was performed in collaboration with Dr. Gómez-Díaz's group, as previously described¹¹². Briefly, Illumina reads were assessed for quality control using FastQC (v.0.11.5)³⁴⁹, trimmed (10 bases from each 3' end) and aligned to the PlasmoDB³⁵¹ *P. falciparum* 3D7 reference genome 42 using Bowtie2 (v.2.3.1)³⁵². For the alignment, default values were used, but suppressing reads that failed the alignment (--no-unal), considering only paired alignment (--no-mixed) and restricting fragment length to 2,000 (-X 2000). Samtools (v.1.4)³⁶⁸ was used to sort, deduplicate and filter read alignments with MAPQ score<10. Qualimap (v.2.2.1)³⁵³ was used to confirm the quality of alignment and QC ataqv (v.0.9.4)³⁶⁹ and Picard Tools (v.2.2.2)³⁵⁴ to plot the distribution of paired-end sequencing fragment sizes.

To perform the nucleosome-free ATAC-seq analysis, nucleosome-free fragments (>130 bp) were extracted using Samtools (v.1.9). We performed a first-round of peak-

calling for each sample using gDNA (10G gDNA) as control using MACS2 (v2.1.2)³⁷⁰ software using the module “callpeak” (parameters: *-g 2.3e+7 -f BAMPE --nomodel --extsize 117 --fe-cutoff 1.5 --broad*). Differential peaks were called using the same module and parameters using one sample as “treatment” and another as “control”. Only differential peaks overlapping a peak in the first peak-calling round and with *qval*<10 were kept for further analysis. Finally, the identified differential peaks were manually curated using Integrative Genomics Viewer (v.2.3.66)³⁵⁶. For visualization, samples were normalized by input against gDNA (10G gDNA) using the MACS2 “callpeak” module (parameters: *-g 2.41e7 --keep-dup all -q 0.01 -f BAMPE -B*) and signal tracks were generated using MACS2 “bdgcmp” module (parameters: *-m ppois*).

16 PRIMERS

16.1 Primers used for cloning

ID	Name	Sequence	Use
C1	ap2hs_sgRNA5'_InF_+885_F	TAAGTATATAATATTCATTCTCAAGAATAA TGTAGTTTTAGAGCTAGAA	sgRNA-5' (ΔPfAP2-HS)
C2	ap2hs_sgRNA5'_InF_+885_R	TTCTAGCTCTAAACTACATTATTCTTGAGA AATGAATATTATATACTTA	sgRNA-5' (ΔPfAP2-HS)
C3	ap2hs_sgRNA3'_InF_+11505_F	TAAGTATATAATATTGAAAGCTAGCTATTGA ATACGTTTTAGAGCTAGAA	sgRNA-3' (ΔPfAP2-HS)
C4	ap2hs_sgRNA3'_InF_+11505_R	TTCTAGCTCTAAACGTATTCAATAGCTAG CTTCAATATTATATACTTA	sgRNA-3' (ΔPfAP2-HS)
C5	HR1_ap2hs_-2_SpeI_F ETF	tggtgtactagtTAATGCAAAATAAAAGTGAATTC	HR1 (ΔPfAP2-HS)
C6	HR1_ap2hs_+808_AflII_R	tggtgtcttaagTAAAGTTTGAGGGATTTAATAG	HR1 (ΔPfAP2-HS) & PCR check (eYFP::PfAP2-HS)
C7	HR2_ap2hs_+11520_EcoRI_F	tggtgtgaattcACAATTAAGGCTTTCCATCGT	HR2 (ΔPfAP2-HS); Sanger sequencing check (PfAP2-HS::DD).
C8	HR2_ap2hs_end_+490_SacII_NcoI_R	tggtgtccatggccgcggATTGAGTAAATCAAATA AGGACA	HR2 (ΔPfAP2-HS)
C9	HR_ap2hs_+9551_NotI_F	tggtgtgcggccgcGTAGCGAAAATAAACAGAAC GC	HR (PfAP2-HS::DD)
C10	HR_ap2hs_+11574_XhoI_R	tggtgtctcgagTAATTTTTCTGTTTTTTTTTTAA ATTAT	HR (PfAP2-HS::DD)
C11	ap2hs_sgRNA-C_InF_+11527_F	TAAGTATATAATATTGGAAAGGTGGATACA ATTAAGTTTTAGAGCTAGAA	sgRNA-C (PfAP2-HS::eYFP & PfAP2-HS::3xHA)
C12	ap2hs_sgRNA-C_InF_+11527_R	TTCTAGCTCTAAACTTAATTGTATCCACCT TTCCAATATTATATACTTA	sgRNA-C (PfAP2-HS::eYFP & PfAP2-HS::3xHA)
C13	InF_ap2hs_HR1.1_SpeI_+10963_F	gcggggaggactagtCGTTTCAAGACACTATAA GC	HR1 (PfAP2-HS::eYFP)
C14	InF_ap2hs_HR1.1_+11499_sgrNAMut_R	TgAgcTGgATCCACCTTCCctgtattc	HR1 (PfAP2-HS::eYFP)
C15	InF_ap2hs_HR1.2_sgRNAMut_PAM_3'_mut_BglII_F	ggtggatCcaGcTCaAGGCaTTtCaCGaCTcAAc AAccTAAAgAAgAAgACtGagAAgcTAagatctgca gcagca	HR1 (PfAP2-HS::eYFP)
C16	InF_ap2hs_HR1.2_sgRNAMut_PAM_3'_mut_BglII_R	tgctgtctcagatctTAgcTTctCaGTcTtCTTTAg gTTgTTgAGtCGgTGaAAtGCCTtGaGCTgGatcc acc	HR1 (PfAP2-HS::eYFP)
C17	HR2_ap2hs_+11577_XhoI_F	ttatcgctcgagAAAAATAATATTATATCTATATA TAATA	HR2, endog. term. (PfAP2-HS::eYFP)
C18	HR2_ap2hs_+12143_AatII_R	cgtaagacgtcTTCTTATTAGTATTATTATCATC C	HR2, endog. term. (PfAP2-HS::eYFP)

ID	Name	Sequence	Use
C19	pHHL_inv_x3HA_+5150_BglII_F	tggtgtagatctACTAGTCCCCGGGCTGCAG	3xHA (PfAP2-HS::3xHA); Sanger sequencing check (PfAP2-HS::3xHA)
C20	pHHL_inv_x3HA_+5254_XhoI_R	tggtgtctcgagTTATTAAGCGTAGTC	3xHA (PfAP2-HS::3xHA)
C21	lnF_HR2(EX)_ap2hs_+11789_EcoRI_F	catcaaatagaattcCCCACAGACATATAGACATA T	HR2, exog. term. (PfAP2-HS::3xHA)
C22	lnF_HR2(EX)_ap2hs_+12143_AatII_R	GTGCCACCTgacgtcTTCTTATTAGTATTATTA TCATCC	HR2, exog. term. (PfAP2-HS::3xHA)
C23	lnF_sgRNA-N_ap2hs_F_+73bp	ttctagctctaaacTGTCATAGAAATGAATACAta atattataactta	sgRNA-N (eYFP::PfAP2-HS)
C24	lnF_sgRNA-N_ap2hs_R_+73bp	taagtataataatattATGTATTCATTTCTATGACAgtt ttagagctagaa	sgRNA-N (eYFP::PfAP2-HS)
C25	HR1_ap2hs_F_-366_SacII	tggtgtccgaggTGATGTTAAATAAAATTATACATA G	HR1 (eYFP::PfAP2-HS); PCR check (eYFP::PfAP2-HS)
C26	HR1_ap2hs_R_0_NcoI	tggtgtccatggTATTATATTATTTAAAACCTTTTTG G	HR1 (eYFP::PfAP2-HS)
C27	HR2.1_ap2hs_F_+88_Shield mut	CCtTGcCATAGAAAcGAgTACATtaataatcaacat aaaaatg	HR2 (eYFP::PfAP2-HS)
C28	HR2.1_ap2hs_R_+767_EcoRI	tggtgtgaattcCACCATGTCATGCTTATTTAC	HR2 (eYFP::PfAP2-HS)
C29	HR2.2_ap2hs_F_+3/+90_Shield mut_SpeI	tggtgtactagtCAAAAcAAGAGTGAgTTtAAAGT ACtAAcAGTAAgGAgTTTTATCAAGAcGAgTA TGAtAAcGTaCCtTGcCATAGAAAcGAgTAC	HR2 (eYFP::PfAP2-HS)
C30	HR2.2_ap2hs_R_+767_EcoRI	tggtgtgaattcCACCATGTC	HR2 (eYFP::PfAP2-HS)
C31	lnF_eYFP_F_+atg	TTAAATAATAATAAtgGTGAGCAAGGGCG AGGAG	eYFP (eYFP::PfAP2-HS)
C32	lnF_eYFP_R	cTCACTcTTgTTTTGCTTGACAGCTCGTCC ATGC	eYFP (eYFP::PfAP2-HS)
C33	hsp70-1_-2096_F_Inf	AATGTCGTCCCAGAATTTCTGTTATAAATA AGAGGC	hsp70-1 promoter (0Gbox_TdT, 1Gbox_TdT and 2Gbox_TdT)
C34	hsp70-1_-0_R_Inf	GCCCTTGCTCACCATTTTTCTTAATTCTTT TG	hsp70-1 promoter (0Gbox_TdT, 1Gbox_TdT and 2Gbox_TdT)
C35	hsp70-1_-1109_1Gbox_Rint_Inf	tattaaCATTTGCCCCCTTCTGTTT	hsp70-1 promoter (1Gbox_TdT)
C36	hsp70-1_-1102_1Gbox_Fint_Inf	GGCGAAATGttaataCATTTTTGGGATTTTTAT TTGG	hsp70-1 promoter (1Gbox_TdT)
C37	hsp70-1_-1121_0Gbox_Rint_Inf	tattaaCATTTCaatataTCTGTTTTTTTTTTTCC TACC	hsp70-1 promoter (0Gbox_TdT)
C38	hsp70-1_-1102_0Gbox_Fint_Inf	attGAAATGttaataCATTTTTGGGATTTTTATTT GG	hsp70-1 promoter (0Gbox_TdT)
C39	Rec166-RecUp	ttaataacaacacaactcttacttcatatgatgatttaattccctg gtccgctactcgactataga	RecUp (Rec166)
C40	Rec166-RecDown	aaataaaaaataaaaaatattaagaggaaataaataatcc catagaatGTAATTCGTGCGCGTCAGagacggc gttaaggcgcataacgataccac	RecDown (Rec166)
C41	ap2hs_-94_F	CAGTTGATGATTACATCTCTG	PCR check (Δ PfAP2-HS); Sanger sequencing check (eYFP::PfAP2-HS)
C42	ap2hs_end_+718_R	TTCATCACTTGTTAAGCATCC	PCR check (Δ PfAP2-HS); Sanger sequencing check (PfAP2-HS::3xHA)
C43	ap2hs_+9284_F	TTTTCCAGTAAATGATTATGG	PCR check (Δ PfAP2-HS, PfAP2-HS::DD & PfAP2-HS::3xHA); Sanger sequencing check (Δ PfAP2-HS)
C44	ap2hs_+10399_F	AGAAATGAACAAAACATATTGGG	PCR check (PfAP2-HS::eYFP)
C45	ap2hs_end_+233_R	ATATGTCTATATGTCTGTGGG	PCR check (Δ PfAP2-HS, PfAP2-HS::DD, PfAP2-HS::eYFP & PfAP2-HS::3xHA); Sanger sequencing check (Δ PfAP2-HS, PfAP2-HS::3xHA, PfAP2-HS::eYFP)
C46	ap2hs_+11520_F	TGGTGTGAATTCACAATTAAGGCTTTCCA TCGT	Sanger sequencing check (PfAP2-HS::DD)
C47	hsp70-1_-1220	TATAGATACCTATAGAAACATGC	Sanger sequencing check (0Gbox_TdT, 1Gbox_TdT and 2Gbox_TdT)
C48	LISP1_+5420_F	TATTTTATTACAATATACAAATACG	PCR check (0Gbox_TdT, 1Gbox_TdT and 2Gbox_TdT)
C49	LISP1_+6006_R	AGTATACCCAGGAGTGGATAA	PCR check (0Gbox_TdT, 1Gbox_TdT and 2Gbox_TdT)

ID	Name	Sequence	Use
C50	rec166_QCR1	tcctgtctacatctatgggcgt	PCR check (Rec166)
C51	rec166_QCR2	tggtttgaaagagccagagca	PCR check (Rec166)
C52	rec166_GT	cccaacaagaatgggtgtca	PCR check (Rec166)
C53	PbGEM-646603_QCR1	tggaatagaacacaggaaa	PCR check (PbGEM-646603 & PbGEM-060890)
C54	PbGEM-646603_QCR2	tcgattgagcatgcttcacgt	PCR check (PbGEM-646603 & PbGEM-060890)
C55	PbGEM-646603_GT	tcggacaagcagaccctaaa	PCR check (PbGEM-646603 & PbGEM-060890)
C56	Generic_GW1	catactagccatttatgtg	PCR check (Rec166)
C57	Generic_GW2	ctttggtgacagatactac	PCR check (PbGEM-646603 & PbGEM-060890)

Table 35. Primers used for cloning or to check correct integration in the genome (by PCR amplification or Sanger sequencing).

16.2 Primers used for qPCR analysis

ID	Name	Sequence
Q1	hsp70-1_+1155_F	TGCAGCTGTACAAGCAGCC
Q2	hsp70-1_+1315_R	GACTCTTTTTAGCAGGTATGG
Q3	hsp90_+1860_F	ATCAGAATTTGGATGGTCCGC
Q4	hsp90_+1989_R	TGATATAATTGGGTGACGAGC
Q5	hsp110c_+1402_F	AAAGGACACATTAACCTTACAGC
Q6	hsp110c_+1543_R	AAAAGGTGGTCATAACGTGGG
Q7	hsp70-3_+1521_F	AGTTACCTTTGATGTTGATGCC
Q8	hsp70-3_+1640_R	TCAATTTCTTCTTGCTTAAACC
Q9	pfap2-hs_F_+10399_F	AGAAATGAACAAAACATATTGGG
Q10	pfap2-hs_R_+10510_R	TTATATTTGTTATAGGTTCTCCTC
Q11	pfUCE_F*	GGTGTAGTGGCTACCAATAGGA
Q12	pfUCE_R*	GTACCACCTCCCATGGAGTA
Q13	PF3D7_1421800_+217_F	GTTGATGATAATGTGAAAACCG
Q14	PF3D7_1421800_+350_R	TATAACGTGTGAAATTCAATATCC
Q15	PF3D7_0303600_+49_F	ACAGCTGAATACGAAAAGTACG
Q16	PF3D7_0303600_+190_R	CACAGTATTTACACCATGAAGC
Q17	PF3D7_1469000_+329_F	GTGTAGTAGTAGAATGCTTAGC
Q18	PF3D7_1469000_+467_R	ATTTGGAATTTACCATATCTCC
Q19	PF3D7_1474700_+1280_F	AATGTCTTGAATATGATGAAAAGG
Q20	PF3D7_1474700_+1436_R	TTATTTTGTATGAAATTAGGATTGG
Q21	PF3D7_0404500_+276_F	TACTACGGCAAAAACCTCACCC
Q22	PF3D7_0404500_+413_R	TTTAATCTGTTTTCGTTCGTACC
Q23	PF3D7_0525000_+1107_F	GTGTAACCAAGGGAATGAAGC
Q24	PF3D7_0525000_+1237_R	TATTGCTATGCATATTGCTATGC
Q25	PF3D7_1201100_+2348_F	ATAATAATAAGAATGGATGTGCG
Q26	PF3D7_1201100_+2514_R	TGACATTGGTCTTTAATCTCC
Q27	PF3D7_0702200_+825_F	ATTTGTGGTAATCATTTTCCG
Q28	PF3D7_0702200_+966_R	AATATCTGAAAAGCAAACCTGACC
Q29	PF3D7_0215300_+852_F	TGATGACGTATCAAGTGTCCC
Q30	PF3D7_0215300_+975_R	ATTACTTAACATAACACCTTTAGG
Q31	PF3D7_1246200_+823_F	TCCACACAACACTTTCAACTC
Q32	PF3D7_1246200_+958_R	CATGGTTGATGGTGAAGGG
Q33	TdTomato_+726_F	TCCGAGGACAACAACATGGC
Q34	TdTomato_+879_R	CTTGGTCACCTTCAGCTTGG
Q35	PBANKA_0711900_+1138_F	GCTGTTGCATATGGTGCTGC
Q36	PBANKA_0711900_+1273_R	ATTTAGTCATAACACCACCTGC
Q37	PBANKA_0615400_+392_F	TGCGAACATGGGGAGAATGC
Q38	PBANKA_0615400_+510_R	ATTTTGTCCATCATTATTGTTACC
Q39	PF07_0073_F (Serine tRNA ligase)**	AAGTAGCAGGTCATCGTGTT
Q40	PF07_0073_R (Serine tRNA ligase)**	TTCCGGCACATTTCCATAA
Q41	RhopH2_P2F**	TGTTGCTGTCCATATTTAGTTTT
Q42	RhopH2_P2R**	AATATATCGCTACATAAATTCGT
Q43	PFL2215w_+823_F (actin I)	TCCACACAACACTTTCAACTC
Q44	PFL2215w_+958_R (actin I)	CATGGTTGATGGTGAAGGG

* PfUCE primers were previously designed by Aguilar et al.³⁷¹

** Previously designed by Crowley, V. M. et al.³³⁸

Table 36. Primers used for RT-qPCR transcriptional analysis.

16.3 ATAC-seq Nextera-indexed primers

ID	Sequence	Use
Ad_F1	AATGATACGGCGACCACCGAGATCTACACTCGTCGGCAGCGTCAGATGTG	All
Ad_R2.1	CAAGCAGAAGACGGGCATACGAGATTCGCCTTAGTCTCGTGGGCTCGGAGATGT	10E-R
Ad_R2.2	CAAGCAGAAGACGGGCATACGAGATCTAGTACGGTCTCGTGGGCTCGGAGATGT	10G-R
Ad_R2.3	CAAGCAGAAGACGGGCATACGAGATTTCTGCCTGTCTCGTGGGCTCGGAGATGT	10E-gDNA
Ad_R2.4	CAAGCAGAAGACGGGCATACGAGATGCTCAGGAGTCTCGTGGGCTCGGAGATGT	10E-N
Ad_R2.5	CAAGCAGAAGACGGGCATACGAGATAGGAGTCCGTCTCGTGGGCTCGGAGATGT	10G-N
Ad_R2.6	CAAGCAGAAGACGGGCATACGAGATCATGCCTAGTCTCGTGGGCTCGGAGATGT	EKO-N
Ad_R2.7	CAAGCAGAAGACGGGCATACGAGATGTAGAGAGGTCTCGTGGGCTCGGAGATGT	10E-HS
Ad_R2.8	CAAGCAGAAGACGGGCATACGAGATCCTCTCTGGTCTCGTGGGCTCGGAGATGT	10G-HS
Ad_R2.9	CAAGCAGAAGACGGGCATACGAGATAGCGTAGCGTCTCGTGGGCTCGGAGATGT	EKO-HS
Ad2.10	CAAGCAGAAGACGGGCATACGAGATCAGCCTCGGTCTCGTGGGCTCGGAGATGT	10G-gDNA
Ad2.11	CAAGCAGAAGACGGGCATACGAGATTGCCTCTTGTCTCGTGGGCTCGGAGATGT	EKO-R

Table 37. Indexed primers used for ATAC-seq library preparation.

17 GENERAL RECIPES

CaCl₂ 2 M (100 ml) 29.4 g CaCl ₂ mqH ₂ O to 100ml	DHA 20 mM (5 ml) 28,435 mg DHA mqH ₂ O to 5 ml
DTT 1 M (10 ml) 1.5 g DTT mqH ₂ O to 10 ml [stored at -20°C]	EDTA 0.1 M (100 ml) 3,772 g EDTA disodium salt dihydrate mqH ₂ O to 100 ml pH 8 (adjusted with NaOH pellets)
EDTA 0.5 M pH 8 (100 ml) 18.61 g EDTA disodium salt dihydrate mqH ₂ O to 100 ml pH 8 (adjusted with ~2 g of NaOH pellets)	EGTA 250 mM pH 8 (100 ml) 9.5 g EGTA mqH ₂ O to 100ml pH 8 (adjusted with NaOH pellets)
H₂O₂ 1 M (10 ml) 1 ml H ₂ O ₂ 30% w/w 8.79 ml complete medium [freshly prepared before use]	Hepes 250 mM/EGTA 20 mM pH 7.6 (100 ml) 5.96 g Hepes 0.76 g EGTA pH 7.6 (adjusted with ~1.4 ml of 10 M KOH) mqH ₂ O to 100ml
Hepes 100 mM pH 7.9 (100 ml) 2,383 g Hepes pH 7.9 (adjusted with NaOH pellets) mqH ₂ O to 100 ml	Igepal 10% (10 ml) 10 ml Igepal CA-630 90 ml mqH ₂ O
KH₂PO₄ 1 M (100 ml) 13.61 g KH ₂ PO ₄ mqH ₂ O to 100 ml	K₂HPO₄/KH₂PO₄ 1 M pH 7.6 (10 ml) 8.66 ml 1 M K ₂ HPO ₄ 1.34 ml 1 M KH ₂ PO ₄ mqH ₂ O to 10 ml pH 7.6
KCl 100 mM (100 ml) 0.745 g KCl mqH ₂ O to 100ml	KCl 2 M (100 ml) 14.91 g KCl mqH ₂ O to 100ml
1 M K₂HPO₄/KH₂PO₄ pH 7.6 (10 ml) 8.66 ml 1 M K ₂ HPO ₄ 1.34 ml 1 M KH ₂ PO ₄ mqH ₂ O to 10 ml pH 7.6	KOH 10 M (10 ml) 5.61 g KOH mqH ₂ O to 10 ml
MgCl₂ 1 M (100 ml) 9.52 g MgCl ₂ mqH ₂ O to 100 ml	NaAc 3 M pH 5.2 (10 ml) 2.46 g NaAc anhydrous mqH ₂ O to 10 ml pH 5.2 (adjusted with acetic acid)

NaCl 2 M (10 ml) 1.169 g NaCl mqH ₂ O to 10 ml	NaCl 4 M (100 ml) 23.376 g NaCl mqH ₂ O to 100 ml
NaCl 5 M (100 ml) 29,22 g NaCl mqH ₂ O to 100 ml	NaHCO₃ 0.5 M pH 9 (100 ml) 4.2 g NaHCO ₃ mqH ₂ O to 100 ml
NaHCO₃ 1.2 M (100 ml) 10,08 g NaHCO ₃ mqH ₂ O to 100 ml	NaOH 10 M (100 ml) 40 g NaOH mqH ₂ O to 100 ml
NaOH 1 M (100 ml) 4 g NaOH mqH ₂ O to 100 ml	Rapamycin 4 mg/ml (2.5 ml) 10 mg Rapamycin 2.5 ml DMA
Rapamycin 100 µM (20 ml) 1.83 mg Rapamycin 20 ml DMSO	SDS 18% (10 ml) 9 ml 20% SDS 1 ml mqH ₂ O
Syto11 0.5 mM (2,600 µl) 260 µl SYTO11 1mM 2,340 µl DMSO	Tris 1 M (100 ml) 12,114 g Tris mqH ₂ O to 100 ml
Tris 5 mM pH 8 (50 ml) 0,3 g Tris base mqH ₂ O to 50 ml pH 8 (adjusted with HCl)	Tris-HCl 2 M pH 7.4 (100 ml) 24.228 g Tris mqH ₂ O to 100 ml pH 7.4 (adjusted with HCl)
WR99210 20 mM (1 ml) 8.6232 mg WR99210 1 ml DMSO [stored at -80°C]	

Table 38. General recipes.



RESULTS

1 PREVIOUS RELEVANT RESULTS

The project presented in this PhD thesis is based on previously published and unpublished results, including the generation of 3D7-A lines adapted to HS by Rovira-Graells et al.¹⁵⁶ and the transcriptional analysis of these lines by the Dr. Cortés' group in collaboration with the Dr. Bozdech's team (unpublished results). Also, in my MSc thesis we optimized the HS assay and studied a putative epigenetic mechanism mediating the HSR.

1.1 Adaptation of the 3D7-A line to periodic HS

In a previous study, Rovira-Graells et al. described two HS-susceptibility phenotypes (HS-sensitive or HS-resistant) among *P. falciparum* 3D7-A subclones¹⁵⁶ (Fig. 17a). They showed that the 10G subclone was HS-sensitive and the 1.2B subclone was HS-resistant, and that these phenotypes were maintained after HS exposure (3 h at 41.5°C) for five consecutive generations (Fig. 17b-c).

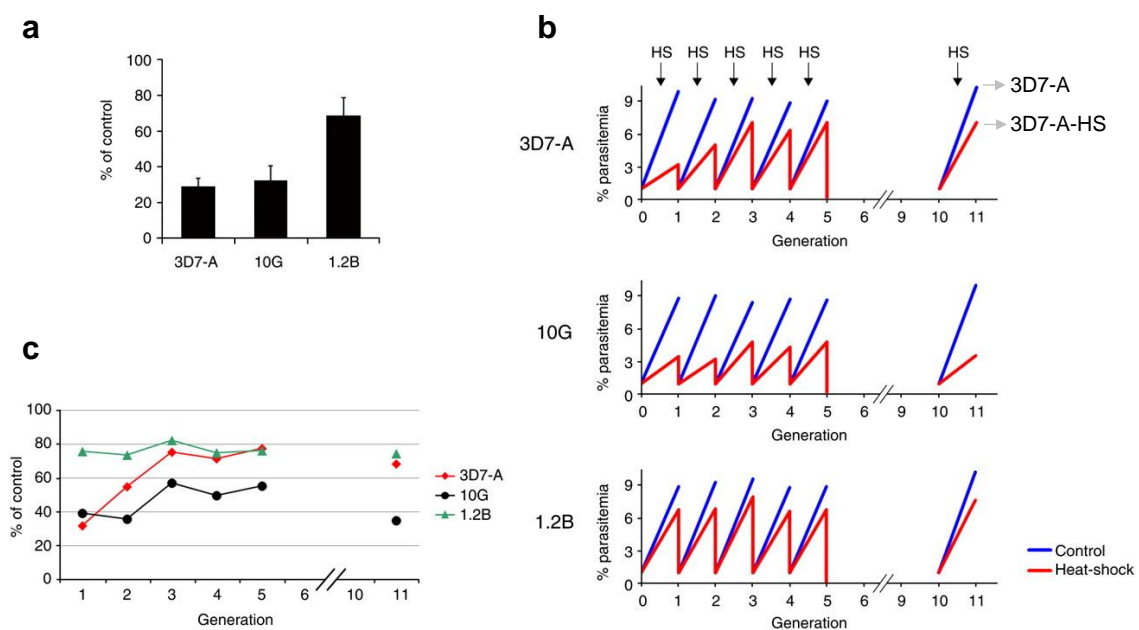


Figure 17. 3D7-A adaptation to periodic HS exposure. **a**, HS survival of 3D7-A, 10G and 1.2B lines, expressed as the percentage (%) respect to their controls maintained at 37°C. **b**, Growth of 3D7-A, 10G and 1.2B cultures maintained at 37°C (blue) or exposed to a 3 h-HS for five consecutive generations at the trophozoite stage (red). After each cycle, cultures exposed to HS were synchronized, adjusted to 1% parasitemia and split into two identical dishes to compare again growth between HS and control (37°C) conditions. Afterwards, cultures were grown without HS in cycles 6-10 and exposed to HS again at cycle 10. The 3D7-A line was able to adapt to HS (3D7-A-HS). **c**, Percentage of growth under HS, relative to normal conditions, calculated from the data in panel **b**¹⁵⁶.

In contrast, after exposing the parental 3D7-A line to periodic HS, a HS-adapted line (named 3D7-A-HS) displaying a 1.2B-like HS-resistant phenotype was obtained (Fig. 17b-c). The ability of the 3D7-A parental line to adapt in only a few cycles and maintain

the resistant phenotype for several generations after the exposure suggested that the parental parasite population contained a selectable subset of parasites resistant to HS, which could have either a genetic or an epigenetic basis.

1.2 Optimization of the heat shock assay

Before analysing the molecular basis of this HS adaptation, in my MSc thesis we first validated and optimized the HS assay. For our assays, we also used a short and severe HS exposure (3 h at 41.5°C), as it allowed to study the immediate HSR.

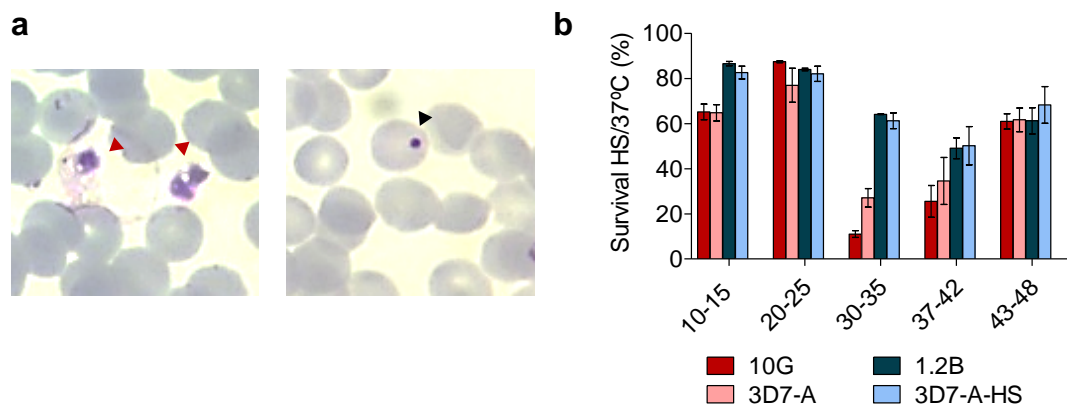


Figure 18. Sensitivity to HS throughout the intraerythrocytic cycle. **a**, Images of “crisis forms” (red arrowheads) and pyknotic (black arrowhead) dead parasites typically observed after HS exposure at the trophozoite stage. **b**, Survival of tightly synchronized cultures exposed to HS at different ages (in h post-invasion). Two HS-sensitive (3D7-A and 10G) and two HS-resistant (3D7-A-HS and 1.2B) lines were tested. The mean and s.e.m. of two independent biological replicates are shown.

We also optimized the HS conditions to differentiate the HS-resistant and HS-sensitive phenotypes. For this, tightly-synchronized cultures were exposed to HS (3 h at 41.5°C) at different stages of the asexual life cycle: early rings (10-15 hpi), late rings (20-25 hpi), trophozoites (30-35 hpi), early schizonts (37-42 hpi) or late schizonts (43-48 hpi). After HS exposure, “crisis forms” and pyknotic parasites described in previous studies were observed, confirming parasite death upon this stress¹³⁰ (**Fig. 18a**). Although we observed a reduced growth after exposure at all the stages, parasites were not equally affected by HS throughout the asexual life cycle. As expected, ring-stage parasites were clearly more resistant than late-stage parasites^{130,231,232}. Similarly, late schizonts (43-48 hpi) also showed high survival levels, probably because all new merozoites were already formed and some schizonts had already burst at the time of HS exposure. Maximal differences between sensitive and resistant parasite lines were observed when exposing parasites at 30-35 hpi, which corresponds to the trophozoite stage (**Fig. 18b**). HS exposure at this time point allowed to clearly identify the sensitive and resistant phenotypes, corresponding to <30% and >60% survival, respectively. Thus,

30-35 hpi was defined as the best time point to compare HS phenotypes between parasite populations and we used it for the following HS analysis.

1.3 Transcriptional analysis of 3D7-A-HS and unselected 3D7-A populations

The rapid and stable adaptation of 3D7-A to HS suggested that epigenetic variation and selection of epigenetic variants may be driving this adaptation. To test this hypothesis, a transcriptomic analysis of two independently selected 3D7-A-HS lines and non-selected cultures maintained in parallel (3D7-A) was performed by Dr. Cortés' group in collaboration with Dr. Bozdech's group before I started working in the project. Transcriptomic data showed only small differences between 3D7-A and 3D7-A-HS, including a total of 33 genes with a >1.5 FC expression (**Fig. 19a**).

Transcriptomic data, obtained from Rovira-Graells et al.¹⁵⁶, of 3D7-A subclones with either a HS-sensitive (10G) or a HS-resistant (1.2B) phenotype was also included in the analysis. This was used to identify common features between populations with the same HS phenotype. A total of three genes showed higher transcript levels in all HS-resistant lines (3D7-A-HS r1, 3D7-A-HS r2 and 1.2B) compared to HS-sensitive lines (3D7-A r1, 3D7-A r2 and 10G): the cytoadherence linked asexual protein 2 gene (*clag2*, PF3D7_0220800), a *var* gene (PF3D7_0711700) and a *rif* pseudogene (PF3D7_0632600) (**Fig. 19b**). All of them are clonally variant genes, such they can provide the epigenetic heterogeneity needed for adaptation via bet-hedging strategies. *var* and *rif* genes encode PfEMP1 and Rifin proteins, respectively, known for their role in antigenic variation³⁷² and unlikely to be related with the HS-resistant phenotype. In contrast, *clag2* is a member of the *clag* family, composed by 5 genes (*clag2*, *clag3.1*, *clag3.2*, *clag8* and *clag9*), some of which are known to play a key role in the formation of the plasmodial surface anion channel (PSAC) responsible for solute permeability in *Plasmodium*-infected erythrocytes.

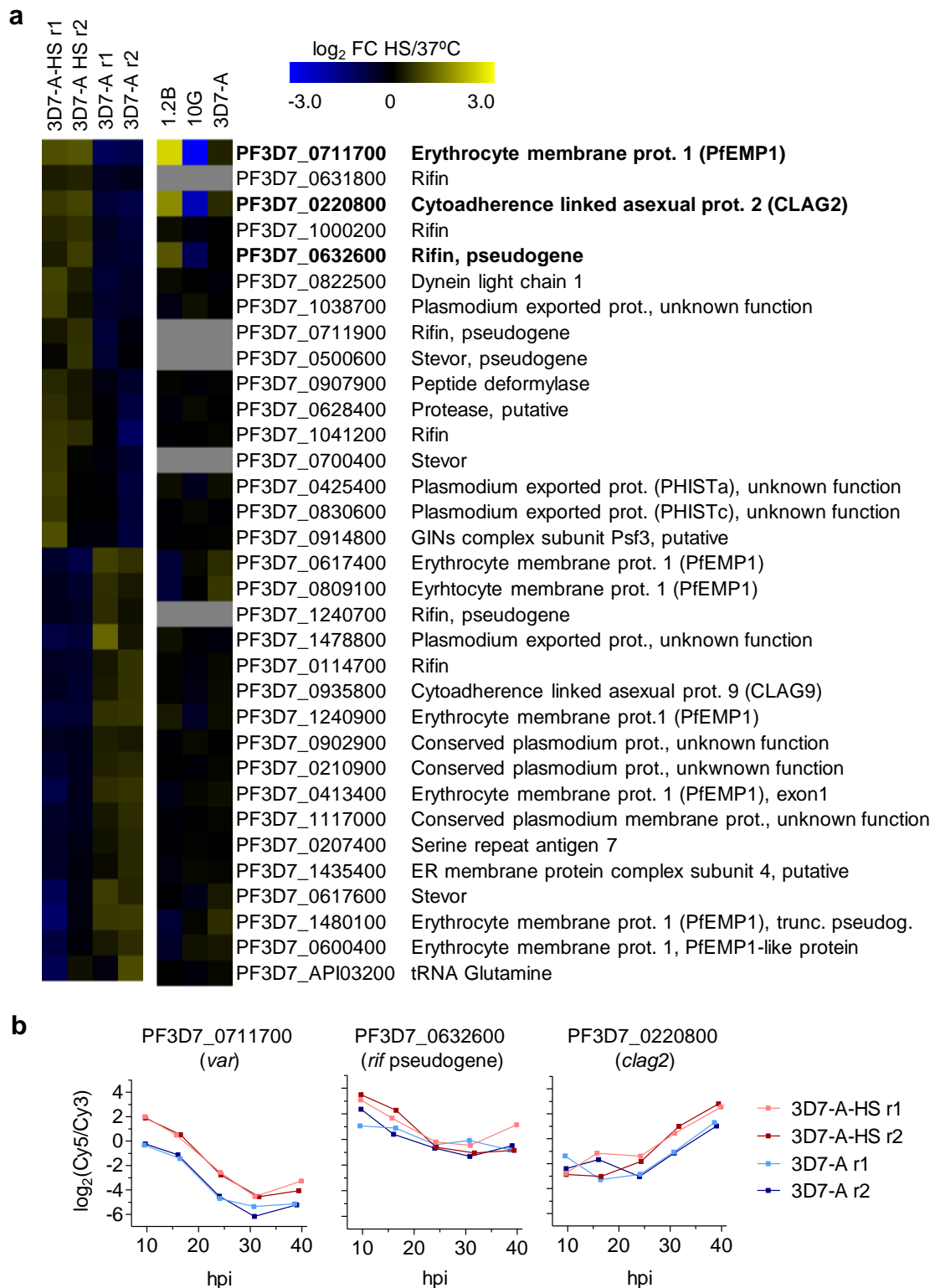


Figure 19. Transcriptional analysis of HS-adapted and control lines. **a**, Microarray comparison of HS-adapted and control parasite lines across the intraerythrocytic asexual cycle. Values are the mean-centered log₂ of the maximum expression fold change (FC) across a time interval corresponding to half the length of the asexual cycle, calculated using the adjusted maximum average fold-change (aMAFC) score as previously described¹⁵⁶. Genes with a >1.5-fold change in expression in two independent 3D7-A-HS-adapted lines (3D7-A-HS r1 and r2) relative to their respective controls (3D7-A r1 and r2) are shown. Data for parasite lines 1.2B, 10G and 3D7-A is from Rovira-Graells et al.¹⁵⁶. **b**, Time-course expression of genes in panel **a** that showed a concordant change in expression between HS-sensitive or HS-resistant lines.

1.4 Assessment of the association between *clag2* and the heat shock-resistant phenotype

In my MSc thesis project, we focused our analysis on *clag2*, hypothesizing that it may mediate the HSR by modulating the uptake of chemical chaperones, cellular osmolytes that stabilize proteins and help in protein folding³⁷³. We first quantified *clag2* transcript levels of HS-adapted (3D7-A-HS) and control lines (3D7-A), which confirmed the higher *clag2* expression in 3D7-A-HS observed in the microarray analysis (Fig. 20). Next, we analysed a collection of 3D7-A parasite subclones (10G, 4D, 6D, 1.2B, 10E, 1.2B, W4-2, W4-5, W4-1 and W4-4), from which we also characterized their HS-susceptibility phenotype. Contrary to what we expected, some subclones were HS-resistant despite having *clag2* silenced, whereas some others were HS-sensitive despite having the gene in an active state. Thus, no correlation was observed between *clag2* expression and the HS-susceptibility phenotype, indicating that *clag2* expression is neither necessary nor sufficient for the HS resistant phenotype (Fig. 20).

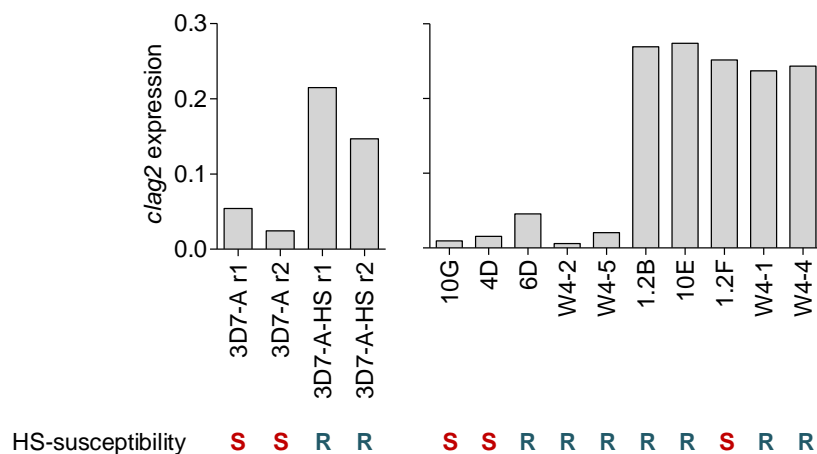


Figure 20. Expression of *clag2* and HS sensitivity. *clag2* transcript levels were tested in the HS-adapted lines (3D7-A-HS r1 and r2) and their controls (3D7-A r1 and r2) (left panel), and in a collection of 3D7-A subclones (right panel). The level of HS-susceptibility of each line is indicated below: S (HS-sensitive) and R (HS-resistant). Values are transcript levels of *clag2* (normalized against *rhoph2*) at the schizont stage, determined by reverse transcription-quantitative PCR (RT-qPCR). Results derived from my MSc thesis project.

2 IDENTIFICATION OF THE DETERMINANT OF HEAT SHOCK SUSCEPTIBILITY

Based on the previous results exposed above, we discarded transcriptional differences between 3D7-A and 3D7-A-HS as the cause of HS resistance and analysed genetic changes as a possible mechanism of HS adaptation in 3D7-A-HS.

2.1 Whole genome sequencing of 3D7-A and 3D7-A-HS lines

In order to analyse whether genomic changes were involved in the HS adaptation of 3D7-A-HS, full genome sequencing of the 3D7-A-HS and 3D7-A lines (from two independent biological selection replicates) was performed. This analysis revealed 22 genetic differences between the two lines that were consistent in both biological replicates (Table 39). Most of them were in non-coding regions and in long AT repeats, or were synonymous mutations that didn't affect the coding sequence. Only a SNP, consisting of a C to T mutation predicted to affect a protein sequence was clearly predominant in both non-selected 3D7-A lines, but almost absent in the 3D7-A-HS lines (Fig. 21a). It was located in chromosome 13, at position 10,249 bp of the PF3D7_1342900 gene, and resulted in a premature stop codon (Q3417X) in the protein encoded. We corroborated the presence of this SNP by Sanger sequencing, which clearly showed a heterogeneous 3D7-A control population with higher frequency of parasites containing the SNP, and a 3D7-A HS-adapted population essentially homogeneous for the reference allele (Fig. 21b). Thus, this result showed that adaptation to HS involved elimination of parasites expressing truncated PF3D7_1342900.

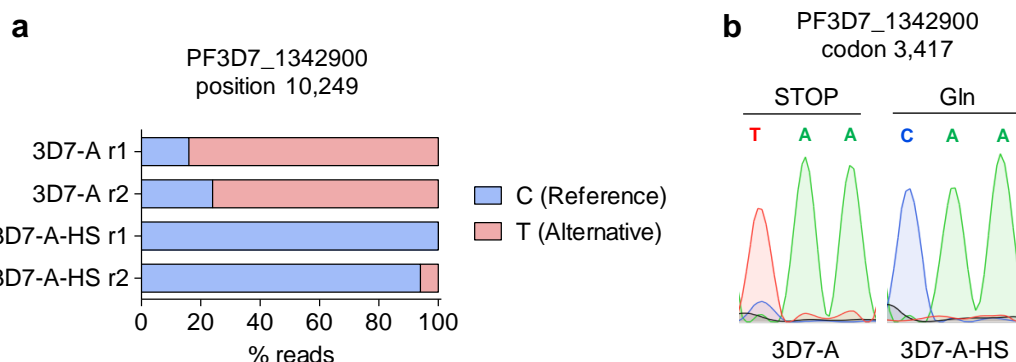


Figure 21. Identification of a single nucleotide polymorphism (SNP) associated with HS sensitivity. **a**, Proportion of Illumina reads with the reference (C) or alternative (T) allele at position 10,249 bp of PF3D7_1342900. Data from two independent HS-adapted cultures (3D7-A-HS r1 and r2) and their controls (3D7-A r1 and r2) is shown. **b**, Sanger sequencing of codon 3,417. The mutation produces an amino acid change from glutamine (Gln) to a stop codon.

a

Chrom.	Position	Ref.	Alt.	Strain	% Alt.		Closest gene at 5'		Closest gene at 3'		Observations
					Repl.1	Repl.2	Gene	Dist.	Gene	Dist.	
4	894147	CAT	C	3D7-A 3D7-A-HS	62% 2%	59% 2%			PF3D7_0419900 (PI 4-K, putative)	281bp	String of TA's
2	24596	T	A	3D7-A 3D7-A-HS	75% 25%	80% 53%	PF3D7_0200100 (PIEMP1)	636bp			String of TA's
9	1221861	AATATAT	A	3D7-A 3D7-A-HS	73% 23%	66% 22%	PF3D7_0930700	126bp			String of TA's
9	1430115	AAT	A	3D7-A 3D7-A-HS	56% 10%	63% 11%	PF3D7_0936000 (REX2)	2093bp	PF3D7_0936100 (ETRAPMP9)	492bp	String of TA's
12	2010358	AATATATAT ATATAT	A	3D7-A 3D7-A-HS	44% 3%	51% 5%	PF3D7_1249200 (conserved)	70bp	PF3D7_1249100 (conserved)	650bp	String of TA's
14	973656	A	AAT	3D7-A 3D7-A-HS	52% 2%	48% 3%	PF3D7_1423900 (snoRNA)	796bp	PF3D7_1424100 (RPL5)	197bp	String of TA's
3	296122	AAT	A	3D7-A 3D7-A-HS	49% 7%	53% 5%	PF3D7_0306300 (GRX1)	28bp			String of TA's
7	858548	AATAT	A	3D7-A 3D7-A-HS	77% 44%	73% 43%	PF3D7_0719500 (CDC50A)	1894bp	PF3D7_0719600 (60S L11a, put.)	194bp	String of TA's
7	935027	A	AAT	3D7-A 3D7-A-HS	61% 12%	68% 14%	PF3D7_0721700 (PSOP1)	470bp			String of TA's
13	2787621	T	TTA	3D7-A 3D7-A-HS	63% 16%	75% 20%	PF3D7_1370300 (MAHRP1)	351bp			String of TA's
8	194766	C	CAT	3D7-A 3D7-A-HS	67% 0%	53% 0%			PF3D7_0802900 (conserved)	382bp	String of TA's
10	318433	C	CAT	3D7-A 3D7-A-HS	57% 4%	56% 12%			PF3D7_1007900 (EIF3D)	153bp	String of TA's
11	622928	TTATATATA TATATATA	T	3D7-A 3D7-A-HS	55% 10%	53% 16%	PF3D7_1116500 (FT2)	1442bp			String of TA's
11	1678870	A	AATAT	3D7-A 3D7-A-HS	49% 16%	48% 12%	PF3D7_1142000 (HPR-cont., putative)	208bp			String of TA's

b

Chrom.	Position	Gene	Reference	Alternative	Strain	% Alt		Observations	Amino acid change
						Repl. 1	Repl. 2		
2	25645	PF3D7_0200100 (PEEMP1)	TAAA	T	3D7-A	78%	67%	String of A's	K>-
					3D7-A-HS	0%	20%		
2	25666	PF3D7_0200100 (PEEMP1)	A	T	3D7-A	74%	57%		E>D
					3D7-A-HS	0%	18%		
2	25669	PF3D7_0200100 (PEEMP1)	G	A	3D7-A	74%	29%		V>V
					3D7-A-HS	0%	0%		
9	1129283	PF3D7_0927800 (COX5B)	CATATATATAT	C	3D7-A	66%	59%	String of TA's, intron	
					3D7-A-HS	9%	10%		
10	734986	PF3D7_1018400 (conserved)	A	AATAT	3D7-A	49%	56%	String of TA's, intron	
					3D7-A-HS	0%	5%		
11	294600	PF3D7_1107100 (nucl. ac. binding.)	A	AATAAT	3D7-A	35%	34%	String of TA's, intron	
					3D7-A-HS	3%	4%		
11	1129182	PF3D7_1129200 (RPN7)	AATATAT	A	3D7-A	59%	63%	String of TA's, intron	
					3D7-A-HS	31%	33%		
13	1683721	PF3D7_1342900 (AplAP2)	G	A	3D7-A	84%	76%	-	Q>X
					3D7-A-HS	0%	6%		

- Deletion
X Stop codon

Table 39. Genetic changes between 3D7-A-HS and control 3D7-A lines identified by whole genome sequencing. Frequency of SNPs and indels (% of reads containing the mutation in Illumina full genome sequencing) in two HS-adapted cultures and their respective controls. Observations about the nature of the genetic change are provided in the last column. **a**, Mutations in intergenic regions. The ID and relative position of the closest upstream and downstream genes are indicated. **b**, Mutations in coding regions and introns. The ID of the affected gene and the amino acid change produced by the mutation (if any) are indicated. Chrom., chromosome; Ref., reference allele; Alt., alternative allele; Repl., biological replicate; Dist., distance to the indicated gene.

2.2 Association of the premature Q3417X mutation in PF3D7_1342900 with the heat shock-sensitive phenotype

The analysis of a collection of 3D7-A subclones corroborated that all subclones with the Q3417X mutation show a HS-sensitive phenotype, whereas all subclones with the wild type allele are HS-resistant (**Fig. 22**). This result provides strong support to the idea that this mutation is the determinant of HS sensitivity in the 3D7-A line. It also confirms our hypothesis that the HS-adaptation observed in the 3D7-A-HS line was driven by the selection of a HS-resistant subpopulation that did not carry the Q3417X mutation. Although only three of our 3D7-A subclones carried this mutation, in the global 3D7-A population the proportion of parasites with the Q3417X mutation was much higher (~80%) (**Fig. 21**), explaining the HS-sensitive phenotype of this line. While this mutation had a clear deleterious effect for parasites during HS, this was not the case under basal conditions. Instead, the appearance and selection of this mutation during normal culture maintenance suggest that it may offer an increased fitness under such conditions.

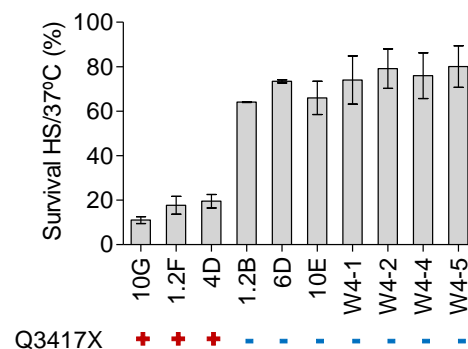


Figure 22. Association of the Q3417X mutation with HS sensitivity. HS susceptibility of 3D7-A subclones carrying (+) or not (-) the Q3417X mutation. Values correspond to the percentage of survival of HS-exposed cultures compared to their controls maintained in parallel at 37°C. Mean with s.e.m. of two independent biological replicates are shown.

2.3 Description of the PF13_42900 gene that carries the Q3417X mutation

As stated above, the Q3417X mutation causes a premature stop codon in the PF3D7_1342900 gene, which encodes an ApiAP2 transcription factor with unknown function. Because of the association of this protein with HS survival, we termed it PfAP2-HS. PfAP2-HS is a 3,858 aa-length protein, containing three AP2 domains (D1, D2 and D3) towards the C-terminal end and a PR domain at the central region. The identified Q3417X mutation results in a truncated PfAP2-HS protein missing the last

442 aa, which include the AP2 domain D3 (PfAP2-HS Δ D3) (Fig. 23). The AP2 domain D1 was previously reported to have *in vitro* specificity for a DNA motif termed G-box ((A/G)NGGGG(C/A))⁸⁴, whereas the role of the other domains is unclear.



Figure 23. Schematic of the PfAP2-HS protein. 10E and 1.2B subclones express the wild type PfAP2-HS, which contains a pentapeptide repeat-like domain (PR, 1,977-2,104 aa) at the central region and three AP2 domains (D1-3, positions 2,363-2,412 aa, 3,066-3,117 aa and 3,789-3,840 aa, respectively). The truncated PfAP2-HS version present in the 10G subclone has a premature stop codon at position 3,417, which leads to the lack of AP2 domain D3 (PfAP2-HS Δ D3).

2.4 Effect of the Q3417X mutation in the the regulation of *hsp70-1* and *hsp90*

The G-box motif is present in the promoter region of more than 500 *P. falciparum* genes, of which only a few carry a tandem G-box (Td-Gbox) (see Results, section 5.2.1) that increases the affinity of the AP2 domain D1 binding^{84,102}. Among these genes with a Td-Gbox are the cytoplasmic *hsp70* (*hsp70-1*, PF3D7_0818900) and *hsp90* (PF3D7_0708400), which have two identical highly conserved tandem copies in opposite strands, separated by 5-6 bp, located within 1.2 kb of the start codon¹⁰² (Fig. 24). Interestingly, in addition to containing this highly conserved Td-Gbox in their promoter, both *hsp70-1* and *hsp90* encode predicted chaperones that are known to participate in the HSR in other eukaryotes²⁶³, reason why they became candidate genes to be regulated by PfAP2-HS during the HSR.

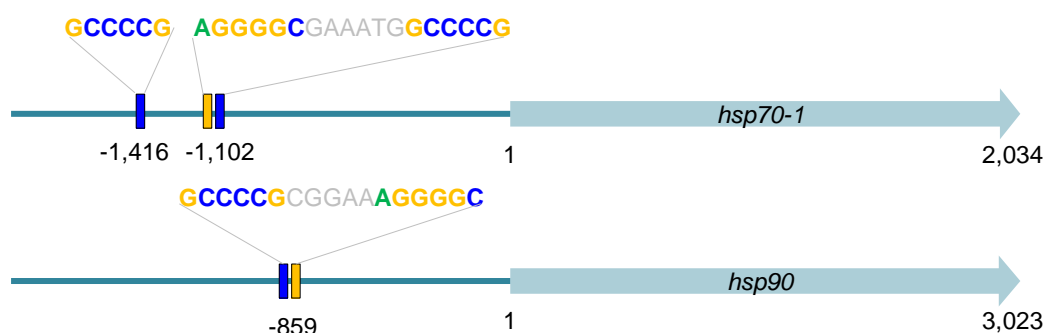


Figure 24. Td-Gbox motifs in the *hsp70-1* and *hsp90* promoter regions. Schematic of the promoter regions of *hsp70-1* and *hsp90*, in which the G-box motifs are highlighted in yellow (sense) or blue (antisense). The positions of the G-box motifs are indicated below as bp relative to the ATG of each gene.

We next tested the ability of parasites expressing wild type PfAP2-HS and PfAP2-HS Δ D3 to mount a transcriptional HSR, focusing on *hsp70-1* and *hsp90* expression.

We observed that both *hsp70-1* and *hsp90* were strongly up-regulated during HS in subclones expressing wild type PfAP2-HS (1.2B, 10E and 6D), whereas in subclones expressing PfAP2-HS Δ D3 (10G, 4D and 1.2F) the response was of much lower magnitude and delayed (Fig. 25a). Although the expression pattern upon HS was similar between both genes, the induction was stronger in *hsp70-1*: *hsp70-1* showed up to 17-fold increased transcript levels, whereas a maximum 8-fold increase was reported for *hsp90*. Altogether, these results indicate that the loss of PfAP2-HS domain D3 impairs the ability to normally induce expression of genes predicted to participate in the transcriptional response to HS, including *hsp70-1* and *hsp90*.

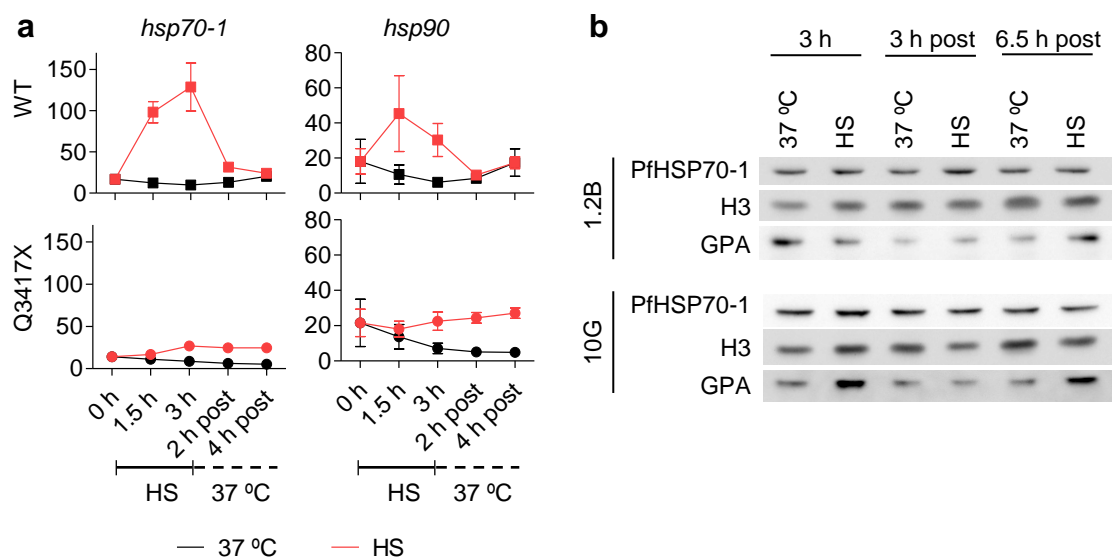


Figure 25. Induction of *hsp70-1* and *hsp90* expression during and after HS. **a**, Transcript levels of *hsp70-1* and *hsp90* (relative to *serine--tRNA ligase*) during and after HS in 3D7-A subclones carrying (Q3417X: 10G, 1.2F and 4D) or not (WT: 1.2B, 6D and 10E) the premature stop codon mutation in the *pfap2-hs* gene. Values are the mean and s.e.m. of three independent assays, each using different subclones. **b**, Western blot analysis of HSP70-1 protein levels in HS-exposed parasites and their controls maintained at 37°C at the end of the HS (3 h) and after HS (3 h post and 6.5 h post), comparing a HS-sensitive (10G) and a HS-resistant (1.2B) subclone. As loading controls, we used anti-histone H3 and anti-glycophorin A (GPA), an erythrocyte protein.

We also attempted to analyse HSP70-1 induction at the protein level, expecting that the high induction of *hsp70-1* transcript levels would lead to higher levels of HSP70-1 protein upon HS. However, HSP70-1 protein levels were not altered between HS and control conditions, or between HS-resistant (1.2B) and HS-sensitive (10G) lines (Fig. 25b). As a delay between transcription and translation was already described in *P. falciparum*¹⁶⁸, we also collected samples up to 6.5 h after the stress, but again we observed no difference. To address the possibility that the anti-HSP70-1 antibody may be crossreactive, we tried different HSP70-1 antibodies, including commercial and custom-made antibodies, as well as monoclonal and polyclonal antibodies. However,

we did not observe a correlation between transcript and protein levels with any of the antibodies (data not shown).

Transcript levels of other chaperone-encoding genes containing a single G-box motif (but not a Td-Gbox) in their upstream region, such as *hsp70-z* (PF3D7_0708800) and *hsp70-3* (PF3D7_1134000), were also analysed. Although an induction of these genes was observed upon HS in the HS-resistant lines, the response was variable and weaker than in *hsp70-1* and *hsp90* (Fig. 26). We also followed the expression of *pfap2-hs* itself, which showed a similar pattern to *hsp70-z* and *hsp70-3*, with a ~2-fold induction after 1.5 h of HS (Fig. 26). Parasites carrying the mutation in *pfap2-hs* had a lower and delayed response compared to the HS-resistant lines, suggesting that the loss of domain D3 of PfAP2-HS may also impair the up-regulation of these chaperones. However, the differences between control and mutant subclones were far smaller than in the case of *hsp70-1* and *hsp90*. Ubiquitin-conjugating enzyme (*uce*, PF3D7_0812600) transcript levels were used as a negative control, as its expression remains unaffected in response to HS (Fig. 26).

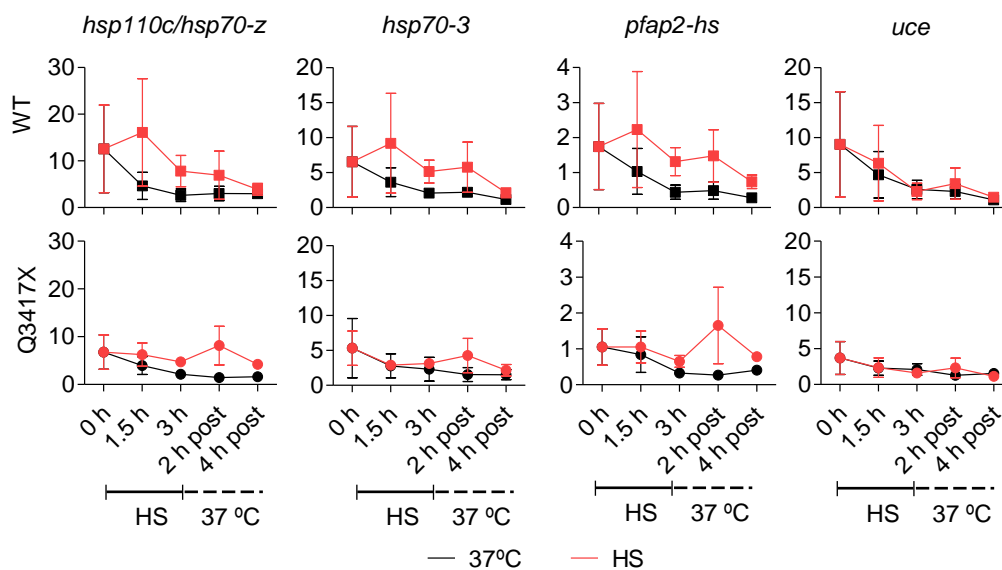


Figure 26. Expression of *hsp70-z*, *hsp70-3* and *pfap2-hs* during and after HS. Transcript levels of *hsp70-z*, *hsp70-3*, *pfap2-hs* and ubiquitin-conjugating enzyme (*uce*) (relative to *serine-tRNA ligase*) during and after HS in 3D7-A subclones carrying (Q3417X) or not (WT) the stop codon mutation in *pfap2-hs* gene. Subclones are the same as in fig. 24a. Values are the mean and s.e.m. of three independent assays, each using different subclones.

3 NEW TOOLS TO STUDY PfAP2-HS

In order to characterize PfAP2-HS localization, activation and functionality, we generated a collection of *P. falciparum* and *P. berghei* transgenic lines. This collection included parasite lines expressing tagged versions of the endogenous protein, as well as parasites expressing versions of the protein with inducible degradation or mislocalization. Constitutive *pfap2-hs*-knockout lines were also generated and became a key tool for subsequent functional analysis.

3.1 Generation of Δ PfAP2-HS transgenic lines

To further characterize the role of PfAP2-HS, we generated PfAP2-HS null mutants (Δ *pfap2-hs*) using CRISPR/Cas9 technology. Because of the large size of the gene (11,577 bp), we used two separate guide RNAs (Fig. 27a).

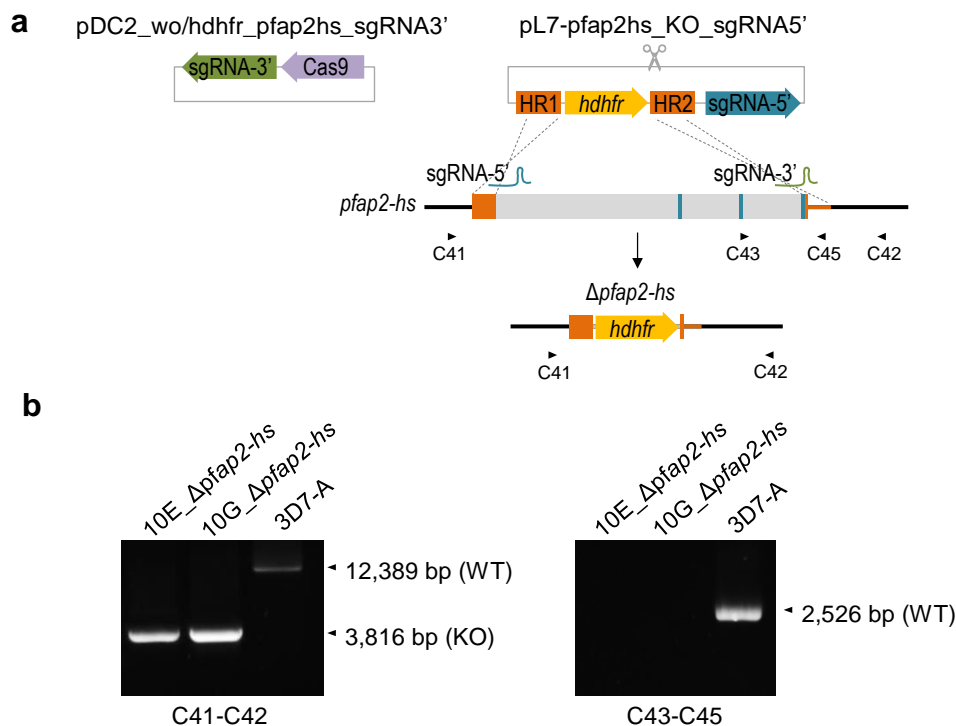


Figure 27. Generation of Δ *pfap2-hs* transgenic parasite lines. **a**, Schematic of the CRISPR/Cas9 strategy used to knock *pfap2-hs* out in the 10E (10E_Δ*pfap2-hs*) and 10G (10G_Δ*pfap2-hs*) lines, using two guide RNAs (sgRNA-5' and sgRNA-3'). A *dhfr* cassette was used as the selection marker. The position and names of the primers used for analytical PCR are indicated by arrowheads and the position of the AP2 domains by blue bars. **b**, Analytical PCR validation of the genetic edition, indicating the expected size of the amplified product in wild type (WT) and correctly edited (KO) parasites.

After several unsuccessful attempts at 37°C (the physiological temperature for *P. falciparum*), we reasoned that PfAP2-HS may play a role in regulating the expression of genes involved in proteostasis under basal conditions, in addition to driving the HSR. Therefore, we attempted to knock *pfap2-hs* out in cultures maintained at 35°C, as mild

hypothermia is expected to reduce protein unfolding and facilitate proteome integrity^{374,375}. At this temperature, the knockout of *pfap2-hs* was readily achieved in both the HS-resistant subclone 10E and the HS-sensitive subclone 10G (10E_Δ*pfap2-hs* and 10G_Δ*pfap2-hs* lines, respectively) (Fig. 27b).

3.2 Generation of transgenic lines with inducible AP2-HS degradation and mislocalization

Two methodologies were used to induce PfAP2-HS degradation or PbAP2-HS mislocalization. First, we added an FKBP destabilization domain (DD) at the C-terminal end of PfAP2-HS in the *P. falciparum* 1.2B line (PfAP2-HS::DD), a tool that allows to induce the degradation of the protein in the absence of the ligand Shield1 (Shld). Two correctly edited populations were obtained after subcloning by limiting dilution (8A_PfAP2-HS::DD and 12E_PfAP2-HS::DD) (Annex II – Fig. 2b-c). This tool was used to control PfAP2-HS degradation or stabilization in the HS assay and, as expected, in the absence of Shld parasites could grow normally at 37°C but showed a HS-sensitive phenotype. However, the resistant phenotype couldn't be rescued by the addition of Shld, indicating that the integration of the construct interfered with the function of the AP2 domain D3, located only 18 aa from the end of the protein (Annex II – Fig. 2d). The impossibility to activate a protective HSR was also observed at the transcriptional level, as expression of *hsp70-1* was not induced in either of the transgenic lines (Annex II – Fig. 2e).

To induce mislocalization of the PbAP2-HS protein, we used the knocksideways (KS) system, by which a wrong localization of the protein is induced with the addition of Rapa, which drives oligomerization of domains FKBP and FBR³³². Using a background line that was previously edited to express FRB fused to a transmembrane protein³³², we generated a transgenic *P. berghei* line that expressed the endogenous PbAP2-HS tagged with a FKBP domain (PbAP2-HS::KS). This was subsequently subcloned by limiting dilution to finally obtain two correctly edited subclones (c2m2_PbAP2-HS::KS and c1m3_PbAP2-HS::KS) (Annex II – Fig. 7). Preliminary HS assays were performed using the KS line and showed that, despite its close proximity to the AP2 domain D3, this tagging did not affect normal PbAP2-HS functionality (see Results, section 6).

3.3 Generation of transgenic lines expressing tagged PfAP2-HS and PbAP2-HS

We also generated a collection of transgenic lines expressing diverse versions of tagged PfAP2-HS and PbAP2-HS. First, we tagged PfAP2-HS with eYFP at the C-terminal end (PfAP2-HS::eYFP), but we observed again that this bulky C-terminal tag also impaired HS survival, resulting in a HS-sensitive phenotype similar to the effect caused by the DD tagging (**Annex II – Fig. 3**). These observations are consistent with interference of the tag with the function of the third AP2 domain located in close proximity to the C-terminus and corroborate the important role of domain D3 in the regulation of the HSR. To avoid disrupting the D3 function, we attempted other tagging strategies, including a smaller tag (3xHA) at C-terminal (PfAP2-HS::3xHA) (**Annex II – Fig. 4**) and an eYFP at N-terminal (eYFP::PfAP2-HS) (**Annex II – Fig. 5**). Although these tags didn't interfere with PfAP2-HS function, the protein could not be detected in any of the assays using anti-3xHA or anti-GFP antibodies. On the one hand, we used Western blot (WB) analysis optimized for large molecular weight protein detection. On the other hand, immunofluorescence assays (IFA) were also performed, but the weak signal observed in the transgenic lines was not specific, as it was also observed in the wild type lines.

In collaboration with Dr. Oliver Bilker's group, we also generated a *P. berghei* line expressing the ortholog of PfAP2-HS (PbAP2-HS, PBANKA_1356000) fused to a 3xHA tag in the C-terminal end (PbAP2-HS::3xHA) (**Annex II – Fig. 8**). However, it was also impossible to detect the protein by WB or IFA and consequently we couldn't perform the ChIP-seq, proteomics and phosphoproteomics analysis initially planned.

4 CHARACTERIZATION OF THE INVOLVEMENT OF PfAP2-HS IN PARASITE DEVELOPMENT

The impossibility to obtain the $\Delta pfap2$ -*hs* lines at 37°C, together with the detection of several growth defects under standard culture maintenance at 35°C, made us think of an important role for PfAP2-HS during asexual growth. Thus, we decided to further characterize the IDC defects of the knockout lines in the absence of HS, both from a phenotypic and a transcriptional point of view.

4.1 Functional characterization of PfAP2-HS under basal conditions

First, we analysed the growth rate of the knockout (10E_ $\Delta pfap2$ -*hs* and 10G_ $\Delta pfap2$ -*hs*) and their parental (10E and 10G) lines by measuring the increase in parasitemia between consecutive cycles at different temperatures. A severe temperature dependence was observed in the two $\Delta pfap2$ -*hs* lines, such that growth was slightly lower than in the parental lines at 35°C but markedly reduced to less than 50% at 37°C or 37.5°C (Fig. 28a). In contrast, both parental lines had similar growth rates at the three temperatures tested, indicating that the Q3417X mutation in the 10G line did not affect parasite asexual growth.

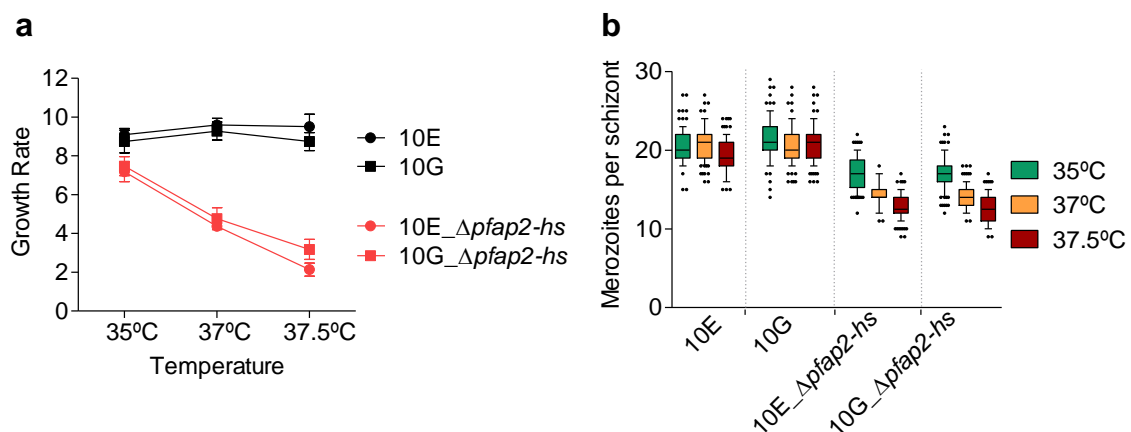


Figure 28. Characterization of the growth of parasite lines lacking PfAP2-HS at different nonstress temperatures. **a**, Growth rate of $\Delta pfap2$ -*hs* (10E_ $\Delta pfap2$ -*hs* and 10G_ $\Delta pfap2$ -*hs*) and parental lines (10E and 10G) at different temperatures (35°C, 37°C and 37.5°C). Values are the mean and s.e.m. of four biological replicates. **b**, Number of merozoites per schizont at different temperatures, obtained from 100 schizonts for each parasite line and condition. Boxes are median and quartiles, whereas whiskers are the 10th and 90th percentiles.

We also analysed the number of merozoites formed in each schizont at the three temperatures tested, observing that both $\Delta pfap2$ -*hs* lines had a smaller number of merozoites per schizont at 35°C compared to their parental lines and that this number decreased at higher temperatures (37°C and 37.5°C) (Fig. 28b). In contrast, the

number of merozoites per schizont was similar at the three temperatures in the parental lines. These results may partly explain the $\Delta pfap2$ -*hs* reduced growth rates at 37 or 37.5°C.

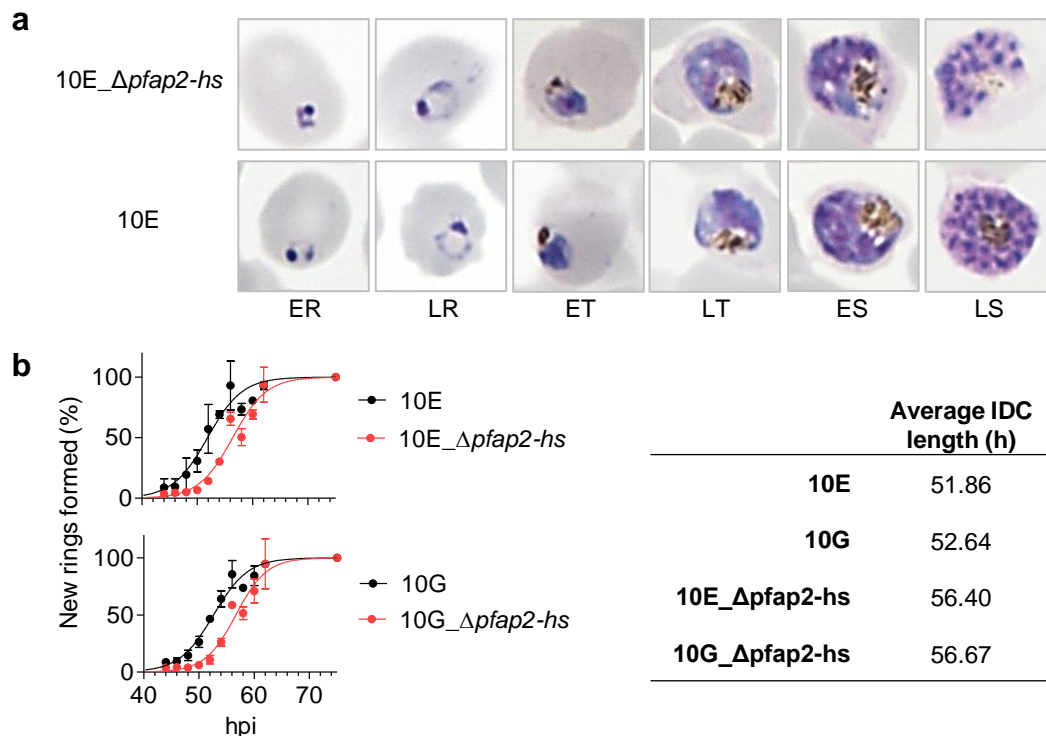


Figure 29. Characterization of the IDC of parasite lines lacking PfAP2-HS under nonstress conditions. a, Representative microscopy images of different intraerythrocytic stages, comparing the 10E_Δ*pfap2*-*hs* and 10E lines. ER, early ring; LR, late ring; ET, early trophozoite; LT, late trophozoite; ES, early schizont; LS, late schizont. **b,** Asexual blood cycle duration of populations lacking PfAP2-HS (10E_Δ*pfap2*-*hs* and 10G_Δ*pfap2*-*hs*) and their parental lines (10E and 10G), estimated from the time when 50% of the newly formed ring-stage parasites appear. The cumulative percentage of new rings formed at each time point is shown. Values are the mean and s.e.m. of two biological replicates, fitted to a sigmoidal dose-response curve.

Following $\Delta pfap2$ -*hs* parasites during the asexual cycle, we observed that they could progress through all the intraerythrocytic stages, showing normal morphology for each stage except for schizonts, which had fewer merozoites than normal (Fig. 29a). We also observed slower progression in both $\Delta pfap2$ -*hs* lines compared to their parental lines. Using an assay to accurately analyse asexual cycle progression³³⁵, we found that the duration of the IDC was ~4.5 h longer in both $\Delta pfap2$ -*hs* lines (Fig. 29b) compared to the parental 10E and 10G lines, even at the permissive temperature (35°C). This lower temperature also affected the cycle length of the parental lines, delaying it ~4 h from the usual 48 h-long *P. falciparum* IDC.

4.2 PfAP2-HS-dependent transcriptional regulation under basal conditions

In order to identify differences in gene expression that could explain the developmental defects of 10E_Δ*pfap2-hs*, microarray analysis was used to study the transcriptome of these parasites under nonstress conditions (35°C), compared to the parental 10E line. We estimated the AFC expression of each gene during a certain period of time (27-30.6 hpi). This analysis revealed a reduced list of genes with an AFC>2 between 10E and 10E_Δ*pfap2-hs* lines, some of which were also differentially expressed in 10G compared to 10E (Fig. 30a). These transcriptional differences between 10E and 10G may correspond to the typical epigenetic variation observed between subclones, rather than being attributable to the PfAP2-HS truncation in 10G. One of the main alterations was a *stevor* (PF3D7_0832600), known to be a clonally variant gene.

As expected, *pfap2-hs* and *hdhfr* were the most differently expressed genes between 10E and 10E_Δ*pfap2-hs* strains, as they had been deleted or added in the knockout parasites, respectively. Both *hsp70-1* and *hsp90* showed reduced expression in 10E_Δ*pfap2-hs*, although in the case of *hsp90* the fold-difference (~1.6-fold) was below the cut-off (Fig. 30b). Indeed, gene set enrichment analysis (GSEA) identified protein folding and response to heat as functional groups with reduced expression in the knockout line, including genes of the T-complex, *Pfj4*, *thioredoxin peroxidase 1*, *cpn10* or *hsp70-3*, among others. These results suggest that PfAP2-HS may play a role in protein homeostasis maintenance under nonstress conditions (Fig. 31).

Many ribosome-related genes were down-regulated in the knockout line, such that 5 rRNAs and RNA-binding proteins showed more than 2-fold lower expression in this line. GSEA analysis corroborated that translation and ribosome formation were highly affected by the PfAP2-HS deletion. The knockout line also showed reduced transcript levels for genes involved in other processes, including merozoite invasion and several metabolic pathways, which could explain the delayed IDC progression and lower growth rate phenotypes observed in the Δ*pfap2-hs* lines (Fig. 31). In contrast, GSEA revealed higher expression of genes encoding exported proteins, as well as phospholipid and polyamine metabolism-related proteins. While some of these transcriptional alterations may be directly related to the *pfap2-hs* deletion, others may correspond to clonal stochastic epigenetic switches and thus may be independent of PfAP2-HS regulation.

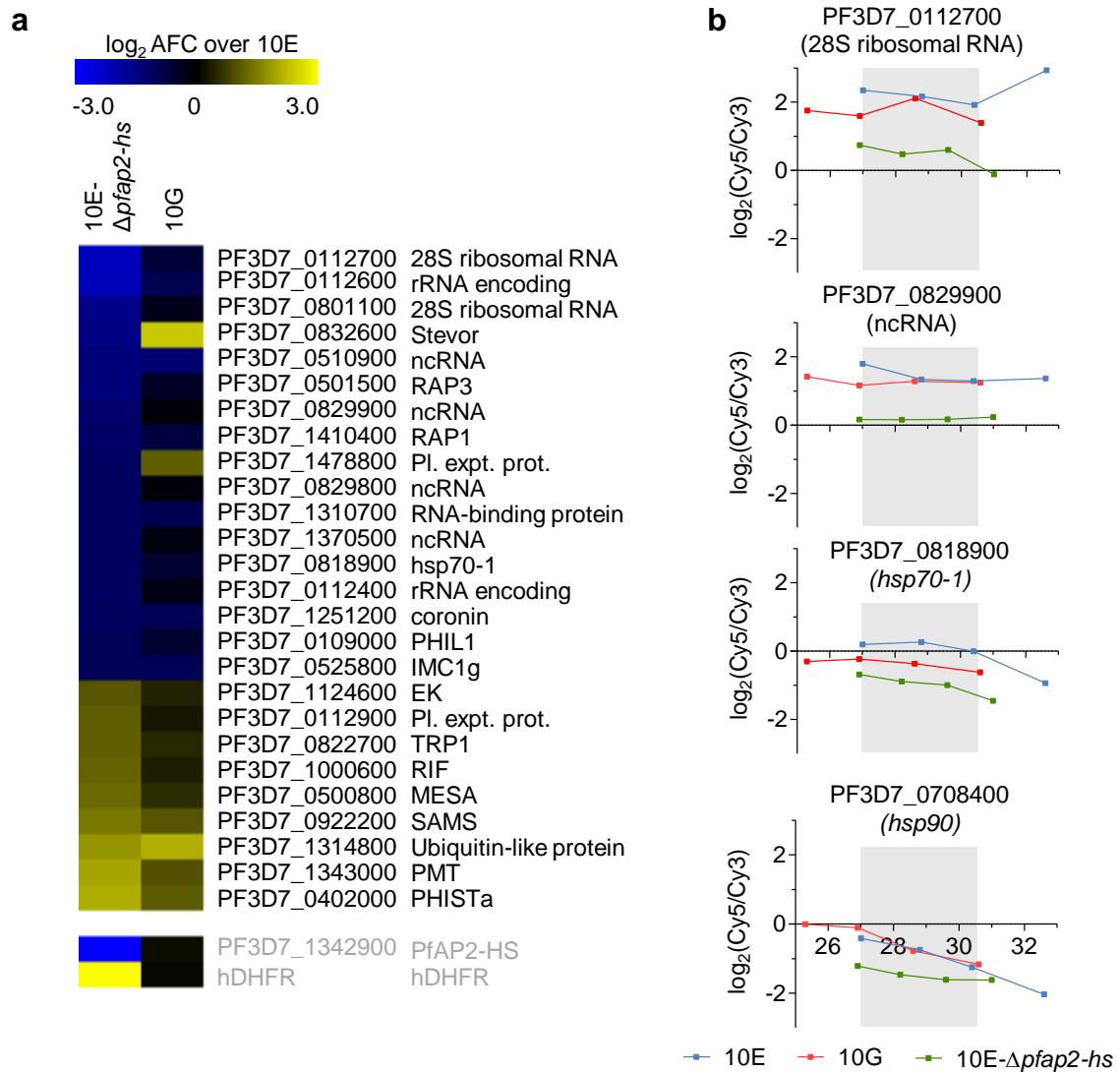


Figure 30. Transcriptional changes associated with the absence of PfAP2-HS under basal conditions (35°C). **a**, Alterations in transcript levels in the absence of HS (35°C) for genes with an average fold-change (AFC) expression >2 between 10E- Δ pfap2-hs and 10E. Values are the \log_2 of the AFC expression relative to 10E across the time period compared (~27-30.5 hpi). Genes edited in the knockout line, which serve as positive and negative controls, are shown at the bottom in grey letters (their values are out of the range displayed). **b**, Expression plots of selected genes under basal conditions. Expression values are plotted against statistically-estimated parasite age, expressed in h post-invasion (hpi). Grey shadow highlights the interval used to calculate the AFC expression.

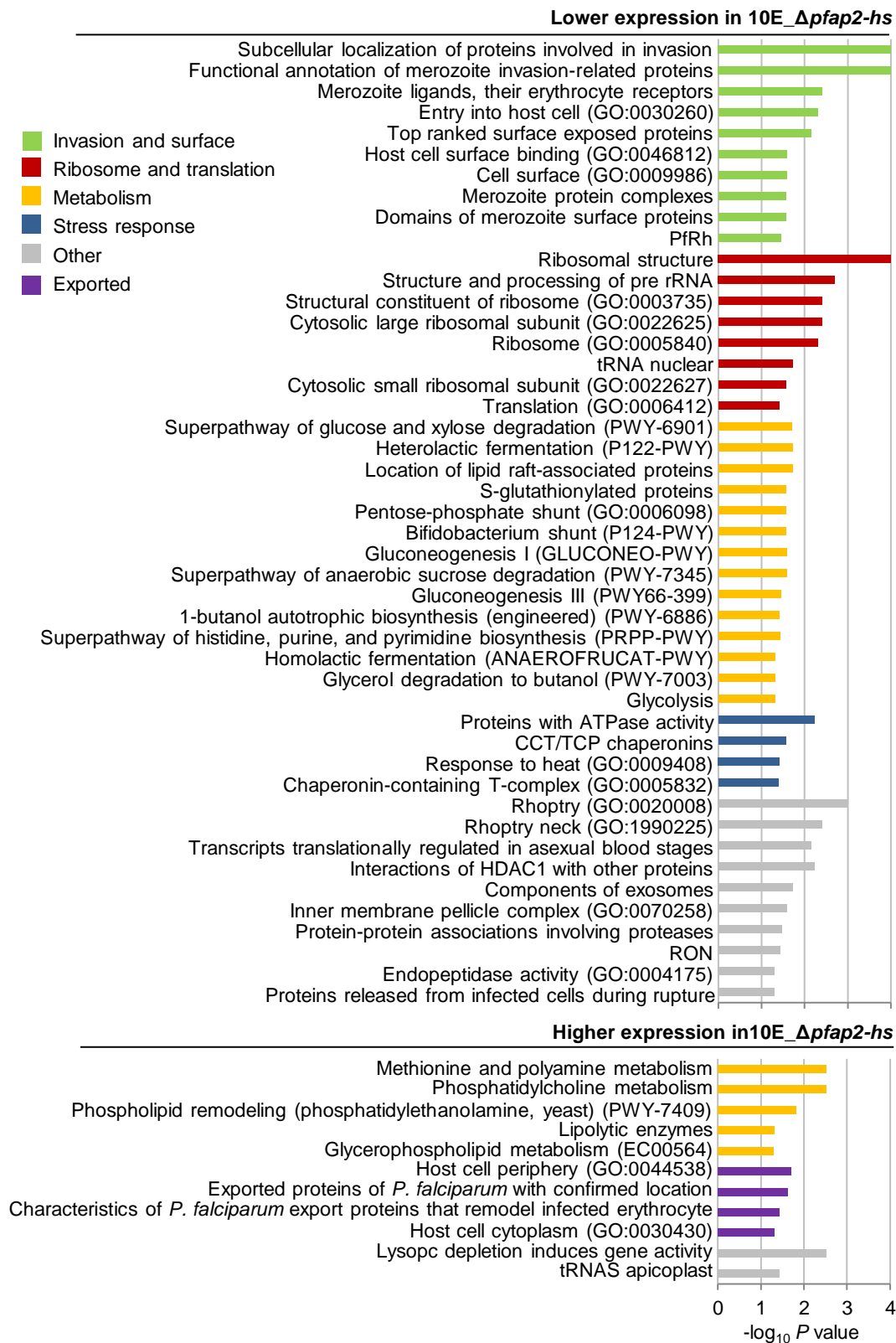


Figure 31. Gene set enrichment analysis (GSEA) of the comparative transcriptomic analysis between 10E and 10E_Δpfap2-hs lines under basal conditions. Genes were ranked based on the fold difference in expression between the Δpfap2-hs and the parental line, and GSEA pre-ranked was used to identify groups of genes differentially expressed between the two parasite lines. Categories were manually grouped by function (invasion and surface, ribosome and translation, metabolism, stress response, exported and other). Only processes showing a significantly enrichment ($P < 0.05$) are shown. The P value for each term is shown as $-\log_{10}(P \text{ value})$.

5 CHARACTERIZATION OF THE ROLE OF PfAP2-HS IN THE HEAT SHOCK RESPONSE

In order to characterize the role of PfAP2-HS in the HSR, we took advantage of the generated transgenic line lacking PfAP2-HS (10E_Δ*pfap2-hs*). We not only analysed the HS susceptibility phenotype, but also the HS-induced transcriptional response in this line compared to wild type and Q3417X-carrying lines.

5.1 Essentiality of PfAP2-HS under heat shock

As expected, the 10E_Δ*pfap2-hs* line had a HS-sensitive phenotype, such that its HS survival rate was 15-fold lower than in the parental line 10E, confirming that PfAP2-HS is necessary to drive a protective HSR. This HS-sensitive phenotype of 10E_Δ*pfap2-hs* was even more severe than in parasites with the Q3417X mutation (10G) (Fig. 32), which suggests that PfAP2-HSΔD3 still had residual activity in the HSR. However, it may also indicate that 10E_Δ*pfap2-hs* parasites have lower basal proteostasis capacity, such that they may already be at the edge of proteostasis collapse under basal conditions and any additional proteostatic damage (e.g. HS exposure) may have a larger impact.

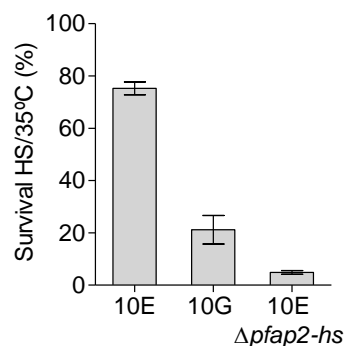


Figure 32. HS survival of parasite lines lacking PfAP2-HS. HS survival analysis, expressed as the percentage of parasitemia in HS-exposed cultures compared to their control cultures maintained at 35°C. Populations expressing different versions of PfAP2-HS were used, including 10E (wild type PfAP2-HS), 10G (PfAP2-HSΔD3) and 10E_Δ*pfap2-hs*. Values are the mean and s.e.m. of five independent biological replicates.

5.2 Transcriptomic analysis of the heat shock response

To further analyse the PfAP2-HS-dependent and independent HSR, we conducted a time-course transcriptomic analysis. Two-colour microarrays were used to compare the expression patterns of the 10E, 10G and 10E_Δ*pfap2-hs* lines before, during and after HS. Control cultures were always maintained at 35°C. This data was further validated analysing the transcript levels of eleven selected genes by RT-qPCR, using samples from an independent biological replicate (Annex III – Fig. 1).

Comparing our data to a reference transcriptome⁵⁸, we estimated the average parasite age of each sample and its IDC progression during the assay using a statistical likelihood-based method previously described³⁵⁹. This global transcriptional analysis revealed that HS results in delayed IDC progression and even growth arrest at the recovery phase, which was more pronounced in 10G and 10E_Δ*pfap2-hs* lines (**Fig. 33a**). In these lines, parasites completely stopped progressing throughout the IDC, possibly as a consequence of the high damage they suffer upon HS exposure, whereas 10E parasites kept progressing during and after HS (**Fig. 33a**). Interestingly, HS-exposed 10E parasites progressed faster than cultures under control conditions and this was maintained until the recovery phase, when the development almost stopped resulting in an overall delayed growth.

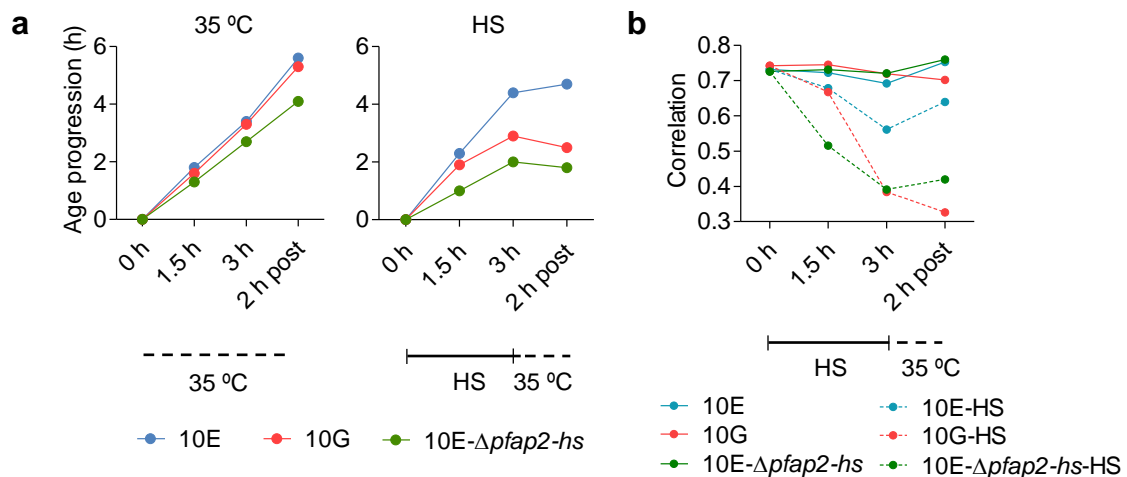


Figure 33. Effect of HS on age progression and on the global transcriptome. **a**, Age progression of wild type (10E), PfAP2-HSΔD3 (10G) and ΔPfAP2-HS (10E_Δ*pfap2-hs*) cultures during the HS assay, comparing HS-exposed and control (35°C) populations. Parasite age was statistically estimated from the transcriptomic data. **b**, Pearson correlation of the genome-wide transcript levels of each culture compared to the most similar time point of a high-density time-course reference transcriptome. Control cultures maintained at 35°C (continuous line) and HS-exposed (dashed line) cultures are shown.

Using this analysis, we could also corroborate that under nonstress conditions the 10E_Δ*pfap2-hs* line had slower IDC progression, consistent with the phenotypic analysis described before. We also showed that HS-exposed parasites were less similar to the reference transcriptome than control parasites (as defined by a lower correlation value) (**Fig. 33b**). In both HS-sensitive lines (10G and 10E_Δ*pfap2-hs*), this correlation sharply decreased after 3 h of HS and remained highly divergent during the recovery phase, supporting the idea that they are highly damaged during and after HS. In contrast, the alteration was less pronounced in 10E parasites during HS and it approached a basal state during the recovery phase, showing that 10E parasites can recover well from the stress. The patterns observed clearly reflected the HS survival rate of each line, such that the higher transcriptomic damage of HS-sensitive strains

was associated with lower survival, whereas the transcriptomic recovery observed in the HS-resistant line results in HS survival.

Fold change expression between HS-exposed and control cultures was calculated for each gene. From the 5,024 total genes analysed, only 361 showed a differential fold change expression greater than four ($FC > 4$) at any time point. Globally, there was a larger number of genes with altered (either up- or down-regulated) transcript levels during HS in 10G and 10E_Δ*pfap2-hs* compared to 10E (253, 240 and 75 genes, respectively) (Fig. 34), indicating that the HS-sensitive lines were undergoing a stronger general damage.

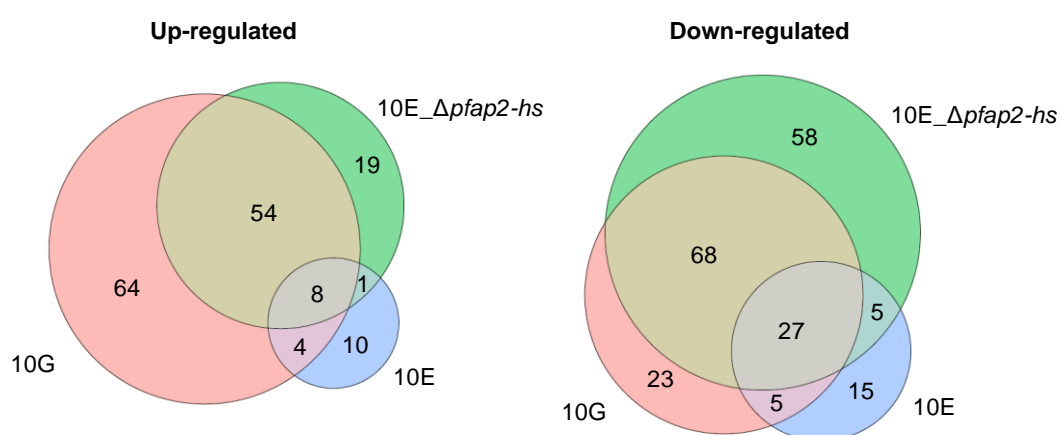


Figure 34. Venn diagrams of the genes with altered expression upon HS. Venn diagrams of genes with a fold change expression between HS-exposed and control conditions above 4 ($FC > 4$) for each of the three lines (10E, 10G and 10E_Δ*pfap2-hs*). Values indicate the number of genes corresponding to the specific section or intersection.

We performed hierarchical clustering of genes with transcript levels $FC > 4$. Clustering was based on changes in transcript levels relative to control cultures during and after HS. This clustering revealed a total of six clusters, which could be grouped in three general transcriptional patterns. (Fig. 35). Cluster I corresponded to the PfAP2-HS-dependent HSR and included genes that only show increased expression during HS in 10E. Clusters II-VI include genes that participate in the PfAP2-HS-independent HSR, showing either down-regulation (clusters II-III) or up-regulation (clusters IV-VI) in all parasite lines.

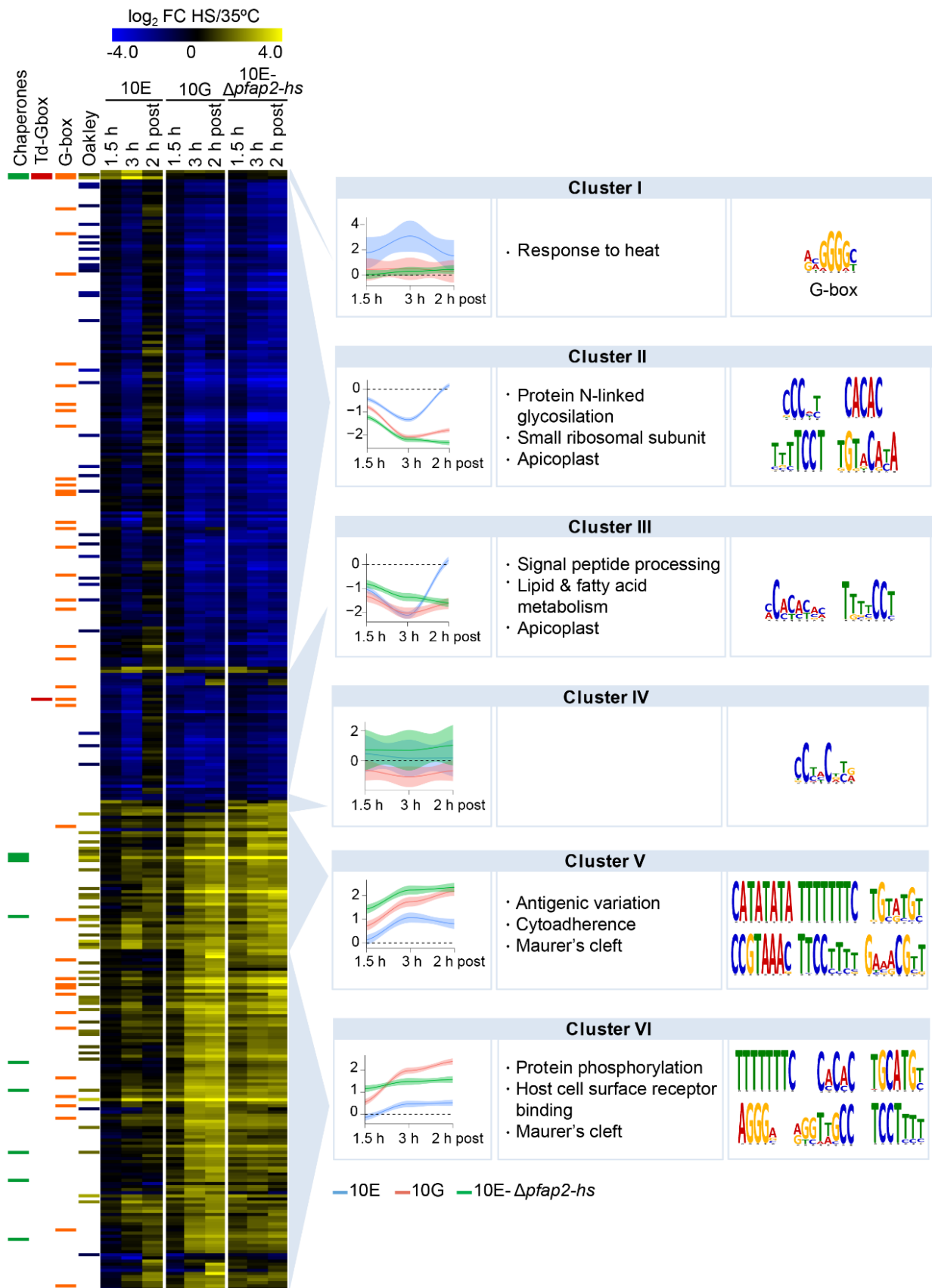


Figure 35. Global transcriptional alterations upon HS. a, Hierarchical clustering showing the \log_2 expression fold-change (FC) of HS-exposed vs. control cultures during HS (1.5 and 3 h) and 2 h after HS (2 h post). Genes with altered transcript levels (≥ 4 FC at any of the time points analysed) are shown. A total of 13 genes had values out of the range displayed (actual range: -4.78 to +4.93). For each cluster, the trend of the alteration upon HS in each parasite line (with 95% confidence interval), the representative enriched GO terms and the 8-mers motifs enriched in the promoter regions are also shown. Columns at the left indicate annotation as chaperone³¹¹, presence of the G-box⁸⁴ or tandem G-box (Td-Gbox) (described in fig. 37) in the upstream region, and \log_2 FC during HS determined in a previous study¹³⁰ (Oakley).

5.2.1 PfAP2-HS-dependent heat shock response

Cluster I corresponded to a small cluster of three genes that show a rapid increase in transcript levels upon HS only in parasites expressing complete PfAP2-HS. This cluster includes a gene of unknown function (PF3D7_1421800), *hsp70-1* (PF3D7_0818900) and *hsp90* (PF3D7_0708400) (**Fig. 36**). All of them show a high induction of expression after 3 h of HS (i.e. ~16-fold induction in *hsp70-1*) and a rapid recovery once the stress has ceased. This pattern, observed only in PfAP2-HS wild type parasites, indicates that these genes are part of the PfAP2-HS-dependent response.

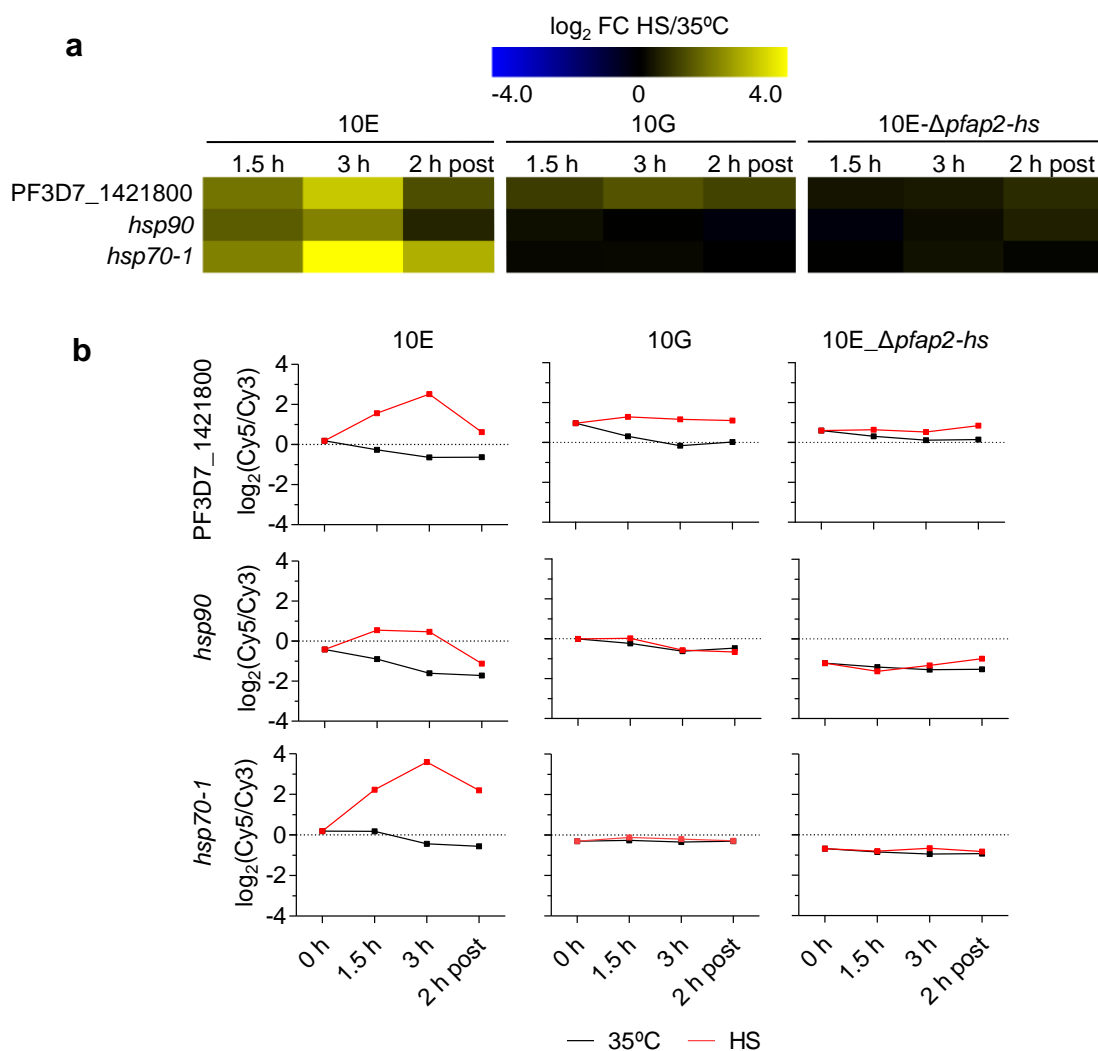


Figure 36. Genes regulated by PfAP2-HS during HS. **a**, Enlarged view of cluster I from fig. 35. Log₂ expression fold-change (FC) of HS-exposed vs control cultures during HS (1.5 and 3 h) and after HS (2 h post) is shown for the genes included in this cluster. **b**, Changes in log₂ expression of the three genes identified in cluster I (PF3D7_1421800, *hsp90* and *hsp70-1*). Data from the three tested populations under control (35°C) or HS conditions are shown.

Both *hsp70-1* and *hsp90* encode chaperones and are known for their involvement in the mechanism of response to heat. In contrast, PF3D7_1421800 is still poorly studied and has not predicted function. However, it was marked as essential in a *piggyBac*

mutagenesis-based screen³⁷⁶ and showed expression at early and late trophozoites¹⁵⁶, as well as in gametocytes and ookinetes³⁷⁷. Thus, so far, we could not predict its function in the mechanism of HSR, although its presumed essentiality indicates that it may play a key role in the IDC under basal conditions.

As expected, a motif resembling the G-box was found to be enriched in the promoter sequences of genes in cluster I (Fig. 35), as both *hsp70-1* and *hsp90* contain a highly conserved Td-Gbox in their regulatory region (Fig. 24). In contrast, the other genes containing a similar (but less conserved) Td-Gbox in their promoter did not show a PfAP2-HS-dependent transcriptional alteration (Fig. 37).

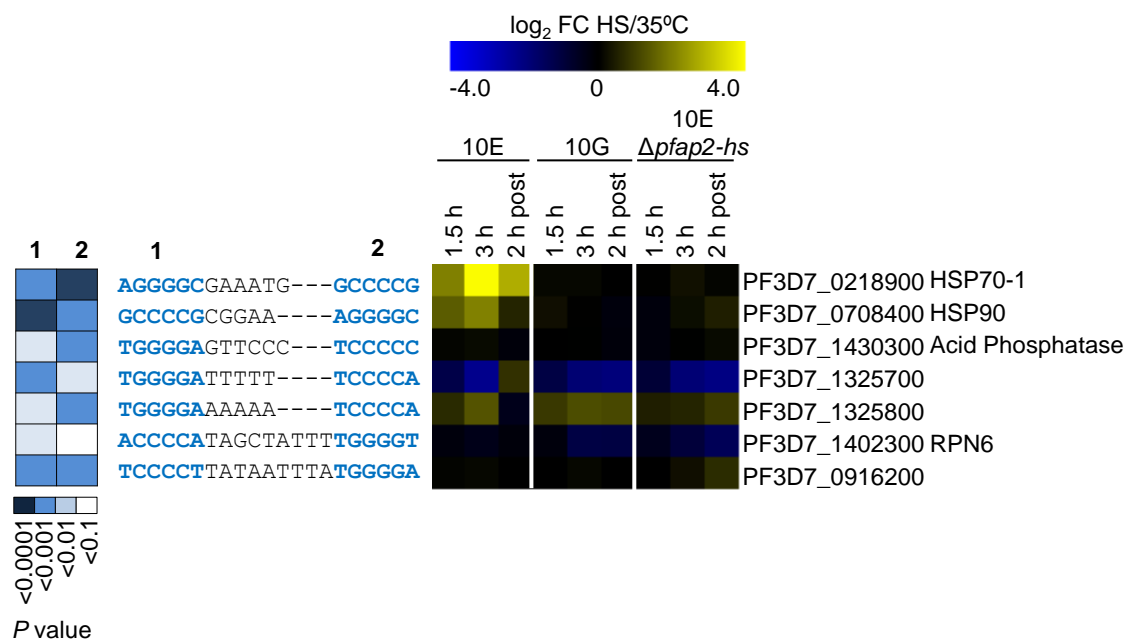


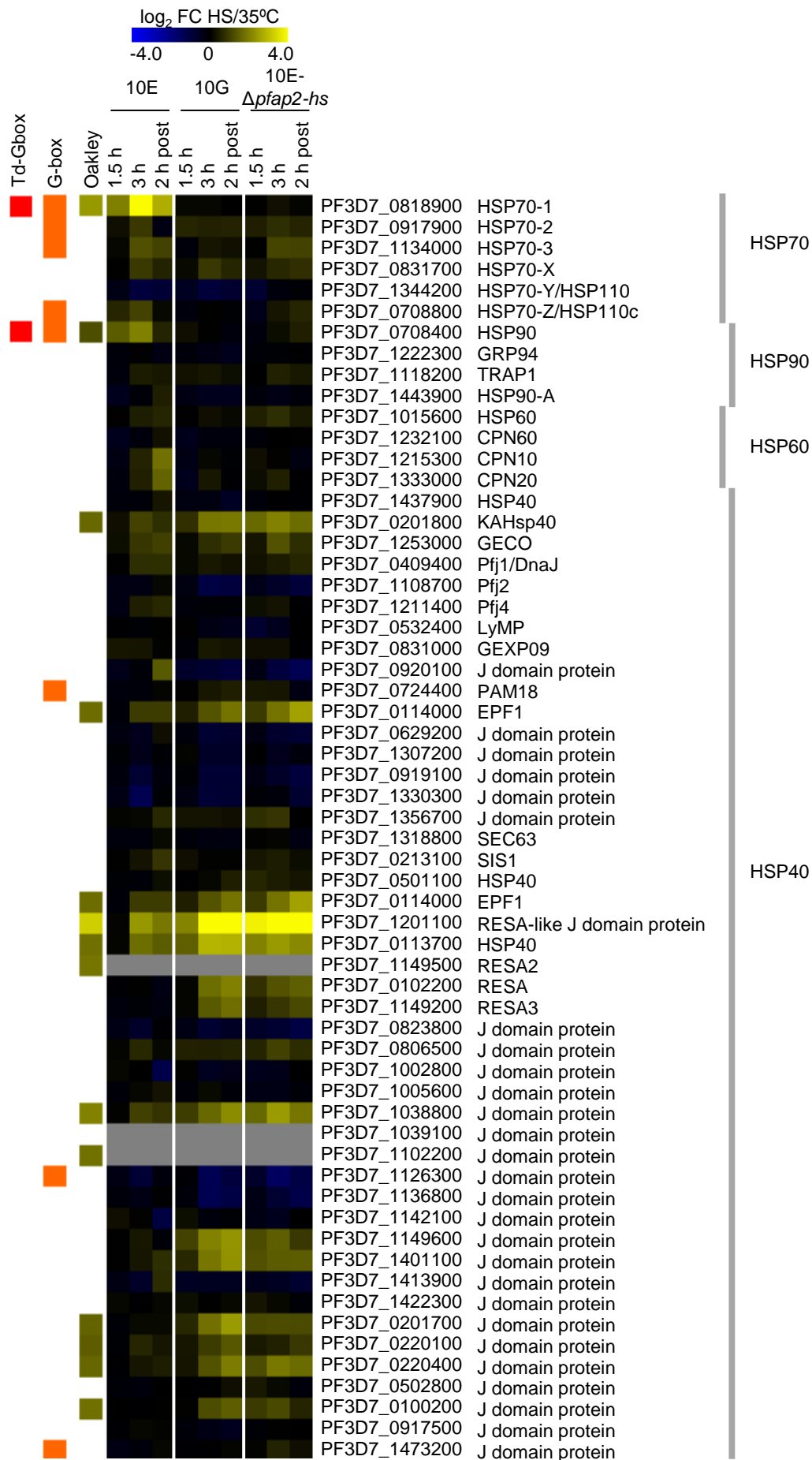
Figure 37. Transcriptional changes in genes containing a Td-Gbox in their promoter region. *P. falciparum* genes that contain a tandem arrangement of the G-box [(A/G)NGGGG(C/A)] motif (separated by maximum 9 bp) in their promoter region (defined as the 2 kb upstream of the start codon or until the previous gene when it is closer). The sequence identified as the G-box is highlighted in blue, and the level of concordance with the consensus G-box motif is expressed as the *P* value of the match (determined using the FIMO v5.0.5 function in the MEME suite). The \log_2 expression fold-change (FC) of HS-exposed vs control cultures during HS (1.5 and 3 h) and after HS (2 h post) for these genes is shown.

5.2.2 PfAP2-HS-independent heat shock response

The vast majority of genes in other clusters (II-VI) showed PfAP2-HS-independent alterations in expression, involving either down-regulation (clusters II and III) or up-regulation (clusters IV-VI) upon HS. Functional analysis showed an enrichment of genes involved in ribosomal formation, lipid and fatty acid metabolism, protein glycosylation and apicoplast location in clusters II-III, whereas clusters V-VI were enriched in genes involved in cytoadherence, host cell binding, protein phosphorylation and Maurer's cleft location (Fig. 35). Cluster IV did not show any enriched function,

probably due to its transcriptional variability and small size. Motifs such as TTTCC or CACA, which resemble the predicted target motifs of other ApiAP2⁸⁴, were enriched in some of these clusters (Fig. 35).

Transcriptional alteration in the expression of these genes (clusters II-VI) was observed in all the strains, but specially in parasites lacking a complete functional PfAP2-HS, in which changes persist during the recovery phase (2 h after HS) (Fig. 35). Instead, 10E parasites recovered normal transcript levels for many of these genes during the recovery phase. This indicates that the sustained alteration of these genes in the HS-sensitive lines was related with their low HS survival and may reflect cell damage or death. In addition to genes reflecting cell damage, clusters II-VI likely included genes that participate in the PfAP2-HS-independent damage response, such as some chaperone-encoding genes (Fig. 35). Apart from *hsp70-1* and *hsp90* from cluster I, only *cpn10*, *cpn20* and PF3D7_0920100 encoding a J domain protein showed lower expression in the defective *pfap2-hs* populations (Fig. 38). However, these genes seem to play a role in the recovery from stress rather than during HS, which suggest a regulation downstream of the PfAP2-HS-dependent response. In general, the expression of most chaperones and chaperonins was not altered by HS and the few alterations observed (e.g. KAHsp40 or RESA-like J domain protein) were PfAP2-HS-independent (Fig. 38). In fact, activation of these genes was higher in PfAP2-HS-defective lines, likely reflecting the most severe damage that they suffer. Increased expression of *pfap2-hs* itself was also observed, although at very low levels (maximum FC~1.8 after 3 h of HS in the 10E line and ~1.4 at 2 h post-HS in the 10G line), suggesting a possible positive feedback loop that may enhance the HSR.



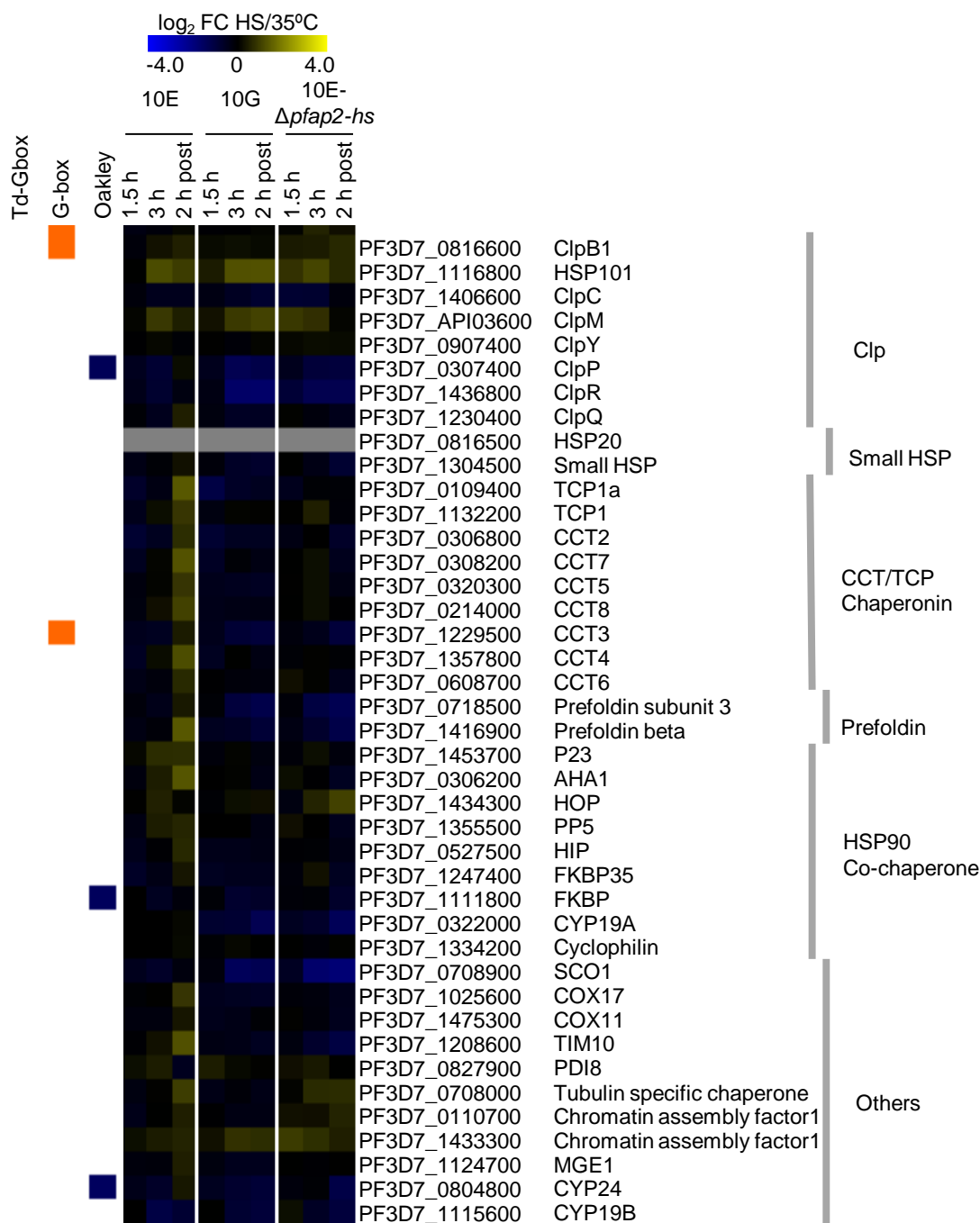


Figure 38. Transcript level changes upon HS in chaperone-encoding genes. \log_2 expression fold-change (FC) (HS relative to control conditions), as in fig. 35, for all chaperone-encoding genes described by Pavithra et al.³¹¹. Columns at the left indicate presence of the G-box⁸⁴ or tandem G-box (Td-Gbox) (described in fig. 37) in the upstream region, and \log_2 FC expression of genes reported to vary during HS in a previous study¹³⁰ (Oakley).

5.2.3 A closer look into the protective heat shock response

To provide a clearer view of the natural HSR, we analysed changes upon HS in the 10E line alone, in which cell damage produced by HS is limited as indicated by its high survival. A total of 935 genes showed above 2-fold alterations in the HS-exposed lines at any of the time points analysed, of which 428 were up-regulated and 507 down-regulated (Fig. 39). A sequential regulation is clearly observed, such that genes are

activated or repressed either early or late in the HSR, or take part in the recovery phase.

Our transcriptional analysis corroborated many of the findings previously described by Oakley et al.¹³⁰ (Fig. 39), despite using different culture synchronization, HS exposure and time point analysis. On the one hand, we observed up-regulation of genes involved in protein folding and stress response during HS, but also in the recovery phase. Among these altered genes, *hsp70-1* and *hsp90* were the most affected, but other members also showed transcriptional alterations, such as HSP70s, HSP40 co-chaperones (RESA-like and DnaJ domain proteins), chaperone co-activators, prefoldins, etc (Fig. 38). Similar to Oakley et al., we found that not all chaperones and chaperonins were affected by HS. Genes related with signal transduction and phosphorylation, mainly members of the calcium-dependent or FIKK serine/threonine kinase families, were also up-regulated during and after HS, suggesting that they play a role in the HSR. Genes involved in rRNA processing and cytoskeletal proteins were also up-regulated (e.g. alpha tubulin II, actin-like and actin-related proteins). Many metabolic pathways were affected, but in several cases genes from the same pathways were found to be altered in opposite directions, except for gluconeogenesis and phospholipid metabolism pathways, which were clearly up-regulated.

On the other hand, genes involved in protein translation and PTMs (e.g. protein glycosylation and signal peptide processing), and several components of the ubiquitin-dependent protein catabolic system, were down-regulated. As hypothesized by Oakley et al., this result might indicate a slowdown of protein synthesis and turnover, to either increase protein half-life or to conserve energy during stress. Also, lower expression was observed for genes involved in transmembrane transport and protein trafficking.

Contrary to Oakley et al. data, we found that expression of genes that participate in antigenic variation and cytoadherence, including *rifin* and *var* genes, was reduced upon HS. We also found down-regulation of genes involved in cell redox homeostasis and with oxidoreductase and antioxidant activity.

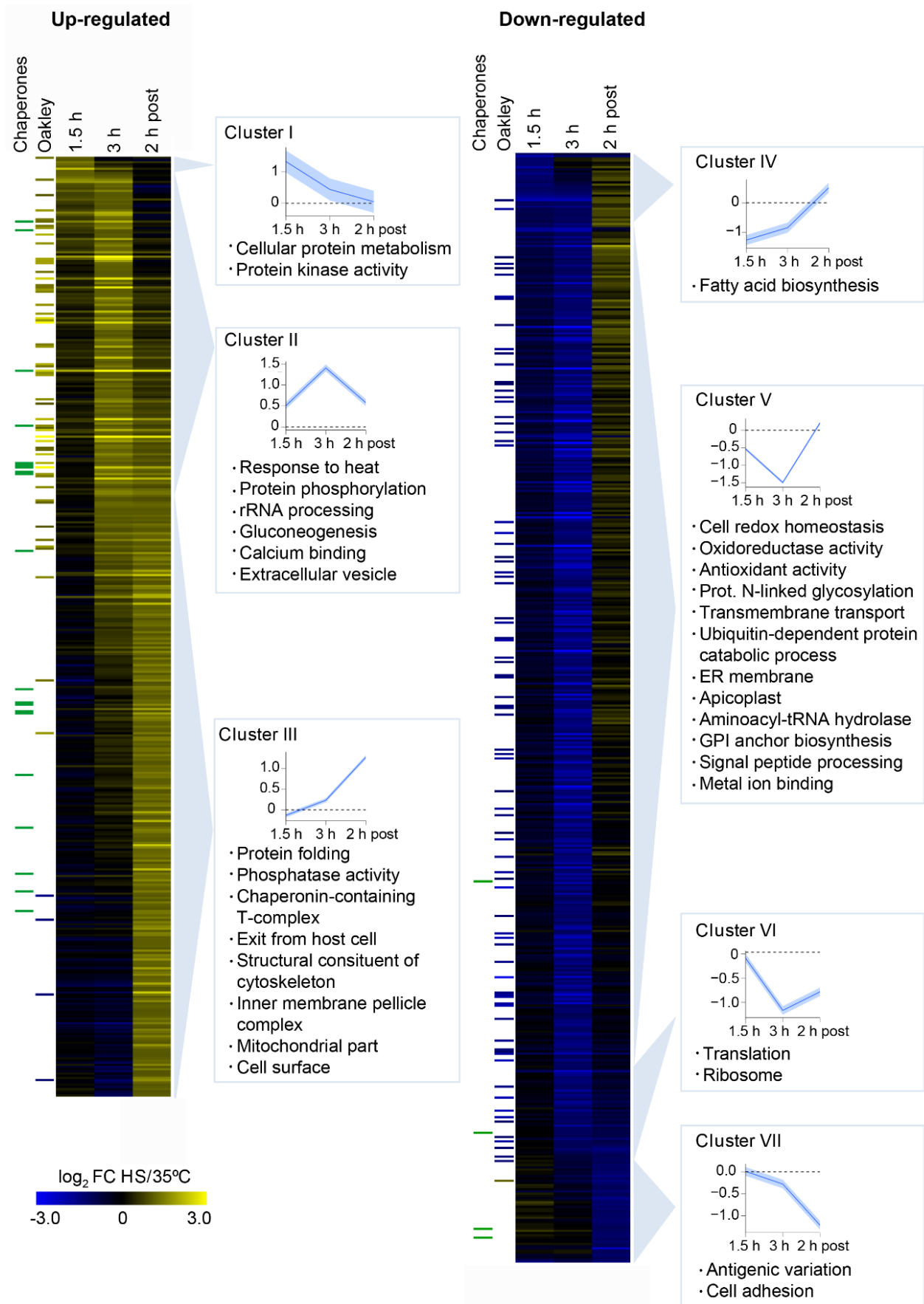


Figure 39. Transcriptomic characterization of the HSR in parasites expressing wild type PfAP2-HS. Hierarchical clustering of genes with a fold change ≥ 2 in the 10E line at any of the time points analysed. Log₂ expression fold-change (FC) (HS relative to control conditions) during (1.5 h and 3 h) and after (2 h post) the HS exposure in the 10E line is shown. The trend of the alteration upon HS (with 95% confidence interval) and representative enriched GO terms are shown for each cluster. Columns at the left indicate log₂ FC expression of genes reported to vary during HS in a previous study¹³⁰ (Oakley), and annotation as chaperone³¹¹. 10 genes had values out of the range displayed (actual range: -3.98 to +4.03).

5.3 PfAP2HS DNA-binding motifs involved in the heat shock response

In order to study the DNA motifs recognized by PfAP2-HS and to identify its direct targets, we first planned to use the transgenic lines expressing tagged PfAP2-HS to perform ChIP-seq analysis. The impossibility to detect the protein suggested that PfAP2-HS abundance is too low for this analysis. Hence, we decided to study it from another perspective, using the ATAC-seq technology to identify chromatin open regions. Also, we used a modified *hsp70-1* promoter driving the expression of *Td-Tomato* to focus on the role of the G-box motif in the HSR.

5.3.1 ATAC-seq analysis of the chromatin open regions under basal conditions

Instead of identifying the sequences directly bound by the protein of interest, the ATAC-seq technique allows the identification of open regions of chromatin, which are free of nucleosomes and often correspond to intergenic sequences where transcription factors are bound³⁶⁷ (Fig. 40a).

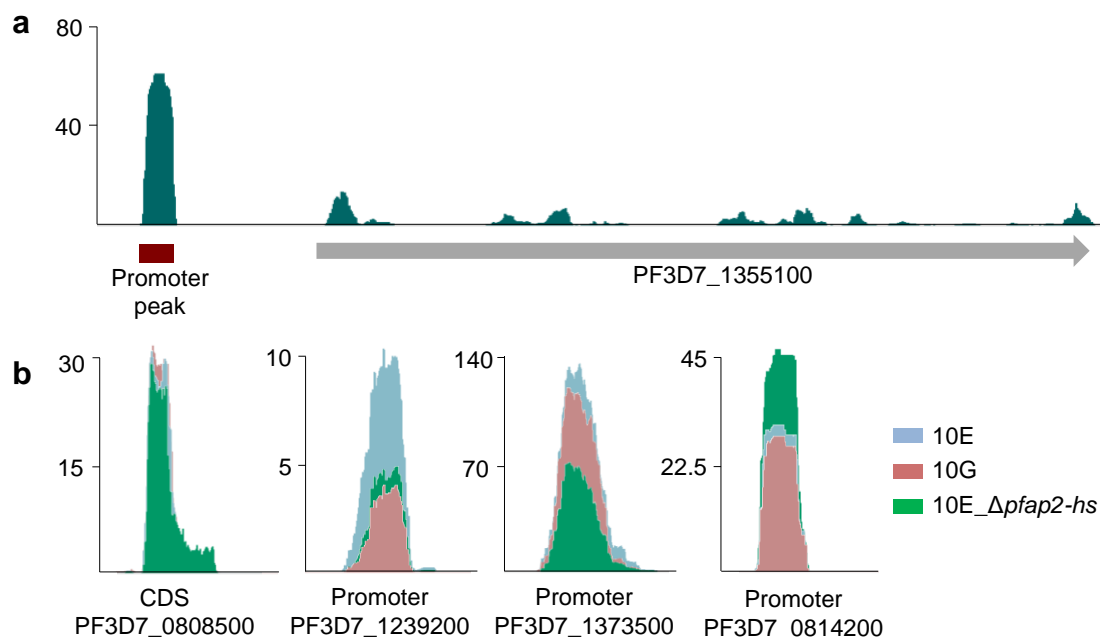


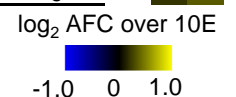
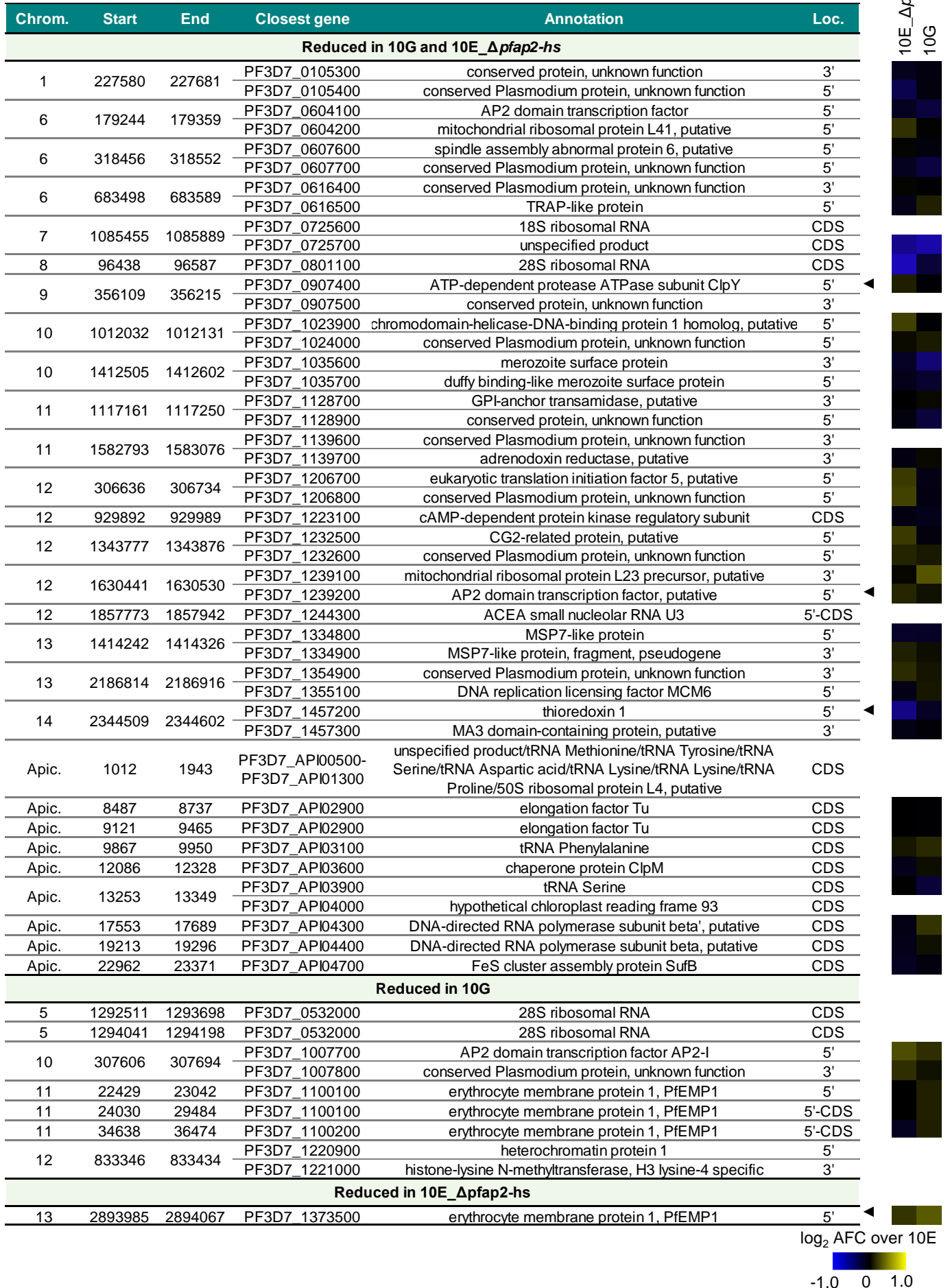
Figure 40. Typical ATAC-seq peak and variations found in the analysis. **a**, ATAC-seq peak located in the promoter of the PF3D7_1355100 gene. Peaks are also commonly found in the coding sequence (CDS). **b**, Examples of common or differential peaks found between 10E, 10G and 10E_Δ*pfap2-hs* strains: equal peak (left), peak reduced in both HS-sensitive strains (middle left); peak reduced only in 10E_Δ*pfap2-hs* (middle right) or peak increased only in 10E_Δ*pfap2-hs* (right). These peaks are all located in the CDS or promoter regions of the genes specified below. Values correspond to the number of reads in each position, normalized by input against genomic DNA.

Thus, by comparing lines expressing Δ PfAP2-HS, PfAP2-HS Δ D3 and wild type PfAP2-HS both under control and HS conditions, we expected to be able to identify the differential peaks of open chromatin that could be attributable to the lack of functional PfAP2-HS. This was a preliminary and exploratory experiment, and consequently further analysis and replicates must be done to make conclusions from this assay.

The ATAC-seq data was first used to compare the control (not exposed to HS) populations, with the aim to identify differences that could support the phenotypes observed under nonstress conditions. In this case, differential peak calling analysis revealed 39 differential peaks among the three populations tested (**Table 40**). However, contrary to what we expected, we did not identify any peak completely absent in the 10E_ Δ *pfap2-hs* line. In the case of *hsp70-1*, for instance, the peak located in the upstream Td-Gbox was present in the 10E, 10G and 10E_ Δ *pfap2-hs*, suggesting that it may not correspond to PfAP2-HS binding. Similarly, other peaks were present in all the lines tested and the difference between strains relied on the magnitude of the peak, which was either reduced or increased compared to 10E. This result suggests that the peaks were not only the consequence of PfAP2-HS binding, but also correspond to attachment of other factors or complexes.

The majority of differential peaks were reduced in both HS-sensitive lines. Some examples were the peaks located in the upstream region of the ATP-dependent protease ATPase subunit ClpY (PF3D7_0907400), an ApiAP2 transcription factor (PF3D7_1239200) (**Fig. 40b**) or the thioredoxin 1 (PF3D7_1457200). In contrast, one peak was found to be significantly reduced only in the 10E_ Δ *pfap2-hs* line, located in the promoter region of a *var* gene (PF3D7_1373500) (**Fig.40b**), which can be explained by its clonally variant expression profile. We also found some peaks that increased in the 10E_ Δ *pfap2-hs* line, such as the peak located in the promoter region of the DNA/RNA-binding protein Alba1 (PF3D7_0814200) (**Fig. 40b**). Although the identified differential peaks were mainly located in 3' or 5' regulatory regions, suggesting a putative role in regulating gene expression, no clear correlation was found between the data derived from ATAC-seq and microarray analysis (**Table 40**). For instance, reduced ATAC-seq peaks were not associated with reduction of transcript levels, and vice versa. This observation contrasts with previous studies in which chromatin accessibility can predict transcript levels^{111,112} and raises questions on whether our assay needs more optimization.

a



b

Chrom.	Start	End	Closest gene	Annotation	Loc.
Increased in 10G					
7	1086528	1088370	PF3D7_0726000	28S ribosomal RNA	CDS
Increased in 10G and 10E_Δpfap2-hs					
8	685145	685233	PF3D7_0814100	conserved Plasmodium protein, unknown function	5'
			PF3D7_0814200	DNA/RNA-binding protein Alba 1	5'
14	1716385	1716485	PF3D7_1442300	adrenodoxin reductase, putative	3'
			PF3D7_1442400	conserved Plasmodium protein, unknown function	5'

Table 40. Differential ATAC-seq peaks between 10E, 10G and 10E_Δpfap2-hs strains under nonstress conditions. List of the differential ATAC-seq peaks between 10E, 10G and 10E_Δpfap2-hs lines under nonstress conditions (maintained at 35°C). Peaks are classified as reduced (**a**) or increased (**b**) versus the control 10E line. Start and end position is indicated for each peak. The annotation of the closest gene for each peak is provided, as well as their position relative to the gene (5' or 3'): upstream (5'), downstream (3') or coding sequence (CDS). The heatmap at the right shows the \log_2 of the average expression fold-change (AFC) for each gene relative to 10E, as determined in the microarray analysis. Arrowheads indicate the genes that are mentioned in the main text. Chrom., chromosome; Loc., location relative to gene.

5.3.2 ATAC-seq analysis of the chromatin open regions upon heat shock

Peak calling analysis comparing HS-exposed vs control cultures revealed similar patterns for all the lines and identified a total of 65 differential peaks (**Table 41**).

Although some peaks were equally affected in all the lines, either being increased or reduced upon HS, we could identify differential peaks that were only altered in specific lines. For instance, we found a 2.8-fold increase of the peak located in the *hsp70-1* coding sequence only in the 10E line upon HS, but not in either of the HS-sensitive strains (**Fig. 41**). Instead of being related to transcription factor binding, this peak may correspond to a high quantity of Pol II molecules attached to this locus and being highly active upon HS, which correlates with the increased transcription also found in the microarray analysis. In contrast, we observed a clear ATAC-seq peak that coincided with the position of the Td-Gbox, but it showed no alteration upon HS in the wild type 10E line, and it was only slightly reduced in 10G and 10E_Δpfap2-hs. A similar pattern was observed in *hsp90*, where the upstream Td-Gbox peak decreased only in the HS-sensitive strains upon HS, but not in the 10E line (**Fig. 41**). Thus, contrary to what we initially expected, there was not increased binding in the Td-Gbox region upon HS in the wild type, but instead we observed reduced binding in the HS-sensitive lines. We still cannot explain this paradoxical result, although it may probably indicate that the observed peak does not correspond to PfAP2-HS binding only, and other factors bind

to the same regions and contribute to generating the open chromatin region around the Td-Gbox.

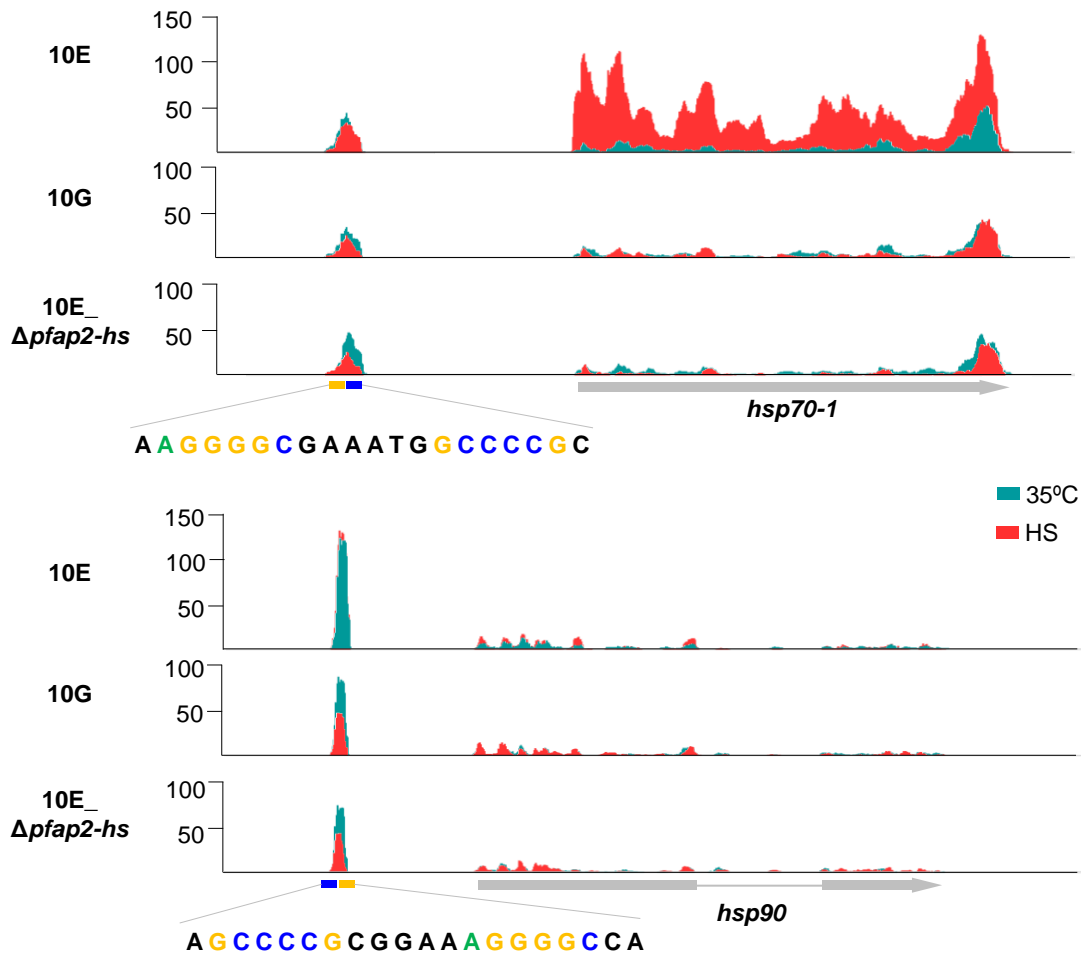


Figure 41. Nucleosome-free regions identified by ATAC-seq analysis of the *hsp70-1* and *hsp90* loci. Peaks corresponding to the chromatin open regions found in *hsp70-1* (up) and *hsp90* (down) ORF and promoter, comparing HS-exposed and control (35°C) cultures. The Td-Gbox and the coding sequence are highlighted in both genes by a yellow/blue and grey lines, respectively, and introns are represented by a thinner line. The sequences corresponding to the Td-Gbox are displayed below. Values correspond to the number of reads in each position, normalized by input against genomic DNA.

Similar to *hsp70-1* and *hsp90*, other peaks were found to be specifically reduced in the HS-sensitive lines (10G and 10E_Δ*pfap2-hs*), such as the peak in the 5' region of *pfap2-exp* (PF3D7_1466400). Other peaks were increased in these two lines, including the ones located in the promoter regions of the heat shock protein 101 (PF3D7_1116800) or the RESA-like protein (PF3D7_1201100). We could also identify some alterations specifically found in 10E_Δ*pfap2-hs* parasites. Some examples are the peaks located in the transcription initiation factor TFIIB (PF3D7_0110800) 5' region or in the 28S rRNA (PF3D7_0532000) coding sequence, which were increased or reduced only in 10E_Δ*pfap2-hs*, respectively (Fig. 42 and Table 41).

Although in some cases the presence of a higher peak was associated with induction of transcript levels upon HS (e.g. *hsp70-1*, PF3D7_1201100 or PF3D7_1252400), a general correlation could not be established between ATAC-seq and microarrays data. Again, this discrepancy highlights the limitations of this analysis and the need of further optimization and replicates to understand the real scenario.

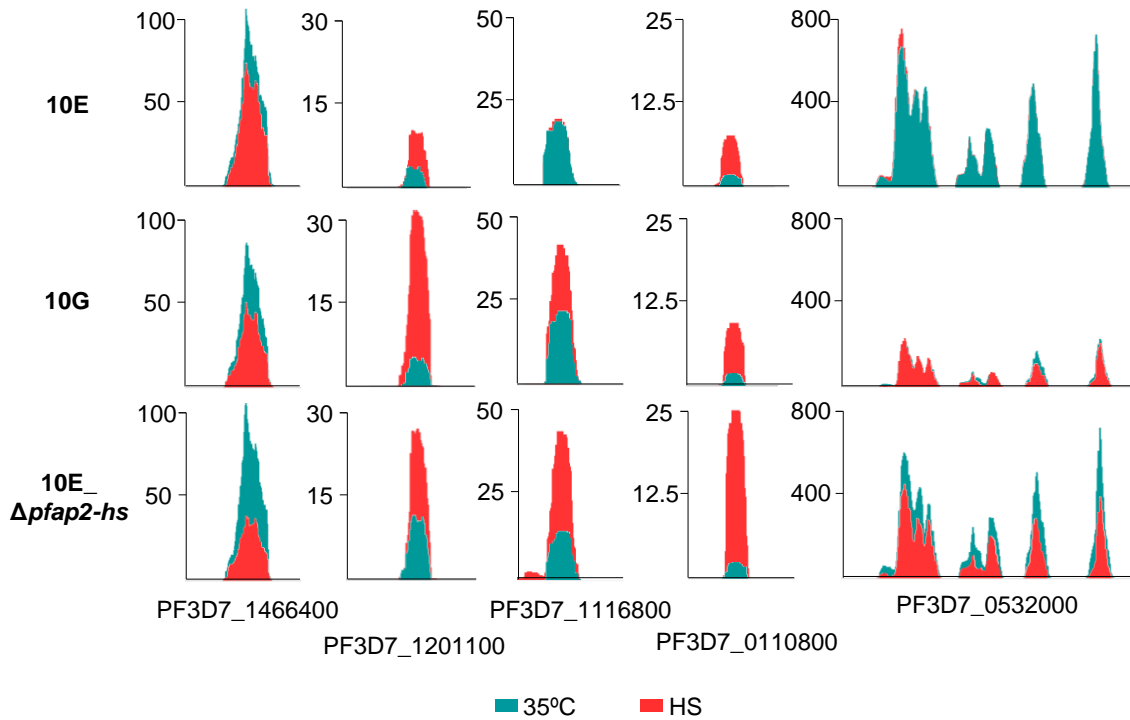


Figure 42. Relevant nucleosome-free regions identified by ATAC-seq analysis. Peaks corresponding to the chromatin open regions found in PF3D7_1466400, PD3D7_1201100, PF3D7_1116800, PF3D7_0110800 promoters and PF3D7_0532000 coding sequence are shown, comparing HS-exposed and control (35°C) cultures. Values correspond to the number of reads in each position, normalized by input against genomic DNA.

b

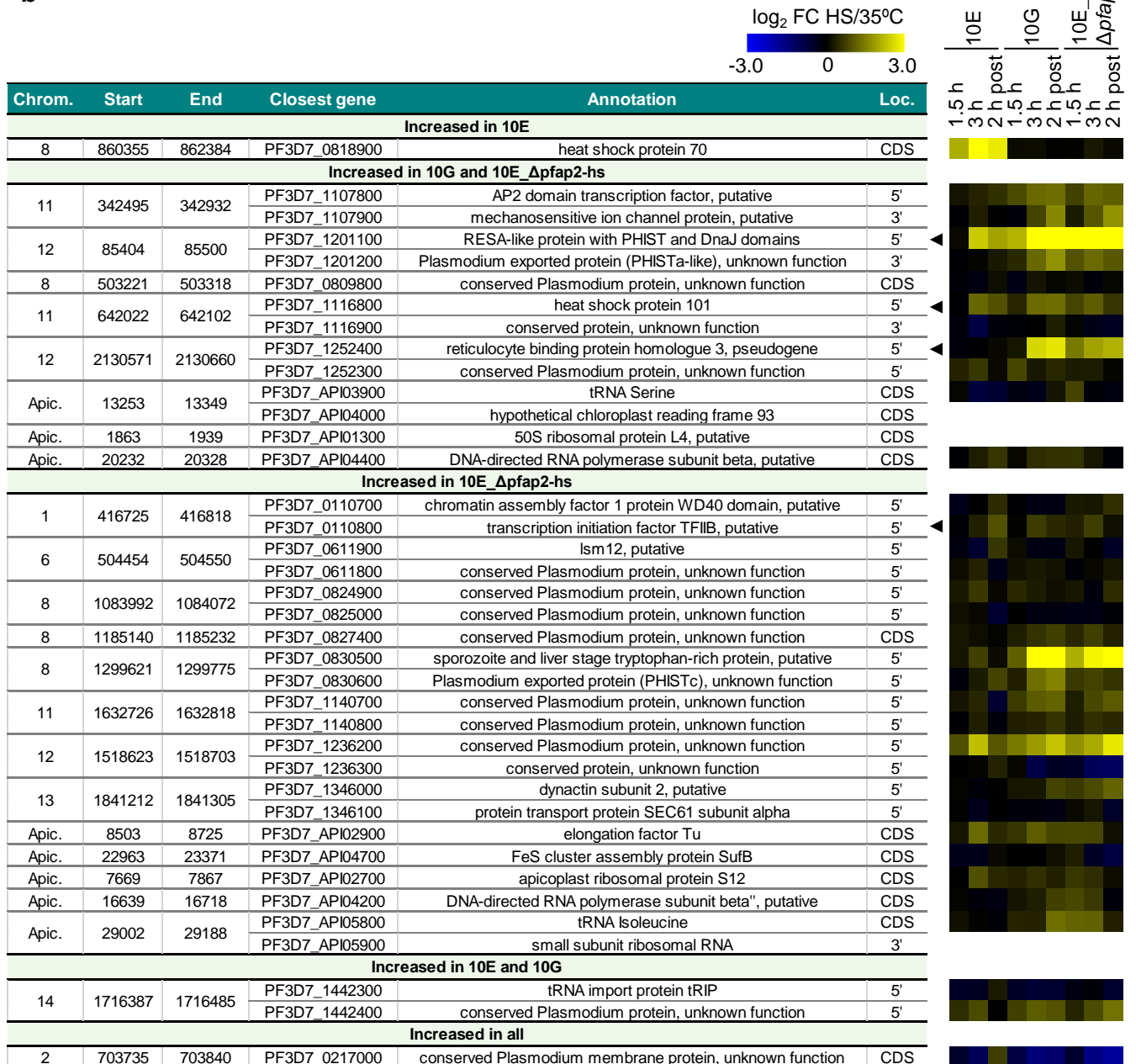


Table 41. Differential ATAC-seq peaks between HS-exposed and control populations. List of the differential ATAC-seq peaks with a fold change above 1.5 identified between HS-exposed and control parasites from 10E, 10G and 10E_Δpfap2-hs cultures. Peaks are classified as reduced (a) or increased (b) upon HS exposure, indicating in which line the peak was altered. Start and end position are indicated for each peak. The annotation of the closest gene for each peak is provided, as well as their position relative to the gene (5' or 3'): upstream (5'), downstream (3') or coding sequence (CDS). The heatmap at the right shows the log₂ of the fold-change (FC) expression values of different time points during the heat shock assay in the three populations, as determined in the microarray analysis. Arrowheads indicate the genes that are mentioned in the main text. Chrom., chromosome; Loc., location relative to gene.

5.3.3 Analysis of the role of the Td-Gbox in *hsp70-1* induction upon heat shock

As the ATAC-seq analysis didn't reveal any conclusive results about the motifs bound by PfAP2-HS, we focused on the role of the G-box motif, previously shown to be recognized by PfAP2-HS⁸⁴. The approach used for this purpose was based on transgenic parasite lines with an exogenous *hsp70-1* promoter driving the expression of a *Td-Tomato* fluorescent marker. This promoter was previously modified, such that the Td-Gbox motif was either maintained or disrupted by changing a single or both G-boxes (Fig. 43a). The construct was integrated in the liver specific protein 1 (*lisp1*, PF3D7_1418100) locus, which is not essential in the asexual intraerythrocytic stages.

We obtained two correctly edited transgenic lines (10E_2Gbox_TdT and 10E_1Gbox_TdT), validated by PCR and Sanger sequencing of the G-box-containing region (Fig. 43b). However, PCR analysis of the 10E_0Gbox_TdT line revealed an unexpected PCR double band, although the integrated promoter had the edited sequence instead of the Td-Gbox. We reasoned that it may be due to a recombination event in the *Td-Tomato* promoter region and, although we used it in our analysis, we took it into account for the interpretation of the results.

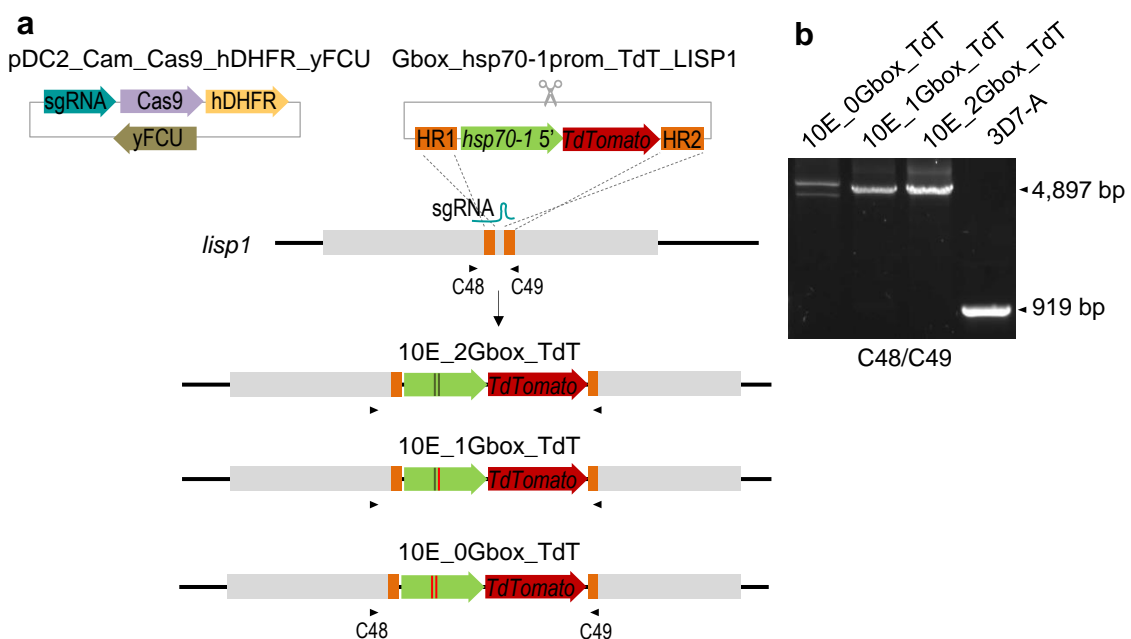


Figure 43. Generation of transgenic lines expressing Td-Tomato driven by a *hsp70-1* promoter containing 0, 1 or 2 G-boxes. Schematic of the CRISPR/Cas9 strategy used to integrate a modified *hsp70-1* promoter driving Td-Tomato expression in the liver specific protein 1 (*lisp1*, PF3D7_1418100) locus. For the promoter, the 2 kb upstream of the ATG from *hsp70-1* were used, which include the Td-Gbox (dark green lines). We also generated two other constructs, in which the Td-Gbox was modified by changing a single G-box or both G-boxes for other sequences (red lines). The position of the primers used for analytical PCR is indicated by arrowheads. The electrophoresis image at the right shows the analytical PCR validation of the genetic edition, indicating the expected size of the amplified product in wild type (3D7-A) and correctly edited (10E_0Gbox_TdT; 10E_1Gbox_TdT and 10E_2Gbox_TdT) parasites.

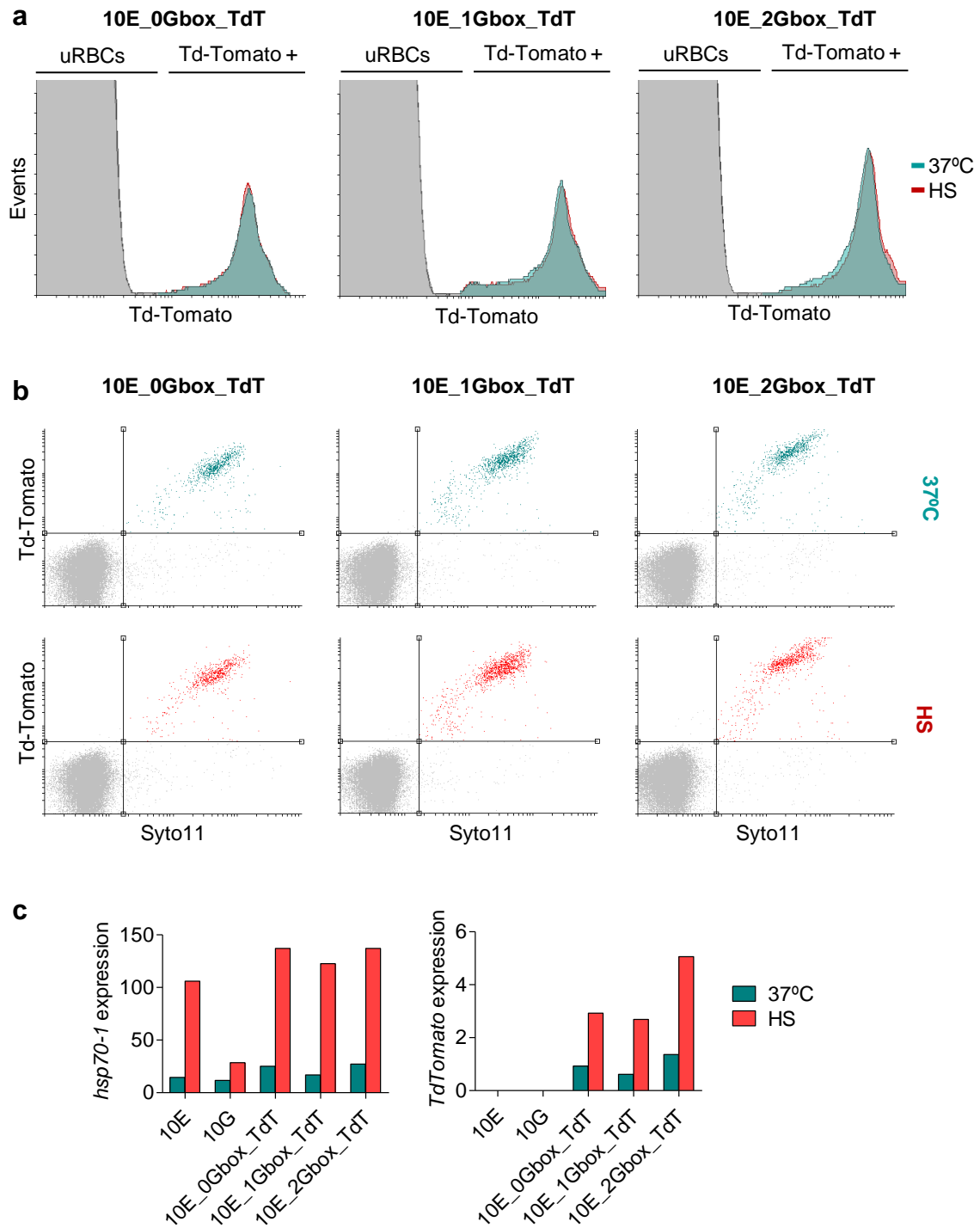


Figure 44. *Td-Tomato* expression driven by the *hsp70-1* promoter containing 0, 1 or 2 G-boxes. a-b, FACS analysis at the trophozoite stage showing the *Td-Tomato* signal from three transgenic lines that contain an exogenous *hsp70-1* promoter with the *Td-Gbox* (10E_2Gbox_TdT), a single G-box (10E_1Gbox_TdT) or both G-boxes totally disrupted (10E_0Gbox_TdT). Data is represented by histogram plots of *Td-Tomato* signal showing the overlapped data from HS-exposed (red) or control (37°C, green) populations (a), or by dot plots of *Td-Tomato* and *Syto11* signal of each sample (b). **c,** Transcript levels of *hsp70-1* and *Td-Tomato* (relative to *serine--tRNA ligase*) after HS in the three transgenic lines. HS-resistant (10E) and HS-sensitive (10G) lines were used as non-edited controls. uRBCs: uninfected RBCs.

The transgenic lines generated were used to quantify the Td-Tomato fluorescence levels by flow cytometry under both nonstress and HS conditions. However, we observed no difference in Td-Tomato fluorescence between HS and control conditions in any of the three different combinations of Td-Gbox (Fig. 44a-b). To confirm that this result was not due to signal saturation, we analysed the expression of Td-Tomato by RT-qPCR. In this case, *Td-tomato* transcript levels did show an increase upon HS (Fig. 44c). However, this induction was driven by all the modified promoters tested, suggesting that the Td-Gbox is not necessary to regulate *hsp70-1* expression upon HS.

Before concluding anything from this unexpected result, some aspects must be considered. First, *Td-Tomato* transcript levels observed under normal conditions were much lower than the levels for the endogenous *hsp70-1*, indicating that the endogenous and exogenous *hsp70-1* promoters were not driving the same level of expression. Similarly, the increase in *Td-Tomato* transcripts upon HS was lower than the FC observed for endogenous *hsp70-1*, suggesting again that the promoter used in these transgenic lines does not have the same activity as the endogenous one. This could be due to the need for a longer *hsp70-1* promoter or a specific 3' region that include more regulatory sequences, a previously described for *hsp90*¹⁰². Also, the chromatin environment in the edited loci may also influence *Td-Tomato* expression. Finally, while equal Td-Tomato signal was detected by flow cytometry in all samples (control and HS-exposed), different transcript levels were observed between these conditions. This effect indicates either that Td-Tomato signal was saturated in all samples or that a delayed translation was taking place, and thus the Td-Tomato signal that we were detecting was not the HS-induced but the background levels.

Altogether, our ATAC-seq and gene reporter experiments neither corroborated nor discarded the function of the tandem and single G-box in PfAP2-HS target gene regulation. Further optimization and generation of more transgenic lines is needed to obtain conclusive results from these experimental approaches.

5.4 Analysis of the role of PfAP2-HS in other types of stress

Protein folding was identified as one of the pathways affected by *pfap2-hs* deletion under nonstress conditions (see Results, section 4.2), likely resulting in a lower capacity for protein homeostasis (proteostasis) maintenance. The ability of $\Delta pfap2-hs$ parasites to grow at 35°C but not at 37°C also suggests that PfAP2-HS is necessary for normal proteostasis. Consequently, stress affecting proteostasis was predicted to have

a higher impact on the $\Delta pfap2$ -*hs* line. To test this hypothesis, we determined the sensitivity to a panel of compounds known to induce different types of stress that lead to a proteotoxic situation, including DTT and H₂O₂, which induce ER-stress and oxidative stress, respectively. Additionally, we added in this analysis the drug DHA, which kills parasites by impairing proteostasis.

5.4.1 Analysis of the role of PfAP2-HS in stress induced by DTT and H₂O₂

We tested the effect of a range of concentrations of different stress-inducing compounds (DTT and H₂O₂) in trophozoite-stage parasites, comparing populations expressing the wild type (1.2B or 10E lines) or PfAP2-HS Δ D3 (10G line) version of PfAP2-HS.

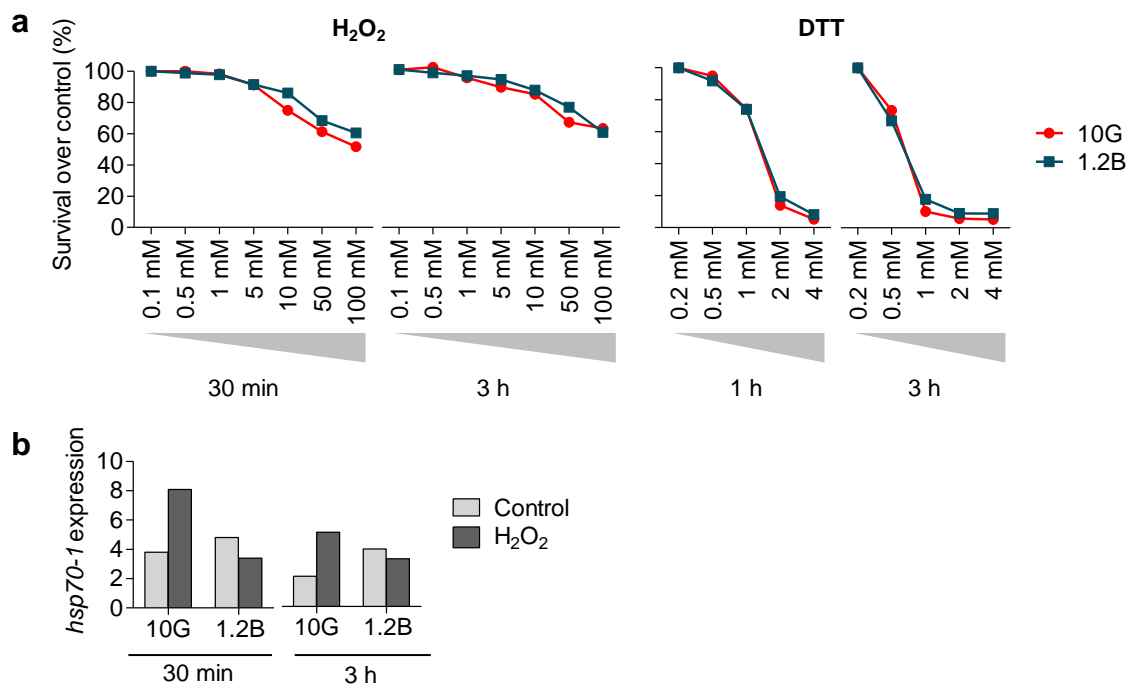


Figure 45. Parasite survival to H₂O₂ and DTT-induced stress. **a**, HS-sensitive (10G) and HS-resistant (1.2B) populations were exposed for 30 min, 1 h or 3 h to several concentrations of either H₂O₂ (0.1 – 100 mM) or DTT (0.2 – 4 mM). Values indicate the survival percentage (%) of stress-exposed cultures versus their controls maintained under nonstress conditions. **b**, Transcript levels of *hsp70-1* (normalized by *actin 1*, as in previous studies¹²⁶) of 10G and 1.2B cultures after being exposed to 50 mM H₂O₂ for 30 min or 3 h.

In the case of DTT and H₂O₂ exposure, only small differences unlikely to have biological relevance were found between the HS-sensitive and the HS-resistant populations at the tested conditions (Fig. 45a). In the case of H₂O₂, concentrations higher than 100 mM were also tested, but all resulted in high damage to RBCs viability, rather than affecting the parasite itself. Also, the high non-specific damage produced by DTT may mask the effect of PfAP2-HS in assisting survival in front of this challenge. Thus, we analysed *hsp70-1* expression as a proxy of PfAP2-HS activity. We selected the 50 mM H₂O₂ condition, which showed the biggest difference at both 30 min and 3 h

exposure. In this case, the exposure to H₂O₂ increase in *hsp70-1* expression in the 10G line after 30 min and 3 h, but not in the wild type 1.2B. Thus, this analysis provided no evidence of PfAP2-HS-dependent response to DTT or H₂O₂ induced stress (Fig. 45b). However, these are just preliminary experiments in which a limited number of drug concentrations and parasite strains were used. New assays should include the 10E_Δ*pfap2-hs* transgenic line as a key tool to determine the implication of PfAP2-HS in the response to these other types of cellular stress.

5.4.2 Analysis of the role of PfAP2-HS in stress induced by DHA

We also studied sensitivity to DHA, the main antimalarial drug currently known to impair proteostasis³⁷⁸. In this case, we characterized the DHA half maximal inhibitory concentration (IC₅₀) in the Δ*pfap2-hs* line compared to 10E and 10G at either the ring or trophozoite stage. Interestingly, the 10E_Δ*pfap2-hs* line showed a >2-fold lower IC₅₀ than its parental 10E line both at the ring and trophozoite stages (Fig. 46). This higher sensitivity may be explained both by the low basal proteostasis maintenance capacity and the lack of a PfAP2-HS-dependent protective response in the knockout parasites.

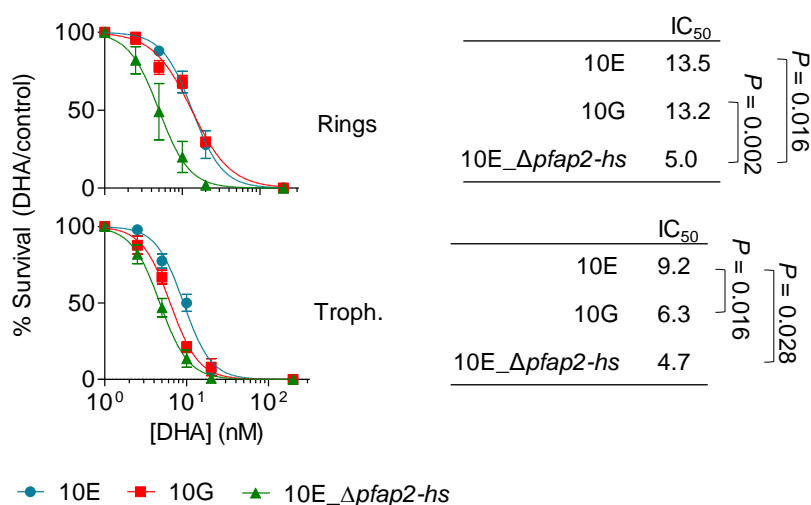


Figure 46. Dihydroartemisinin sensitivity of parasite lines expressing different versions of PfAP2-HS. Survival (%) after a 3 h pulse of different dihydroartemisinin (DHA) concentrations (2.5 – 20 nM). Parasites were exposed to DHA either at the ring (upper panel) or trophozoite stages (lower panel). Values are the mean and s.e.m. of three biological replicates, fitted to a sigmoidal dose-response curve. IC₅₀ and significant *P* values (*P*<0.05), calculated using a two-tailed paired *t*-test, are shown. All cultures were maintained at 35°C. Troph., trophozoites.

Parasites carrying the Q3417X mutation (10G line) also resulted significantly more sensitive to DHA than the 10E line at the trophozoite stage. In this case, the mutation does not induce any deleterious effect under basal conditions, indicating that this increased DHA sensitivity was due to the lack of a correct PfAP2-HS-driven protective response. However, this difference between 10G and 10E lines was only observed in

trophozoites, whereas at the ring stage both lines showed similar DHA sensitivity, similar to the pattern of HS survival (**Fig. 46**).

Altogether these results suggest that a directed response driven by PfAP2-HS may also play a role in the stress response to DHA, highlighting its importance in stress conditions beyond HS.

6 PRELIMINARY CHARACTERIZATION OF THE *P. BERGHEI* ORTHOLOG OF PfAP2-HS

AP2-HS is highly conserved among *Plasmodium* species, suggesting that its functions throughout the IDC may be also conserved. Thus, we used the rodent-infective species *P. berghei* to test a possible role of the PfAP2-HS ortholog (PbAP2-HS, PBANKA_1356000) as a housekeeping and HSR regulator.

We generated a construct to reproduce in *P. berghei* the stop codon mutation Q3417X found to be associated with HS sensitivity in *P. falciparum* (**Annex II – Fig. 9**). After 2 attempts, we could not obtain PbAP2-HS Δ D3 lines. Genetic edition in *P. berghei* is much more efficient than in *P. falciparum*, such that the impossibility to obtain a specific transgenic line indicates that such edited parasites are not viable. Thus, we concluded that parasites carrying the premature stop codon mutation were not viable *in vivo*, consequently suggesting that a fully functional PbAP2-HS is essential in *P. berghei*. We didn't try to obtain the full knockout of *pbap2-hs*, as previous studies already reported its essentiality in *P. berghei* and *P. yoelii*^{85,90,379}.

In order to study the role of PbAP2-HS *in vivo*, we used the c2m2_PbAP2-HS::KS transgenic line, in which PbAP2-HS mislocalization can be induced by the addition of Rapa (**Annex II – Fig. 7**). We first attempted to study its essentiality *in vivo* by directly injecting Rapa to mice, but the results obtained were not consistent nor conclusive, and it was not possible to perform more replicates due to technical and logistic issues.

We also used this transgenic line to study the implication of PbAP2-HS in the HSR in *P. berghei in vivo* infections. As mice do not experience fever in response to *Plasmodium* infection, we exposed parasites to HS *ex vivo*, adding or not Rapa to the culture, and afterwards we injected the resultant HS-exposed parasites to mice to follow the evolution of the infection *in vivo*. Apart from ensuring the same HS episode in all conditions, this design also allowed us to overcome the obstacle of PbAP2-HS essentiality *in vivo* and to specifically test its role during HS stress. The temperature of HS was also adapted, as we observed that a 3 h at 41.5°C HS resulted in ~30% survival in the wild type *P. berghei* cl15cy1 line (**Fig. 47a**), reason why we decided to use a lower temperature (40°C) for the *P. berghei* HS assay that resulted in ~90% survival. Doing this assay, we observed that addition of Rapa during the HS had an effect on the HSR, such that parasites showed ~20% less survival than their controls maintained without Rapa or the wild type line (PbANKA cl15cy1) (**Fig. 47b**). Moreover, while the two controls (c2m2_PbAP2-HS::KS without Rapa and PbANKA cl15cy1)

showed a modest induction of *hsp70-1* transcript levels after the 3 h of HS, the population treated with Rapa was unable to induce this response (Fig. 47c). Altogether, our results suggest that the role of AP2-HS may be conserved in *P. berghei*, such that a functional PbAP2-HS is needed for the activation of the protective HSR, including the correct induction of *hsp70-1* upon HS. It is still unclear whether the housekeeping role of PbAP2-HS is also conserved, although its predicted essentiality *in vivo* is suggestive of key role for this transcription factor under basal conditions. Although our results are promising, these are only exploratory experiments and further replicates using more mice and optimized protocols are needed to overcome the high variability observed between mice and replicates.

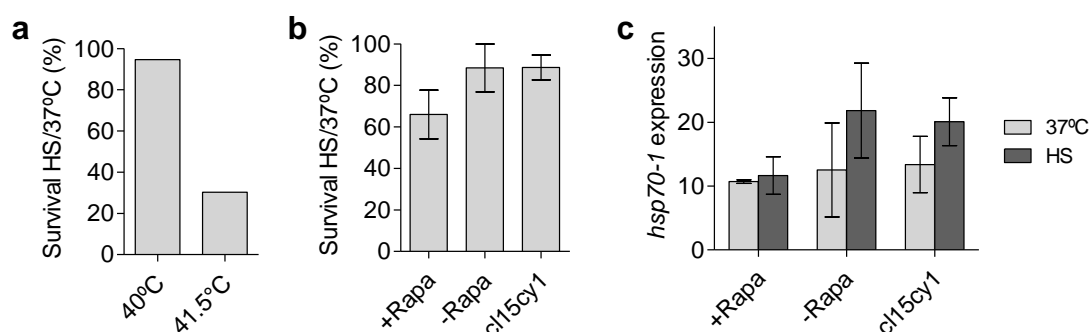


Figure 47. Role of PbAP2-HS during HS in *P. berghei*. **a**, Survival to HS (performed either at 40°C or 41.5°C) of the wild type PbANKA cl15cy1 clone, expressed as the percentage of parasitemia of HS-exposed cultures versus their controls maintained at 37°C. **b**, HS survival of the c2m2_PbAP2-HS::KS line maintained with (+Rapa) or without (-Rapa) Rapamycin during the HS stress. The wild type PbANKA cl15cy1 line was used as control. Values are expressed as the mean and s.e.m. of two independent biological replicates. **c**, *hsp70-1* transcript levels (normalized against *serine-tRNA ligase*) either under nonstress (37°C) or HS conditions, immediately after the stress. Values were obtained by RT-qPCR, and correspond to the mean and s.e.m. of two independent biological replicates.



DISCUSSION

1 *P. FALCIPARUM* PARASITES CAN RESPOND TO HEAT STRESS

In this thesis, we have characterized the whole transcriptional alteration occurring in *P. falciparum* parasites upon heat stress, discerning the alterations that reflect the protective response from the ones related with cell damage. We identified PfAP2-HS, a transcription factor of the ApiAP2 family, as the key regulator of the *P. falciparum* protective HSR. The PfAP2-HS-dependent HSR is largely restricted to a rapid activation of *hsp70-1* and *hsp90*. Moreover, we observed that PfAP2-HS was also involved in the maintenance of proteostasis and in parasite growth under basal conditions, as well as in the response to other types of stress such as the induced by DHA. This is the first identification of a transcription factor that drives a protective transcriptional response to an environmental condition in *P. falciparum* blood stages. This finding not only corroborates the ability of malaria parasites to induce directed responses, but also provides a much-needed system to study such type of transcriptional responses in *Plasmodium sp.*

1.1 *P. falciparum* can activate directed transcriptional responses

Directed responses play a key role in eukaryotes, driving the induction of a transient transcriptional change with the final aim of ensuring survival to a specific external condition. However, as we explained in the introduction chapter, there is an ongoing controversy about the capacity of *P. falciparum* to drive such directed responses to fluctuating conditions in its environment¹¹⁴ (Fig. 48). Previous studies reported transcriptional alterations upon different types of stress, although these changes were of low magnitude, sometimes non-reproducible and mainly consequence of cell damage or direct inhibition of a specific pathway, rather than part of a protective response^{115–119}. Based on these results, the hypothesis that *Plasmodium sp.* have a hard-wired transcriptome was proposed¹¹⁵.

Contrary to this idea, we characterized in detail the transcriptional changes occurring upon HS and identified the main regulator of the protective HSR (PfAP2-HS), analogue to the conserved eukaryotic transcription factor HSF1. Other responses to fluctuating conditions have been reported in *P. falciparum*^{123–130}. Among them, two recent studies are especially relevant and corroborate the capacity of malaria parasites to sense stress. First, the KIN kinase was found to act as a nutrient sensor and initiate a response before a nutrient starvation¹³³. Second, LysoPC depletion induces sexual

commitment and changes in the expression of metabolic enzymes (ethanolamine kinase and methyl transferase)^{134,380}. While in both examples are a proof of concept of stress sensing in *Plasmodium*, the factor responsible for the transcriptional response was not identified. Hence, PfAP2-HS is the first transcription factor identified in *P. falciparum* asexual stages involved in a response to external cues, corroborating the capacity of the parasites to both sense an external change and drive a specific transcriptional response. However, the mechanism of HS sensing that leads to PfAP2-HS activation is still unclear. By similarity to other model eukaryotes, we propose some sensing mechanisms that are discussed below, mainly based on the sensing of unfolded proteins by chaperones and the subsequent PfAP2-HS activation by several post-translational modifications. Nevertheless, further studies should focus on this aspect to determine the mechanisms involved in HS sensing and HSR activation.

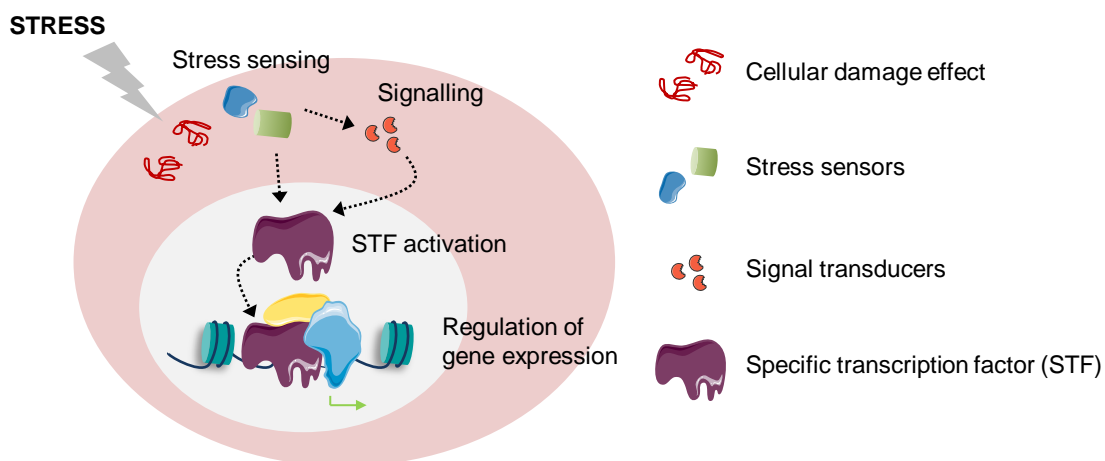


Figure 48. Schematic of a putative directed stress response. The accumulation of cellular damage or specific signals trigger the specific stress response, characterized by a sensing mechanism, signalling transduction and specific transcription factor (STF) activation, which finally leads to regulation of target genes expression that mediate survival under the new condition.

1.2 Heat shock induces global transcriptional alterations

Similar to the HSR in mammals, in *P. falciparum* the number of down-regulated genes was higher than the number of up-regulated genes^{261,263,267}. We found that HS mainly activated genes involved in protein folding, cytoskeleton, signalling pathways and rRNA processing, whereas it inhibited translation, ribosomal formation, metabolism, transport, protein degradation and antigenic variation. This overall response observed in *P. falciparum* shares some similarities with the global transcriptional alteration reported in other organisms. Mammalian HSR, for instance, mainly includes chaperone up-regulation, but also increased expression of cytoskeletal and apoptotic genes, as well as down-regulation of genes related with cell cycle, metabolism, protein synthesis,

mRNA processing and transport²⁶¹ (see Discussion, section 1.3.3). In yeast, HS induces up-regulation of genes involved protein folding and degradation, respiration and glycolysis, and down-regulation of genes related with ribosomal formation, rRNA processing, protein synthesis and metabolism^{131,381,382}. Thus, up-regulation of genes involved in protein folding and down-regulation of protein synthesis genes are conserved between humans, yeast and *P. falciparum*.

Oakley et al. also described the global transcriptional alterations occurring in *P. falciparum* upon HS exposure¹³⁰. However, our approach provides some advantages such as the time-course instead of a single time point sample collection, as well as the use of tightly synchronous populations rather than asynchronous cultures. Despite the experimental differences, we observed that the effect of HS on the parasites was generally consistent between the two studies. Thus, our study not only validated many of their results, but also provided higher accuracy and allowed the identification of a higher number of genes altered upon heat stress, in addition to distinguishing between PfAP2-HS-dependent and -independent targets. A similar detailed transcriptional response has not been characterized in other Apicomplexa, in which the heat stress is mainly studied as the initiator of specific developmental steps rather than as a threatening environmental change^{383–385}.

The most characteristic altered genes of the HSR are chaperones and *hsp* genes, which are highly and continuously up-regulated during HS²⁶¹. Although this regulation is reported to be extremely rapid in mammals (<2 min)²⁶¹, our approach did not have such high temporal resolution, but instead we analysed the effect of HS both during the HS and at the recovery phase. We observed that HS highly induces transcription of specific *hsps* immediately and persistently in *P. falciparum*, whereas expression decreases to basal levels in the recovery phase.

1.3 Different mechanisms are involved in the heat shock response

Although a HS-induced transcriptional alteration was already described in *Plasmodium* parasites, the mechanism driving this response was still unknown. To study the mechanism associated with survival during HS, we took advantage of the 3D7-A line, which showed low survival to HS, and the HS-adapted 3D7-A line.

1.3.1 CLAG2 is neither necessary nor sufficient for heat shock survival

We first identified *clag2* as a candidate gene to be necessary for survival during HS. On the one hand, it is a clonally variant gene, such that it is either in an active or silenced transcriptional state in different individual parasites¹⁶³. This characteristic offers the transcriptional heterogeneity needed for a bet-hedging adaptation strategy^{52,157}. On the other hand, its role in the PSAC formation suggested that it may mediate the entrance of osmolytes (e.g. glycerol, proline or trehalose) that behave as chemical chaperones. For instance, some osmolytes have been shown to control protein stability and suppress protein aggregation in yeast³⁸⁶, as well as to stabilize molecular chaperones in bacteria^{387,388}. Malaria parasites may take advantage of a similar *clag2*-driven channel for the uptake of circulating host metabolites with the final aim to help protein stabilization under heat stress.

However, this hypothesis was later discarded, as *clag2* expression appeared to be neither necessary nor sufficient for HS resistance. Thus, the selection of parasites with active *clag2* expression in 3D7-A-HS observed in the two independent biological replicates may be explained by other reasons, such as stochasticity (a random event) or co-selection with other HS-resistance markers during HS adaptation.

1.3.2 PfAP2-HS is essential to drive the protective heat shock response

Our results indicate that resistance to high temperature is driven by the PfAP2-HS transcription factor, which regulates the expression of key stress response genes during HS to ensure parasite survival. Its role in the HSR was demonstrated in two ways. First, the identification of a premature stop codon mutation (Q3417X) in *pfap2-hs* present in the HS-sensitive lines and its high association with HS sensitivity in all subclones analysed indicated a need of a fully functional PfAP2-HS for survival during HS. Second, we generated $\Delta pfap2-hs$ parasite lines that directly proved the essentiality of this gene to mount a protective HSR and survive the HS.

The identification of PfAP2-HS as the main regulator of the HSR opens a new window of study regarding the role of ApiAP2s in the adaptation to changes in the environment. It is expected that other ApiAP2s may drive protective responses, as it is the most expanded family of transcription factors in *Plasmodium*⁷⁸. The homologous AP2 proteins from plants have also been implicated in response to stress such as heat, salt, cold and drought³⁸⁹, in addition to regulate developmental processes. Although most of the ApiAP2s characterized so far in *Plasmodium sp.* have been related to several steps of parasite life cycle progression, our data shows that ApiAP2 transcription factors are

not only involved in development, but also in stress response mechanisms, similar to plants. This raises the question of whether PfAP2-HS is the only that can respond to stress or other ApiAP2s may also play a role in stress responses, each of them being specialized in a specific response.

Moreover, our results suggest that different roles may be driven by a single ApiAP2 member, as PfAP2-HS plays a role during the normal IDC progression and under heat stress. This capacity, together with the combinatorial mode of gene regulation proposed in *P. falciparum*⁷⁴, may explain the paucity of STFs observed in malaria parasites. Thus, only a few transcription factors may be enough to drive all the transcriptional changes needed during the parasite life cycle progression.

1.3.3 Other transcription factors may drive the PfAP2-HS-independent response

Among the global alterations occurring upon HS, we could discern the immediate protective transcriptional response driven by PfAP2-HS from the rest of alterations related with cell damage and later responses. In fact, we observed that only a reduced number of genes were regulated by PfAP2-HS during the HSR, whereas the vast majority of transcriptional alterations were independent from this factor. Similarly, the eukaryotic HSF1 transcription factor only drives 10-13% of the global transcriptional changes occurring upon HS^{131,261}, and in the case of mammals only a subset of nine genes were described as HSF1-dependent²⁶³. The PfAP2-HS-independent alterations were mainly related with cell damage and death, and mostly found in HS-sensitive parasites due to the enhanced heat-induced proteotoxic effect consequence of the absence of a fully functional PfAP2-HS. A similar phenotype was also reported in HSF1^{-/-} mammalian cells, where the HS had a higher damaging effect than in wild type cells²⁶³.

In addition to reflecting damage, some of the PfAP2-HS-independent transcriptional alterations may play a protective role. These responses are likely regulated by diverse transcription factors upon HS. In yeast, for instance, Msn2/4 transcription factors contribute to the regulation of heat-induced transcription, although they are more related with long-term HS exposure^{264,265}. In mammals, transcription factors such as SRF or NFE2L2 regulate the specific pathways of the HSR, which mainly involve transient and delayed induction of cytoskeletal and apoptotic genes²⁶¹ (**Fig. 49**). Our analysis showed some enriched motifs (mainly CACA- and TTTCC-based sequences) in genes involved in the PfAP2-HS-independent HSR. These enriched sequences match with the cognate DNA binding motif of other ApiAP2 transcription factors, such

as PF3D7_0420300 and PF3D7_0802100, both essential during the IDC, or PF3D7_1456000, also expressed in the asexual stages but not essential. Other factors recognizing these motifs are PF3D7_1305200 and PF3D7_0730300, although due to their time of expression (stage V gametocytes and liver stages, respectively) they probably have no association with the HSR. Thus, although the protective HSR driven by PfAP2-HS is essential, as shown by the phenotype of PfAP2-HS-deficient lines, we can speculate that other ApiAP2s may take part in the response, driving parallel mechanisms of HSR similar to the situation in mammals (Fig. 49). Hence, a tightly controlled ApiAP2 network may be in charge of the survival and recovery to stress. In a previous study, a putative network including PfAP2-HS and PF3D7_0420300 was previously proposed for DTT-induced stress based on bioinformatics predictions, although it was not experimentally confirmed¹²⁶. However, we found that the DTT concentration used in this study was lethal, and consequently the results shown may reflect cell death, rather than a protective response to DTT.



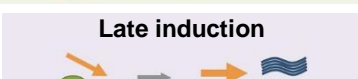
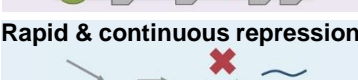

	Mammals		<i>P. falciparum</i>	
	TF	Regulated genes	TF	Regulated genes
Rapid & continuous induction		HSF1 - HSPs - Other chaperones	PfAP2-HS	- HSP70-1 & HSP90 - Pf3D7_1421800
Rapid & transient induction		SRF	Other TFs	- Cytoskeleton - rRNA processing - Gluconeogenesis - Cell surface - Chaperones - Kinases & phosphatases
Late induction		NFE2L2		- Apoptosis
Rapid & continuous repression		?		- Metabolism - Cell cycle
Late repression		?		- mRNA processing

Figure 49. Transcription factors that drive HS-induced transcriptional changes. PfAP2-HS plays an equivalent role to HSF1 from mammals, by mainly inducing *hsp* genes expression. We predict that the other transcriptional changes observed upon HS in *P. falciparum* may be attributable to other transcription factors (TFs), such as other ApiAP2 members, with a similar role to mammalian SRF or NFE2L2. Adapted from Mahat et al.²⁶¹.

A major confounder to study transcriptional responses to stress is that transcription is highly deregulated upon any type of stress. By comparing the response in wild type versus $\Delta pfap2$ -*hs* parasites, we could start to disentangle protective alterations from alterations reflecting cell damage or death. Nevertheless, it is still unclear which of the PfAP2-HS-independent transcriptional changes are part of a parallel protective response and which are part of the damaging effect induced by HS.

2 PfAP2-HS IS ANALOGOUS TO THE EUKARYOTIC HSF1

2.1 PfAP2-HS is structurally different from HSF1

In most eukaryotic organisms, the chaperone-based branch of the protective HSR is mainly activated by the transcription factor HSF1. However, comparative genomic analysis couldn't find any apicomplexan protein structurally similar to HSF1, except for *E. histolytica*^{71,320}, suggesting that malaria parasites either do not activate the HSR or possess a non-canonical regulatory mechanism. The identification of PfAP2-HS as the transcription factor analogous to HSF1 and its essential role in the protective HSR show that *Plasmodium* parasites also activate the HSR, similar to other eukaryotes. This result highlights the limitations derived from using only sequence similarity to identify conserved features between *Plasmodium* species and model eukaryotes and the need of new approaches based on protein functionality rather than sequence or structure characteristics.

2.1.1 Comparison of the structural features between HSF1 and PfAP2-HS

In terms of structure, PfAP2-HS and HSF1 proteins are highly divergent. Indeed, structural variability is also observed between HSF1s from different species, although they all maintain a high degree of conservation at the DNA-binding domain. For instance, mammalian HSF1 contains an N-terminal DNA-binding domain (DBD), a central regulatory domain (RD) and a C-terminal transcriptional activation domain (TAD), as well as three heptad repeats (HR) oligomerization domains (**Fig. 50b**). In addition to the DNA-binding domain and the oligomerization domain, *S. cerevisiae* HSF1 (SchHSF1) also contains two transcriptional activation domains (AR1 and AR2) that are only needed for stress response activation, a unique heptapeptide domain (CE2) that represses HSF1 activity, and a C-terminal modulator domain (CTM) needed for HSF1 binding to *atypical* HSEs and for regulation of CE2²⁷⁵ (**Fig. 50c**).

In contrast, PfAP2-HS is an ApiAP2 protein containing three AP2 domains towards the C-terminal end and a pentapeptide repeat-like (PR) domain at the central region (**Fig. 50a**). Moreover, we could identify two transmembrane (TM) domains located between domains D1-D2 and D2-D3. These TM domains are not predicted by the TMHMM algorithm used by PlasmoDB, but many other algorithms identified them (e.g. SPLIT, PHOBIUS, OCTOPUS, TMMOD and TOPCONS), although they have not been

functionally validated. The presence of two potential TM domains in a transcription factor is intriguing, as they may play important regulatory roles.

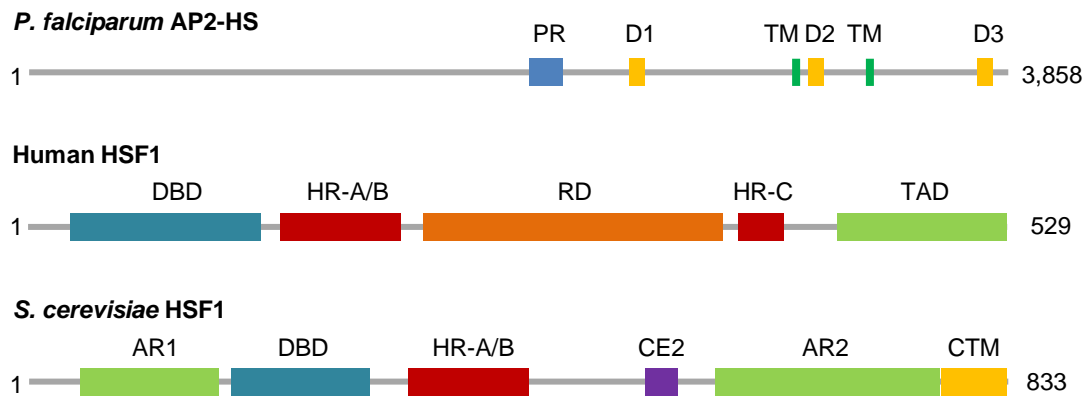


Figure 50. Schematic of PfAP2-HS and the HSF1 from mammals and yeast. **a**, PfAP2-HS. The pentapeptide-like repeat (PR), the three AP2 domains (D1, D2 and D3) and the predicted transmembrane regions (TM) are shown. **b**, Mammalian HSF1 in which the DNA-binding domain (DBD), the heptad repeat domains (HR-A/B and HR-C), the regulatory domain (RD) and the transactivation domain (TAD) are shown. **c**, Yeast HSF1 (from *S. cerevisiae*). The transcriptional activation domains (AR1 and AR2), the DBD, the HR-A/B, the negative regulatory domain conserved element 2 (CE2) and the C-terminal modulator domain (CTM) are shown.

AP2 domains are typically related with DNA and protein binding, and proteins containing these domains are known to be involved in stress response and development in plants^{76,390,391}. As protein binding microarrays analysis did not find any DNA-binding sequence for AP2 domains D2 and D3⁸⁴, we suggest that these domains may rather be related with protein-protein interaction or PfAP2-HS activation. Thus, although PfAP2-HS and HSF1 are structurally different, some features could be maintained between proteins. For instance, the AP2 domain D1 may be analogous to the DBD domain, whereas domains D2 and D3 could play a similar role to domains AR1 and AR2 of ScHSF1, only acting during the HSR. Moreover, based on the essential role of domain D3 in the HS survival, we suggest that this domain could also play an analogous role to the CTM domain of ScHSF1, regulating specific DNA-binding (see Discussion, section 2.5.2), or to the HR-A/B domains, mediating protein oligomerization only under HS.

Lastly, although no specific function has been described for the PfAP2-HS PR domain, tandem repeats are assumed to facilitate transient protein-protein interactions and associate with functional domains, by which they are often involved in adaptation and tolerance to environmental conditions³⁹². Hence, the PR domain may be involved in complex formation or oligomerization of PfAP2-HS. It may also play a similar function to the heptapeptide CE2 domain of ScHSF1³⁹³, acting as a negative regulator of PfAP2-HS activity. We are aware that these functions are speculative, and biochemical

and genetic analysis will be needed to establish the role of the different PfAP2-HS domains.

2.1.2 PfAP2-HS AP2 domain D3 plays a key role in the heat shock response

PfAP2-HS is characterized by its large size (3,858 aa), the second largest ApiAP2 protein in *P. falciparum*. It contains three AP2 domains towards the C-terminal end (D1-3) and a central PR domain. While domain D1 is predicted to bind to the G-box motif⁸⁴, the role of the other domains (D2 and D3) is completely unknown. By homology to the analogous AP2 domains from plants, domains D2 and D3 are also expected to interact with DNA or with other proteins, although no DNA-binding motif was identified using protein binding microarrays analysis⁸⁴. However, the identification of a premature stop codon mutation (Q3417X) before the AP2 domain D3, which leads to a truncated protein that lacks the third AP2 domain (PfAP2-HS Δ D3), allowed us to study the role of this domain under nonstress and stress conditions.

This mutation appeared spontaneously and was selected during culture maintenance (raising to a ~80% frequency in 3D7-A), suggesting that the lack of D3 offers a fitness advantage. Although we couldn't identify any apparent advantage, we demonstrated that D3 is not essential during the IDC under nonstress conditions, as PfAP2-HS Δ D3 parasites can grow and progress throughout the asexual cycle equally to wild types with no apparent defect. In contrast, the Δ PfAP2-HS parasite line has lower proteostasis capacity, such that they cannot grow efficiently under basal physiological conditions.

However, parasites lacking D3 were more sensitive to heat stress and could not activate the protective transcriptional response, indicating that this domain is needed to mount a protective response to this stress situation. We observed these phenotypes not only in the PfAP2-HS Δ D3 lines, but also in the transgenic lines where PfAP2-HS was tagged at the C-terminal end. In these cases, bulky tags did not have an effect on normal growth under basal conditions, but severely affected HS survival, indicating that the proximity of the tag to domain D3 was impairing its role during the HSR. Domain D3 was also needed for normal survival upon DHA-induced stress at the trophozoite stage, when the HSR appears to be mounted. This suggests that parasites can produce a PfAP2-HS-dependent protective response to DHA, an antimalarial drug known to impair proteostasis³⁷⁸. In contrast, domain D3 played no role in other stress conditions induced by compounds such as DTT or H₂O₂, which lead to ER stress and oxidative stress, respectively^{126,394}.

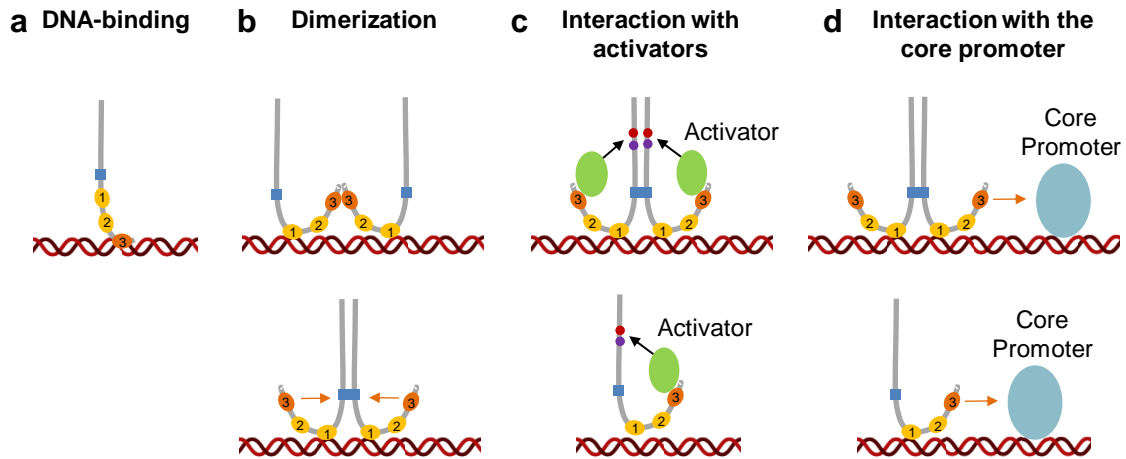


Figure 51. Putative roles of the AP2 domain D3 of PfAP2-HS in the HSR. Domain D3 may be involved either in DNA-binding (a) or protein-binding (b-d). In this latter case, it could mediate PfAP2-HS oligomerization either directly (top) or indirectly (bottom) (b), binding to other activating factors (c) or binding to the core promoter (d). In both scenarios c and d PfAP2-HS may play its role either in a dimeric or monomeric manner. PfAP2-HS domain PR (blue box) and AP2 domains (yellow circles, numbers stand for D1, D2 and D3) are indicated.

Although our data indicates that the AP2 domain D3 is essential for the stress response but dispensable for the basal proteostasis maintenance, the mechanism by which it participates in the activation of the HSR still remains unclear. One possibility relies on the capacity to bind specific DNA motifs, needed to correctly drive PfAP2-HS to its target genes upon HS (Fig. 51a). However, the presence of a Td-Gbox in the promoter of the PfAP2-HS-dependent genes suggests that domain D1, rather than D3, is mainly involved in the DNA-binding. Another hypothesis is that domain D3 is needed for protein-protein interactions during HS (Fig. 51b-d). For instance, it could mediate PfAP2-HS dimerization upon HS, either being the oligomerization domain itself or helping the interaction of other oligomerization domains. It could also mediate PfAP2-HS activation by interacting with activator proteins (e.g. kinases) or induce the transcriptional enhancer or repressor activity by interacting with factors of the core promoter. However, the molecular mechanism by which domain D3 activates transcription has not been studied in detail, as this was beyond the objective of this thesis and should be subject of future investigations. New transgenic lines with the specific deletion of this domain may be used in ChIP-seq analysis to study DNA-binding defects compared to the wild type. Also, interactions with DNA or other proteins may be explored by using recombinant domain D3 in PBMs, electrophoretic mobility shift assays (EMSA) or affinity chromatography.

2.2 Genetic variations in *pfap2-hs*

Only a few SNPs have been identified in the human *hsf1*. Some of the non-synonymous SNPs are predicted to impair HSF1 structure and function³⁹⁵, whereas

others located in intergenic regions such as introns or the 3' UTR were shown to be associated with thermotolerance³⁹⁶.

Some synonymous and non-synonymous mutations are also described in the *pfap2-hs* gene, as well as in other ApiAP2 family members. Claessens et al. identified three premature stop codon mutations that spontaneously appeared *in vitro* during culture adaptation of field samples³⁹⁷. Intriguingly, in this case, the truncation of the protein by more than half of its length and a consequent loss of all three AP2 domains similarly to our Δ PfAP2-HS line, did not have a growth effect and was even predicted to confer a growth advantage during culture adaptation. This result differs from our observations, as we showed that Δ PfAP2-HS parasites cannot grow at standard temperature. One possible explanation would be that the culture conditions in that study differ from our standard conditions (i.e. the actual temperature of the incubators may be below 37°C), but we cannot rule out other possible explanations involving the genetic background of the parasites. Future studies with these culture-adapted parasite lines will shed light on this apparent discrepancy.

Regarding the *in vivo* variability, a study working with a single field isolate from a febrile patient found 8 non-synonymous and 1 synonymous modifications in the PfAP2-HS *P. vivax* ortholog (PVX_083040), only one of them affecting an AP2 domain³⁹⁸. However, these numbers are not exceptional compared to other genes and can be explained by its large size (11,550 bp in the *P. vivax* ortholog). In fact, in the same study, the AP2 family of transcription factors presented a variability rate of 3.4 SNPs/kb, lower than other polymorphic families such as the SERA family (15.3 SNPs/kb), but higher than the median variability of all *P. vivax* genes (1.5 SNPs/kb)³⁹⁹. In *P. falciparum*, the analysis of the genome of more than 3,000 field isolates (MalariaGEN⁴⁰⁰) revealed more than 200 synonymous and 800 non-synonymous SNPs in PfAP2-HS, although many of them have low quality or low frequency within the infection. From these, only one of the 3,000 isolates carried a relevant non-sense mutation (C3168X) in a *P. falciparum* infected patient, also resulting in a truncated PfAP2-HS at the C-terminal end that lacks D3. The very low frequency of non-sense mutations in PfAP2-HS in the field suggest that the fully functional PfAP2-HS may be essential in human infections and that this specific C3168X mutation reported in a single patient may correspond to a dead-end infection. Although no information is available about this specific patient, the presence of such mutation *in vivo* could be explained if this patient was afebrile, in which case the lack of the AP2 domain D3 is not essential under nonstress conditions. However, further characterization of the role of PfAP2-HS *in vivo* is needed.

The genetic alteration of ApiAP2 transcription factors could result in increased expression to new downstream targets, such as drug resistance genes, being a possible mechanism of evolution to offer new responses to environmental stress conditions. Although the Q3417X mutation had the opposite effect on the parasite, impairing the protective HSR, it offered an advantageous phenotype under normal conditions, as it was selected during culture maintenance. Other mutations leading to increased PfAP2-HS function, for instance, may be relevant regarding DHA and HS resistance. Variability in the *pfap2-hs* coding sequence or regulatory regions should be studied in the field to determine if they confer increased PfAP2-HS functionality, and thus provide drug resistance markers.

2.3 PfAP2-HS and HSF1 play a similar role under basal and stress conditions

Despite the structural differences, convergent evolution would have led to an analogous role for both PfAP2-HS and HSF1 under stress and nonstress conditions (Fig. 52). The transcriptional program driven under each condition is distinct, although some target genes may be shared.

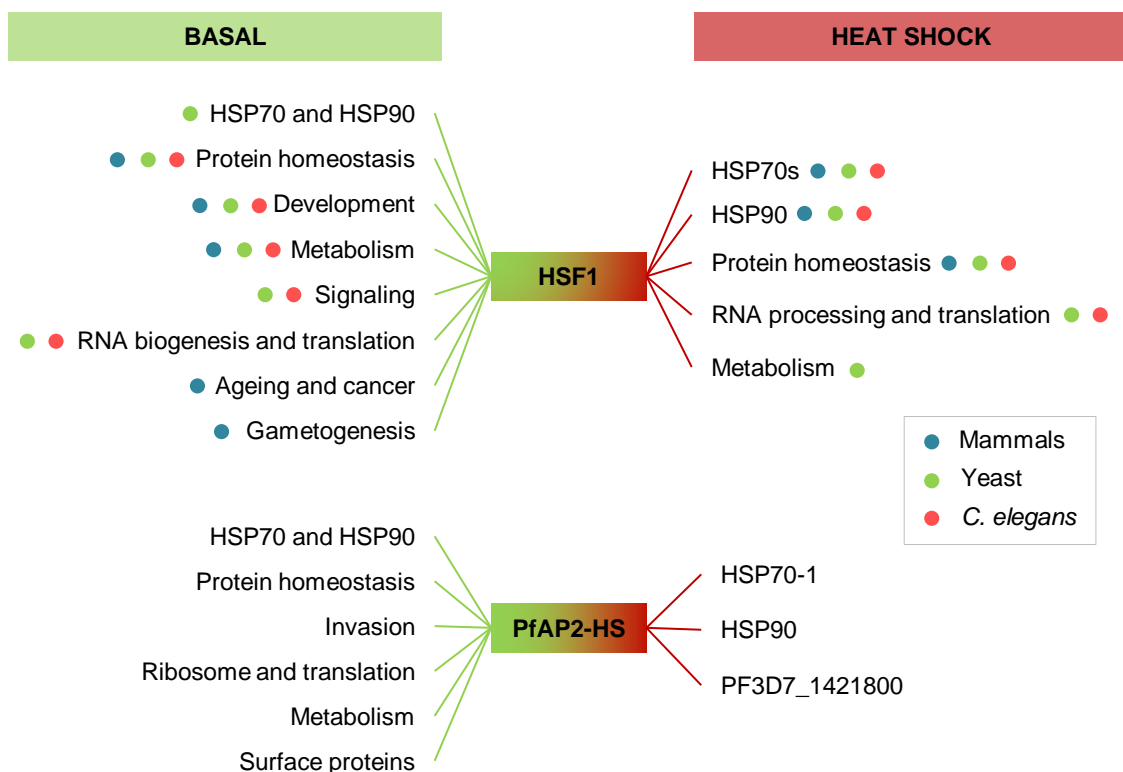


Figure 52. Dual role of HSF1 and PfAP2-HS. Comparison of the functions driven by PfAP2-HS in *P. falciparum* and by the HSF1 in mammals^{261,263} (blue dot), yeast^{263,276,401} (green dot) and *C. elegans*²⁷³ (red dot). Both roles under basal (left) and HS (right) conditions are shown.

2.3.1 PfAP2-HS is essential for the HSR

As regulators of the HSR, both HSF1 and PfAP2-HS induce a transcriptional response mainly involving chaperone expression. In mammals, a total of nine genes are regulated in an HSF1-dependent manner during the HSR²⁶³. These include four members of the HSP70 family, an HSP90, three co-chaperones (HSP40 and others) and a non-chaperone gene. In *S. cerevisiae*, most of the ScHSF1 target genes induced by HS are also stress response genes, including the orthologs of HSP70, HSP90 and small HSPs^{264,285} (**Fig. 52**).

This reduced transcriptional program matches with the response that we reported in *P. falciparum*, where only three genes showed PfAP2-HS-dependent regulations. HSP70 and HSP90 family members are also represented in the *P. falciparum* HSR, as well as another non-chaperone gene (PF3D7_1421800) (**Fig. 52**). From these genes, *hsp70-1* showed the highest level of induction, reaching transcript levels up to 17-fold higher upon HS than under basal conditions. However, this induction was not detected at the protein level during HS or up to 6.5 h after the stress. This discrepancy between mRNA and protein levels after heat stress had been already described for HSP70 and HSP90 in other eukaryotes^{402,403}, although the reason is still not fully understood. Some studies proposed that the high *hsp70-1* mRNA levels are translated only when the stress is life threatening⁴⁰², while others suggest that mRNA degradation and protein instability is accelerated in HS-exposed cells^{322,404}. However, we cannot exclude the possibility that this lack of HSP70-1 increased levels may be due to technical issues.

2.3.2 PfAP2-HS plays a role in other types of stress

In eukaryotic organisms, HS induces a proteotoxic effect in the cytoplasm, which is the signal to activate the HSR. Similar to HS, other types of stress causing a cytoplasmic proteotoxic effect also trigger an HSF1-dependent response²⁶². Although it has not been described in *P. falciparum*, the mechanism of stress sensing may be conserved in this apicomplexan parasite. Thus, other types of stress affecting *Plasmodium* proteostasis, such as DHA-induced stress, may also involve a PfAP2-HS-dependent response. In this sense, we observed that PfAP2-HS is needed to deal with DHA-induced stress, as parasites lacking a functional PfAP2-HS have lower survival to this drug. Whether this transcription factor activates the protective transcriptional HSR under DHA stress or it only contributes to a basal proteostasis maintenance is still unknown. The increased DHA sensitivity observed in parasites carrying the Q3417X mutation in *pfap2-hs* suggests that the HSR mechanism is also activated in DHA-induced stress, whereas the high sensitivity of the knockout line suggest that this line

was at the edge of proteostasis collapse under basal conditions and any further damage was lethal.

However, we could observe that PfAP2-HS was not associated with survival to other types of stress, induced by DTT or H₂O₂ exposure. One possibility is that DHA and HS specifically affect parasite proteome integrity, whereas DTT and H₂O₂ may also induce a severe effect on the erythrocyte. Thus, at low doses they may have a minimal proteotoxic effect, whereas at high doses they destroy the erythrocytes infected by parasites carrying either wild type or mutated PfAP2-HS, reason why we cannot distinguish a PfAP2-HS-dependent response. Another possible explanation relies on the type of stress, which is mostly oxidative stress in the case of H₂O₂ and ER stress in the case of DTT, rather than being a cytoplasmic proteotoxic stress such as the induced by HS. In fact, DTT is known to activate the UPR in other organisms, which differs from the HSR, although they share some components^{405–407}.

2.3.3 PfAP2-HS is needed for proteostasis maintenance and development during the asexual cycle

In the absence of stress, HSF1 is involved in many other processes related with proteostasis, growth, development and metabolism (**Fig. 52**). In all these cases, the transcriptional program activated by HSF1 is different from the one regulated upon HS. For instance, HSF1 plays an important role in protein homeostasis maintenance by driving basal gene expression of chaperones and proteins involved in ubiquitination and proteolysis²⁸⁵. In *S. cerevisiae*, where ScHSF1 is essential for growth and viability under basal conditions, its main essential function relies on the regulation of *hsp70* and *hsp90*^{263,273}.

P. berghei studies attempted without success to disrupt *pbap2-hs* and reported a potential essentiality of this transcription factor for asexual blood stage growth *in vivo*⁸⁵. Interestingly, we could generate PfAP2-HS knockout parasite lines *in vitro*, which also presented lower expression levels of both *hsp70-1* and *hsp90*, as well as other genes related with stress response and protein folding, indicating that the HSF1 role in proteostasis maintenance is conserved in PfAP2-HS. In yeast, a comparable phenotype was also observed after ScHSF1 inactivation, which led to decreased expression of chaperones, followed by proteostasis collapse and cell death at basal conditions²⁶³. Our Δ *pfap2-hs* lines were also highly thermosensitive, such that standard temperature conditions (37°C) induced lower growth and multiplication, whereas lower temperature (35°C) rescued the normal growth phenotype. This is consistent with a key role for PfAP2-HS in regulating proteostasis under basal conditions.

In addition to protein folding, eukaryotic HSF1 participates in development, metabolism and protein biogenesis^{273,285,408}. Similarly, we found that PfAP2-HS is involved in parasite intraerythrocytic development, impairing normal merozoite formation in the mature schizont stages and delaying the asexual cycle. A lower expression of genes involved in invasion, metabolism, ribosome formation and translation was found in the $\Delta pfap2-hs$ line, corroborating the important role of PfAP2-HS in the IDC progression. This developmental role was also observed in a previous study, where a 50% attenuated growth was reported in parasites presenting a *piggyBac* transposon-based disruption of *pfap2-hs*⁴⁰⁹. A similar growth phenotype was described in PfSir2A overexpressing parasites, which causes down-regulation of rRNA transcripts linked to a decreased growth rate and a lower number of merozoites per schizont⁴¹⁰. Interestingly, genes involved in ribosomal formation were one of the main affected groups in $\Delta pfap2-hs$ parasites.

PfAP2-HS expression in stage V gametocytes³⁷⁷ and sporozoite-stage parasites suggests other roles for this protein beyond the asexual cycle. In *P. yoelii*, expression of the *pfap2-hs* orthologue was also shown to be up-regulated in salivary gland sporozoites and liver stages⁷⁸. This high expression in sporozoites could be linked to the HSR role, as at this stage parasites suffer a dramatic thermal change of more than 10°C when they are inoculated in the mammalian host. Nevertheless, the role of PfAP2-HS at these stages awaits experimental characterization.

2.4 Possible mechanisms of PfAP2-HS regulation analogous to HSF1

Although our data shows that PfAP2-HS plays a fundamental role in the HSR, the HS sensing mechanism and the downstream events that lead to PfAP2-HS activation are still unknown. We can hypothesize that some of the regulatory mechanisms that control HSF1 activation may also control PfAP2-HS, but further analyses are needed to determine if these mechanisms are conserved in malaria parasites.

2.4.1 Possible mechanisms of PfAP2-HS activation

Under nonstress conditions, inhibitory chaperones maintain HSF1 in its inactive monomeric form and only a low proportion can trimerize, bind to *degenerated* HSE motifs and drive expression of housekeeping genes^{273,294}. In contrast, increasing numbers of denatured proteins induced by heat stress compete with HSF1 for binding to inhibitory chaperones, releasing HSF1 and inducing high levels of HSF1 trimerization. This protein-based mechanism permits to measure all deviations from

physiological conditions and acts as a very sensitive and integrative thermometer itself⁴¹¹. Upon stress, HSF1 also undergoes several activating PTMs and translocation to the nucleus to bind to the *canonical* HSE and regulate transcription of stress-response genes. Another model has been proposed in *S. cerevisiae*. In this case, a high proportion of ScHSF1 is constitutively trimeric and bound to DNA^{279,280}, whereas HS mainly induces its hyperphosphorylation and change of conformation that lead to a more efficient interaction of the factor with other components of the transcriptional machinery.

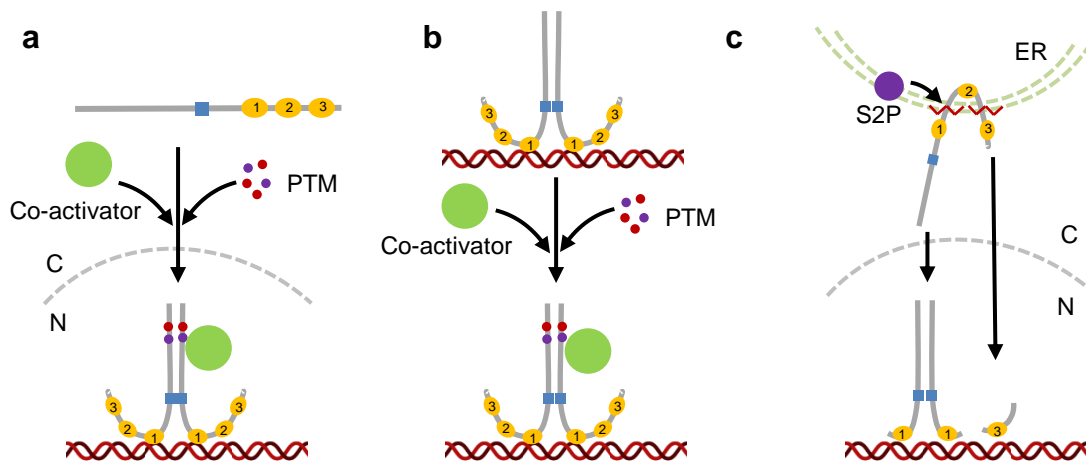


Figure 53. Proposed mechanisms of PfAP2-HS activation upon HS. Based on model eukaryotes, different mechanisms could mediate PfAP2-HS activation upon HS. The PfAP2-HS domain PR (blue box) and AP2 domains (yellow circles, numbers stand for D1, D2 and D3) are indicated. **a**, PfAP2-HS may be maintained as a repressed form in the cytoplasm (C), and upon HS accumulate in the nucleus (N) and be activated by dimerization and several post-translational modifications (PTM) and co-activator factors. **b**, PfAP2-HS may be constitutively bound to the promoter region and activated by PTMs, a conformational change or co-activators. **c**, PfAP2-HS may be attached in the endoplasmic reticulum (ER) membrane by its transmembrane domains. A protease (e.g. S2P) may sense stress and cut PfAP2-HS, such that an activated form containing either domain D1 or domain D3 may be released.

In *P. falciparum* we could not characterize the activation and localization of PfAP2-HS due to the impossibility to detect the protein. However, the presence of a nuclear localization signal⁸⁰ corroborates its transcriptional function, although it does not clarify whether PfAP2-HS is constitutively located in the nucleus or only translocates to the nucleus after activation. Consequently, both yeast and mammalian HSF1 activation mechanisms, as well as other unrelated mechanisms, are plausible for PfAP2-HS activation. On the one hand, the presence of an upstream identical inverted Td-Gbox motif conserved in both *hsp70-1* and *hsp90* suggests that a dimerization step may be involved in the activation of PfAP2-HS, similar to mammal HSF1 trimerization (Fig. 53a). On the other hand, ATAC-seq data revealed the presence of peaks in the G-box-containing regions upstream of *hsp70-1* and *hsp90* under nonstress conditions, suggesting that PfAP2-HS may be already bound there, similar to ScHSF1 (Fig. 53b). However, these peaks were also observed in the knockout line, indicating that they

may not only correspond to PfAP2-HS, but also to other factors attached to these promoter regions. As in other eukaryotes, interaction with co-activators, as well as phosphorylation and other PTMs may also be involved in the mechanism of PfAP2-HS activation. In this sense, a phosphorylation step is also needed to activate the constitutive AP2/ERF proteins, the ApiAP2 homologue family in plants⁴¹².

The large size of the PfAP2-HS protein and the prediction of two TM domains located between the AP2 domains D1-D2 and D2-D3 also suggest that cleavage may be another possible activation mechanism (Fig. 53c). In fact, a previous study proposed PfAP2-HS as a putative target protein of the Site-2 protease (S2P, PF3D7_1305600), which drives cleavage of membrane-bound transcription factors of the ER⁴¹³. There is not a consensus sequence described for S2P-driven cleavage, but it is known that its cleavage site resides inside or near the TM region⁴¹⁴. In PfAP2-HS, this cleavage may occur in either of the two TM domains. If the protein is cut in the first TM domain, the N-terminal region of PfAP2-HS would be released, containing the nuclear localization signal, the PR and the AP2 domain D1. Instead, if cleavage occurred after the second TM domain, only the C-terminal region, containing the AP2 domain D3, would be released. In eukaryotes, a similar activation mechanism is observed for ATF6, a transcription factor involved in the UPR that is activated by S2P-driven cleavage when unfolded proteins accumulate in the ER^{415,416}. Nevertheless, none of the proposed activation mechanisms could be studied in our project.

2.4.2 Proposed mechanisms of PfAP2-HS inhibition

Different mechanisms inhibit HSF1 under nonstress conditions or during recovery from stress. These mechanisms mostly include repression by HSP90 and HSP70, both of which are target genes of HSF1^{284,417}. While HSP90 inhibition relies on the ability to interact with the HSF1 monomers, HSP70 binds to the TAD domain of HSF1^{418,419}. PfAP2-HS also drives expression of *hsp70-1* and *hsp90*, which suggest that a similar regulatory mechanism may occur in *P. falciparum*.

Another inhibitory mechanism is driven by HSBP1, which interacts with HSP70 and also with the trimerization motif HR-A/B of HSF1, thereby negatively regulating HSF1²⁸⁸. HSBP1 has been identified in the genome of every organism studied so far, except for *S. cerevisiae*, in which HSF1 is mainly bound to DNA under nonstress conditions²⁸⁹. The ortholog of HSBP1 has also been identified in *P. falciparum* (PfHSBP), sharing a 28% sequence identity with the human³²¹. Similar to other species, PfHSBP also interacts with HSP70-1 in the cytoplasm³²¹. However, the

relevance of HSBP1 in regulating HSF1 activity remains unclear, and a possible role of PfHSBP in the regulation of PfAP2-HS has not been studied.

2.5 DNA-binding motifs that recruit PfAP2-HS under basal and heat shock conditions

Our transcriptional analysis revealed a small subset of genes regulated by PfAP2-HS under nonstress or heat stress conditions, although the *cis*-acting sequence that recruits PfAP2-HS in each situation still remains poorly understood.

2.5.1 Role of the G-box in the heat shock response

Previous studies identified the G-box motif as the DNA-binding sequence of the AP2 domain D1 of PfAP2-HS⁸⁴, and this motif was found to be enriched in the promoter of *hsp* genes using *in silico* approaches¹⁰². Gene reporter assays with the *hsp90* promoter also suggested an important role for this sequence¹⁰². The G-box motif is present in the promoter region of more than 500 genes in *P. falciparum*, including ten chaperones and chaperonins. However, our microarray data did not reveal a consistent expression pattern of these G-box-containing genes upon HS. While some of them were up-regulated in a PfAP2-HS-independent manner, others were down-regulated or even not altered upon heat stress. Thus, we concluded that the single G-box motif is unlikely to act as the DNA-binding motif of PfAP2-HS during HS.

In model eukaryotes, trimerized HSF1 binds to a conserved triple inverted nGAAn sequence^{268,269}. Similarly, in *P. falciparum*, the fact that a perfect inverted Td-Gbox is found upstream of both *hsp70-1* and *hsp90* genes suggests that this tandem sequence may be needed for PfAP2-HS regulation during HS. In contrast, other genes containing a similar but less conserved upstream Td-Gbox motif did not show relevant transcriptional alterations upon HS, indicating that a highly conserved Td-Gbox motif is needed for such regulation. However, we could not directly confirm its essentiality for recruiting PfAP2-HS to the promoters of its target genes, as our approach using the *Td-Tomato* gene reporter expression driven by *hsp70-1* promoter was not successful. Despite the impossibility to continue the study in this direction, several lines of evidence lead us to propose that the Td-Gbox may play a key role in the HSR. First, the presence of a tandem resembles to the architecture of the HSF1 binding sequence, formed by three inverted nGAAn motifs^{268–270}. Second, the two only genes in the *P. falciparum* genome with a perfect Td-Gbox are among the PfAP2-HS-induced genes upon HS. Third, the AP2 domain D1 preferentially interacts with Td-Gbox, whereas the binding affinity substantially decreases in the presence of a single G-box copy *in vitro*⁸⁴.

Finally, gene reporter assays suggest that both the promoter (containing the Td-Gbox) and the 3' regions of *hsp90* are necessary for its expression¹⁰². Apart from the Td-Gbox, PfAP2-HS binding and target gene transcriptional activation may also involve other regulatory mechanisms. For instance, further sequences either at the promoter region or at the 3' UTR, as well as the epigenetic context or the subnuclear localization, may influence on PfAP2-HS activity.

2.5.2 Differential DNA-binding under basal or heat shock conditions

As explained above, HSF1 can perform distinct functions and regulate different transcriptional programs under basal and heat stress conditions. In *C. elegans*, this specificity is mainly established by the architecture of the promoter region, in which the presence of co-activators (e.g. E2F/DP) and specific HSEs modulate the intrinsic affinity of HSF1. In the absence of stress, trimerized HSF1 preferentially binds to promoters that have a *degenerated* HSE and adjacent binding sites for co-activators²⁷³. In contrast, under HS, HSF1 trimers bind to *consensus* HSEs in the promoter (**Fig. 54**).

	<i>C. elegans</i>	<i>S. cerevisiae</i>	<i>P. falciparum</i>
Basal	Degenerated n <u>RA</u> nn <u>TTC</u> nn <u>GAN</u> n	Perfect n <u>TTC</u> nn <u>GAA</u> nn <u>TTC</u> n Step n <u>TTC</u> n(5 bp)n <u>TTC</u> n(5 bp)n <u>TTC</u> n	Single G-box (?) <u>RNGGGGC</u> n Unknown motif (?)
	HS	Consensus n <u>GAA</u> nn <u>TGG</u> nn <u>GAA</u> n	Perfect n <u>TTC</u> nn <u>GAA</u> nn <u>TTC</u> n Gap n <u>TTC</u> nn <u>GAA</u> n(5 bp)n <u>GAA</u> n

Figure 54. Proposed PfAP2-HS-binding motifs under basal and HS conditions compared to HSF1-binding motifs in *C. elegans* and *S. cerevisiae*. Different architectures of the heat shock element (HSE) are described in *C. elegans* and *S. cerevisiae* and show different affinity to HSF1 under basal and HS conditions. In *P. falciparum*, the single or tandem conformation of the G-box motif may be a regulation layer of PfAP2-HS binding to DNA. The tandem G-box motif showed corresponds to the highly conserved sequence found in *hsp70-1* and *hsp90* promoter regions. The conserved GAA and G-box motifs are underlined. R, A or G; N, A or C or G or T.

SchSF1 can also bind to HSEs with different architecture (*perfect*, *gap* and *step* types) (**Fig. 54**). *Perfect* HSEs are high affinity-binding sites for SchSF1 and are related with the constitutive SchSF1 binding. In contrast, both *gap*- and *step*-types are low affinity-binding motifs, and SchSF1 is only recruited there when the transcriptional activation of the gene is needed. While *step*-type HSEs are involved in basal constitutive transcription and low-level activation, *gap*-type HSEs are involved in moderate stress-induced transcription⁴²⁰. SchSF1 transcriptional activity is induced differently depending on the HSE architecture, a process that is regulated by domains AR1 and

AR2. Both domains can induce gene expression upon HS when ScHSF1 is bound to a *perfect* HSE upstream, whereas only AR2 can induce the expression of genes with the *gap*-type HSE, such as the *hsp90* orthologs²⁷⁷. In addition to the AR2 domain, the CTM domain is also needed to mount the HSR, as it regulates the transcriptional activator function of ScHSF1 when it is specifically bound to a *gap*-type HSE. Interestingly, alterations in the CTM impair growth at 38°C but not at lower temperature (28°C), similar to our observations when the AP2 domain D3 of PfAP2-HS is truncated. This similitude suggests that D3 may play a regulatory role similar to the CTM domain.

In *Plasmodium*, we could not determine the binding specificity for each condition. However, our microarray data showed that the PfAP2-HS-regulated genes during HS contain an upstream Td-Gbox motif, suggesting that it is needed for the HSR. Based on mechanisms described in the other organisms, we suggest that the C-terminal AP2 domain D3 modulates PfAP2-HS activation (e.g. mediating dimerization) or interaction with other proteins (e.g. co-activator or core promoter factors) specifically upon HS. However, these models are speculative and based on the HSF1 mode of action. Hence, further experimental analyses are needed to decipher the mechanism of gene activation by PfAP2-HS under different conditions. For instance, the generation of new transgenic lines expressing different PfAP2-HS versions (e.g. lacking domain D2 or domain D1) could be used to functionally validate the role of each AP2 domain in the HSR. ChIP-seq analysis would be especially valuable to elucidate the differential DNA-binding specificity among the diverse conditions.

2.6 Conservation of the role of PfAP2-HS in other *Plasmodium* species

The PfAP2-HS protein sequence is highly conserved among *Plasmodium* species, suggesting that its function in development and in the HSR may also be maintained. We tested this hypothesis in *P. berghei*, a *Plasmodium* species infecting rodent.

Previous studies reported that the ortholog of PfAP2-HS in *P. berghei* (PbAP2-HS, PBANKA_1356000) and *P. yoelii* (PY17X_1361700) are likely essential *in vivo*^{85,90,379}, consistent with an important role during life cycle progression. We also tried to study the role of PbAP2-HS *in vivo*. Our preliminary results showed that the AP2 domain D3 may be essential, indicating that a fully functional PbAP2-HS protein is needed in *P. berghei* *in vivo* infections. This result is in contrast with our *P. falciparum* *in vitro* data, where the lack of this PfAP2-HS domain was not detrimental and even may confer a fitness advantage. While this may reflect difference between *Plasmodium* species, it

may also reflect difference between *in vivo* and *in vitro* models, as parasites are probably more exposed to environmental variability and stress *in vivo* than in culture conditions.

Interestingly, *P. berghei* infection in rats and mice is associated with a fall of body temperature (hypothermia) instead of fever^{421,422}. Despite the absence of fever in infected mice, the role of PbAP2-HS in regulating the HSR may be maintained as a strategy to induce a protective response to other proteotoxic stress conditions. Our preliminary data showed that PbAP2-HS mislocalization may result in lower HS survival and impaired induction of *hsp70-1* expression, indicating that PbAP2-HS is needed to drive a protective HSR.

Despite the high variability observed in these assays, our preliminary results suggest that the PfAP2-HS developmental role in the asexual life cycle and its role as the regulator of the HSR may be conserved in *P. berghei*. Further analysis and careful optimization of the assays should be performed to determine in detail the role of PbAP2-HS *in vivo*.

3 UNANSWERED QUESTIONS AND FUTURE PERSPECTIVES

In this project we have described the mechanism of response to heat stress, a new adaptive strategy of *Plasmodium* parasites that relies on the role of an ApiAP2 transcription factor to drive the protective transcriptional response. As expected, after identifying the first malaria transcription factor driving a directed protective response, many new questions about the mechanism of response have arisen. Although we have already mentioned many of them, there are still some burning questions and unexpected results that remain unclear. Here we summarize the main unanswered questions that were beyond the objective of this PhD thesis.

- [Characterization of the role of the domains described in PfAP2-HS.](#)

Not much is known about the PfAP2-HS mechanism of action. The AP2 domain D1 is the only one described to bind to DNA, but the role of the rest of domains is poorly understood. Our data shows that domain D3 is essential to drive a protective HSR, and some hypotheses have arisen about its putative role. However, further analysis focused on the functional characterization of either of the AP2 or PR domains must be performed to understand the whole mechanism of PfAP2-HS-mediated gene regulation.

- [PfAP2-HS protein detection.](#)

Despite generating several transgenic lines expressing tagged versions of PfAP2-HS and PbAP2-HS and using different protein detection strategies, we could not detect the proteins. This has been a big obstacle, as it was needed to perform many of the planned assays (e.g. IFAs, ChIP-seq, proteomics...). We still unknown the reason why we could not detect the proteins. The impossibility to detect them in WB analysis could be due to the large size of the protein (~456 kDa). A low protein abundance may also explain the impossibility to detect it and may require more sensitive methods of protein detection.

- [Mechanism of sensing and PfAP2-HS activation.](#)

This includes the HS sensing mechanism and the signalling cascade that regulate the active or repressed state of PfAP2-HS. Our aim was to perform IFAs to analyse putative changes in the subcellular location of PfAP2-HS upon HS. Also, we wanted to perform proteomic and phosphoproteomic analysis to identify protein interactions and phosphorylation sites involved in PfAP2-HS activation. However,

the impossibility to detect the PfAP2-HS protein was a major obstacle for these assays.

- [Direct targets of PfAP2-HS and DNA motif.](#)

We used two different approaches to study the binding of PfAP2-HS to DNA under basal and stress conditions. On the one hand, comparative ATAC-seq was used to link a chromatin accessibility pattern to the presence of functional PfAP2-HS. However, our analysis were only preliminary and new replicates are needed to be performed. On the other hand, an approach with transgenic parasites was also used to study the role of the inverted Td-Gbox in driving *hsp70-1* expression. In this case, technical issues affected the normal activity of the *hsp70-1* modified promoter, entangling the interpretation of the results. Altogether, new experiments should be performed to identify the *cis*-acting element recognized by PfAP2-HS *in vivo*, both under nonstress and stress conditions. Ideally, ChIP-seq and PBMs analysis could be used to determine the specific PfAP2-HS DNA binding sites, although theses analyses depend on the ability to detect the protein, which has been impossible so far.

- [Interaction of PfAP2-HS with the core promoter and characterization of its enhancer or repressor activity.](#)

The molecular changes occurring in the *hsp70* promoter driven by HSF1 have been characterized in model eukaryotes. In this thesis we have not studied this mechanism, although the characterization of the interaction between PfAP2-HS and the target core promoter during the HSR will be key to understand the whole mechanisms of transcriptional activation during the stress response.

- [Heat shock response at a protein level.](#)

Although a high transcriptional induction was observed for *hsp70-1* upon HS, we could not detect an equivalent induction of the HSP70-1 protein. Further analysis must be focused on this and determine whether it is due to a technical issue or is a characteristic trait of the *P. falciparum* HSR.

- [Role of PfAP2-HS in other types of stress.](#)

The role of this transcription factor in the response to stress other than HS is unclear. While we determined a link between PfAP2-HS and DHA-induced stress resistance, no association was found with DTT or H₂O₂ resistance. New research must determine the types of stress to which PfAP2-HS activates a protective

response, as well as the putative link to other known protective mechanisms (e.g. UPR).

- [Role of PfAP2-HS in *P. berghei*](#)

All the experiments with *P. berghei* were performed during a short stay in Dr. Billker's group. The difficulties that arose during transgenic generation and adaptation of the HS assay and the impossibility of the team to continue the experiments after the stay were a big obstacle to perform all the experiments and replicates needed to obtain conclusive results. Thus, more replicates must be performed to determine if the role of PfAP2-HS is conserved in *P. berghei*. Other *Plasmodium* species that induce fever during the could also be studied, such as *P. knowlesi*, which causes malaria in monkeys.

- [Role of PfAP2-HS during human infections.](#)

We have hypothesized about the importance of the role of PfAP2-HS in field infections, highlighting its association with fever and DHA sensitivity. Thus, it would be worth to study in more detail the presence of PfAP2-HS mutations *in vivo* in symptomatic patients with fever and under DHA treatment, and to analyse their effect in the stress response mechanism.

The background of the slide is a repeating pattern of circular cells, each containing different internal structures such as nuclei, nucleoli, and various organelles, rendered in a light teal color. A solid teal horizontal band is positioned across the middle of the slide, containing the word 'CONCLUSIONS' in white, bold, uppercase letters.

CONCLUSIONS

The following conclusions are derived from this doctoral thesis:

- *P. falciparum* has an intrinsic capacity to sense heat stress and activate a specific transcriptional response similar to other eukaryotes.
- The eukaryotic HSR is mediated by the transcription factor HSF1, which is absent in malaria parasites. In contrast, the *P. falciparum* HSR is driven by the transcription factor PfAP2-HS, a member of the ApiAP2 family. Although it structurally differs from the eukaryotic HSF1, they both have an analogous role during the HSR.
- The lack of a fully functional PfAP2-HS impairs the protective HSR and leads to a HS-sensitive phenotype characterized by cell growth arrest and death upon HS.
- The PfAP2-HS-dependent HSR includes a small subset of genes (*hsp70-1*, *hsp90* and Pf3D7_1421800), for which expression is highly and rapidly induced upon HS. Both HSP70-1 and HSP90 are mainly related with protein folding and stress response and contain a conserved Td-Gbox motif in their promoter region.
- Heat stress induces a broad range of PfAP2-HS-independent transcriptional alterations. Other transcription factors may take part in this HSR, mediating parallel mechanisms to PfAP2-HS. Nevertheless, many of the observed alterations are associated with cell damage or death, rather than to a protective response, and are exacerbated in the absence of a functional PfAP2-HS.
- PfAP2-HS is also needed for survival to DHA exposure, the frontline antimalarial drug.
- Similar to HSF1, PfAP2-HS plays a basal role under nonstress conditions in IDC progression, being essential for the correct parasite development. Its basal function is mainly related with proteostasis maintenance, ribosome formation, translation, invasion and metabolism. Parasites lacking PfAP2-HS can grow efficiently at 35°C but not at 37°C, consistent with a key role for PfAP2-HS in maintaining proteostasis.
- The third AP2 domain (D3) of PfAP2-HS is essential for the HSR but dispensable for growth under nonstress conditions.

- The Td-Gbox motif may be associated with PfAP2-HS DNA binding upon HS, although we could not confirm the direct association between the presence of the motif and the induction of the target gene expression. The DNA motif of PfAP2-HS under basal conditions remains unclear.
- The dual role of PfAP2-HS in the normal IDC progression and in the HSR may be conserved in other *Plasmodium* species.



ACKNOWLEDGEMENTS

Els que més em coneixeu, ja sabeu que sempre havia pensat que la meua tesi no tindria agraïments, que “la gent que ha sigut important, ja n’és més que conscient”. Però fa només uns dies algú em va dir que a tots ens agrada sentir-nos una mica especials i que, tot i que ja ho sapiguem, ens encanta que algú ens ho faci veure i compartir-ho plegats. I és ben veritat. Així que permeteu-me rectificar. Espero que en aquest petit recull d’agraïments us hi pogueu sentir reflectits perquè, poc o molt, tots vosaltres heu sigut importants en aquest camí i l’heu fet únic.

Primer de tot, vull agrair la dedicació del meu director de tesi. Alfred, moltes gràcies per tot, no només a nivell científic, sinó també a nivell personal. Gràcies per haver confiat en mi fa cinc anys i donar-me l’oportunitat d’entrar al món de la malària, quan tot just era recent sortida de la universitat. Gràcies per l’esforç i el temps que has dedicat en mi, per guiar-me i donar-me suport en tot moment, per ensenyar-me a fer ciència clara i sincera, per la teua paciència i per recortar-me després de cada experiment fallit. Estic convençuda que no hagués pogut trobar un lloc millor on passar aquests anys i si calgués ho repetiria sense pensar-m’ho dues vegades!

Epis, vosaltres sou els que ho heu viscut més de prop, i m’heu vist riure, estar estressada i fins i tot plorar. Heu fet que aquests anys hagin passat com res. Gràcies Núria i Cristina, les *hippies* que em vaig trobar al grup quan vaig entrar, per acollir-me i ensenyar-me tot el que sé, i per encomanar-me aquest esperit actiu i vital que tant us caracteritza. Gràcies en general a tots els *epis*, per fer-me sentir com a casa, ajudar-me en tot moment i en definitiva ser molt més que companys de lab: l’*epi-boy* (Oriol), la *princesita* (Sofía), la *gym girl* (Anastasia), el *senyor wikipedia* (Lucas), el *Dr. Love & chismes* (Harvie) i els *epis* que han estat de pas (Sara, Júlia, Carla i Rafa). Sense un grup com vosaltres, amb qui fer tonteries i parlar sense embuts, aquests anys haurien sigut molt i molt diferents. Així que, de veritat, gràcies per ser *epis* i deixar-me formar-ne part.

No em puc oblidar de la resta de futurs *Philosophiae Doctors* que heu fet que un dinar sense les vostres converses ja no sigui el mateix i heu convertit la *china* en un punt de trobada sagrat: Eli *mamasita*, Elena, Arnau, Ger, Martinha, Borja, Inés, Cris, María, Marta, Vicky... i tota la resta de *glycos*, *nanos*, *falcis*, *vivax*, *chagas*, *micros* i *immunos* per fer que l’ambient a la 1a planta sigui l’enveja del CEK! Gràcies a tots i totes per compartir experiments, viatges, intimitats, celebracions i moments de desànim. Us asseguro que guardo un munt d’històries i bons records inesborrables amb vosaltres!

I would also like to render thanks to Oliver Bilker and his group, as well as to other members of the malaria community in the Wellcome Trust Sanger Institute, to receive me with open arms. Thank you all for your kind help and for all the beers, parties, trainings and many things that made me feel like home. I am especially grateful to Claire and Tom, who were essential and worked a lot to move my experiments forward!

Gràcies també als *metges moleculars* que volten pel CEK (Ana, Helena, Elena i Josep) per fer-me sentir que els anys no passen al vostre costat. Haig de confessar que m'ha encantat tenir com a excusa pujar a la 3a a fer petar la xerrada de tant en tant. Gràcies especialment a tu, Ana, per ser el punt de suport que sovint necessitava i convertir els dijous en el dia especial de la setmana. Ha estat un plaer compartir aquesta etapa juntes. I també gràcies a totes aquelles que no esteu al lab però que sabeu que sou igual d'essencials (*jel2a2* i Anna).

Gràcies també als que m'he anat creuant pel camí durant aquests anys i que poc o molt heu hagut d'aguantar la meua època al laboratori. A les dues *nenes* de tota la vida, al *peix al cove* i la resta de colla granollerina, als *guais*, als *blautònics*, les *bohèmies*... I especialment a tu, Albert, el meu "segon doctorat", gràcies per les abraçades, els viatges, les *rises* i les reflexions en els moments més crucials. Ha sigut una època de canvis pels dos, però què és la vida si no... tal com va dir algun savi, "hemos venido a jugar"! Un plaer haver compartit aquest camí junts, xalant com ho hem fet.

I ja per acabar, gràcies als de casa. Família, sembla que si tot va bé aviat seré doctora. Dra. Tintó-Font! Durant aquests anys m'heu preguntat una vegada i una altra "quina feina faig" i "per a què serveix". Encara em costa explicar-vos-ho, però espero que amb aquest *llibre* us feu una idea més clara dels últims anys de la vostra filla-germana-néta-cosina-neboda. Mare, pare i Sílvia, no em posaré *romanticona* que ja sabeu que no és el meu estil, però simplement vull deixar per escrit una cosa que poques vegades us he dit: gràcies per ser al meu costat en tot moment i sobretot pels gairebé 28 anys d'esforços que heu hagut de fer perquè jo hagi pogut arribar fins aquí.

moltes
gràcies!



BIBLIOGRAPHY

1. World Health Organization. *World malaria report 2018*. (2018).
2. Li, X. H. *et al.* A historical review of WHO certification of malaria elimination. *Trends Parasitol.* **35**, 163–171 (2019).
3. Our World in Data, Malaria Incidence in 2017. (2018). Available at: <https://ourworldindata.org/grapher/the-incidence-of-malaria-per-1000-population>.
4. Maitland, K. Severe malaria in African children - The need for continuing investment. *N. Engl. J. Med.* **375**, 2416–2417 (2016).
5. Sinka, M. E. *et al.* The dominant Anopheles vectors of human malaria in Africa, Europe and the Middle East: occurrence data, distribution maps and biologic précis. *Parasit. Vectors* **3**, 117 (2010).
6. Miller, L. H., Baruch, D. I., Marsh, K. & Doumbo, O. K. The pathogenic basis of malaria. *Nature* **415**, 673–679 (2002).
7. White, N. J. *et al.* Malaria. *Lancet* **383**, 723–735 (2014).
8. Lee, A. H., Symington, L. S. & Fidock, D. A. DNA repair mechanisms and their biological roles in the malaria parasite *Plasmodium falciparum*. *Microbiol. Mol. Biol. Rev.* **78**, 469–486 (2014).
9. Cowman, A. F., Healer, J., Marapana, D. & Marsh, K. Malaria: biology and disease. *Cell* **167**, 610–624 (2016).
10. Tiburcio, M. *et al.* A switch in infected erythrocyte deformability at the maturation and blood circulation of *Plasmodium falciparum* transmission stages. *Blood* **119**, e172–e180 (2012).
11. Aly, A. S. I., Vaughan, A. M. & Kappe, S. H. I. Malaria parasite development in the mosquito and infection of the mammalian host. *Annu. Rev. Microbiol.* **63**, 195–221 (2009).
12. Snow, R. W. *et al.* Relation between severe malaria morbidity in children and level of *Plasmodium falciparum* transmission in Africa. *Lancet* **349**, 1650–1654 (1997).
13. Bartoloni, A. & Zammarchi, L. Clinical aspects of uncomplicated and severe malaria. *Mediterr. J. Hematol. Infect. Dis.* **4**, e2012026 (2012).
14. Laishram, D. D. *et al.* The complexities of malaria disease manifestations with a focus on asymptomatic malaria. *Malar. J.* **11**, 29 (2012).
15. Bousema, T., Okell, L., Felger, I. & Drakeley, C. Asymptomatic malaria infections: detectability, transmissibility and public health relevance. *Nat. Rev. Microbiol.* **12**, 833–840 (2014).
16. Grobusch, M. P. & Kremsner, P. G. Malaria: drugs, disease and post-genome biology. in *Curr Top Microbiol Immunol* (eds. Compans, R. W. *et al.*) **295**, 83–104 (Springer-Verlag, 2005).
17. World Health Organization. Severe malaria. *Trop. Med. Int. Heal.* **19**, 7–131 (2014).

18. Chotivanich, K. *et al.* Platelet-induced autoagglutination of Plasmodium falciparum-infected red blood cells and disease severity in Thailand. *J. Infect. Dis.* **189**, 1052–1055 (2004).
19. Wassmer, S. C. *et al.* Investigating the pathogenesis of severe malaria: a multidisciplinary and cross-geographical approach. *Am. J. Trop. Med. Hyg.* **93**, 42–56 (2015).
20. Doumbo, O. K. *et al.* High levels of Plasmodium falciparum rosetting in all clinical forms of severe malaria in african children. *Am. J. Trop. Med. Hyg.* **81**, 987–993 (2009).
21. Sharma, L. & Shukla, G. Placental malaria: a new insight into the pathophysiology. *Front. Med.* **4**, 1–6 (2017).
22. Desai, M. *et al.* Epidemiology and burden of malaria in pregnancy. *Lancet Infect. Dis.* **7**, 93–104 (2007).
23. Newman, R. D. *et al.* Burden of malaria during pregnancy in areas of stable and unstable transmission in Ethiopia during a nonepidemic year. *J. Infect. Dis.* **187**, 1765–1772 (2003).
24. WHO. World Health Organization, Diagnostic testing. (2019). Available at: <https://www.who.int/malaria/areas/diagnosis/en/>.
25. Maltha, J., Gillet, P. & Jacobs, J. Malaria rapid diagnostic tests in endemic settings. *Clin. Microbiol. Infect.* **19**, 399–407 (2013).
26. Roth, J. M., Korevaar, D. A., Leeflang, M. M. G. & Mens, P. F. Molecular malaria diagnostics: a systematic review and meta-analysis. *Crit. Rev. Clin. Lab. Sci.* **53**, 87–105 (2016).
27. Tse, E. G., Korsik, M. & Todd, M. H. The past, present and future of anti-malarial medicines. *Malar. J.* **18**, 93 (2019).
28. Blasco, B., Leroy, Di. & Fidock, D. A. Antimalarial drug resistance: Linking Plasmodium falciparum parasite biology to the clinic. *Nat. Med.* **23**, 917–928 (2017).
29. Srivastava, I. K., Rottenberg, H. & Vaidya, A. B. Atovaquone, a broad spectrum antiparasitic drug, collapses mitochondrial membrane potential in a malarial parasite. *J. Biol. Chem.* **272**, 3961–3966 (1997).
30. Srivastava, I. K. & Vaidya, A. B. A mechanism for the synergistic antimalarial action of atovaquone and proguanil. *Antimicrob. Agents Chemother.* **43**, 1334–9 (1999).
31. Combrinck, J. M. *et al.* Insights into the role of heme in the mechanism of action of antimalarials. *ACS Chem. Biol.* **8**, 133–137 (2013).
32. Tilley, L., Straimer, J., Gnädig, N. F., Ralph, S. A. & Fidock, D. A. Artemisinin action and resistance in Plasmodium falciparum. *Trends Parasitol.* **32**, 682–696 (2016).
33. Haldar, K., Bhattacharjee, S. & Safeukui, I. Drug resistance in Plasmodium. *Nat. Rev. Microbiol.* **16**, 156–170 (2018).

34. WHO. *World Health Organization. Guidelines for the treatment of malaria, 3rd edition.* (2015).
35. Tizifa, T. A. *et al.* Prevention efforts for malaria. *Curr. Trop. Med. Reports* **5**, 41–50 (2018).
36. WHO. World Health Organization, Preventive Therapies. (2019). Available at: https://www.who.int/malaria/areas/preventive_therapies/en/.
37. Cohen, J., Nussenzweig, V., Vekemans, J. & Leach, A. From the circumsporozoite protein to the RTS,S/AS candidate vaccine. *Hum. Vaccin.* **6**, 90–96 (2010).
38. Ouattara, A. & Laurens, M. B. Vaccines against malaria. *Clin. Infect. Dis.* **60**, 930–936 (2015).
39. RTS,S Clinical Trials Partnership. Efficacy and safety of RTS,S/AS01 malaria vaccine with or without a booster dose in infants and children in Africa: final results of a phase 3, individually randomised, controlled trial. *Lancet* **386**, 31–45 (2015).
40. Smith Gueye, C. *et al.* Strategies and approaches to vector control in nine malaria-eliminating countries: a cross-case study analysis. *Malar. J.* **15**, 2 (2016).
41. WHO. *World Health Organization. Global Technical Strategy for Malaria 2016-2030.* (2016).
42. WHO. *World Health Organization. The use of DDT in malaria vector control.* (2011).
43. Beier, J. C., Müller, G. C., Gu, W., Arheart, K. L. & Schlein, Y. Attractive toxic sugar bait (ATSB) methods decimate populations of *Anopheles malaria* vectors in arid environments regardless of the local availability of favoured sugar-source blossoms. *Malar. J.* **11**, 31 (2012).
44. Gardner, M. J. *et al.* Genome sequence of the human malaria parasite *Plasmodium falciparum*. *Nature* **419**, 498–511 (2002).
45. Creasey, A. *et al.* Maternal inheritance of extrachromosomal DNA in malaria parasites. *Mol. Biochem. Parasitol.* **65**, 95–8 (1994).
46. Zilversmit, M. M. *et al.* Low-complexity regions in *Plasmodium falciparum*: missing links in the evolution of an extreme genome. *Mol. Biol. Evol.* **27**, 2198–2209 (2010).
47. Miles, A. *et al.* Indels, structural variation, and recombination drive genomic diversity in *Plasmodium falciparum*. *Genome Res.* **26**, 1288–1299 (2016).
48. Nair, S. *et al.* Recurrent gene amplification and soft selective sweeps during evolution of multidrug resistance in malaria parasites. *Mol. Biol. Evol.* **24**, 562–573 (2006).
49. Guler, J. L. *et al.* Asexual populations of the human malaria parasite, *Plasmodium falciparum*, Use a two-step genomic strategy to acquire accurate, beneficial DNA amplifications. *PLoS Pathog.* **9**, e1003375 (2013).

50. Jeffares, D. C. *et al.* Genome variation and evolution of the malaria parasite *Plasmodium falciparum*. *Nat. Genet.* **39**, 120–125 (2007).
51. Volkman, S. K. *et al.* A genome-wide map of diversity in *Plasmodium falciparum*. *Nat. Genet.* **39**, 113–119 (2007).
52. Llorà-Batlle, O., Tintó-Font, E. & Cortés, A. Transcriptional variation in malaria parasites: why and how. *Brief. Funct. Genomics* **00**, 1–13 (2019).
53. Mu, J. *et al.* Multiple transporters associated with malaria parasite responses to chloroquine and quinine. *Mol. Microbiol.* **49**, 977–989 (2003).
54. Lehane, A. M. & Kirk, K. Efflux of a range of antimalarial drugs and ‘chloroquine resistance reversers’ from the digestive vacuole in malaria parasites with mutant PfCRT. *Mol. Microbiol.* **77**, no-no (2010).
55. Djimdé, A. *et al.* A molecular marker for chloroquine-resistant falciparum malaria. *N. Engl. J. Med.* **344**, 257–263 (2001).
56. Cowman, A. F., Morry, M. J., Biggs, B. A., Cross, G. A. & Foote, S. J. Amino acid changes linked to pyrimethamine resistance in the dihydrofolate reductase-thymidylate synthase gene of *Plasmodium falciparum*. *Proc. Natl. Acad. Sci.* **85**, 9109–9113 (1988).
57. Sutherland, C. J. *et al.* Novel pfdhps haplotypes among imported cases of *Plasmodium falciparum* malaria in the United Kingdom. *Antimicrob. Agents Chemother.* **53**, 3405–3410 (2009).
58. Bozdech, Z. *et al.* The transcriptome of the intraerythrocytic developmental cycle of *Plasmodium falciparum*. *PLoS Biol.* **1**, e5 (2003).
59. Le Roch, K. G. Discovery of gene function by expression profiling of the malaria parasite life cycle. *Science* **301**, 1503–1508 (2003).
60. Otto, T. D. *et al.* New insights into the blood-stage transcriptome of *Plasmodium falciparum* using RNA-Seq. *Mol. Microbiol.* **76**, 12–24 (2010).
61. Levine, M. & Tjian, R. Transcription regulation and animal diversity. *Nature* **424**, 147–151 (2003).
62. Tuteja, R., Ansari, A. & Chauhan, V. S. Emerging functions of transcription factors in malaria parasite. *J. Biomed. Biotechnol.* **2011**, 1–6 (2011).
63. Butler, J. E. F. The RNA polymerase II core promoter: a key component in the regulation of gene expression. *Genes Dev.* **16**, 2583–2592 (2002).
64. Coleman, B. I. & Duraisingh, M. T. Transcriptional control and gene silencing in *Plasmodium falciparum*. *Cell. Microbiol.* **10**, 1935–1946 (2008).
65. Callebaut, I., Prat, K., Meurice, E., Mornon, J.-P. & Tomavo, S. Prediction of the general transcription factors associated with RNA polymerase II in *Plasmodium falciparum*: conserved features and differences relative to other eukaryotes. *BMC Genomics* **6**, 100 (2005).

66. Bischoff, E. & Vaquero, C. In silico and biological survey of transcription-associated proteins implicated in the transcriptional machinery during the erythrocytic development of *Plasmodium falciparum*. *BMC Genomics* **11**, 34 (2010).
67. Coulson, R. M. R. Comparative genomics of transcriptional control in the human malaria parasite *Plasmodium falciparum*. *Genome Res.* **14**, 1548–1554 (2004).
68. Ruvalcaba-Salazar, O. K. *et al.* Recombinant and native *Plasmodium falciparum* TATA-binding-protein binds to a specific TATA box element in promoter regions. *Mol. Biochem. Parasitol.* **140**, 183–196 (2005).
69. Calderwood, M. S., Gannoun-Zaki, L., Wellems, T. E. & Deitsch, K. W. *Plasmodium falciparum* var genes are regulated by two regions with separate promoters, one upstream of the coding region and a second within the intron. *J. Biol. Chem.* **278**, 34125–34132 (2003).
70. Cooper, G. Regulation of Transcription in Eukaryotes. in *The Cell: A Molecular Approach. 2nd edition* (Sinauer Associates., 2000).
71. Iyer, L. M., Anantharaman, V., Wolf, M. Y. & Aravind, L. Comparative genomics of transcription factors and chromatin proteins in parasitic protists and other eukaryotes. *Int. J. Parasitol.* **38**, 1–31 (2008).
72. Balaji, S. Discovery of the principal specific transcription factors of Apicomplexa and their implication for the evolution of the AP2-integrase DNA binding domains. *Nucleic Acids Res.* **33**, 3994–4006 (2005).
73. Essien, K., Hannehalli, S. & Stoeckert, C. J. Computational analysis of constraints on noncoding regions, coding regions and gene expression in relation to *Plasmodium* phenotypic diversity. *PLoS One* **3**, e3122 (2008).
74. Vannoort, V. & Huyen, M. Combinatorial gene regulation in *Plasmodium falciparum*. *Trends Genet.* **22**, 73–78 (2006).
75. Riechmann, J. L. *et al.* Arabidopsis transcription factors: genome-wide comparative analysis among eukaryotes. *Science* **290**, 2105–2110 (2000).
76. Riechmann, J. L. & Meyerowitz, E. M. The AP2/EREBP family of plant transcription factors. *Biol. Chem.* **379**, 633–46 (1998).
77. Lindner, S. E., De Silva, E. K., Keck, J. L. & Llinás, M. Structural determinants of DNA binding by a *P. falciparum* ApiAP2 transcriptional regulator. *J. Mol. Biol.* **395**, 558–567 (2010).
78. Painter, H. J., Campbell, T. L. & Llinás, M. The Apicomplexan AP2 family: integral factors regulating *Plasmodium* development. *Mol. Biochem. Parasitol.* **176**, 1–7 (2011).
79. Jeninga, M., Quinn, J. & Petter, M. ApiAP2 transcription factors in apicomplexan parasites. *Pathogens* **8**, 47 (2019).
80. De Silva, E. K. *et al.* Specific DNA-binding by apicomplexan AP2 transcription factors. *Proc. Natl. Acad. Sci. U. S. A.* **105**, 8393–8 (2008).

81. LaCount, D. J. *et al.* A protein interaction network of the malaria parasite *Plasmodium falciparum*. *Nature* **438**, 103–107 (2005).
82. Josling, G. A. *et al.* A *Plasmodium Falciparum* bromodomain protein regulates invasion gene expression. *Cell Host Microbe* **17**, 741–751 (2015).
83. Chandler, J. W., Cole, M., Flier, A., Grewe, B. & Werr, W. The AP2 transcription factors DORNROSCHEN and DORNROSCHEN-LIKE redundantly control *Arabidopsis* embryo patterning via interaction with PHAVOLUTA. *Development* **134**, 1653–1662 (2007).
84. Campbell, T. L., De Silva, E. K., Olszewski, K. L., Elemento, O. & Llinás, M. Identification and genome-wide prediction of DNA binding specificities for the ApiAP2 family of regulators from the malaria parasite. *PLoS Pathog.* **6**, e1001165 (2010).
85. Modrzynska, K. *et al.* A knockout screen of ApiAP2 genes reveals networks of interacting transcriptional regulators controlling the *Plasmodium* life cycle. *Cell Host Microbe* **21**, 11–22 (2017).
86. Zhang, M. *et al.* Uncovering the essential genes of the human malaria parasite *Plasmodium falciparum* by saturation mutagenesis. *Scienc.* **360**, eaap7847 (2018).
87. Santos, J. M. *et al.* Red blood cell invasion by the malaria parasite is coordinated by the PfAP2-I transcription factor. *Cell Host Microbe* **21**, 731–741.e10 (2017).
88. Sinha, A. *et al.* A cascade of DNA-binding proteins for sexual commitment and development in *Plasmodium*. *Nature* **507**, 253–257 (2014).
89. Kafsack, B. F. C. *et al.* A transcriptional switch underlies commitment to sexual development in malaria parasites. *Nature* **507**, 248–252 (2014).
90. Zhang, C. *et al.* Systematic CRISPR-Cas9-mediated modifications of *Plasmodium yoelii* ApiAP2 genes reveal functional insights into parasite development. *MBio* **8**, 1–17 (2017).
91. Yuda, M. *et al.* Identification of a transcription factor in the mosquito-invasive stage of malaria parasites. *Mol. Microbiol.* **71**, 1402–1414 (2009).
92. Kaneko, I., Iwanaga, S., Kato, T., Kobayashi, I. & Yuda, M. Genome-wide identification of the target genes of AP2-O, a *Plasmodium* AP2-family transcription factor. *PLOS Pathog.* **11**, e1004905 (2015).
93. Yuda, M., Iwanaga, S., Shigenobu, S., Kato, T. & Kaneko, I. Transcription factor AP2-Sp and its target genes in malarial sporozoites. *Mol. Microbiol.* **75**, 854–863 (2010).
94. Iwanaga, S., Kaneko, I., Kato, T. & Yuda, M. Identification of an AP2-family protein that is critical for malaria liver stage development. *PLoS One* **7**, e47557 (2012).
95. Flueck, C. *et al.* A major role for the *Plasmodium falciparum* ApiAP2 Protein PfSIP2 in chromosome end biology. *PLoS Pathog.* **6**, e1000784 (2010).

96. Martins, R. M. *et al.* An ApiAP2 member regulates expression of clonally variant genes of the human malaria parasite *Plasmodium falciparum*. *Sci. Rep.* **7**, 14042 (2017).
97. Sierra-Miranda, M. *et al.* Pf AP2Tel, harbouring a non-canonical DNA-binding AP2 domain, binds to *Plasmodium falciparum* telomeres. *Cell. Microbiol.* **19**, e12742 (2017).
98. Gissot, M., Briquet, S., Refour, P., Boschet, C. & Vaquero, C. PfMyb1, a *Plasmodium falciparum* transcription factor, is required for intra-erythrocytic growth and controls key genes for cell cycle regulation. *J. Mol. Biol.* **346**, 29–42 (2005).
99. Boschet, C. *et al.* Characterization of PfMyb1 transcription factor during erythrocytic development of 3D7 and F12 *Plasmodium falciparum* clones. *Mol. Biochem. Parasitol.* **138**, 159–163 (2004).
100. Komaki-Yasuda, K., Okuwaki, M., Nagata, K., Kawazu, S. & Kano, S. Identification of a novel and unique transcription factor in the intraerythrocytic stage of *Plasmodium falciparum*. *PLoS One* **8**, e74701 (2013).
101. Lima, W. R. *et al.* The PfNF-YB transcription factor is a downstream target of melatonin and cAMP signalling in the human malaria parasite *Plasmodium falciparum*. *J. Pineal Res.* **54**, 145–153 (2013).
102. Militello, K. T., Dodge, M., Bethke, L. & Wirth, D. F. Identification of regulatory elements in the *Plasmodium falciparum* genome. *Mol. Biochem. Parasitol.* **134**, 75–88 (2004).
103. Gunasekera, A. M. *et al.* Regulatory motifs uncovered among gene expression clusters in *Plasmodium falciparum*. *Mol. Biochem. Parasitol.* **153**, 19–30 (2007).
104. Elemento, O., Slonim, N. & Tavazoie, S. A universal framework for regulatory element discovery across all genomes and data types. *Mol. Cell* **28**, 337–350 (2007).
105. Young, J. A. *et al.* In silico discovery of transcription regulatory elements in *Plasmodium falciparum*. *BMC Genomics* **9**, 70 (2008).
106. Russell, K., Emes, R. & Horrocks, P. Triaging informative cis-regulatory elements for the combinatorial control of temporal gene expression during *Plasmodium falciparum* intraerythrocytic development. *Parasit. Vectors* **8**, 81 (2015).
107. Painter, H. J. *et al.* Genome-wide real-time in vivo transcriptional dynamics during *Plasmodium falciparum* blood-stage development. *Nat. Commun.* **9**, 2656 (2018).
108. Imamura, H., Persampieri, J. H. & Chuang, J. H. Sequences conserved by selection across mouse and human malaria species. *BMC Genomics* **8**, 372 (2007).
109. Wu, J., Sieglaff, D. H., Gervin, J. & Xie, X. S. Discovering regulatory motifs in the *Plasmodium* genome using comparative genomics. *Bioinformatics* **24**, 1843–1849 (2008).

110. Pons, N. *et al.* Nucleosome landscape and control of transcription in the human malaria parasite. *Genome Res.* **20**, 228–238 (2010).
111. Toenhake, C. G. *et al.* Chromatin accessibility-based characterization of the gene regulatory network underlying *Plasmodium falciparum* blood-stage development. *Cell Host Microbe* **23**, 557–569.e9 (2018).
112. Ruiz, J. L. *et al.* Characterization of the accessible genome in the human malaria parasite *Plasmodium falciparum*. *Nucleic Acids Res.* **46**, 9414–9431 (2018).
113. Harris, E. Y., Pons, N., Le Roch, K. G. & Lonardi, S. Chromatin-driven de novo discovery of DNA binding motifs in the human malaria parasite. *BMC Genomics* **12**, 601 (2011).
114. Deitsch, K. *et al.* Mechanisms of gene regulation in *Plasmodium*. *Am. J. Trop. Med. Hyg.* **77**, 201–8 (2007).
115. Ganesan, K. *et al.* A genetically hard-wired metabolic transcriptome in *Plasmodium falciparum* fails to mount protective responses to lethal antifolates. *PLoS Pathog.* **4**, e1000214 (2008).
116. Gunasekera, A. M., Myrick, A., Roch, K. Le, Winzeler, E. & Wirth, D. F. *Plasmodium falciparum*: Genome wide perturbations in transcript profiles among mixed stage cultures after chloroquine treatment. *Exp. Parasitol.* **117**, 87–92 (2007).
117. Kato, N. *et al.* Gene expression signatures and small-molecule compounds link a protein kinase to *Plasmodium falciparum* motility. *Nat. Chem. Biol.* **4**, 347–356 (2008).
118. Kritsiriwuthinan, K. *et al.* Global gene expression profiling of *Plasmodium falciparum* in response to the anti-malarial drug pyronaridine. *Malar. J.* **10**, 242 (2011).
119. Le Roch, K. G. *et al.* A systematic approach to understand the mechanism of action of the bithiazolium compound T4 on the human malaria parasite, *Plasmodium falciparum*. *BMC Genomics* **9**, 513 (2008).
120. Hu, G. *et al.* Transcriptional profiling of growth perturbations of the human malaria parasite *Plasmodium falciparum*. *Nat. Biotechnol.* **28**, 91–98 (2010).
121. Tamez, P. A. *et al.* An erythrocyte vesicle protein exported by the malaria parasite promotes tubovesicular lipid import from the host cell surface. *PLoS Pathog.* **4**, e1000118 (2008).
122. Dahl, E. L. *et al.* Tetracyclines specifically target the apicoplast of the malaria parasite *Plasmodium falciparum*. *Antimicrob. Agents Chemother.* **50**, 3124–3131 (2006).
123. Zuzarte-Luís, V. & Mota, M. M. Parasite sensing of host nutrients and environmental cues. *Cell Host Microbe* **23**, 749–758 (2018).
124. Babbitt, S. E. *et al.* *Plasmodium falciparum* responds to amino acid starvation by entering into a hibernatory state. *Proc. Natl. Acad. Sci.* **109**, E3278–E3287 (2012).

125. Fang, J. *et al.* Ambient glucose concentration and gene expression in *Plasmodium falciparum*. *Mol. Biochem. Parasitol.* **133**, 125–9 (2004).
126. Chaubey, S., Grover, M. & Tatu, U. Endoplasmic reticulum stress triggers gametocytogenesis in the malaria parasite. *J. Biol. Chem.* **289**, 16662–16674 (2014).
127. Natalang, O. *et al.* Dynamic RNA profiling in *Plasmodium falciparum* synchronized blood stages exposed to lethal doses of artesunate. *BMC Genomics* **9**, 388 (2008).
128. Torrentino-Madamet, M. *et al.* Global response of *Plasmodium falciparum* to hyperoxia: a combined transcriptomic and proteomic approach. *Malar. J.* **10**, 4 (2011).
129. Chou, E. S. *et al.* A high parasite density environment induces transcriptional changes and cell death in *Plasmodium falciparum* blood stages. *FEBS J.* **285**, 848–870 (2018).
130. Oakley, M. S. M. *et al.* Molecular factors and biochemical pathways induced by febrile temperature in intraerythrocytic *Plasmodium falciparum* parasites. *Infect. Immun.* **75**, 2012–2025 (2007).
131. Gasch, A. P. *et al.* Genomic expression programs in the response of yeast cells to environmental changes. *Mol. Biol. Cell* **11**, 4241–4257 (2000).
132. Causton, H. C. *et al.* Remodeling of yeast genome expression in response to environmental changes. *Mol. Biol. Cell* **12**, 323–337 (2001).
133. Mancio-Silva, L. *et al.* Nutrient sensing modulates malaria parasite virulence. *Nature* **547**, 213–216 (2017).
134. Brancucci, N. M. B. *et al.* Lysophosphatidylcholine regulates sexual stage differentiation in the human malaria parasite *Plasmodium falciparum*. *Cell* **171**, 1532–1544.e15 (2017).
135. Filarsky, M. *et al.* GDV1 induces sexual commitment of malaria parasites by antagonizing HP1-dependent gene silencing. *Science* **359**, 1259–1263 (2018).
136. Ponts, N. *et al.* Genome-wide mapping of DNA methylation in the human malaria parasite *Plasmodium falciparum*. *Cell Host Microbe* **14**, 696–706 (2013).
137. Miao, J. *et al.* The malaria parasite *Plasmodium falciparum* histones: organization, expression, and acetylation. *Gene* **369**, 53–65 (2006).
138. Duffy, M. F., Selvarajah, S. A., Josling, G. A. & Petter, M. The role of chromatin in *Plasmodium* gene expression. *Cell. Microbiol.* **14**, 819–828 (2012).
139. Trojer, P. & Reinberg, D. Facultative Heterochromatin: Is There a Distinctive Molecular Signature? *Mol. Cell* **28**, 1–13 (2007).
140. Hernandez-Rivas, R., Pérez-Toledo, K., Herrera Solorio, A.-M., Delgadillo, D. M. & Vargas, M. Telomeric heterochromatin in *Plasmodium falciparum*. *J. Biomed. Biotechnol.* **2010**, 1–11 (2010).

141. Flueck, C. *et al.* Plasmodium falciparum heterochromatin protein 1 marks genomic loci linked to phenotypic variation of exported virulence factors. *PLoS Pathog.* **5**, e1000569 (2009).
142. Hoeijmakers, W. A. M. *et al.* Plasmodium falciparum centromeres display a unique epigenetic makeup and cluster prior to and during schizogony. *Cell. Microbiol.* **14**, 1391–1401 (2012).
143. Horrocks, P., Wong, E., Russell, K. & Emes, R. D. Control of gene expression in Plasmodium falciparum – Ten years on. *Mol. Biochem. Parasitol.* **164**, 9–25 (2009).
144. Bechtsi, D. P. & Waters, A. P. Genomics and epigenetics of sexual commitment in Plasmodium. *Int. J. Parasitol.* **47**, 425–434 (2017).
145. Fan, Q., An, L. & Cui, L. Plasmodium falciparum histone acetyltransferase, a yeast GCN5 homologue involved in chromatin remodeling. *Eukaryot. Cell* **3**, 264–276 (2004).
146. Joshi, M. B. *et al.* Molecular cloning and nuclear localization of a histone deacetylase homologue in Plasmodium falciparum. *Mol. Biochem. Parasitol.* **99**, 11–9 (1999).
147. Cui, L., Fan, Q., Cui, L. & Miao, J. Histone lysine methyltransferases and demethylases in Plasmodium falciparum. *Int. J. Parasitol.* **38**, 1083–1097 (2008).
148. Cui, L. & Miao, J. Chromatin-mediated epigenetic regulation in the malaria parasite Plasmodium falciparum. *Eukaryot. Cell* **9**, 1138–1149 (2010).
149. Perez-Toledo, K. *et al.* Plasmodium falciparum heterochromatin protein 1 binds to tri-methylated histone 3 lysine 9 and is linked to mutually exclusive expression of var genes. *Nucleic Acids Res.* **37**, 2596–2606 (2009).
150. Briquet, S. *et al.* High-mobility-group box nuclear factors of Plasmodium falciparum. *Eukaryot. Cell* **5**, 672–682 (2006).
151. Vembar, S. S., Scherf, A. & Siegel, T. N. Noncoding RNAs as emerging regulators of Plasmodium falciparum virulence gene expression. *Curr. Opin. Microbiol.* **20**, 153–161 (2014).
152. Weiner, A. *et al.* 3D nuclear architecture reveals coupled cell cycle dynamics of chromatin and nuclear pores in the malaria parasite Plasmodium falciparum. *Cell. Microbiol.* **13**, 967–977 (2011).
153. Duraisingh, M. T. *et al.* Heterochromatin silencing and locus repositioning linked to regulation of virulence genes in Plasmodium falciparum. *Cell* **121**, 13–24 (2005).
154. Ralph, S. A., Scheidig-Benatar, C. & Scherf, A. Antigenic variation in Plasmodium falciparum is associated with movement of var loci between subnuclear locations. *Proc. Natl. Acad. Sci.* **102**, 5414–5419 (2005).
155. Ay, F. *et al.* Three-dimensional modeling of the P. falciparum genome during the erythrocytic cycle reveals a strong connection between genome architecture and gene expression. *Genome Res.* **24**, 974–988 (2014).

156. Rovira-Graells, N. *et al.* Transcriptional variation in the malaria parasite *Plasmodium falciparum*. *Genome Res.* **22**, 925–938 (2012).
157. Carey, J. N. *et al.* Regulated stochasticity in a bacterial signaling network permits tolerance to rapid environmental change. *Cell* **173**, 196–207.e14 (2018).
158. Deitsch, K. W. & Dzikowski, R. Variant gene expression and antigenic variation by malaria parasites. *Annu. Rev. Microbiol.* **71**, 625–641 (2017).
159. Abdi, A. I. *et al.* Global selection of *Plasmodium falciparum* virulence antigen expression by host antibodies. *Sci. Rep.* **6**, 19882 (2016).
160. Salanti, A. *et al.* Selective upregulation of a single distinctly structured var gene in chondroitin sulphate A-adhering *Plasmodium falciparum* involved in pregnancy-associated malaria. *Mol. Microbiol.* **49**, 179–191 (2003).
161. Lavazec, C., Sanyal, S. & Templeton, T. J. Expression switching in the stevor and Pfmc-2TM superfamilies in *Plasmodium falciparum*. *Mol. Microbiol.* **64**, 1621–1634 (2007).
162. Fernandez, V. Small, clonally variant antigens expressed on the surface of the *Plasmodium falciparum*-infected erythrocyte are encoded by the rif gene family and are the target of human immune responses. *J. Exp. Med.* **190**, 1393–1404 (1999).
163. Cortés, A. Switching *Plasmodium falciparum* genes on and off for erythrocyte invasion. *Trends Parasitol.* **24**, 517–524 (2008).
164. Mira-Martínez, S. *et al.* Expression of the *Plasmodium falciparum* clonally variant clag3 genes in human infections. *J. Infect. Dis.* **215**, 938–945 (2017).
165. Mira-Martínez, S. *et al.* Epigenetic switches in clag3 genes mediate blasticidin S resistance in malaria parasites. *Cell. Microbiol.* **15**, n/a-n/a (2013).
166. Sharma, P. *et al.* An epigenetic antimalarial resistance mechanism involving parasite genes linked to nutrient uptake. *J. Biol. Chem.* **288**, 19429–19440 (2013).
167. Le Roch, K. G. Global analysis of transcript and protein levels across the *Plasmodium falciparum* life cycle. *Genome Res.* **14**, 2308–2318 (2004).
168. Foth, B. J. *et al.* Quantitative time-course profiling of parasite and host cell proteins in the human malaria parasite *Plasmodium falciparum*. *Mol. Cell. Proteomics* **10**, M110.006411 (2011).
169. Vembar, S. S., Droll, D. & Scherf, A. Translational regulation in blood stages of the malaria parasite *Plasmodium* spp. : systems-wide studies pave the way. *Wiley Interdiscip. Rev. RNA* **7**, 772–792 (2016).
170. Braks, J. A. M., Mair, G. R., Franke-Fayard, B., Janse, C. J. & Waters, A. P. A conserved U-rich RNA region implicated in regulation of translation in *Plasmodium* female gametocytes. *Nucleic Acids Res.* **36**, 1176–1186 (2008).
171. Brancucci, N. M. B., Witmer, K., Schmid, C. & Voss, T. S. A var gene upstream element controls protein synthesis at the level of translation initiation in *Plasmodium falciparum*. *PLoS One* **9**, e100183 (2014).

172. Vembar, S. S., Macpherson, C. R., Sismeiro, O., Coppée, J.-Y. & Scherf, A. The PfAlba1 RNA-binding protein is an important regulator of translational timing in *Plasmodium falciparum* blood stages. *Genome Biol.* **16**, 212 (2015).
173. Wen, B. *et al.* Translational Repression is essential for *Plasmodium* sexual development and mediated by a DDX6-type RNA helicase. *Science* **313**, 667–669 (2006).
174. Gunderson, J. *et al.* Structurally distinct, stage-specific ribosomes occur in *Plasmodium*. *Science* **238**, 933–937 (1987).
175. Eshar, S. *et al.* PFSR1 controls alternative splicing and steady-state RNA levels in *Plasmodium falciparum* through preferential recognition of specific RNA motifs. *Mol. Microbiol.* **96**, 1283–1297 (2015).
176. Zhang, Q. *et al.* Exonuclease-mediated degradation of nascent RNA silences genes linked to severe malaria. *Nature* **513**, 431–435 (2014).
177. Shock, J. L., Fischer, K. F. & DeRisi, J. L. Whole-genome analysis of mRNA decay in *Plasmodium falciparum* reveals a global lengthening of mRNA half-life during the intra-erythrocytic development cycle. *Genome Biol.* **8**, R134 (2007).
178. Painter, H. J., Carrasquilla, M. & Llinás, M. Capturing in vivo RNA transcriptional dynamics from the malaria parasite *Plasmodium falciparum*. *Genome Res.* **27**, 1074–1086 (2017).
179. Hasday, J. D., Fairchild, K. D. & Shanholtz, C. The role of fever in the infected host. *Microbes Infect.* **2**, 1891–1904 (2000).
180. Sajadi, M. M. & Mackowiak, P. A. Temperature Regulation and the Pathogenesis of Fever. in *Principles and Practice of Infectious Diseases* (eds. Mandell, Douglas & Bennett's) 708–731 (ScienceDirect, 2015).
181. Blatteis, C. M. Fever: pathological or physiological, injurious or beneficial? *J. Therm. Biol.* **28**, 1–13 (2003).
182. Roth, J., Rummel, C., Barth, S. W., Gerstberger, R. & Hübschle, T. Molecular aspects of fever and hyperthermia. *Immunol. Allergy Clin. North Am.* **29**, 229–245 (2009).
183. Dinarello, C. A. Infection, fever, and exogenous and endogenous pyrogens: some concepts have changed. *J. Endotoxin Res.* **10**, 201–222 (2004).
184. Netea, M. G., Kullberg, B. J. & Van der Meer, J. W. M. Circulating cytokines as mediators of fever. *Clin. Infect. Dis.* **31**, S178–S184 (2000).
185. Romanovsky, A. A. *et al.* Fever and hypothermia in systemic inflammation: recent discoveries and revisions. *Front. Biosci.* **10**, 2193–216 (2005).
186. Adams, G. R. Cytokine regulation of fever: studies using gene knockout mice. *J Appl Physiol* **93**, 1159–1167 (2002).
187. Roth, J. Endogenous antipyretics. *Clin. Chim. Acta* **371**, 13–24 (2006).

188. Scammell, T. E., Elmquist, J. K., Griffin, J. D. & Saper, C. B. Ventromedial preoptic prostaglandin E2 activates fever-producing autonomic pathways. *J. Neurosci.* **16**, 6246–54 (1996).
189. Roth, J. & de Souza, G. E. P. Fever induction pathways: evidence from responses to systemic or local cytokine formation. *Brazilian J. Med. Biol. Res.* **34**, 301–314 (2001).
190. Hopkins, S. J. Central nervous system recognition of peripheral inflammation: a neural, hormonal collaboration. *Acta Biomed.* **78 Suppl 1**, 231–47 (2007).
191. Blatteis, C. M. The onset of fever: new insights into its mechanism. *Prog. Brain Res.* **162**, 3–14 (2007).
192. Blasius, A. L. & Beutler, B. Intracellular Toll-like Receptors. *Immunity* **32**, 305–315 (2010).
193. Aderem, A. & Ulevitch, R. J. Toll-like receptors in the induction of the innate immune response. *Nature* **406**, 782–787 (2000).
194. Rivest, S. Molecular insights on the cerebral innate immune system. *Brain. Behav. Immun.* **17**, 13–9 (2003).
195. Conti, B., Tabarean, I., Andrei, C. & Bartfai, T. Cytokines and fever. *Front. Biosci.* **9**, 1433–49 (2004).
196. Turrin, N. P. & Rivest, S. Unraveling the molecular details involved in the intimate link between the immune and neuroendocrine systems. *Exp. Biol. Med.* **229**, 996–1006 (2004).
197. Romanovsky, A. A., Steiner, A. & Matsumura, K. Cells that trigger fever. *Cell Cycle* **5**, 2195–2197 (2006).
198. Ushikubi, F. *et al.* Impaired febrile response in mice lacking the prostaglandin E receptor subtype EP3. *Nature* **395**, 281–284 (1998).
199. Rummel, C. *et al.* Localized vs. systemic inflammation in guinea pigs: a role for prostaglandins at distinct points of the fever induction pathways? *Am. J. Physiol. Integr. Comp. Physiol.* **289**, R340–R347 (2005).
200. Oakley, M. S., Gerald, N., McCutchan, T. F., Aravind, L. & Kumar, S. Clinical and molecular aspects of malaria fever. *Trends Parasitol.* **27**, 442–449 (2011).
201. Schumacker, P. T., Rowland, J., Saltz, S., Nelson, D. P. & Wood, L. D. Effects of hyperthermia and hypothermia on oxygen extraction by tissues during hypovolemia. *J. Appl. Physiol.* **63**, 1246–1252 (1987).
202. Jiang, Q. *et al.* Febrile-range temperature modifies early systemic tumor necrosis factor alpha expression in mice challenged with bacterial endotoxin. *Infect. Immun.* **67**, 1539–46 (1999).
203. Jiang, Q. *et al.* Exposure to febrile temperature upregulates expression of pyrogenic cytokines in endotoxin-challenged mice. *Am. J. Physiol. Integr. Comp. Physiol.* **276**, R1653–R1660 (1999).

204. Karunaweera, N. D., Grau, G. E., Gamage, P., Carter, R. & Mendis, K. N. Dynamics of fever and serum levels of tumor necrosis factor are closely associated during clinical paroxysms in *Plasmodium vivax* malaria. *Proc. Natl. Acad. Sci.* **89**, 3200–3203 (1992).
205. Gravenor, M. B. & Kwiatkowski, D. An analysis of the temperature effects of fever on the intra-host population dynamics of *Plasmodium falciparum*. *Parasitology* **117**, 97–105 (1998).
206. Dicko, A. *et al.* Season, fever prevalence and pyrogenic threshold for malaria disease definition in an endemic area of Mali. *Trop. Med. Int. Heal.* **10**, 550–556 (2005).
207. Gatton, M. L. & Cheng, Q. Evaluation of the pyrogenic threshold for *Plasmodium falciparum* malaria in naive individuals. *Am. J. Trop. Med. Hyg.* **66**, 467–473 (2002).
208. Rogier, C., Trape, J.-F. & Commenges, D. Evidence for an age-dependent pyrogenic threshold of *Plasmodium falciparum* parasitemia in highly endemic populations. *Am. J. Trop. Med. Hyg.* **54**, 613–619 (1996).
209. Roucher, C. *et al.* Changing malaria epidemiology and diagnostic criteria for *Plasmodium falciparum* clinical malaria. *PLoS One* **7**, e46188 (2012).
210. Iwalokun, B. *et al.* Reduction in febrile episodes and dynamics of pyrogenic threshold in Nigerian children with *Plasmodium falciparum* malaria. *J. Pediatr. Infect. Dis.* **06**, 185–194 (2015).
211. Dollat, M. *et al.* Measuring malaria morbidity in an area of seasonal transmission: pyrogenic parasitemia thresholds based on a 20-year follow-up study. *PLoS One* **14**, e0217903 (2019).
212. Gazzinelli, R. T., Kalantari, P., Fitzgerald, K. A. & Golenbock, D. T. Innate sensing of malaria parasites. *Nat. Rev. Immunol.* **14**, 744–757 (2014).
213. Kalantari, P. The emerging role of pattern recognition receptors in the pathogenesis of malaria. *Vaccines* **6**, 13 (2018).
214. Krishnegowda, G. *et al.* Induction of proinflammatory responses in macrophages by the glycosylphosphatidylinositols of *Plasmodium falciparum*. *J. Biol. Chem.* **280**, 8606–8616 (2005).
215. Gowda, D. C. TLR-mediated cell signaling by malaria GPIs. *Trends Parasitol.* **23**, 596–604 (2007).
216. Nebl, T., De Veer, M. J. & Schofield, L. Stimulation of innate immune responses by malarial glycosylphosphatidylinositol via pattern recognition receptors. *Parasitology* **130**, S45–S62 (2005).
217. Durai, P., Govindaraj, R. G. & Choi, S. Structure and dynamic behavior of Toll-like receptor 2 subfamily triggered by malarial glycosylphosphatidylinositols of *Plasmodium falciparum*. *FEBS J.* **280**, 6196–6212 (2013).
218. Naik, R. S. *et al.* Glycosylphosphatidylinositol anchors of *Plasmodium falciparum*. *J. Exp. Med.* **192**, 1563–1576 (2000).

219. Kurucz, R., Seeberger, P. H. & Varón Silva, D. Glycosylphosphatidylinositols in malaria: GPI biosynthesis and GPI-derived proteins. in *Encyclopedia of Malaria* **192**, 1–13 (Springer New York, 2013).
220. Gazzinelli, R. T. & Denkers, E. Y. Protozoan encounters with Toll-like receptor signalling pathways: implications for host parasitism. *Nat. Rev. Immunol.* **6**, 895–906 (2006).
221. Jaramillo, M. *et al.* Hemozoin-inducible proinflammatory events in vivo: potential role in malaria infection. *J. Immunol.* **172**, 3101–3110 (2004).
222. Coronado, L. M., Nadovich, C. T. & Spadafora, C. Malarial hemozoin: from target to tool. *Biochim. Biophys. Acta - Gen. Subj.* **1840**, 2032–2041 (2014).
223. Parroche, P. *et al.* Malaria hemozoin is immunologically inert but radically enhances innate responses by presenting malaria DNA to Toll-like receptor 9. *Proc. Natl. Acad. Sci.* **104**, 1919–1924 (2007).
224. Coban, C. *et al.* Toll-like receptor 9 mediates innate immune activation by the malaria pigment hemozoin. *J. Exp. Med.* **201**, 19–25 (2005).
225. Baccarella, A., Fontana, M. F., Chen, E. C. & Kim, C. C. Toll-like receptor 7 mediates early innate immune responses to malaria. *Infect. Immun.* **81**, 4431–4442 (2013).
226. Wu, J. *et al.* Strain-specific innate immune signaling pathways determine malaria parasitemia dynamics and host mortality. *Proc. Natl. Acad. Sci.* **111**, E511–E520 (2014).
227. Figueiredo, R. T. *et al.* Characterization of heme as activator of toll-like receptor 4. *J. Biol. Chem.* **282**, 20221–20229 (2007).
228. Orengo, J. M. *et al.* Plasmodium-induced inflammation by uric acid. *PLoS Pathog.* **4**, e1000013 (2008).
229. McGuire, W. *et al.* Levels of tumour necrosis factor and soluble TNF receptors during malaria fever episodes in the community. *Trans. R. Soc. Trop. Med. Hyg.* **92**, 50–53 (1998).
230. Hensmann, M. & Kwiatkowski, D. Cellular basis of early cytokine response to Plasmodium falciparum. *Infect. Immun.* **69**, 2364–2371 (2001).
231. Kwiatkowski, D. Febrile temperatures can synchronize the growth of Plasmodium falciparum in vitro. *J. Exp. Med.* **169**, 357–361 (1989).
232. Long, H. Y., Lell, B., Dietz, K. & Kremsner, P. G. Plasmodium falciparum: in vitro growth inhibition by febrile temperatures. *Parasitol. Res.* **87**, 553–5 (2001).
233. Engelbrecht, D. & Coetzer, T. L. Turning up the heat: heat stress induces markers of programmed cell death in Plasmodium falciparum in vitro. *Cell Death Dis.* **4**, e971–e971 (2013).
234. Porter, H., Gamette, M. J., Cortes-Hernandez, D. G. & Jensen, J. B. Asexual blood stages of Plasmodium falciparum exhibit signs of secondary necrosis, but not classical apoptosis after exposure to febrile temperature (40 C). *J. Parasitol.* **94**, 473–480 (2008).

235. Pavithra, S. R., Banumathy, G., Joy, O., Singh, V. & Tatu, U. Recurrent fever promotes *Plasmodium falciparum* development in human erythrocytes. *J. Biol. Chem.* **279**, 46692–46699 (2004).
236. Aunpad, R. *et al.* The effect of mimicking febrile temperature and drug stress on malarial development. *Ann. Clin. Microbiol. Antimicrob.* **8**, 19 (2009).
237. McKenzie, F. E., Jeffery, G. M. & Collins, W. E. Gametocytemia and fever in human malaria infections. *J. Parasitol.* **93**, 627–633 (2007).
238. Kwiatkowski, D. & Greenwood, B. M. Why is malaria fever periodic? A hypothesis. *Parasitol. Today* **5**, 264–6 (1989).
239. Greischar, M. A., Read, A. F. & Bjørnstad, O. N. Synchrony in malaria infections: how intensifying within-host competition can be adaptive. *Am. Nat.* **183**, E36–E49 (2014).
240. Udomsangpetch, R. *et al.* Febrile temperatures induce cytoadherence of ring-stage *Plasmodium falciparum*-infected erythrocytes. *Proc. Natl. Acad. Sci.* **99**, 11825–11829 (2002).
241. Zhang, R., Chandramohanadas, R., Lim, C. T. & Dao, M. Febrile temperature elevates the expression of phosphatidylserine on *Plasmodium falciparum* (FCR3CSA) infected red blood cell surface leading to increased cytoadhesion. *Sci. Rep.* **8**, 15022 (2018).
242. Marinkovic, M. *et al.* Febrile temperature leads to significant stiffening of *Plasmodium falciparum* parasitized erythrocytes. *Am. J. Physiol. Physiol.* **296**, C59–C64 (2009).
243. Liu, Y. & Chang, A. Heat shock response relieves ER stress. *EMBO J.* **27**, 1049–1059 (2008).
244. Fulda, S., Gorman, A. M., Hori, O. & Samali, A. Cellular stress responses: cell survival and cell death. *Int. J. Cell Biol.* **2010**, 1–23 (2010).
245. Galluzzi, L., Yamazaki, T. & Kroemer, G. Linking cellular stress responses to systemic homeostasis. *Nat. Rev. Mol. Cell Biol.* **19**, 731–745 (2018).
246. de Nadal, E., Ammerer, G. & Posas, F. Controlling gene expression in response to stress. *Nat. Rev. Genet.* **12**, 833–845 (2011).
247. Anckar, J. & Sistonen, L. Regulation of HSF1 function in the heat stress response: implications in aging and disease. *Annu. Rev. Biochem.* **80**, 1089–1115 (2011).
248. Hartl, F. U., Bracher, A. & Hayer-Hartl, M. Molecular chaperones in protein folding and proteostasis. *Nature* **475**, 324–332 (2011).
249. Chaari, A. Molecular chaperones biochemistry and role in neurodegenerative diseases. *Int. J. Biol. Macromol.* **131**, 396–411 (2019).
250. Glover, J. R. & Lindquist, S. Hsp104, Hsp70, and Hsp40: a novel chaperone system that rescues previously aggregated proteins. *Cell* **94**, 73–82 (1998).

251. Taipale, M., Jarosz, D. F. & Lindquist, S. HSP90 at the hub of protein homeostasis: emerging mechanistic insights. *Nat. Rev. Mol. Cell Biol.* **11**, 515–528 (2010).
252. Johnson, B. D., Schumacher, R. J., Ross, E. D. & Toft, D. O. Hop modulates hsp70/hsp90 interactions in protein folding. *J. Biol. Chem.* **273**, 3679–3686 (1998).
253. Daugaard, M., Rohde, M. & Jäättelä, M. The heat shock protein 70 family: Highly homologous proteins with overlapping and distinct functions. *FEBS Lett.* **581**, 3702–3710 (2007).
254. Bracher, A. & Verghese, J. The nucleotide exchange factors of Hsp70 molecular chaperones. *Front. Mol. Biosci.* **2**, 1–9 (2015).
255. Xu, H. Cochaperones enable Hsp70 to use ATP energy to stabilize native proteins out of the folding equilibrium. *Sci. Rep.* **8**, 13213 (2018).
256. Minami, Y., Höhfeld, J., Ohtsuka, K. & Hartl, F.-U. Regulation of the heat-shock protein 70 reaction cycle by the mammalian DnaJ homolog, Hsp40. *J. Biol. Chem.* **271**, 19617–19624 (1996).
257. Frydman, J. Folding of newly translated proteins in vivo: the role of molecular chaperones. *Annu. Rev. Biochem.* **70**, 603–647 (2001).
258. Bukau, B. & Horwich, A. L. The Hsp70 and Hsp60 chaperone machines. *Cell* **92**, 351–366 (1998).
259. Taylor, R. P. & Benjamin, I. J. Small heat shock proteins: a new classification scheme in mammals. *J. Mol. Cell. Cardiol.* **38**, 433–444 (2005).
260. Haslbeck, M. sHsps and their role in the chaperone network. *Cell. Mol. Life Sci.* **59**, 1649–57 (2002).
261. Mahat, D. B., Salamanca, H. H., Duarte, F. M., Danko, C. G. & Lis, J. T. Mammalian heat shock response and mechanisms underlying its genome-wide transcriptional regulation. *Mol. Cell* **62**, 63–78 (2016).
262. Åkerfelt, M., Morimoto, R. I. & Sistonen, L. Heat shock factors: integrators of cell stress, development and lifespan. *Nat. Rev. Mol. Cell Biol.* **11**, 545–555 (2010).
263. Solís, E. J. *et al.* Defining the essential function of yeast Hsf1 reveals a compact transcriptional program for maintaining eukaryotic proteostasis. *Mol. Cell* **63**, 60–71 (2016).
264. Boy-Marcotte, E. *et al.* The heat shock response in yeast: differential regulations and contributions of the Msn2p/Msn4p and Hsf1p regulons. *Mol. Microbiol.* **33**, 274–283 (1999).
265. Verghese, J., Abrams, J., Wang, Y. & Morano, K. A. Biology of the heat shock response and protein chaperones: budding yeast (*Saccharomyces cerevisiae*) as a model system. *Microbiol. Mol. Biol. Rev.* **76**, 115–158 (2012).
266. Yamamoto, N., Maeda, Y., Ikeda, A. & Sakurai, H. Regulation of thermotolerance by stress-induced transcription factors in *Saccharomyces cerevisiae*. *Eukaryot. Cell* **7**, 783–790 (2008).

267. Duarte, F. M. *et al.* Transcription factors GAF and HSF act at distinct regulatory steps to modulate stress-induced gene activation. *Genes Dev.* **30**, 1731–1746 (2016).
268. Amin, J., Ananthan, J. & Voellmy, R. Key features of heat shock regulatory elements. *Mol. Cell. Biol.* **8**, 3761–3769 (1988).
269. Xiao, H. & Lis, J. Germline transformation used to define key features of heat-shock response elements. *Science* **239**, 1139–1142 (1988).
270. Guertin, M. J., Petesch, S. J., Zobeck, K. L., Min, I. M. & Lis, J. T. Drosophila heat shock system as a general model to investigate transcriptional regulation. *Cold Spring Harb. Symp. Quant. Biol.* **75**, 1–9 (2010).
271. Santoro, N., Johansson, N. & Thiele, D. J. Heat shock element architecture is an important determinant in the temperature and transactivation domain requirements for heat shock transcription factor. *Mol. Cell. Biol.* **18**, 6340–52 (1998).
272. Liu, X.-D. Conservation of a stress response: human heat shock transcription factors functionally substitute for yeast HSF. *EMBO J.* **16**, 6466–6477 (1997).
273. Li, J., Chauve, L., Phelps, G., Brielmann, R. M. & Morimoto, R. I. E2F coregulates an essential HSF developmental program that is distinct from the heat-shock response. *Genes Dev.* **30**, 2062–2075 (2016).
274. Qu, Z., Titus, A. S. C. L. S., Xuan, Z. & D’Mello, S. R. Neuroprotection by heat shock factor-1 (HSF1) and trimerization-deficient mutant identifies novel alterations in gene expression. *Sci. Rep.* **8**, 17255 (2018).
275. Veri, A. O., Robbins, N. & Cowen, L. E. Regulation of the heat shock transcription factor Hsf1 in fungi: implications for temperature-dependent virulence traits. *FEMS Yeast Res.* **18**, 1–11 (2018).
276. Eastmond, D. L. & Nelson, H. C. M. Genome-wide analysis reveals new roles for the activation domains of the *Saccharomyces cerevisiae* heat shock transcription factor (Hsf1) during the transient heat shock response. *J. Biol. Chem.* **281**, 32909–32921 (2006).
277. Hashikawa, N. & Sakurai, H. Phosphorylation of the yeast heat shock transcription factor is implicated in gene-specific activation dependent on the architecture of the heat shock element. *Mol. Cell. Biol.* **24**, 3648–3659 (2004).
278. Mosser, D. D., Theodorakis, N. G. & Morimoto, R. I. Coordinate changes in heat shock element-binding activity and HSP70 gene transcription rates in human cells. *Mol. Cell. Biol.* **8**, 4736–4744 (1988).
279. Vujanac, M., Fenaroli, A. & Zimarino, V. Constitutive nuclear import and stress-regulated nucleocytoplasmic shuttling of mammalian heat-shock factor 1. *Traffic* **6**, 214–229 (2005).
280. Jakobsen, B. K. & Pelham, H. R. Constitutive binding of yeast heat shock factor to DNA in vivo. *Mol. Cell. Biol.* **8**, 5040–5042 (1988).

281. Pincus, D. *et al.* Genetic and epigenetic determinants establish a continuum of Hsf1 occupancy and activity across the yeast genome. *Mol. Biol. Cell* **29**, 3168–3182 (2018).
282. Gomez-Pastor, R., Burchfiel, E. T. & Thiele, D. J. Regulation of heat shock transcription factors and their roles in physiology and disease. *Nat. Rev. Mol. Cell Biol.* **19**, 4–19 (2018).
283. Zheng, X. *et al.* Dynamic control of Hsf1 during heat shock by a chaperone switch and phosphorylation. *Elife* **5**, 3–5 (2016).
284. Voellmy, R. On mechanisms that control heat shock transcription factor activity in metazoan cells. *Cell Stress Chaperones* **9**, 122 (2004).
285. Hahn, J.-S., Hu, Z., Thiele, D. J. & Iyer, V. R. Genome-wide analysis of the biology of stress responses through heat shock transcription factor. *Mol. Cell Biol.* **24**, 5249–5256 (2004).
286. Shi, Y., Mosser, D. D. & Morimoto, R. I. Molecular chaperones as HSF1-specific transcriptional repressors. *Genes Dev.* **12**, 654–666 (1998).
287. Neef, D. W. *et al.* A direct regulatory interaction between chaperonin TRiC and stress-responsive transcription factor HSF1. *Cell Rep.* **9**, 955–966 (2014).
288. Satyal, S. H., Chen, D., Fox, S. G., Kramer, J. M. & Morimoto, R. I. Negative regulation of the heat shock transcriptional response by HSBP1. *Genes Dev.* **12**, 1962–1974 (1998).
289. Liu, X. *et al.* Crystal structure of the hexamer of human heat shock factor binding protein 1. *Proteins Struct. Funct. Bioinforma.* **75**, 1–11 (2009).
290. Shamovsky, I., Ivannikov, M., Kandel, E. S., Gershon, D. & Nudler, E. RNA-mediated response to heat shock in mammalian cells. *Nature* **440**, 556–560 (2006).
291. Zhong, M., Orosz, A. & Wu, C. Direct sensing of heat and oxidation by *Drosophila* heat shock transcription factor. *Mol. Cell* **2**, 101–8 (1998).
292. Hentze, N., Le Breton, L., Wiesner, J., Kempf, G. & Mayer, M. P. Molecular mechanism of thermosensory function of human heat shock transcription factor Hsf1. *Elife* **5**, 1–24 (2016).
293. Yamamoto, A., Mizukami, Y. & Sakurai, H. Identification of a novel class of target genes and a novel type of binding sequence of heat shock transcription factor in *Saccharomyces cerevisiae*. *J. Biol. Chem.* **280**, 11911–11919 (2005).
294. Vihervaara, A. & Sistonen, L. HSF1 at a glance. *J. Cell Sci.* **127**, 261–266 (2014).
295. Page, T. J. *et al.* Genome-wide analysis of human HSF1 signaling reveals a transcriptional program linked to cellular adaptation and survival. *Mol. Biosyst.* **2**, 627 (2006).
296. Sandqvist, A. *et al.* Heterotrimerization of heat-shock factors 1 and 2 provides a transcriptional switch in response to distinct stimuli. *Mol. Biol. Cell* **20**, 1340–1347 (2009).

297. Morano, K. A., Grant, C. M. & Moye-Rowley, W. S. The response to heat shock and oxidative stress in *Saccharomyces cerevisiae*. *Genetics* **190**, 1157–1195 (2012).
298. Vihervaara, A., Duarte, F. M. & Lis, J. T. Molecular mechanisms driving transcriptional stress responses. *Nat. Rev. Genet.* **19**, 385–397 (2018).
299. Fujimoto, M. *et al.* RPA assists HSF1 access to nucleosomal DNA by recruiting histone chaperone FACT. *Mol. Cell* **48**, 182–194 (2012).
300. Fay, A. *et al.* Cohesin selectively binds and regulates genes with paused RNA polymerase. *Curr. Biol.* **21**, 1624–1634 (2011).
301. Li, J. *et al.* Kinetic Competition between Elongation Rate and Binding of NELF Controls Promoter-Proximal Pausing. *Mol. Cell* **50**, 711–722 (2013).
302. Trinklein, N. D., Murray, J. I., Hartman, S. J., Botstein, D. & Myers, R. M. The role of heat shock transcription factor 1 in the genome-wide regulation of the mammalian heat shock response. *Mol. Biol. Cell* **15**, 1254–1261 (2004).
303. Park, J. M., Werner, J., Kim, J. M., Lis, J. T. & Kim, Y. J. Mediator, not holoenzyme, is directly recruited to the heat shock promoter by HSF upon heat shock. *Mol. Cell* **8**, 9–19 (2001).
304. Lis, J. T., Mason, P., Peng, J., Price, D. H. & Werner, J. P-TEFb kinase recruitment and function at heat shock loci. *Genes Dev.* **14**, 792–803 (2000).
305. Sullivan, E. K., Weirich, C. S., Guyon, J. R., Sif, S. & Kingston, R. E. Transcriptional activation domains of human heat shock factor 1 recruit human SWI/SNF. *Mol. Cell. Biol.* **21**, 5826–5837 (2001).
306. Petesch, S. J. & Lis, J. T. Activator-induced spread of poly(ADP-Ribose) polymerase promotes nucleosome loss at Hsp70. *Mol. Cell* **45**, 64–74 (2012).
307. Vonlaufen, N., Kanzok, S. M., Wek, R. C. & Sullivan Jr, W. J. Stress response pathways in protozoan parasites. *Cell. Microbiol.* **10**, 2387–2399 (2008).
308. Przyborski, J. M., Diehl, M. & Blatch, G. L. Plasmodial HSP70s are functionally adapted to the malaria parasite life cycle. *Front. Mol. Biosci.* **2**, 1–7 (2015).
309. Liu, K. & Houry, W. A. Chaperones and Proteases of *Plasmodium falciparum*. in *Heat Shock Proteins of Malaria* 161–187 (Springer Netherlands, 2014). doi:10.1007/978-94-007-7438-4_9
310. Acharya, P., Kumar, R. & Tatu, U. Chaperoning a cellular upheaval in malaria: heat shock proteins in *Plasmodium falciparum*. *Mol. Biochem. Parasitol.* **153**, 85–94 (2007).
311. Pavithra, S. R., Kumar, R. & Tatu, U. Systems analysis of chaperone networks in the malarial parasite *Plasmodium falciparum*. *PLoS Comput. Biol.* **3**, e168 (2007).
312. Banumathy, G., Singh, V., Pavithra, S. R. & Tatu, U. Heat shock protein 90 function is essential for *Plasmodium falciparum* growth in human erythrocytes. *J. Biol. Chem.* **278**, 18336–18345 (2003).

313. Gitau, G. W., Mandal, P., Blatch, G. L., Przyborski, J. & Shonhai, A. Characterisation of the Plasmodium falciparum Hsp70–Hsp90 organising protein (PfHop). *Cell Stress Chaperones* **17**, 191–202 (2012).
314. Kumar, N., Koski, G., Harada, M., Aikawa, M. & Zheng, H. Induction and localization of Plasmodium falciparum stress proteins related to the heat shock protein 70 family. *Mol. Biochem. Parasitol.* **48**, 47–58 (1991).
315. Chen, Y. *et al.* Repurposing drugs to target the malaria parasite unfolding protein response. *Sci. Rep.* **8**, 10333 (2018).
316. Vincensini, L. *et al.* Proteomic analysis identifies novel proteins of the maurer's clefts, a secretory compartment delivering Plasmodium falciparum proteins to the surface of its host cell. *Mol. Cell. Proteomics* **4**, 582–593 (2005).
317. Grover, M., Chaubey, S., Ranade, S. & Tatu, U. Identification of an exported heat shock protein 70 in Plasmodium falciparum. *Parasite* **20**, 2 (2013).
318. Muralidharan, V., Oksman, A., Pal, P., Lindquist, S. & Goldberg, D. E. Plasmodium falciparum heat shock protein 110 stabilizes the asparagine repeat-rich parasite proteome during malarial fevers. *Nat. Commun.* **3**, 1310 (2012).
319. Botha, M., Pesce, E.-R. & Blatch, G. L. The Hsp40 proteins of Plasmodium falciparum and other apicomplexa: Regulating chaperone power in the parasite and the host. *Int. J. Biochem. Cell Biol.* **39**, 1781–1803 (2007).
320. Nieto, A., Pérez Ishiwara, D. G., Orozco, E., Sánchez Monroy, V. & Gómez García, C. A novel heat shock element (HSE) in Entamoeba histolytica that regulates the transcriptional activation of the EhPgp5 gene in the presence of emetine drug. *Front. Cell. Infect. Microbiol.* **7**, 115–122 (2017).
321. Sayeed, S. K. *et al.* Identification of heat shock factor binding protein in Plasmodium falciparum. *Malar. J.* **13**, 118 (2014).
322. Biswas, S. & Sharma, Y. D. Enhanced expression of Plasmodium falciparum heat shock protein PFHSP70-I at higher temperatures and parasite survival. *FEMS Microbiol. Lett.* **124**, 425–429 (1994).
323. Joshi, B., Biswas, S. & Sharma, Y. D. Effect of heat-shock on Plasmodium falciparum viability, growth and expression of the heat-shock protein 'PFHSP70-I' gene. *FEBS Lett.* **312**, 91–94 (1992).
324. Botha, M. *et al.* Plasmodium falciparum encodes a single cytosolic type I Hsp40 that functionally interacts with Hsp70 and is upregulated by heat shock. *Cell Stress Chaperones* **16**, 389–401 (2011).
325. Watanabe, J. Cloning and characterization of heat shock protein DnaJ homologues from Plasmodium falciparum and comparison with ring infected erythrocyte surface antigen. *Mol. Biochem. Parasitol.* **88**, 253–258 (1997).
326. Pesce, E. *et al.* The Plasmodium falciparum heat shock protein 40, Pfj4, associates with heat shock protein 70 and shows similar heat induction and localisation patterns. *Int. J. Biochem. Cell Biol.* **40**, 2914–2926 (2008).

327. Su, X. & Wellems, T. E. Sequence, transcript characterization and polymorphisms of a *Plasmodium falciparum* gene belonging to the heat-shock protein (HSP) 90 family. *Gene* **151**, 225–230 (1994).
328. Turner, G. D. *et al.* An immunohistochemical study of the pathology of fatal malaria. Evidence for widespread endothelial activation and a potential role for intercellular adhesion molecule-1 in cerebral sequestration. *Am. J. Pathol.* **145**, 1057–69 (1994).
329. Cortés, A. A chimeric *Plasmodium falciparum* Pfnbp2b/Pfnbp2a gene originated during asexual growth. *Int. J. Parasitol.* **35**, 125–130 (2005).
330. Cortes, A. Ability of *Plasmodium falciparum* to invade Southeast Asian ovalocytes varies between parasite lines. *Blood* **104**, 2961–2966 (2004).
331. Cortés, A. *et al.* Epigenetic silencing of *Plasmodium falciparum* genes linked to erythrocyte invasion. *PLoS Pathog.* **3**, e107 (2007).
332. Hughes, K. R. & Waters, A. P. Rapid inducible protein displacement in *Plasmodium* in vivo and in vitro using knocksideways technology. *Wellcome Open Res.* **2**, 18 (2017).
333. Janse, C. J., Ramesar, J., van den Berg, F. M. & Mons, B. *Plasmodium berghei*: In vivo generation and selection of karyotype mutants and non-gametocyte producer mutants. *Exp. Parasitol.* **74**, 1–10 (1992).
334. Urbán, P., Estelrich, J., Cortés, A. & Fernández-Busquets, X. A nanovector with complete discrimination for targeted delivery to *Plasmodium falciparum*-infected versus non-infected red blood cells in vitro. *J. Control. Release* **151**, 202–211 (2011).
335. Rovira-Graells, N., Aguilera-Simón, S., Tintó-Font, E. & Cortés, A. New assays to characterise growth-related phenotypes of *Plasmodium falciparum* reveal variation in density-dependent growth inhibition between parasite lines. *PLoS One* **11**, e0165358 (2016).
336. Cytomation. Summit™ software system. (2006). Available at: <http://www.cyto.purdue.edu/cdroms/cyto5/sponsors/cytomate/summit.htm>.
337. Terho, P. Flowing software. (2013). Available at: <http://flowingsoftware.btk.fi/>.
338. Crowley, V. M., Rovira-Graells, N., de Pouplana, L. R. & Cortés, A. Heterochromatin formation in bistable chromatin domains controls the epigenetic repression of clonally variant *Plasmodium falciparum* genes linked to erythrocyte invasion. *Mol. Microbiol.* **80**, 391–406 (2011).
339. Schwach, F. *et al.* PlasmoGEM, a database supporting a community resource for large-scale experimental genetics in malaria parasites. *Nucleic Acids Res.* **43**, D1176–D1182 (2015).
340. PlasmoGEM. PlasmoGEM. Generation of Gene Targeting Vectors using Recombineering -Small scale (single tube) protocol. (2014). Available at: https://plasmogem.sanger.ac.uk/static/supporting_pdfs/Small_Scale_Recombineering_and_Gateway_protocol_WTAC_Mal_Exp_Gen_2013.pdf.

341. Ghorbal, M. *et al.* Genome editing in the human malaria parasite *Plasmodium falciparum* using the CRISPR-Cas9 system. *Nat. Biotechnol.* **32**, 819–821 (2014).
342. Lim, M. Y.-X. *et al.* UDP-galactose and acetyl-CoA transporters as *Plasmodium* multidrug resistance genes. *Nat. Microbiol.* **1**, 16166 (2016).
343. Bancells, C. *et al.* Revisiting the initial steps of sexual development in the malaria parasite *Plasmodium falciparum*. *Nat. Microbiol.* **4**, 144–154 (2019).
344. Knuepfer, E., Napiorkowska, M., van Ooij, C. & Holder, A. A. Generating conditional gene knockouts in *Plasmodium* – a toolkit to produce stable DiCre recombinase-expressing parasite lines using CRISPR/Cas9. *Sci. Rep.* **7**, 3881 (2017).
345. Llorà-Batlle, O., Michel-Todó, L. & Cortés, A. Ectopic heterochromatin formation by specific regions of the *Plasmodium falciparum* pfap2-g gene (unpublished work).
346. Portugaliza, H. P., Llorà-Batlle, O., Rosanas-Urgell, A. & Cortés, A. Reporter lines based on the gexp02 promoter enable early quantification of sexual conversion rates in the malaria parasite *Plasmodium falciparum*. *Sci. Rep.* **9**, 14595 (2019).
347. Pankova, T. G., Igonina, T. M., Kobzev, V. F. & Merkulova, T. I. Study of the binding of nuclear proteins from *Plasmodium berghei* strains with different chloroquine sensitivity to oligonucleotides corresponding to regulatory elements of multidrug resistance (*mdr1*) gene. *Biomed. Khim.* **53**, 547–56 (2008).
348. Schneider, C. A., Rasband, W. S. & Eliceiri, K. W. NIH Image to ImageJ: 25 years of image analysis. *Nat. Methods* **9**, 671–5 (2012).
349. Bioinformatics, B. FastQC. (2012). Available at: <http://www.bioinformatics.babraham.ac.uk/projects/fastqc/>.
350. Martin, M. Cutadapt removes adapter sequences from high-throughput sequencing reads. *EMBnet.journal* **17**, 10 (2011).
351. Bahl, A. *et al.* PlasmoDB: The *Plasmodium* genome resource. A database integrating experimental and computational data. *Nucleic Acids Res.* **31**, 212–215 (2003).
352. Langmead, B. & Salzberg, S. L. Fast gapped-read alignment with Bowtie 2. *Nat. Methods* **9**, 357–359 (2012).
353. García-Alcalde, F. *et al.* Qualimap: evaluating next-generation sequencing alignment data. *Bioinformatics* **28**, 2678–2679 (2012).
354. Picard toolkit. (2016). Available at: <https://github.com/broadinstitute/picard>.
355. McKenna, A. *et al.* The Genome Analysis Toolkit: a MapReduce framework for analyzing next-generation DNA sequencing data. *Genome Res.* **20**, 1297–1303 (2010).
356. Robinson, J. T. *et al.* Integrative genomics viewer. *Nat. Biotechnol.* **29**, 24–26 (2011).

357. Kafsack, B. F. C., Painter, H. J. & Llinás, M. New Agilent platform DNA microarrays for transcriptome analysis of *Plasmodium falciparum* and *Plasmodium berghei* for the malaria research community. *Malar. J.* **11**, 187 (2012).
358. Painter, H. J., Altenhofen, L. M., Kafsack, B. F. C. & Llinás, M. Whole-genome analysis of *Plasmodium* spp. utilizing a new Agilent Technologies DNA microarray platform. in **923**, 213–219 (2012).
359. Lemieux, J. E. *et al.* Statistical estimation of cell-cycle progression and lineage commitment in *Plasmodium falciparum* reveals a homogeneous pattern of transcription in ex vivo culture. *Proc. Natl. Acad. Sci.* **106**, 7559–7564 (2009).
360. Saeed, A. I. *et al.* [9] TM4 microarray software suite. in *Methods in Enzymology* **411**, 134–193 (2006).
361. Bailey, T. L., Williams, N., Misleh, C. & Li, W. W. MEME: discovering and analyzing DNA and protein sequence motifs. *Nucleic Acids Res.* **34**, W369–W373 (2006).
362. Bauer, S., Grossmann, S., Vingron, M. & Robinson, P. N. Ontologizer 2.0—a multifunctional tool for GO term enrichment analysis and data exploration. *Bioinformatics* **24**, 1650–1651 (2008).
363. Alexa, A., Rahnenfuhrer, J. & Lengauer, T. Improved scoring of functional groups from gene expression data by decorrelating GO graph structure. *Bioinformatics* **22**, 1600–1607 (2006).
364. Subramanian, A. *et al.* Gene set enrichment analysis: a knowledge-based approach for interpreting genome-wide expression profiles. *Proc. Natl. Acad. Sci.* **102**, 15545–15550 (2005).
365. Ginsburg, H. Progress in in silico functional genomics: the malaria Metabolic Pathways database. *Trends Parasitol.* **22**, 238–240 (2006).
366. Kavishe, R. A. *et al.* Localization of the ATP-binding cassette (ABC) transport proteins PfMRP1, PfMRP2, and PfMDR5 at the *Plasmodium falciparum* plasma membrane. *Malar. J.* **8**, 205 (2009).
367. Buenrostro, J. D., Giresi, P. G., Zaba, L. C., Chang, H. Y. & Greenleaf, W. J. Transposition of native chromatin for fast and sensitive epigenomic profiling of open chromatin, DNA-binding proteins and nucleosome position. *Nat. Methods* **10**, 1213–1218 (2013).
368. Li, H. *et al.* The sequence alignment/map format and SAMtools. *Bioinformatics* **25**, 2078–2079 (2009).
369. A toolkit for QC and visualization of ATAC-seq results. (2017). Available at: <https://github.com/ParkerLab/ataqv>.
370. Zhang, Y. *et al.* Model-based analysis of ChIP-Seq (MACS). *Genome Biol.* **9**, R137 (2008).
371. Aguilar, R. *et al.* Molecular evidence for the localization of *Plasmodium falciparum* immature gametocytes in bone marrow. *Blood* **123**, 959–966 (2014).

372. Scherf, A., Lopez-Rubio, J. J. & Riviere, L. Antigenic variation in *Plasmodium falciparum*. *Annu. Rev. Microbiol.* **62**, 445–470 (2008).
373. Welch, W. J. & Brown, C. R. Influence of molecular and chemical chaperones on protein folding. *Cell Stress Chaperones* **1**, 109 (1996).
374. Dobson, C. M., Šali, A. & Karplus, M. Protein folding: a perspective from theory and experiment. *Angew. Chemie Int. Ed.* **37**, 868–893 (1998).
375. Masterton, R. J., Roobol, A., Al-Fageeh, M. B., Carden, M. J. & Smales, C. M. Post-translational events of a model reporter protein proceed with higher fidelity and accuracy upon mild hypothermic culturing of Chinese hamster ovary cells. *Biotechnol. Bioeng.* **105**, 215–220 (2010).
376. Zhang, M. *et al.* Uncovering the essential genes of the human malaria parasite *Plasmodium falciparum* by saturation mutagenesis. *Science* **360**, eaap7847 (2018).
377. López-Barragán, M. J. *et al.* Directional gene expression and antisense transcripts in sexual and asexual stages of *Plasmodium falciparum*. *BMC Genomics* **12**, 587 (2011).
378. Bridgford, J. L. *et al.* Artemisinin kills malaria parasites by damaging proteins and inhibiting the proteasome. *Nat. Commun.* **9**, 3801 (2018).
379. Lin, J., Janse, C. J. & Khan, S. M. RMgm-913: PBANKA_1356000 disruption (unpublished work). *RMgmDB* (2013). Available at: <https://www.pberghei.eu/index.php?rmgm=913>.
380. Brancucci, N. M. B. *et al.* Probing *Plasmodium falciparum* sexual commitment at the single-cell level. *Wellcome Open Res.* **3**, 70 (2018).
381. Castells-Roca, L. *et al.* Heat shock response in yeast involves changes in both transcription rates and mRNA stabilities. *PLoS One* **6**, (2011).
382. Mager, W. H. & De Kruijff, A. J. Stress-induced transcriptional activation. *Microbiol. Rev.* **59**, 506–31 (1995).
383. Clos, J. & Krobitch, S. Heat shock as a regular feature of the life cycle of *Leishmania* parasites. *Am. Zool.* **39**, 848–856 (1999).
384. Morimoto, R. I. Regulation of the heat shock transcriptional response: cross talk between a family of heat shock factors, molecular chaperones, and negative regulators. *Genes Dev.* **12**, 3788–3796 (1998).
385. Van der Ploeg, L., Giannini, S. & Cantor, C. Heat shock genes: regulatory role for differentiation in parasitic protozoa. *Science* **228**, 1443–1446 (1985).
386. Singer, M. A. & Lindquist, S. Multiple effects of trehalose on protein folding in vitro and in vivo. *Mol. Cell* **1**, 639–648 (1998).
387. Diamant, S., Eliahu, N., Rosenthal, D. & Goloubinoff, P. Chemical chaperones regulate molecular chaperones in vitro and in cells under combined salt and heat stresses. *J. Biol. Chem.* **276**, 39586–39591 (2001).

388. Voziyan, P. A. & Fisher, M. T. Chaperonin-assisted folding of glutamine synthetase under nonpermissive conditions: Off-pathway aggregation propensity does not determine the co-chaperonin requirement. *Protein Sci.* **9**, 2405–2412 (2000).
389. Najafi, S., Sorkheh, K. & Nasernakhaei, F. Characterization of the APETALA2/Ethylene-responsive factor (AP2/ERF) transcription factor family in sunflower. *Sci. Rep.* **8**, 11576 (2018).
390. Ohme-Takagi, M. & Shinshi, H. Ethylene-inducible DNA binding proteins that interact with an ethylene-responsive element. *Plant Cell* **7**, 173–182 (1995).
391. Jofuku, K. D., den Boer, B. G., Van Montagu, M. & Okamoto, J. K. Control of Arabidopsis flower and seed development by the homeotic gene APETALA2. *Plant Cell* **6**, 1211–1225 (1994).
392. Sharma, M. & Pandey, G. K. Expansion and function of repeat domain proteins during stress and development in plants. *Front. Plant Sci.* **6**, 1–15 (2016).
393. Jakobsen, B. K. & Pelham, H. R. A conserved heptapeptide restrains the activity of the yeast heat shock transcription factor. *EMBO J.* **10**, 369–75 (1991).
394. Rahbari, M. *et al.* Hydrogen peroxide dynamics in subcellular compartments of malaria parasites using genetically encoded redox probes. *Sci. Rep.* **7**, 10449 (2017).
395. Bridges, T. M. *et al.* Polymorphisms in human heat shock factor-1 and analysis of potential biological consequences. *Cell Stress Chaperones* **20**, 47–59 (2015).
396. Li, Q.-L. *et al.* Two novel SNPs in HSF1 Gene are associated with thermal tolerance traits in Chinese holstein cattle. *DNA Cell Biol.* **30**, 247–254 (2011).
397. Claessens, A., Affara, M., Assefa, S. A., Kwiatkowski, D. P. & Conway, D. J. Culture adaptation of malaria parasites selects for convergent loss-of-function mutants. *Sci. Rep.* **7**, 41303 (2017).
398. Dharia, N. V. *et al.* Whole-genome sequencing and microarray analysis of ex vivo *Plasmodium vivax* reveal selective pressure on putative drug resistance genes. *Proc. Natl. Acad. Sci.* **107**, 20045–20050 (2010).
399. Chen, S.-B. *et al.* Whole-genome sequencing of a *Plasmodium vivax* clinical isolate exhibits geographical characteristics and high genetic variation in China-Myanmar border area. *BMC Genomics* **18**, 131 (2017).
400. MalariaGEN. Genomic Epidemiology Network. (2019). Available at: <https://www.malariagen.net/>.
401. Nicholls, S., Leach, M. D., Priest, C. L. & Brown, A. J. P. Role of the heat shock transcription factor, Hsf1, in a major fungal pathogen that is obligately associated with warm-blooded animals. *Mol. Microbiol.* **74**, 844–861 (2009).
402. Li, J. *et al.* Kinetic competition between elongation rate and binding of NELF controls promoter-proximal pausing. *Mol. Cell* **50**, 711–722 (2013).

403. Islam, A. *et al.* The role of Hsp90 α in heat-induced apoptosis and cell damage in primary myocardial cell cultures of neonatal rats. *Genet. Mol. Res.* **12**, 6080–6091 (2013).
404. Theodorakis, N. G., Drujan, D. & De Maio, A. Thermotolerant cells show an attenuated expression of Hsp70 after heat shock. *J. Biol. Chem.* **274**, 12081–12086 (1999).
405. Weindling, E. & Bar-Nun, S. Sir2 links the unfolded protein response and the heat shock response in a stress response network. *Biochem. Biophys. Res. Commun.* **457**, 473–478 (2015).
406. Gosline, S. J. C. *et al.* Intracellular eukaryotic parasites have a distinct unfolded protein response. *PLoS One* **6**, e19118 (2011).
407. Hollien, J. Evolution of the unfolded protein response. *Biochim. Biophys. Acta - Mol. Cell Res.* **1833**, 2458–2463 (2013).
408. Li, J., Labbadia, J. & Morimoto, R. I. Rethinking HSF1 in stress, development, and organismal health. *Trends Cell Biol.* **27**, 895–905 (2017).
409. Balu, B., Singh, N., Maher, S. P. & Adams, J. H. A genetic screen for attenuated growth identifies genes crucial for intraerythrocytic development of *Plasmodium falciparum*. *PLoS One* **5**, e13282 (2010).
410. Mancio-Silva, L., Lopez-Rubio, J. J., Claes, A. & Scherf, A. Sir2a regulates rDNA transcription and multiplication rate in the human malaria parasite *Plasmodium falciparum*. *Nat. Commun.* **4**, 1530 (2013).
411. Richter, K., Haslbeck, M. & Buchner, J. The heat shock response: life on the verge of death. *Mol. Cell* **40**, 253–266 (2010).
412. Phukan, U. J., Jeena, G. S., Tripathi, V. & Shukla, R. K. Regulation of apetala2/ethylene response factors in plants. *Front. Plant Sci.* **8**, 1–18 (2017).
413. Koussis, K. *et al.* Targeted deletion of a *Plasmodium* site-2 protease impairs life cycle progression in the mammalian host. *PLoS One* **12**, e0170260 (2017).
414. Rawson, R. B. The site-2 protease. *Biochim. Biophys. Acta - Biomembr.* **1828**, 2801–2807 (2013).
415. Ye, J. *et al.* ER stress induces cleavage of membrane-bound ATF6 by the same proteases that process SREBPs. *Mol. Cell* **6**, 1355–64 (2000).
416. Murakami, T. *et al.* Cleavage of the membrane-bound transcription factor OASIS in response to endoplasmic reticulum stress. *J. Neurochem.* **96**, 1090–1100 (2006).
417. Guo, Y. *et al.* Evidence for a mechanism of repression of heat shock factor 1 transcriptional activity by a multichaperone complex. *J. Biol. Chem.* **276**, 45791–45799 (2001).
418. Kijima, T. *et al.* HSP90 inhibitors disrupt a transient HSP90-HSF1 interaction and identify a noncanonical model of HSP90-mediated HSF1 regulation. *Sci. Rep.* **8**, 6976 (2018).

419. Shi, Y., Kroeger, P. E. & Morimoto, R. I. The carboxyl-terminal transactivation domain of heat shock factor 1 is negatively regulated and stress responsive. *Mol. Cell. Biol.* **15**, 4309–4318 (1995).
420. Sakurai, H. & Enoki, Y. Novel aspects of heat shock factors: DNA recognition, chromatin modulation and gene expression. *FEBS J.* **277**, 4140–9 (2010).
421. Cordeiro, R. S. B. *et al.* Plasmodium berghei : physiopathological changes during infections in mice. *Ann. Trop. Med. Parasitol.* **77**, 455–465 (1983).
422. Dascombe, M. J. & Sidara, J. Y. The absence of fever in rat malaria is associated with increased turnover of 5-hydroxytryptamine in the brain. in *Temperature Regulation: Recent Physiological and Pharmacological Advances* (ed. Milton, A. S.) 47–52 (Birkhäuser Basel, 1994).

The background of the entire page is a repeating pattern of stylized, circular organisms or cells. Each cell is outlined in a light teal color and contains various internal patterns, such as small dots, larger irregular shapes, or simple outlines, representing different stages or types of cells. A solid teal horizontal band runs across the middle of the page, containing the word "ANNEX" in white, bold, uppercase letters.

ANNEX

ANNEX – I

Product references

Name	Complete product name	Vendor	Reference
aa-dUTP	AA-dUTP (5-Aminoallyl-dUTP), lyophilized powder, 1mg (Biotium)	Labnet Biotechnica	BT-40020-1
Acetonitrile	Acetonitrile LC-MS Ultra ChromaSolv	FLUKA (Sigma)	14261-1L
Acrylamide	40% Acrylamide/Bis Solution, 37.5:1, 500ml	BioRad	161-0148
Agarose	Low EEO agarose (D1) 250g	Conda	1070801022
Agilent gasket	Hybridization Gasket Slide Kit (5) - 8 microarrays per slide	Agilent	G2534-60014
Agilent microarray slide	Microarrays HD-CGH custom-made (8X15K), AMADID 085763	Agilent	G4427A
Alsever's Solution	Alsever's Solution	Sigma-Aldrich	A3551
Ampicillin	Ampicillin sodium salt	Sigma-Aldrich	A9518-5G
AMPure XP® Beads	Agencourt AMPure XP	Beckman Coulter	A63880
AMV reverse transcription kit	Reverse Transcription System (100 reactions)	Promega	A3500
Anti-3xHA antibody	Anti-HA High Affinity, from rat IgG1	Roche	11867423001
Anti-GFP antibody	GFP Polyclonal Antibody	Invitrogen	A-11122
Anti-GPA antibody	Monoclonal Anti-Glycophorin A,B (α,δ) antibody produced in mouse	Sigma-Aldrich	G7650
Anti-H3 antibody	Histone H3 Antibody	Cell Signaling Technology	9715
Anti-HSP70-1 antibody	HSP70 (P. falciparum) Antibody	StressMarq Biosciences	SPC-186C
Anti-HSP70-1, monoclonal antibody	Anti-HSP70-1 (P. falciparum), monoclonal	Kindly provided by J. Przyborsky	
Anti-HSP70-1, polyclonal antibody	Anti-HSP70-1 (P. falciparum), polyclonal	Kindly provided by J. Przyborsky	
Anti-mouse HRP antibody	Anti-Mouse IgG (whole molecule)–Peroxidase antibody produced in goat	Sigma-Aldrich	A4416
Anti-rabbit Alexa 488 antibody	Goat anti-Rabbit IgG (H+L) Highly Cross-Adsorbed Secondary Antibody, Alexa Fluor 488	Invitrogen	A11034
Anti-rabbit HRP antibody	Goat Anti-Rabbit IgG Antibody, (H+L) HRP conjugate	Millipore	AP307P
Anti-rat Alexa 488 antibody	Goat anti-Rat IgG (H+L) Cross-Adsorbed Secondary Antibody, Alexa Fluor 488	Invitrogen	A11006
Anti-rat HRP antibody	Goat anti-Rat IgG (H+L) Cross-Adsorbed Secondary Antibody, HRP	Invitrogen	A10549
APS	10 g, ammonium persulfate (APS) catalyst	BioRad	161-0700
Bromophenol blue	Bromophenol Blue sodium salt	Sigma-Aldrich	B5525
BSA	Bovine serum albumin (BSA), Biowest, 100G	Labclinics	P6154-100G
CaCl ₂ · 2 H ₂ O	Calcium chloride dihydrate, for molecular biology, ≥99.0%	Sigma-Aldrich	C3306
Carbenicillin	Carbenicillin disodium salt (250 mg)	Sigma-Aldrich	C1389-250MG
Chloroform	Chloroform, contains 100-200 ppm amylenes as stabilizer, ≥99.5%.	Sigma-Aldrich	C2432-500ML
Cy3 and Cy5	CyDye Post-Labeling Reactive Dye Pack	GE Healthcare	RPN5661
DAPI	DAPI, AppliChem lifescience	AppliChem	A4099.0005
DH5 α	MAX Efficiency® DH5 α ™ Competent Cells	Life Technologies	18258012
DHA	Dihydroartemisinin mixture of α and β isomers, 50mg	Sigma-Aldrich	D7439-50MG
DMA	N,N-Dimethylacetamide, ReagentPlus®, ≥99%	Sigma-Aldrich	185884
DMF	N,N-Dimethylformamide, anhydrous, 99.8%	Sigma-Aldrich	227056
DMSO	Dimethyl sulfoxide	Sigma-Aldrich	D8418-50ML
DNA-free Kit, DNase treatment & Removal Reagents	DNA-free™ DNA Removal Kit	Invitrogen	AM1906
DNeasy Blood & Tissue Kit	DNeasy Blood and Tissue Kit (50)	Qiagen	69504
dNTP mix (for Taq Pol)	Deoxynucleotide (dNTP) Solution Mix, 10 mM each	NEB	N0447S
dNTP Set (for microarrays)	dNTP Set (100 mM)	Life Technologies	10297018
DTT	DL-Dithiothreitol, ≥98% (HPLC), ≥99.0% (titration)	Sigma-Aldrich	D0632-5G
EDTA	EDTA (Acido Etilendiaminotetraacético) PA-ACS, 500g	Panreac	131026.1210
EGTA	EGTA for molecular biology	Sigma-Aldrich	E3889-10G
Electroporation cuvettes	Gene Pulser®/MicroPulser™ Electroporation Cuvettes, 0.2 cm gap (50 units)	BioRad	1652086
Ethanol	Ethanol absolute for analysis EMSURE® ACS, ISO, Reag. Ph. Eur. (HDPE plastic bottle)	Merck	1.00983.1011
Fetal bovine serum (FBS)	Bovine Serum, heat inactivated, New Zealand origin	Gibco/Life	26170035

		Technologies	
GE blocking agent	Gene Expression Hybridization Kit	Agilent	5188-5242
GeneRuler DNA Ladder Mix	GeneRuler DNA Ladder Mix	Life Technologies	SM0331
GFX PCR DNA & gel band purification kit	ILLUSTRATE GFX, PCR-DNA AND GEL-BAND PURIFICATION KIT, 100	GE Healthcare	28-9034-70
Giemsa	Azur-eosina-azul de metileno según Giemsa en solución, 500ml	Sigma-Aldrich	1092040500
Glucose	D-(+)-Glucose, 100g	Sigma-Aldrich	G8270-100G
Glutamine	L-Glutamine 200mM 100ml	Life Technologies	25030024
Glycerol	Glycerol for molecular biology, ≥99%, 500ml	Sigma-Aldrich	G5516-500ML
Glycine	Glycine, BioUltra for molecular biology, 250g	Sigma-Aldrich	50046-250G
GoTaq	GoTaq® Green Master Mix, 1000 Reactions	Promega	M7123
H₂O₂	Hydrogen Peroxide 30% EMSURE® ISO for analysis 500ml	Merck Millipore	1.07209.0500
HCl	Hydrochloric acid 37% PA-ACS-ISO	Panreac	471020.1611
Heparin	Heparin sodium salt from porcine intestinal mucosa, ≥180 USP units/mg	Sigma-Aldrich	H4784-1G
Hepes	HEPES ≥ 99,5%	Sigma-Aldrich	H3375-250G
High Capacity cDNA Reverse Transcription Kit	High Capacity cDNA Reverse Transcription Kit	Applied Biosystems	4368814
Hi-RPM hybridization buffer	Gene Expression Hybridization Kit	Agilent	5188-5242
Hydrophobic pen	Super PAP Pen, Small	Electron Microscopy Sciences	71312
Igepal CA-630	Igepal® CA-630 for molecular biology	Sigma	I8896
Incubator chamber	Modular Incubator Chamber	Billups-Rothenberg Inc	MIC-101
In-Fusion	In-Fusion® HD Cloning Kit w/Competent Cells	Takara	639642
Isopropanol	2-Propanol, BioReagent, for molecular biology, ≥99% (Sigma), 500ml	Sigma-Aldrich	I9516-500ML
K₂HPO₄	Potassium phosphate dibasic (K ₂ HPO ₄) anhydrous for molecular biology, BioUltra, ≥99.0% (T)	Sigma-Aldrich	60353-250G
KAPA HiFi polymerase	KAPA HiFi HotStart ReadyMix	Roche	KR0370
KCl	Potassium chloride for molecular biology ≥99.0%, 500g	Sigma-Aldrich	P9541-500G
Ketamine	Anesketin inj. (cd sch 2)		905525
KH₂PO₄	Potassium phosphate monobasic, BioUltra, for molecular biology, anhydrous, ≥99.5% (T)	Sigma-Aldrich	60218-100G
KHCO₃	Potassium bicarbonate, ACS reagent, 99.7%, powder, crystals or granules	Sigma-Aldrich	237205
LA Taq Polymerase	LA Taq® DNA Polymerase (125u)	Takara	RR002A
LB agar	LB agar (Lennox)	Conda	1083
LB broth	LB Broth (Lennox)	Conda	1231
LightCycler® 480 SYBR Green I Master	LightCycler® 480 SYBR Green I Master	Roche	4707516001
Maxiprep	Qiagen EndoFree Plasmid Maxi Kit (10)	Qiagen	50912362
β-Mercaptoethanol	β-Mercaptoethanol for molecular biology, 100ml	Vidrafoc	A1108.0100
Methanol	Methanol (Reag. Ph. Eur.) PA-ACS-ISO, 5l	Vidrafoc	131091.1214
MgCl₂·6 H₂O	Magnesium chloride hexahydrate, ACS reagent, 99.0-102.0%	Sigma-Aldrich	M9272
Mice	BALB/c mice and Theiler's original mice	Harlan Laboratories, UK	
Milk powder	Milk powder Sveltesse - 600g	Nestle	8410100002378
MinElute PCR purification kit	MinElute PCR Purification Kit (250), Qiagen	Qiagen	28006
Mini Trans-Blot® module	Mini-PROTEAN Tetra cell with Mini Trans-Blot module	BioRad	165-8029SP
Miniprep	QIAprep Spin Miniprep Kit Qiagen (250)	Qiagen	27106
Mini-PROTEAN® Tetra cell	Mini-PROTEAN Tetra cell with Mini Trans-Blot module	BioRad	165-8029SP
Na₂EDTA	Ethylenediaminetetraacetic acid disodium salt dihydrate, for electrophoresis, for molecular biology, 99.0-101.0% (titration)	Sigma-Aldrich	E5134
Na₂HPO₄	Sodium phosphate dibasic	Sigma-Aldrich	71636-250G
NaAc	Sodium acetate anhydrous (DNase, RNase, protease, none detected)	Sigma-Aldrich	S2889-250G
NaCl	Sodium chloride, ≥98% (titration), 1kg	Sigma-Aldrich	S3014-1KG
NaH₂PO₄	Sodium phosphate monobasic, BioReagent, for molecular biology, anhydrous, ≥98%	Sigma-Aldrich	S3139-250G
NaHCO₃	Sodium bicarbonate, powder, BioReagent, for molecular	Sigma-Aldrich	S5761

	biology, suitable for cell culture		
NaOH	Sodium hydroxide, ACS reagent, ≥97.0%, pellets, 500g	Sigma-Aldrich	221465-500G
NEB2 buffer	NEBuffer™ 2	NEB	B7002S
NEBNext DNA Library Prep Master Mix Set	NEBNext® DNA Library Prep Master Mix Set for Illumina®	NEB	E6040S
Nextera-indexed primers	For primer sequences, see Table 37.	IDT	n/a
NH ₄ Cl	Ammonium chloride, for molecular biology, suitable for cell culture, ≥99.5%	Sigma-Aldrich	A9434
N-laurylsarcosine	N-Lauroylsarcosine sodium salt solution	Sigma-Aldrich	L7414-10ML
Nucleocuvette™ Strip 16-well	Inspection Equipment 4D-Nucleofector™ 16-well Strip	Lonza	AXP-1004
NuPAGE® Transfer Buffer	NuPAGE™ Transfer Buffer (20X)	Invitrogen	NP00061
NuPAGE™ 3-8% Tris-acetate precast gels	NuPAGE™ 3-8% Tris-Acetate Protein Gels, 1.0 mm, 10-well	Invitrogen	EA0375BOX
NuPAGE™ LDS Sample Buffer	NuPAGE™ LDS Sample Buffer (4X)	Invitrogen	NP0007
NuPAGE™ Sample Reducing Agent	NuPAGE™ Sample Reducing Agent (10X)	Invitrogen	NP0004
NuPAGE™ Tris-Acetate SDS Running Buffer	NuPAGE™ Tris-Acetate SDS Running Buffer (20X)	Invitrogen	LA0041
Nycodenz	Histodenz, nonionic density gradient medium	Sigma-Aldrich	D2158-100G
Oligo-dT 25-mer primer	n/a	IDT	n/a
Optical adhesive film	MicroAmp® Optical Adhesive Covers, 100/Pkg	Life Technologies	4311971
Orange G	Orange G	Sigma-Aldrich	O3756-25G
P3 Primary Cell 4D-Nucleofector	P3 Primary Cell 4D-Nucleofector™ X Kit S	Lonza	V4XP-3032
PageRuler Plus™ Prestained Protein Ladder	PageRuler Plus™ Prestained Protein Ladder, Pierce, 2x 250ul	Thermo Scientific	26619
PBS 10x	PBS, 10X, pH 7.4 (500ml)	Invitrogen	70011036
PBS 1x	PBS DULBECCO'S W/O CA MG 1X (10x500ml)	Life Technologies	14190169
Penicillin/Streptomycin	Penicillin-Streptomycin (10,000 U/mL)	Gibco/Life Technologies	1514-0122
Percoll	Percoll 1000ml	GE Healthcare	17-0891-01
PES 0.22 filters	Syringe-driven filters. 30 mm, PES membrane, 0.22µm, sterile.	Jet Biofil	FPE-204-030
PFA (Paraformaldehyde)	16% Paraformaldehyde (formaldehyde) aqueous solution, Electron Microscopy Sciences. 10x10ml	ANAME Instrumentación Científica	RT15710
Phenol:chloroform	Phenol:Chloroform pH 6.7/8.0 premixed with isoamyl alcohol (25:24:1)	Amresco	0883-100ML
Protease inhibitor cocktail	Protease inhibitor cocktail for plant, cell and tissue extracts	Sigma-Aldrich	P9599-1ML
Pierce™ ECL Western Blotting Substrate	Pierce™ ECL Western Blotting Substrate	Thermo Scientific	32109
Plasmodipur Filters	Plasmodipur Filters	EuroProxima	8011Filter25u
Polyethylene glycol (MW 400)	Polyethylene glycol 400 for synthesis. CAS 25322-68-3, pH 5 - 7 (100 g/l, H ₂ O, 20 °C)	Sigma-Aldrich	8.07485
Primers	For primer sequences see Tables 35 and 36.	IDT	n/a
PVDF 0.22 filters	Filtration unit Millex-GV; 0,22 µm, PVDF, 13 mm, sterile.	Merck Millipore	SLGV013SL
Pyrimethamine	Pyrimethamine VETRANAL™, analytical standard	Supelco	46706
Qiagen MiniElute Kit	MinElute Reaction Cleanup kit (50) Qiagen	Qiagen	28204
Qiagen PCR Cleanup Kit	MinElute PCR Purification Kit (250), Qiagen	Qiagen	28006
qPCR reaction plates 384-well	MicroAmp® Optical 384-Well Reaction Plate with Barcode, Applied Biosystems (50 u)	Life Technologies	4309849
qPCR reaction plates 96-well	LightCycler® 480 Multiwell Plate 96	Roche	4729692001
Random 9-mer primer	n/a	IDT	n/a
Rapamycin	Rapamycin from Streptomyces hygroscopicus, ≥95% (HPLC), powder	Sigma-Aldrich	R0395
Restriction enzymes NEB	AatII, BbsI, BtgZI, EagI, NotI and PvuII restriction enzymes	NEB	n/a
Restriction enzymes Takara	AflII, BglII, EcoRI, NcoI, NotI, SacII, Sall, SpeI and XhoI restriction enzymes	Clontech	n/a
RevertAid H Minus M-MuLV Reverse Transcriptase kit	RevertAid H Minus Reverse Transcriptase (200 U/µL), (Fermentas) 5 x 10,000 units	Life Technologies	EP0452
RNase-free DNase I kit	RNase-Free DNase Set (50) Qiagen	Qiagen	79254
RNase-free H ₂ O	UltraPure DEPC-treated water (4x100ml)	Invitrogen	750024
RNeasy MinElute cleanup kit	RNeasy MinElute Cleanup Kit (50) Qiagen	Qiagen	74204
RPMI	RPMI 1640 Med Powder 10 litres	Life Technologies	51800035
Custom made RPMI-Albumax	RPMI [+]AlbuMAX®-II (041-91762A)	Invitrogen	041-91762A

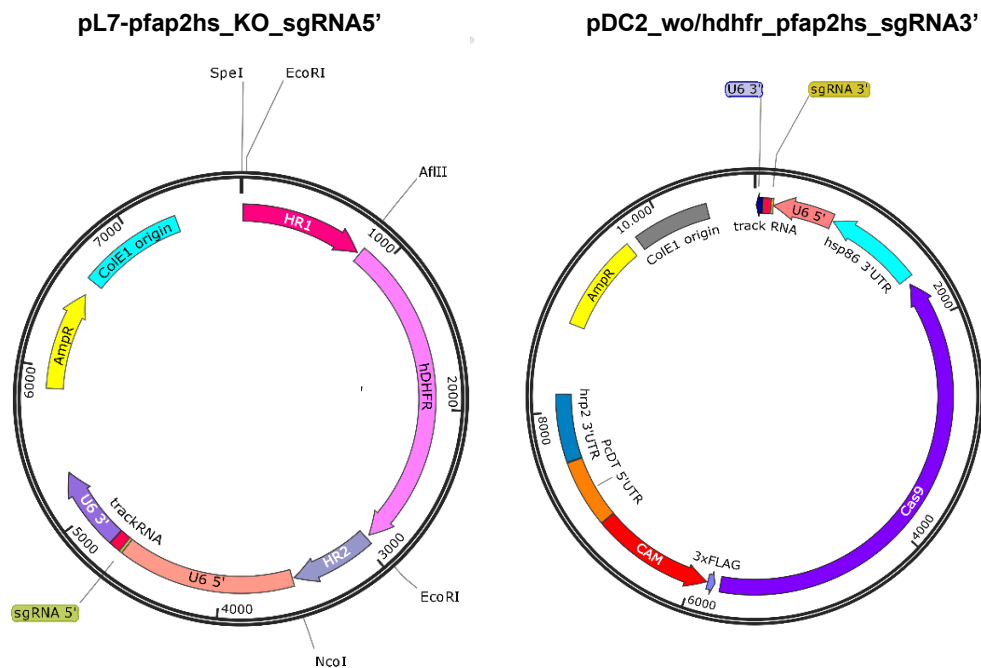
RPMI-1640 (25 mM Hepes)	RPMI-1640 Medium, with HEPES	Sigma-Aldrich	52400-025
Saponin	Saponin from quillaja bark	Sigma-Aldrich	S7900-25G
SDS	SDS, 20% Solution, Ambion® molecular biology grade, 250ml	Invitrogen	AM9820
Shield1	AquaShield-1	Cheminpharma	CIP-AS1-0001
Sorbitol	D-Sorbitol 500g	Sigma-Aldrich	S3889-500G
Stellar cells	In-Fusion® HD Cloning Kit w/Competent Cells	Takara	639642
Stripping solution	Pierce Restore Western blot stripping reagent, 500 ml	Thermo Scientific	21059
SYBR Green Master Mix	Power SYBR® Green PCR Master Mix, 10-Pack (10 x 5 mL)	Life Technologies	4368708
SYBR Safe	Sybr Safe DNA gel stain 400 µl	Life Technologies	S33102
SYTO11	SYTO® 11 green fluorescent nucleic acid stain - 5 mM solution in DMSO	Fisher Scientific	S7573
T4 ligase	T4 DNA Ligase 100U (Roche)	Sigma-Aldrich	10481220001
Taq Polymerase	Taq DNA Polymerase (500u)	Invitrogen	10342020
TE	Used from "Qiagen EndoFree Plasmid Maxi Kit"	Qiagen	50912362
TEMED	N,N,N',N'-Tetramethylethylenediamine, BioReagent, suitable for electrophoresis, ~99%	Sigma-Aldrich	T9281-25ML
Tn5	Nextera DNA library prep kit	Illumina	20018704
Tris	Trizma base, Biotechnology Performance Certified, ≥99.9% (titration), 1Kg	Sigma-Aldrich	T6066-1KG
Tris-HCl	Trizma® hydrochloride. BioPerformance Certified, cell culture tested, ≥99.0% (titration)	Sigma-Aldrich	T5941-100G
Triton X-100	Triton X-100 non-ionic, viscous liquid	Roche	10789704001
TRizol	Trizol reagent 200ml	Invitrogen	15596-018
Tween-20	Tween 20 for molecular biology	Panreac	A4974.0250
Vectashield	Vectashield mounting medium, 10ml, Vector Labs.	Palex Medical	H 1000
WR99210	WR99210	Jacobus Pharmaceuticals	
XCell II™ Blot Module	XCell II™ Blot Module	Invitrogen	EI9051
XCell SureLock™ Mini-Cell Electrophoresis System	XCell SureLock™ Mini-Cell	Invitrogen	EI0001
Xylazine	Xylacare 2& inj.		1442

Annex I - Table 1. List of products and reagents used in the thesis.

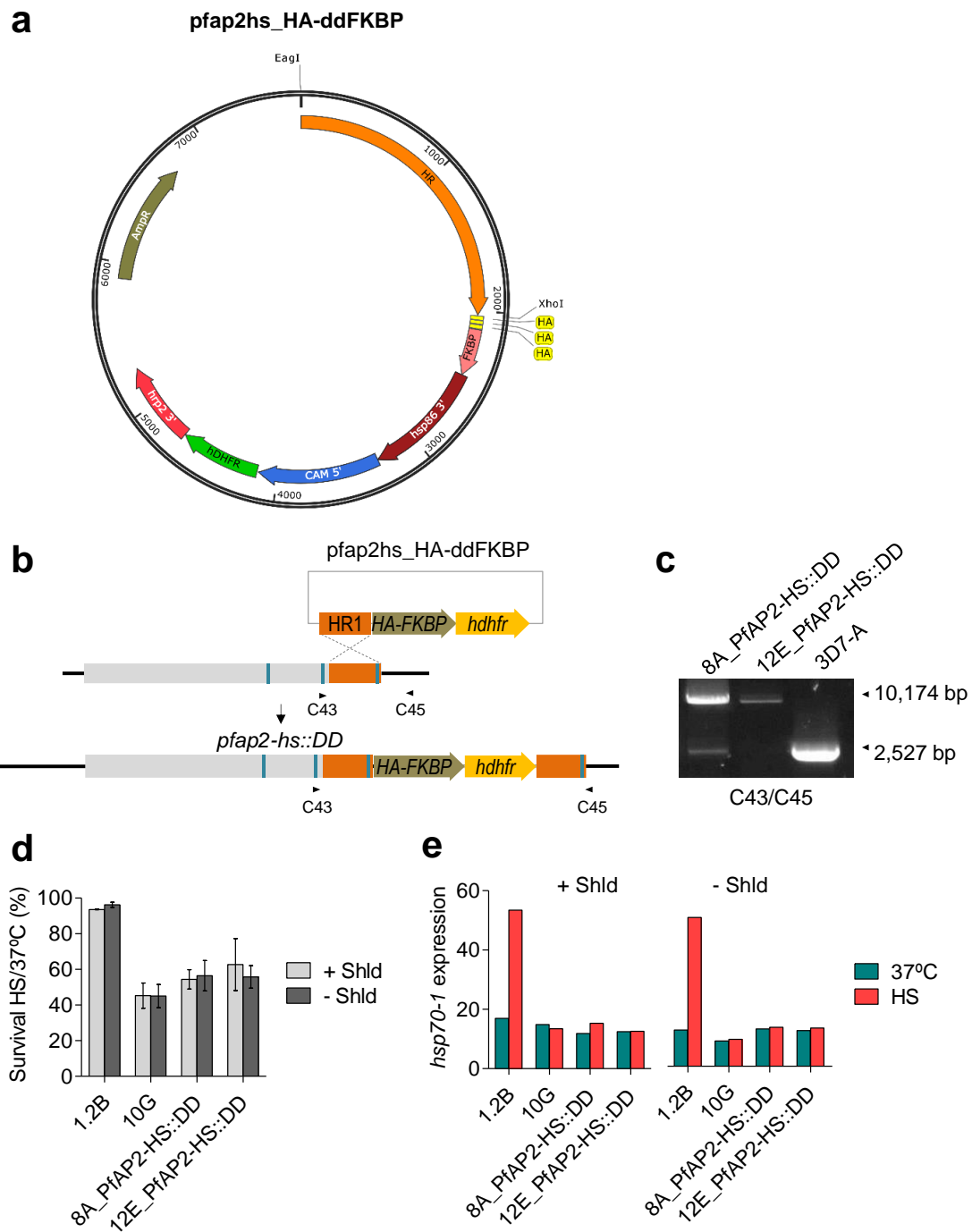
ANNEX – II

Generation and characterization of *P. falciparum* and *P. berghei* transgenic lines

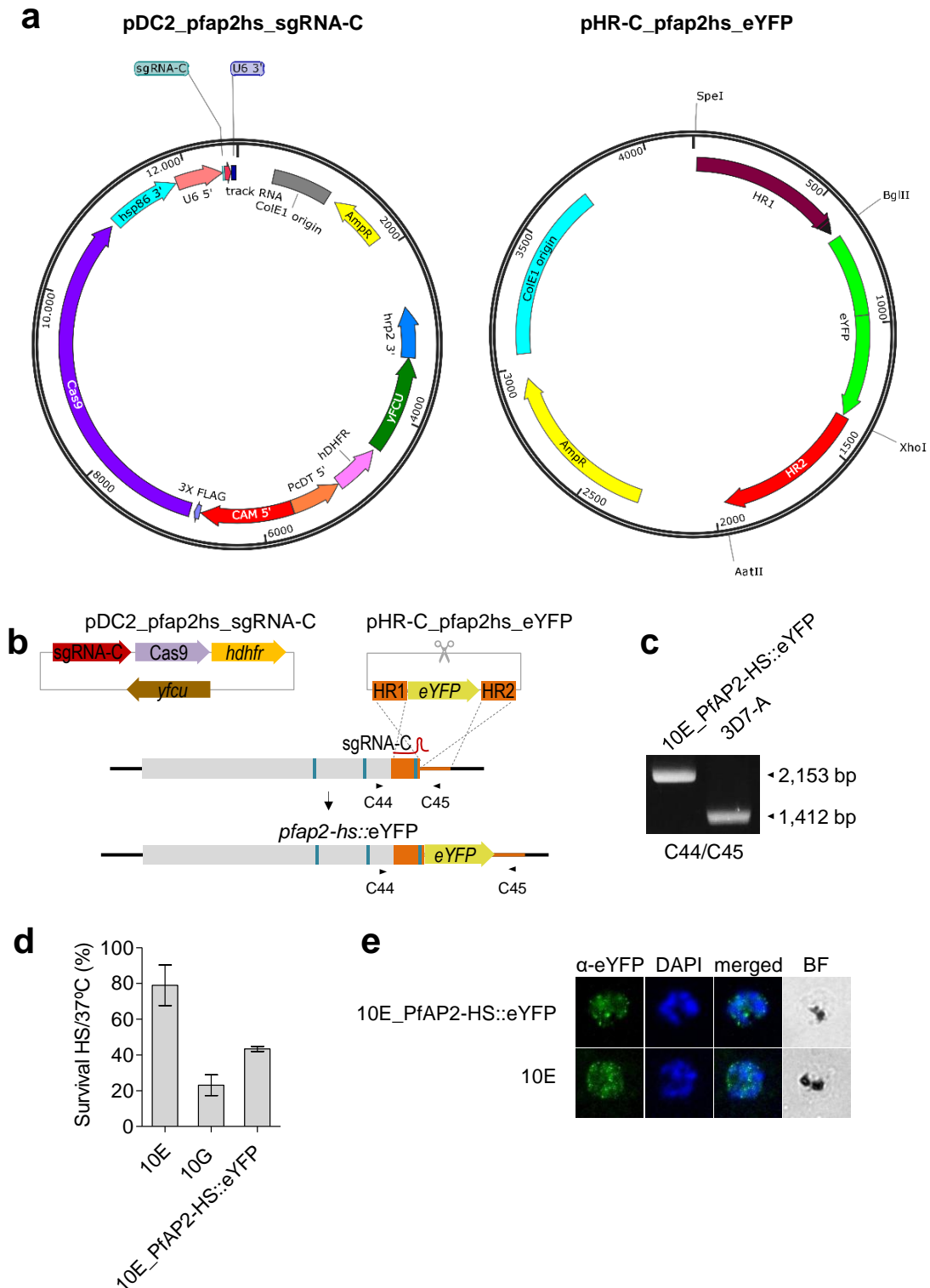
- *P. falciparum* transgenic lines



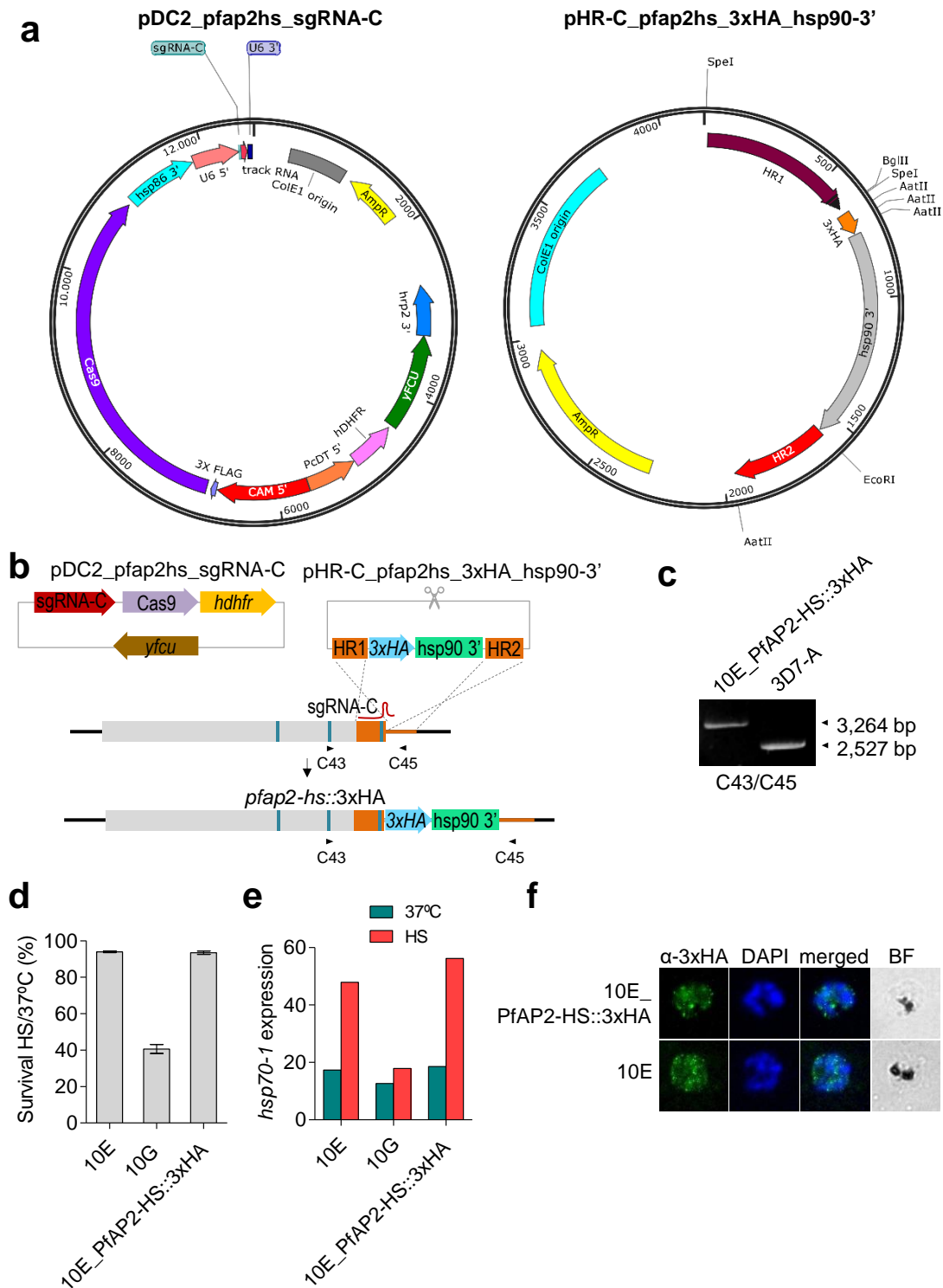
Annex II - Figure 1. Constructs used to generate $\Delta pfap2$ -*hs* lines. Maps of the donor plasmid (pL7-pfap2hs_KO_sgRNA5') and the Cas9-containing plasmid (pDC2_wo/hdhfr_pfap2hs_sgRNA3') used for the deletion of *pfap2*-*hs*.



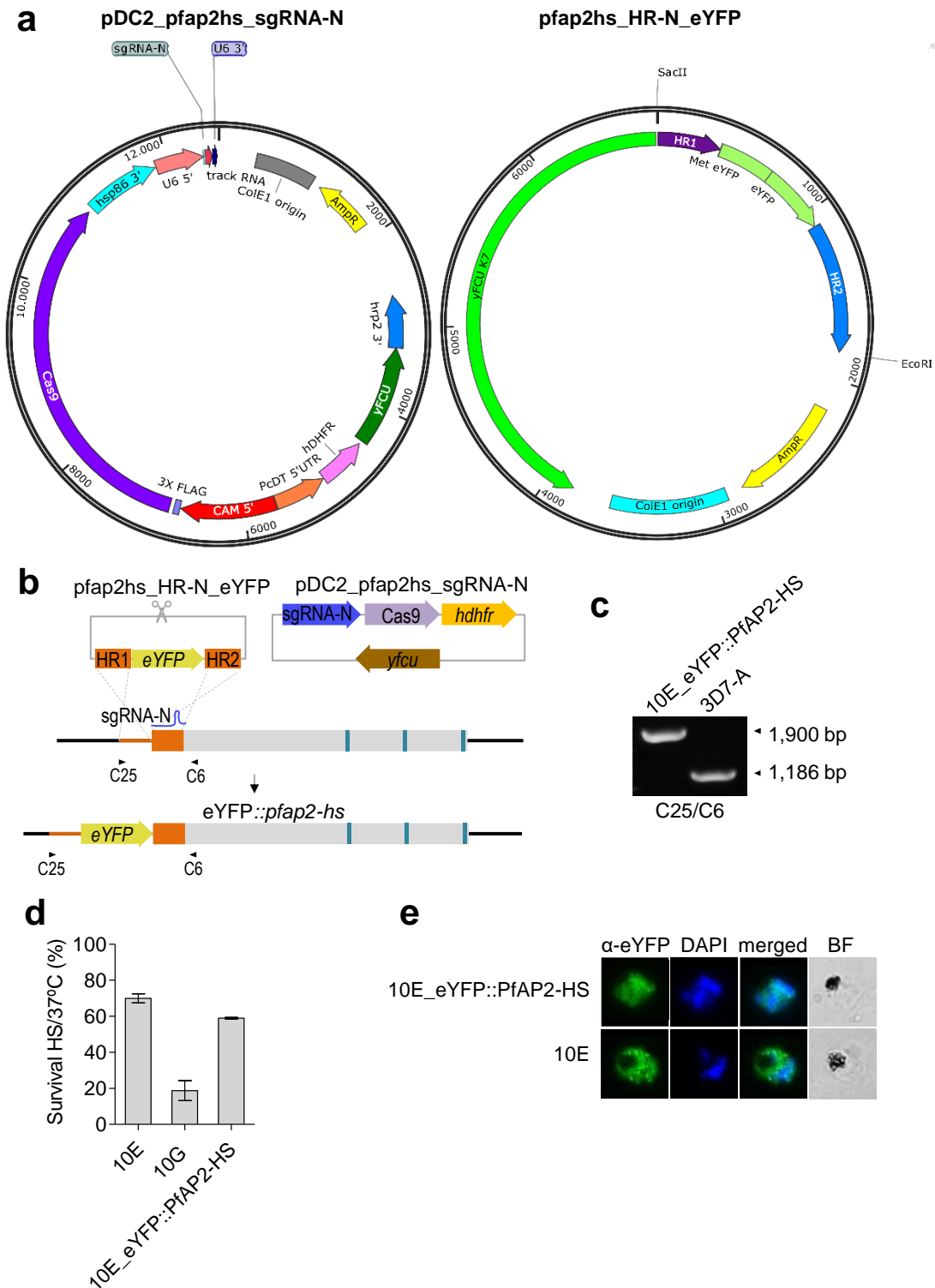
Annex II - Figure 2. Generation and characterization of transgenic parasite lines expressing an endogenous *pfap2-hs* tagged by a destabilization FKBP domain. **a**, Map of the *pfap2hs_HA-ddFKBP* vector used for the C-terminal tagging of the endogenous PfAP2-HS with a 3xHA epitope and a FKBP destabilization domain (ddFKBP, DD). **b**, Schematic of the single homologous recombination strategy used in the 1.2B background, generating the 8A_PfAP2-HS::DD and 12E_PfAP2-HS::DD subclones. Primers used for PCR validation are shown by arrowheads. **c**, Analytical PCR validating edition in 8A_PfAP2-HS::DD and 12E_PfAP2-HS::DD. It shows a mixture of parasites with correct plasmid integration and wild type parasites in subclone 8A, and correct integration in subclone 12E. **d**, HS survival of the transgenic subclones cultured in the presence (+Shld) or absence (-Shld) of Shield1, using HS-resistant (1.2B) and HS-sensitive (10G) subclones as controls. **e**, Transcript levels of *hsp70-1* (normalized by *serine-tRNA ligase*) after HS exposure or control (37°C) conditions of the transgenic lines and its controls cultured in presence or absence of Shield1.



Annex II - Figure 3. Generation and characterization of transgenic parasite lines expressing an endogenous *pfap2-hs* tagged by eYFP at the C-terminal end. **a**, Map of the Cas9-containing plasmid (pDC2_pfap2hs_sgRNA-C) and the donor plasmid (pHR-C_pfap2hs_eYFP) used for the eYFP C-terminal tagging of the endogenous PfAP2-HS. **b**, Schematic of the CRISPR/Cas9 edition strategy used in the 10E background, generating the 10E_PfAP2-HS::eYFP transgenic line. The position of primers used for PCR validation are indicated by arrowheads. **c**, Analytical PCR validating the correct and clean edition of the resultant 10E_PfAP2-HS::eYFP transgenic line. **d**, HS survival of the transgenic line, together with a HS-resistant (10E) and a HS-sensitive (10G) line as controls. **e**, Immunofluorescence assay images detecting the eYFP tag (green) and DNA (DAPI, blue) both in the transgenic and parental lines. Bright field (BF) images are also shown.

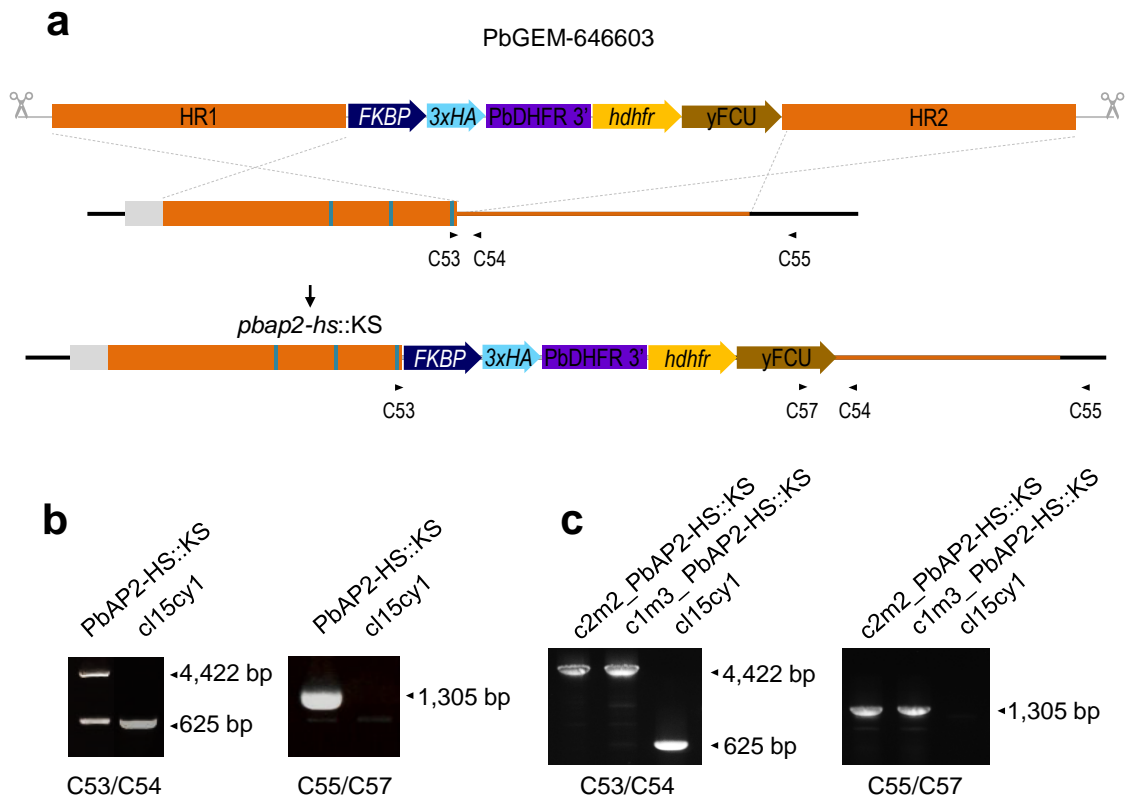


Annex II - Figure 4. Generation and characterization of transgenic parasite lines expressing an endogenous *pfap2-hs* tagged with 3xHA at the C-terminal end. **a**, Map of the Cas9-containing plasmid (pDC2_pfap2hs_sgRNA-C) and the donor plasmid (pHR-C_pfap2hs_3xHA_hsp90-3') used for the 3xHA C-terminal tagging of the endogenous PfAP2-HS. **b**, Schematic of the CRISPR/Cas9 edition strategy used in the 10E background, generating the 10E_PfAP2-HS::3xHA transgenic line. The position of primers used for PCR validation are indicated by arrowheads. **c**, Analytical PCR validating the correct and clean edition of the resultant 10E_PfAP2-HS::3xHA transgenic line. **d**, HS survival of the transgenic line, together with a HS-resistant (10E) and a HS-sensitive (10G) lines as controls. **e**, Transcript levels of *hsp70-1* (normalized by *serine-tRNA ligase*) after HS exposure or control (37°C) conditions of the transgenic line and its controls. **f**, Immunofluorescence assay images detecting the 3xHA tag (green) and DNA (DAPI, blue) both in the transgenic and parental lines. Bright field (BF) images are also shown.

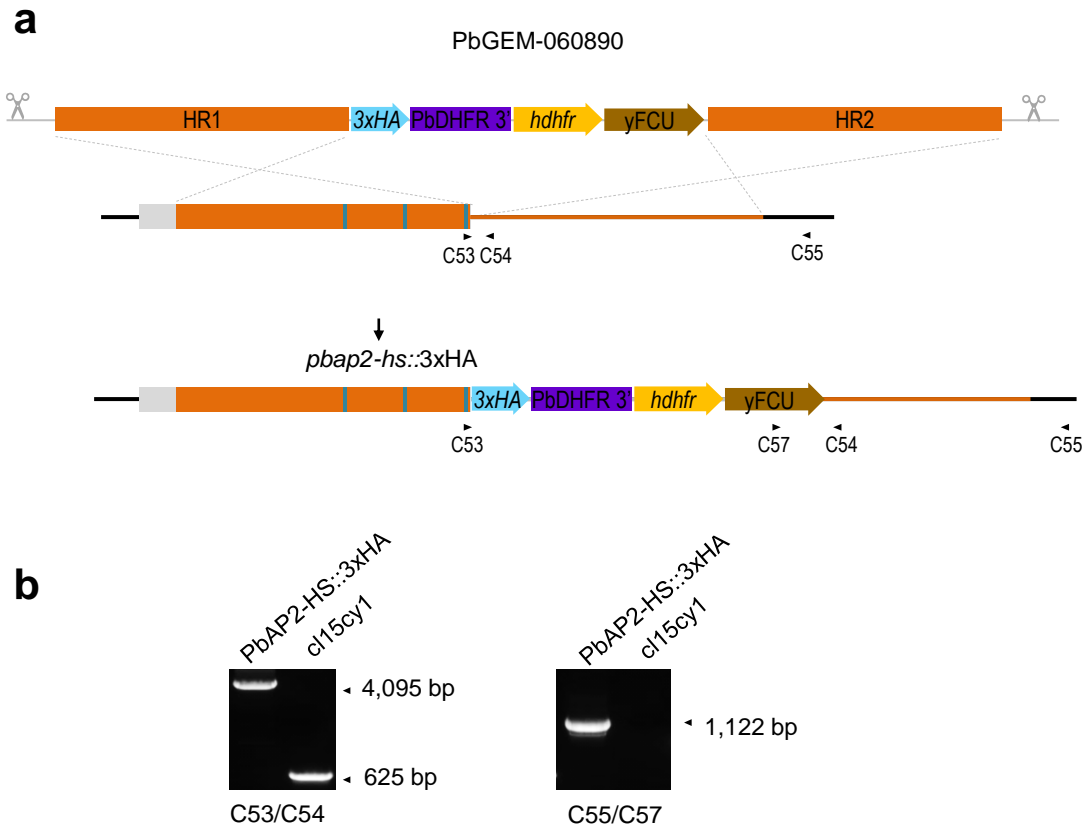


Annex II - Figure 5. Generation and characterization of transgenic parasite lines expressing an endogenous *pfap2-hs* tagged with eYFP at the N-terminal end. **a**, Map of the Cas9-containing plasmid (pDC2_pfap2hs_sgRNA-N) and the donor plasmid (pfap2hs_HR-N_eYFP) used for the eYFP N-terminal tagging of the endogenous PfAP2-HS. **a**, Schematic of the CRISPR/Cas9 edition strategy used in the 10E background, generating the 10E_eYFP::PfAP2-HS transgenic line. The position of primers used for PCR validation are indicated by arrowheads. **b**, Analytical PCR validating the correct and clean edition of the resultant 10E_eYFP::PfAP2-HS transgenic line. **c**, HS survival of the transgenic line, together with a HS-resistant (10E) and a HS-sensitive (10G) lines as controls. **d**, Immunofluorescence assay images detecting the eYFP tag (green) and DNA (DAPI, blue) both in the transgenic and parental lines. Bright field (BF) images are also shown.

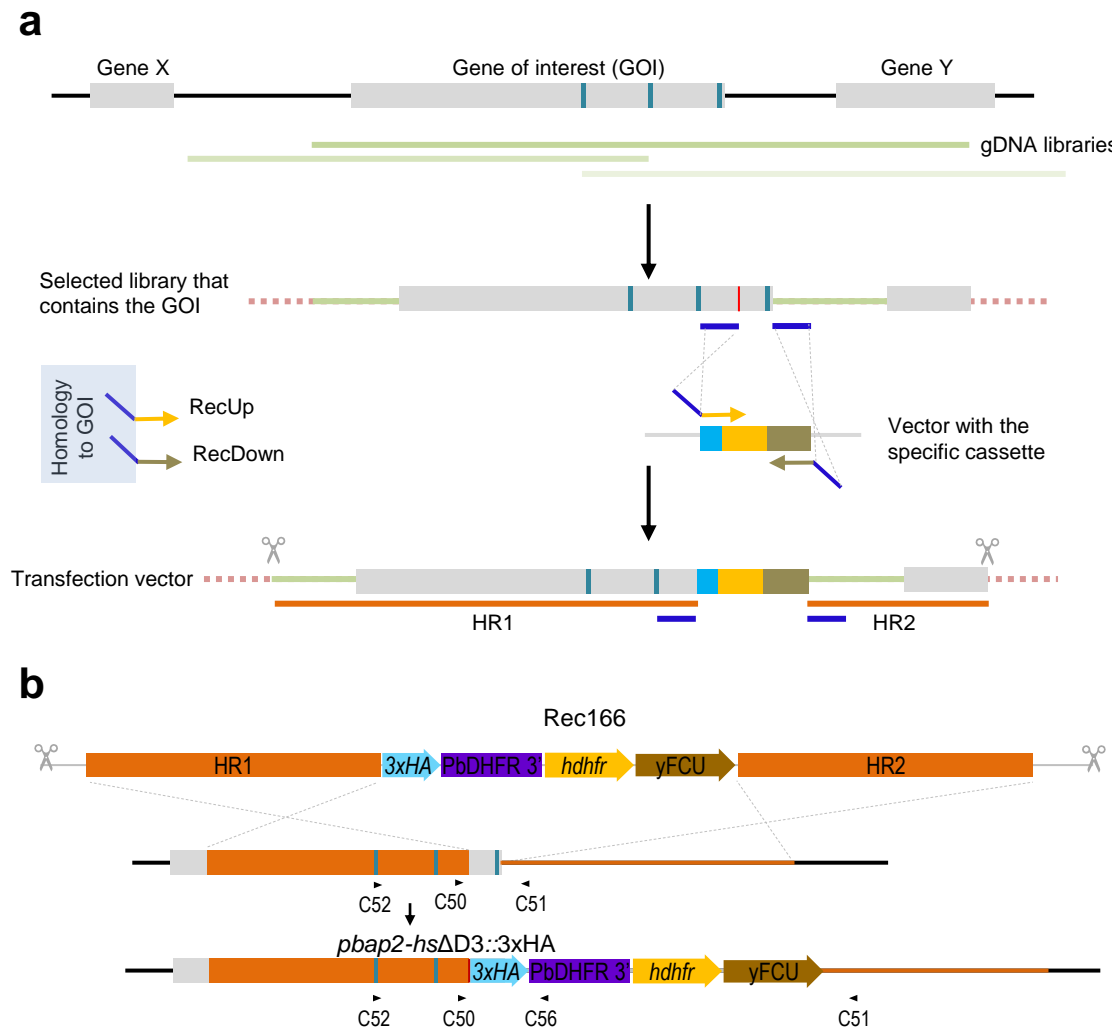
- P. berghei* transgenic lines



Annex II - Figure 7. Generation and characterization of a knocksideways transgenic parasite line for *pbap2-hs*. **a**, Schematic of the C-terminal FKBP and 3xHA tagging of the endogenous PfAP2-HS in the PbANKA cl15cy1 clone using a double recombination strategy. The FKBP domain drives the mislocalization of the protein in absence of Rapamycin ligand (knocksideways system, KS). The position of primers used for PCR validation is indicated by arrowheads. **b-c**, Analytical PCR validating the edition of the resultant PbAP2-HS::KS transgenic line before (**b**) or after (**c**) subcloning (subclones c2m2 and c1m3 are shown). C53/C54 primers were used to determine the presence of wild type and edited parasites, and C55/C57 primers were used to identify only edited parasites.



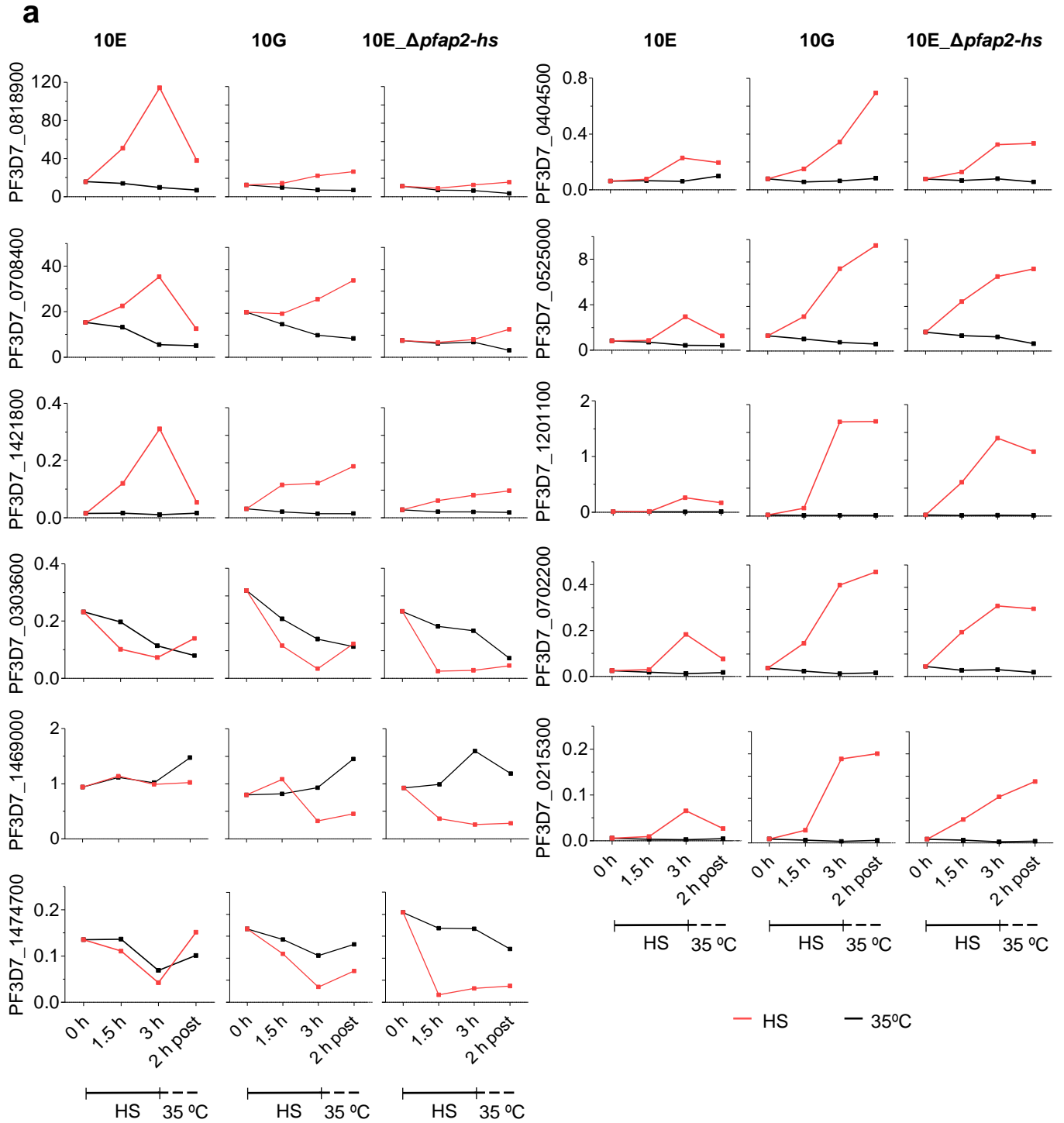
Annex II - Figure 8. Generation and characterization of transgenic parasite lines expressing an endogenous PbAP2-HS tagged with 3xHA at the C-terminal end in *P.berghei* parasites. **a**, Schematic of the C-terminal tagging of the endogenous PfAP2-HS in the PbANKA cl15cy1 clone using a double recombination strategy. The position of primers used for PCR validation is indicated by arrowheads. **b**, Analytical PCR validating the correct and clean edition of the resultant PbAP2-HS::3xHA transgenic line. C53/C54 primers were used to check for wild type and edited parasites, and C55/C57 primers were used to check edited parasites.

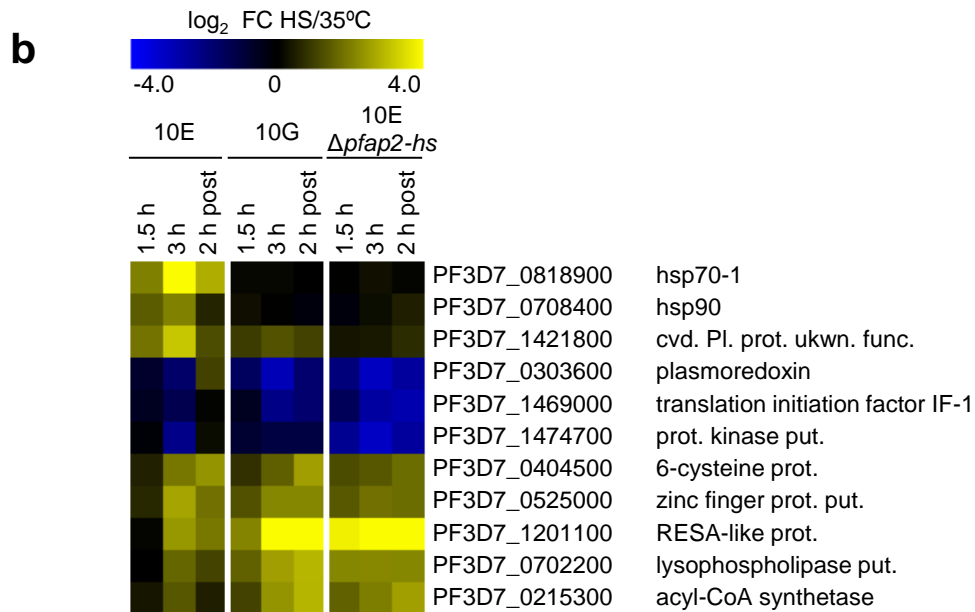


Annex II - Figure 9. Strategy used to obtain transgenic parasites expressing a truncated PbAP2-HS tagged with 3xHA at the C-terminal end in *P.berghei* parasites. a, Schematic of the PlasmogEM-based cloning strategy used to obtain the desired vector. Rec166-RecUp and Rec166-RecDown primers are represented. b, Schematic of the transfection vector used to truncate the PbAP2-HS protein (simulating the Q3714X mutation identified in *P. falciparum*) and tag it with a 3xHA, using a double recombination approach in the PbANKA cl15cy1 parasite background. The position of primers designed for PCR validation is indicated by arrowheads.

ANNEX – III

RT-qPCR validation of microarray analysis





Annex III – Figure 1. Reverse transcription-quantitative PCR (RT-qPCR) validation of the transcriptomic analysis of the HSR. a, RT-qPCR analysis of transcript levels (normalized against *serine--tRNA ligase*) of the genes in panel a, using biological samples independent from the samples used for microarray analysis. Values are the average of triplicate reactions. **b,** Log₂ expression fold-change (FC) (HS relative to control conditions) as determined by microarray analysis (Fig. 35) of the genes selected for validation. Two genes had values out of the range displayed (actual range: -3.1 to +4.93).

ANNEX – IV

Published and unpublished work

- **Work directly derived from the thesis results (unpublished)**

Tintó-Font E., Michel-Todó L., Bozdech Z., Cortés A. An ApiAP2 transcription factor drives protection from febrile temperatures in malaria parasites. [Under review]

- **Work not directly derived from the thesis results**

Llorà-Batlle O., **Tintó-Font E.**, Cortés A. Transcriptional variation in malaria parasites: why and how. *Brief Funct Genomics*. 2019 May 22. doi: 10.1093/bfpg/elz009. [Epub ahead of print]

Mira-Martínez S., Pickford A. K., Rovira-Graells N., Guetens P., **Tintó-Font E.**, Cortés A., Rosanas-Urgell A. Identification of antimalarial compounds that require CLAG3 for their uptake by *Plasmodium falciparum*-infected erythrocytes. *Antimicrob Agents Chemother*. 2019 Apr 25;63(5). doi: 10.1128/AAC.00052-19.

Rovira-Graells N., Aguilera-Simón S., **Tintó-Font E.**, Cortés A. New Assays to Characterise Growth-related phenotypes of *Plasmodium falciparum* reveal variation in density-dependent growth inhibition between parasite lines. *PLoS One*. 2016 Oct 25;11(10):e0165358. doi: 10.1371/journal.pone.0165358. eCollection 2016.